Cyanobacterial bioactive metabolites for anticancer drug discovery: characterization of new compounds and molecular mechanisms in physiologically relevant 3D cell culture

Maria Lígia da Silva Sousa
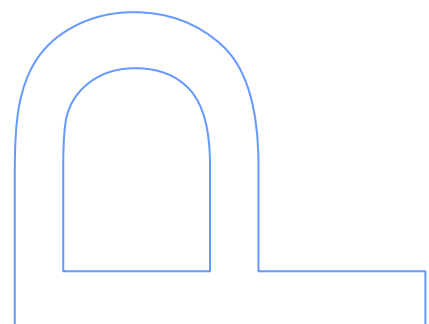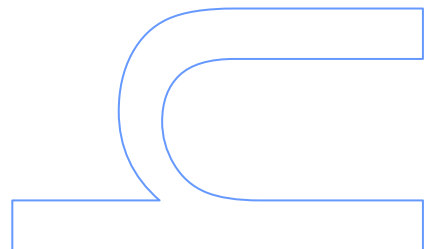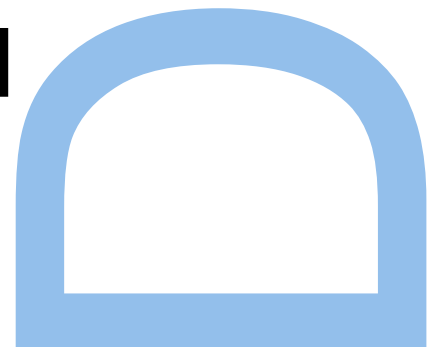Doutoramento em Biologia
Departamento de Biologia
2019
Orientador
Ralph Urbatzka, CIIMAR
Coorientador
Vítor Vasconcelos, FCUP and CIIMAR

FCUP | iii
Cyanobacterial bioactive metabolites for anticancer drug
discovery: characterization of new compounds and
molecular mechanisms in physiologically relevant 3D cell
culture

"A Lígia tem o coração dividido entre o violino e a investigação"
Professora primária Paula Rebocho 1998

"Lígia's heart is divided between violin and research"
Primary school teacher Paula Rebocho 1998

À minha família

To my family

FCUP | iv
Cyanobacterial bioactive metabolites for anticancer drug
discovery: characterization of new compounds and
molecular mechanisms in physiologically relevant 3D cell
culture

FCUP v
Cyanobacterial bioactive metabolites for anticancer drug
discovery: characterization of new compounds and
molecular mechanisms in physiologically relevant 3D cell
culture

Cyanobacterial bioactive metabolites for anticancer drug discovery: characterization of new compounds and molecular mechanisms in physiologically relevant 3D cell culture

SFRH/BD/108314/2015

Maria Lígia da Silva Sousa

Blue Biotechnology and Ecotoxicology (BBE), Interdisciplinary Centre of Marine and Environmental Research (CIIMAR), Portugal

Department of Medical and Health Sciences (IMH), Division of Drug Research (LÄFO), Linköping University, Sweden

Department of Oncology-Pathology, Karolinska Institutet, Sweden

Supervisor: Ralph Urbatzka, CIIMAR

Co-supervisors:

Vítor Vasconcelos FCUP, CIIMAR

Rosário Martins ESS-IPP, CIIMAR

Faculty of Sciences of the University of Porto, 2019

FCUP | vi

Cyanobacterial bioactive metabolites for anticancer drug discovery: characterization of new compounds and molecular mechanisms in physiologically relevant 3D cell culture

Acknowledgments

Personal Acknowledgments

These last four years were the most challenging that I have ever embrace. This journey was not done alone and therefore I would like to thank and dedicate the present work to all of those that directly or indirectly helped me.

Since the beginning, Professor Vítor believed in me and in my project and received me in his lab as if I was part of it already. I cannot thank you enough for the opportunity of joining the best lab in CIIMAR. I thank also Rosário, who always cared about me and my work, always ready to help.

I worked in BBE alongside great scientists who are role models to me and, not less important I became part of the family. I thank to all BBE team but I have to name Mariana, Joana Azevedo, Pedro and Marco, for and the help and counsel regarding the chemistry part of my project; Leonor, especially during this last year, for her commitment to always getting more and better results; to João for always keep the "silence" in the room; to Mica, for taking good care of us all; to CNP, for having me as "CNP's favourite".

I must thank to the best supervisor of all times, Ralph Urbatzka. It is not the first time that you accept the challenge of supervising this enthusiastic young student, very persistent (let's not call it stubborn, ok? 😊), willing to do and know always more. Thank you for letting me learn from you, helping me to grow as a scientist, believing in me, support my work, for always being comprehensive and (definitely) thanks for your endless patience with me!

To my nonofficial supervisor, Stig Linder, I cannot express my appreciation for you and thank you enough. Thanks for being and exceptional person, a brilliant scientist but also the best professor, for all you taught me but also for your hospitality, good mood and for teach me that Sweden is the second best country in the world (Portugal is the first, sorry!). I also thank you the opportunity to meet and work with the most amazing scientists that made my time in Sweden bright and soft: Maria Miquel, Paola, Arjan, Padraig, Karthik, Maria, Nan and Niclas…Thank you!

My final thank goes to the most important people of my life: my family. My husband, for believing in me more than myself. And my parents, for being proud of their daughter and always believe and support every single step I made.

Thank you!

FCUP   ix

Cyanobacterial bioactive metabolites for anticancer drug discovery: characterization of new compounds and molecular mechanisms in physiologically relevant 3D cell culture

Abstract

Cyanobacteria are versatile microorganisms that ubiquitously inhabit terrestrial and aquatic ecosystems. They adapt to external threats by producing secondary metabolites. Therefore, cyanobacteria have been recognized as producer of natural products with potential biotechnological applications.

As a starting point for this project, compounds already isolated from cyanobacterial strains from the LEGE CC culture collection hosted at CIIMAR, and extracts of marine cyanobacteria isolated from the Portuguese coast with described promising anticancer activity from previous screenings, were studied regarding their cytotoxicity and antitumoral activity on colon carcinoma cells (HT-29 and HCT116) cultured as monolayer (2D) or as multicellular culture systems (MSC). Such advanced *in vitro* model (MSC) is a physiologically more representative of a real tumour, therefore, interesting to characterize effects and mechanisms of actions of compounds, and to screen for new compounds.

The compounds studied on the present thesis were nocuolin A (NocA) re-isolated from the cyanobacteria strain *Nodularia* sp. LEGE06071, portoamides A and B (PAB) isolated from the strain *Phormidium* sp. LEGE 05929, hierridins B and C isolated from the strain *Cyanobium sp.* LEGE06113, bartoloside A isolated from the strain *Nodosilinea sp.* LEGE 06102 and bartolosides B and C re-isolated from the strain *Synechocystis salina* LEGE 06155.

NocA exposure of HCT116 cells, cultured both as 2D and MSC, decreased ATP in a dose-dependent manner. Oxygen consumption was also decreased, impairing normal mitochondrial respiration function. These results were additionally observed in immortalized retinal normal cells (RPE-1^{hTERT}), although not accompanied by a reduction of viability. Also, exposure to NocA induced the protein level of the autophagy marker LC3B-II and the presence of autophagic vacuoles, as well as cell death. Apoptosis was confirmed by the M30 Apoptosense assay. The obtained results suggest that NocA targets mitochondria by impairing cell respiration, which makes it an interesting candidate for further studies, considering the high energy requirements of cancer cells.

A second set of compounds studied consisted in a mixture of portoamides A and B (PAB) at the proportion of 3:1, its natural occurrence proportion. PAB were tested against a battery of cancer cell lines and non-cancer cell lines and its activity further explored in

FCUP | x
Cyanobacterial bioactive metabolites for anticancer drug
discovery: characterization of new compounds and
molecular mechanisms in physiologically relevant 3D cell
culture

the colon adenocarcinoma cell lines HT-29 (2D) and HCT116 (cultured both in 2D and as MSC). Although PAB are molecules with high molecular weight (A ≈ 1532 g/mol and B ≈ 1502 g/mol), the results indicated that they enter into cells through an energy-independent mechanism. PAB cytotoxicity was effective not only in 2D, but also on the outer layers of MSC, the most metabolic active and proliferative cells. A proteomics approach reveal upregulation of proteins related with oxidative stress response transaldolase (TALDO), peroxiredoxin- 4 (PRDX4) and peroredoxin-6 (PRDX6), upregulation of two subunits of proteasome (PSA6_HUMAN e PSB4_HUMAN) but also proteins related with the functioning of complex I of the mitochondrial respiratory chain: NADH dehydrogenase and NADH: ubiquinone oxidoreductase (NDUFS3). Enzymatic assays and HCT116 cells transfected with a pTRAF plasmid containing using Nrf2 reporter genes reveal that PAB were not significantly inducing oxidative stress but rather indicated that mitochondria were being disrupted. ATP was reduced and OXPHOS with a significant decrease of maximal mitochondrial respiration, due to the hyperpolarization of mitochondria and PTEN-induced putative kinase 1 (PINK1) upregulated expression. PAB revealed specificity on targeting mitochondria, penetrating the outer layer of MSC.

Bartolosides A and C did not show any activity against MSC of HCT116 cells. Yet, bartoloside B showed a decreasing of the MSC size accompanied with some cell disaggregation. However, a decrease in MSC viability or induction of apoptosis were not confirmed. Hierridin B and C were also tested on MSC of HCT116 cells, but no alterations were observed on the spheroid size. Both hierridins reduced p21 protein level, and increased p53 and c-myc proteins. These results are in accordance with previous work on 2D cultured HT-29, where a cell cycle arrest was observed for cells exposed to hierridin B.

In the last chapter of the present thesis, MSC were explored for the screening of cyanobacterial extracts, in order to guide future work on the isolation of novel compounds using a physiological relevant model. The choice of MSC and different viability assays (acid phosphatase, staining of MSC with dyes for cell death and cytoplasmic esterase activity) allowed us to select eight promising cyanobacteria extracts from a total of 81. The metabolic profile was studied by HR-LC–MS/MS followed by data analysis with GNPS. Such exploration of the MS/MS data led to the identification of the most promising strains, characterized by bioactivity and the potential to produce not known metabolites. The strain *Lusitaniella coriacea* LEGE 07167 was identified as most promising strain,

which had cytotoxic activity in previous works on 2D cultures of several cancer cell lines and the presence of PKS gene clusters.

With the present study we aimed to contribute to increase the knowledge on cyanobacterial secondary metabolites aplications and their importance to the society. We also aimed to demonstrate that using *in vitro* models we can approximate laboratory results to *in vivo* situations and hopefully help to increase the success on drug discovery in the future.

Resumo

As cianobactérias são microorganismos versáteis que habitam todos os ecossistemas terrestres e aquáticos. A sua adaptação a diferentes ambientes deve-se à capacidade de produzir metabolitos secundários. Desta forma, as cianobactérias têm sido reconhecidas como produtoras auspiciosas de novas substâncias naturais com várias aplicações biotecnológicas.

Como ponto de partida para este projeto, foram estudados compostos já isolados de estirpes de cianobactérias da coleção de culturas LEGE CC e extratos de cianobactérias marinhas isoladas da costa portuguesa, anteriormente descritas como tendo potencial anticancerígeno, aqui estudadas quanto à sua citotoxicidade e atividade antitumoral em células de cancro do colon (HT-29 e HCT116), cultivadas em monocamada (2D) ou em sistemas de cultura multicelular (MSC). Este modelo avançado *in vitro* (MSC) é um modelo fisiologicamente mais representativo de um tumor real, e, portanto, um modelo interessante para caracterizar não só efeitos e mecanismos de ação de compostos, mas também como modelo de triagem para novos compostos.

Os compostos estudados neste trabalho foram a nocuolina A (NocA), re-isolada da estirpe de cianobactéria *Nodularia* sp. LEGE06071, as portoamidas A e B (PAB) isoladas de *Phormidium* sp. LEGE 05929, as hierridinas B e C isoladas de *Cyanobium* sp. LEGE06113, a bartolosida A isolada da estirpe *Nodosilinea* sp. LEGE 06102 e e as bartolosidas B e C re-isoladas da estirpe *Synechocystis salina* LEGE 06155.

A NocA exposta às células HCT116, cultivadas em 2D e MSC, induziram uma diminuição de ATP a par da diminuição do consumo de oxigénio, prejudicando o normal funcionamento da respiração mitocondrial. Estes resultados também foram observados

FCUP xii
Cyanobacterial bioactive metabolites for anticancer drug
discovery: characterization of new compounds and
molecular mechanisms in physiologically relevant 3D cell
culture

em células normais imortalizadas da retina (RPE-1^{hTERT}), embora não acompanhados de redução da viabilidade. Além disso, a exposição à NocA induziu a expressão do marcador da autofagia LC3B-II, tendo sido possível visualizar em microsopia de fluorescência a marcação dos vacúolos autofágicos, bem como a indução de morte celular. A apoptose foi confirmada pelo ensaio M30 Apoptosense. Uma vez que a NocA atinge as mitocôndrias prejudicando a respiração celular, este composto torna-se particularmente interessante para estudos futuros de desenvolvimento de fármacos destinados ao tratamento do cancro, tendo em conta que as células de cancro requerem elevados níveis de energia para proliferarem.

O segundo conjunto de compostos aqui estudado é uma mistura de portoamidas A e B (PAB) na proporção de 3:1, a proporção a que naturalmente ocorrem. PAB foi testado em várias linhagens de células cancerígenas e não cancerígenas e a sua atividade explorada em duas linhas celulares de adenocarcinoma do cólon HT-29 (2D) e HCT116 (cultivadas em 2D e como MSC). Embora PAB sejam moléculas com elevado peso molecular (A ≈ 1532 g / mol e B ≈ 1502 g / mol), verificou-se que entram nas células através de um mecanismo independente de energia e sua citotoxicidade é eficaz não apenas em 2D, mas também nas camadas mais exteriores de MSC, a camada com células metabolicamente mais ativas e proliferativas. Através de análises de proteómica foi possivel identificar proteínas sobreexpressas cuja atividade está relacionada com a resposta aos stress oxidativo, como a transaldolase (TALDO), a peroxiredoxina- 4 (PRDX4) e a peroredoxin-6 (PRDX6); verificou-se também a sobreexpressão de duas subunidades do proteosoma (PSA6_HUMAN e PSB4_HUMAN), e de proteínas relacionadas com o funcionamento de complexo I da cadeia respiratória mitocondrial: NADH desidrogenase e NADH: ubiquinona oxidoredutase (NDUFS3). Ensaios enzimáticos e ensaios com células HCT116 transfetadas com um plasmídeo pTRAF contendo genes repórter Nrf2 revelam que o PAB não induz stress oxidativo, mas por outro lado indiciam que as mitocôndrias poderiam estar danificadas. A produção de ATP estava diminuída e a o funcionamento da cadeira de fosforilação oxidativa alterado, traduzindo-se numa significativa diminuição da respiração mitocondrial, devido à hiperpolarização da membrana das mitocôndrias, o que foi confirmado pela sobreexpressão de PTEN-induced putative kinase 1 (PINK1). As PAB revelam assim atuar especificamente nas mitocôndrias e têm capacidade de penetrar na camada externa dos MSC.

FCUP xiii
Cyanobacterial bioactive metabolites for anticancer drug
discovery: characterization of new compounds and
molecular mechanisms in physiologically relevant 3D cell
culture

As bartolosidas A e C não mostraram nenhuma atividade em MSC de células HCT116. No entanto, o bartolosida B induziu uma diminuição do tamanho dos MSC em comparação ao controlo, acompanhado de alguma desagregação celular da estrutura, embora não se tenha verificado diminuição da viabilidade nem indução de apoptose. Em relação às hierridinas, foram testadas em MSC e, embora não houvesse alterações no tamanho dos MSC, foi detectada a diminuição da expressão da proteína p21 e uma sobreexpressão das proteínas p53 e c-myc. Estes resultados estão de acordo com o trabalho anterior realizado com células HT-29 cultivadas em 2D, onde foi registada uma paragem da progressão do ciclo celular em células expostas à hierridina B. No entanto, neste trabalho demonstrou-se a primeira indicação de que isso também pode ocorrer com a hierridina C.

O último capítulo da presente tese explora o uso de MSC como modelo para a triagem de extratos de cianobactérias com promissoras propriedades anticancerígenas, descritas em trabalhos anteriores. Através do uso de MSC e testada a sua viabilidade com ensaios de fosfatase ácida e fluorescência com marcadores de morte celular (iodeto de propídeo) e viabilidade (calceína AM), foi possível selecionar oito extratos de cianobactérias. Esses extratos foram analisados por HR-LC-MS/MS e posterior análise de GNPS. Com estes métodos, foi possível identificar as estirpes mais promissoras, nas quais destacamos a *Lusitaniella coriacea* LEGE 07167. A seleção desta estirpe baseou-se não só nos resultados de viabilidade apresentados neste trabalho, mas também na análise de trabalhos anteriores, que utilizaram várias linhagens de células cancerígenas cultivadas em 2D e na identificação de clusters de genes que estão envolvidos na produção de metabolitos secundários (PKS) no genoma desta cianobactéria.

Com o presente estudo, pretendemos contribuir para aumentar o conhecimento sobre os metabolitos secundários de cianobactérias e sua importância para a sociedade. Foi também um importante objetivo a utilização de modelos avançados *in vitro* de forma a aproximar os resultados obtidos em laboratório às situações reais e assim aumentar o sucesso na descoberta de novos fármacos.

Keywords/ Palavras chave

Cyanobacteria, metabolites, anticancer, spheroid, mitochondria, natural products, nocuolin A, portoamides, bartolosides, hierridins
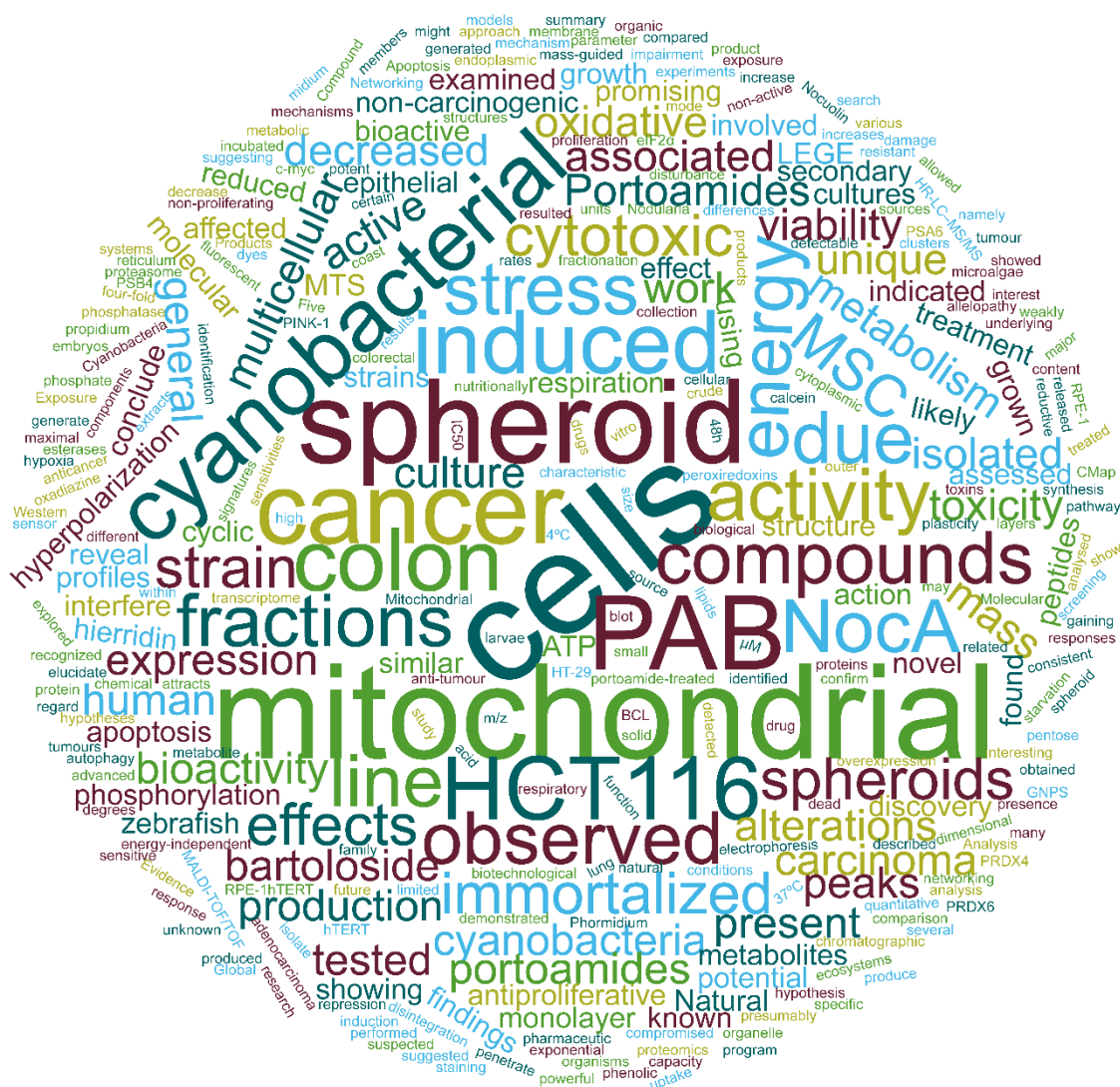
FCUP | xvi
Cyanobacterial bioactive metabolites for anticancer drug
discovery: characterization of new compounds and
molecular mechanisms in physiologically relevant 3D cell
culture

Table of Contents

FCUP   xviii
Cyanobacterial bioactive metabolites for anticancer drug
discovery: characterization of new compounds and
molecular mechanisms in physiologically relevant 3D cell
culture

FCUP xix
Cyanobacterial bioactive metabolites for anticancer drug
discovery: characterization of new compounds and
molecular mechanisms in physiologically relevant 3D cell
culture

List of Figures

Introduction

Antiproliferative effects of the natural oxadiazine nocuolin A are associated with impairment of mitochondrial oxidative phosphorylation

Cytotoxicity of portoamides in human cancer cells and analysis of the molecular mechanisms of action

FCUP | xx
Cyanobacterial bioactive metabolites for anticancer drug
discovery: characterization of new compounds and
molecular mechanisms in physiologically relevant 3D cell
culture

Portoamides A and B are mitochondrial toxins and induce cytotoxicity on the proliferative cell layer of in vitro microtumours

Cytotoxicity assessment of the alkylresorcinols bartolosides A, B and C and hierridins B and C on multicellular culture systems of the colon carcinoma cell line HCT116

Assessing promising bioactivity of cyanobacterial strains on a 3D in vitro model of solid tumours

Discussion

FCUP xxii
Cyanobacterial bioactive metabolites for anticancer drug
discovery: characterization of new compounds and
molecular mechanisms in physiologically relevant 3D cell
culture

List of Tables

Abbreviations

2DGE - two-dimensional gel electrophoresis

ADC - antibody–drug conjugates

ADC (MMAE) - antibody–drug conjugates (Monomethyl Auristatin E)

AO - acridine orange

ATP - adenosine triphosphate

BBE - Laboratory of Blue Biotechnology and Ecotoxicology

BiP - binding immunoglobulin protein

CCCP - carbonyl cyanide m-chlorophenyl hydrazone

CH$_2$Cl$_2$ - dichloromethane

CSC – cancer stem cells

DCFDA - dichlorofluorescin diacetate

DMSO - dimethylsulphoxide

DNA - deoxyribonucleic acid

DPF - days post-fertilization

eIF2α - eukaryotic Initiation Factor 2

ER – endoplasmic reticulum

EtOAc – ethyl acetate

FADH$^+$ - flavin adenine dinucleotide

FADH$_2$ – reduced flavin adenine dinucleotide

FCCP - Carbonyl cyanide-4-phenylhydrazone

FDA - Food and Drug Administration

GNPS - Global Natural Products Social Molecular Networking program

GO - Gene Ontology

GSEA – Gene Set Enrichment Analysis

GSH - reduced glutathione

HMOX-1 - heme oxygenase-1

HO - hoechst

HPLC – high performance liquid chromatography

HR-LC–MS/MS - high -resolution liquid chromatography coupled with MS-MS

IC$_{50}$ - maximal inhibitory concentration~

LC/MS – liquid chromatography / mass spectrometry

LC$_{50}$ - median lethal dose

LDH - lactate dehydrogenase

LEGE CC - LEGE Culture Collection

MALDI-TOF/TOF - matrix-assisted laser desorption/ionization time-of-flight mass spectrometer

MDC - monodansylcadaverine

MeCN - Acetonitrile

MeOH - Methanol

MSC - multicellular spheroid cultures**MTS** - multicellular spheroids

MTT - 3-(4,5-dimethylthiazol-2-yl)-2,5-diphenyltetrazolium bromide

NAD$^+$ - nicotinamide adenine dinucleotide

NADH – reduced nicotinamide adenine dinucleotide

FCUP xxiv
Cyanobacterial bioactive metabolites for anticancer drug
discovery: characterization of new compounds and
molecular mechanisms in physiologically relevant 3D cell
culture

NADPH – reduced nicotinamide adenine dinucleotide phosphate

NocA – nocuolin a

Nrf2 - Nuclear factor erythroid 2-related factor 2

NRPS - nonribosomal peptide

OXPHOS - oxidative phosphorylation

PAB – portoamides A and B

PARP - poly (ADP-ribose) polymerase

PI – propidium iodide

PINK1 - PTEN-induced putative kinase 1

PKS - polyketide synthases

PPP - pentose phosphate pathway

PRDX4 - peroxiredoxin- 4

PRDX6 - peroredoxin-6

RiPP - ribosomally synthesized and post-translationally modified peptide

RNA - ribonucleic acid

ROS – reactive oxidative species

TALDO – transaldolase

TCA - tricarboxylic acid

TLC - thin Layer Chromatography

TMRE - tetramethylrhodamine, ethyl ester

t-RNA - Transfer ribonucleic acid

UV – ultraviolet

FCUP | 1
Cyanobacterial bioactive metabolites for anticancer drug
discovery: characterization of new compounds and
molecular mechanisms in physiologically relevant 3D cell
culture

INTRODUCTION

1. Natural compounds

Since the 60's decade of the past century, several natural compounds, semi-synthetic compounds or synthetic compounds inspired in nature were discovered or developed and are nowadays used in anticancer therapeutics[1]. Plants and animals are historically the major sources of natural products[2]. Regarding anticancer treatment, from 1940s until 2014, 49% of the approved drugs are either natural products or natural products derivatives[3]. Vinca alkaloids were the first famous group of anticancer compounds isolated or derived from a viny ornamental plants, being Vinblastine, an inhibitor of microtubules polymerization, approved in 1961 by FDA for cancer treatment[1]. This compound was also particularly important since it unveiled a new mode of action of anticancer compounds, namely the inhibition of microtubule polymerization, causing defects on chromosome segregation and consequent cell death[4].

Another famous example of a natural anticancer compound is Paclitaxel (taxol), extracted from the yew *Taxus brevifolia*. It was discovered in 1967, its mechanism of action (inhibition of breakdown on fiber microtubules) elucidated in 1979[5] and approved by FDA in 1992, being currently one of the mostly administrated anticancer compounds in the world[1]. After this, other improved derivatives of taxol appeared, such as Docetaxel, in 1989, and Cabazitaxel in 2000[1]. In 1984, it was discovered that Etoposide and Teniposide, two derivatives of Podophyllotoxins, supress Topoisomerase II, a protein responsible to overwinding or underwinding DNA during replication[6]. Camptothecins were described in 1985 as potential anticancer compounds that act on Topoisomerase I, another enzyme responsible for the regulation of DNA structure[7]. Approved by FDA in 2012 for the treatment of chronic myeloid leukemia, Homorringtonine (HHT) is an alkaloid extracted from the yew *Cephaoltaxus harringtonia*, which binds to the A-receptor of the subunit 60S of the ribosome and consequently blocks the biding of t-RNA and the correct translation of proteins on cancer cells[8].

These above-mentioned examples refer to compounds that were isolated from superior eukaryotes, namely plants. However, the microbial world is an immense ocean of opportunities, regarding the exploration of new compounds and new modes of action. Ixabepilone was inspired on compounds isolated from the culture medium of *Sorangium cellulosum*, in 1995 (Epothilone A and B), and acts similarly to paclitaxel, but has cytotoxicity on paclitaxel resistant cells[1]. Notwithstanding of the definition of antibiotics as compounds that kill bacteria, compounds such as Actinomycin D[9], Bleomycin[10] or

FCUP 4
Cyanobacterial bioactive metabolites for anticancer drug
discovery: characterization of new compounds and
molecular mechanisms in physiologically relevant 3D cell
culture

Anthracyclines (such as Doxorubicin or Daunorobicin)[11], isolated from different bacteria of the genus *Streptomyces*, are currently used in anticancer treatments because of its DNA damaging activity via several pathways, from topoisomerase inhibition or intercalation with the DNA backbone, and on different cancer types[1].

1.1. Marine origin compounds for cancer treatment

If we consider the importance of the "microbial world" on the discovery of new compounds, then the marine environment is a whole universe of potential new drug discovery[12]. Currently approved drugs with marine origin are not necessarily from microorganisms (**Table 1**). The most ancient example of a marine drug for cancer treatment is cytorabine (Cytosar-U®), which was approved in 1969 for treatment of leukaemia and was isolated from the sponge *Cryptothethya crypta*[13-14]. More recent examples are Halichrondrin B discovered in 1985, a polyether macrolide isolated from the sea sponge *Halichondria okadai*, which was further developed to Eribulin[15], and approved for treatment of breast cancer since 2010 by FDA[1, 16]. Brentuximab Vedotin (Adcetris®)[17-19] approved in 2011, was the first compound inspired in cyanobacteria, since it is antibody conjugated [20] for the treatment of anaplastic large T-cell systemic malignant lymphoma in Hodgkin's disease. Trabectedin (Yondelis ®)[21] approved in 2015 for soft tissue sarcoma and ovarian cancer treatment was initially isolated from the tunicate *Ecteinascidia turbinate* but later suggested to be produced by the marine bacterial symbiont *Candidatus Endoecteinascidia frumentensis*[22]. The most recent approved compound (not ADC) from marine origin is Plitidepsin (Aplidin®), isolated from the Tunicate *Aplidium albicans*[23], approved in 2018 in Australia for treatment of multiple myeloma, leukemia and lymphoma.

Table 1 – Currently approved marine drugs for cancer therapies. * FDA Years Approved ** Australia Dec 2018 Approved. Adapted from Mayer, A. Marine Pharmaceutical: The Clinical Pipeline. Available online: http://marinepharmacology.midwestern.edu/clinical_pipeline.html (accessed 20 October 2019).

Compound name	Trademark	Marine organism	Chemical class	Molecular target	Cancer treatment	Company
Polatuzumab vedotin (DC DS-4501A)	Polivy TM (2019)*	Mollusk/ cyanobacteria	ADC (MMAE)	CD79b & microtubules	Non-Hodgkin lymphoma, Chronic lymphocytic leukemia, Lymphoma B-Cell, Follicular lymphoma	Roche Genentech
Plitidepsin	Aplidin® (2018)**	Tunicate	Depsipeptide	eEF1A2	Multiple myeloma, leukemia lymphoma	PharmaMar
Trabectedin (ET-743)	Yondelis® (2015)*	Tunicate/ proteobacteria	Alkaloid	Minor groove of DNA	Soft tissue sarcoma, Ovarian cancer	PharmaMar
Brentuximab vedotin (SGN-35)	Adcetris® (2011)*	Mollusk/ cyanobacteria	ADC (MMAE)	CD30 & microtubules	Anaplastic large T-cell systemic maglinant lymphoma, Hodgkin's disease	SeattleGenetics
Eribulin Mesylate (E7389)	Halaven® (2010)*	Sponge	Macrolide	Microtubules	Metastatic breast cancer	Eisai
Cytarabine (Ara-C)	Cytosar-U® (1969)*	Sponge	Nucleoside	DNA polymerase	Leukemia	Pfizer

1.2. Cyanobacteria as a source of natural compounds

As previously referred, Brentuximab vedotin was the first compound (as an antibody drug conjugate) approved for clinical use, that has a cyanobacterial origin. If we carefully

analyse the marine pipeline on clinical trials (**Table 2**), compounds isolated from cyanobacteria symbionts appear as the next generation of marine origin compounds; all of them are conjugated with antibodies, in order to target the cancer cells[20, 24]. **Table 2** presented below summarises the list of cyanobacterial derived drugs currently undergoing clinical trials. It is clearly visible that there are a variety of companies that are involved on clinical trials with cyanobacterial compounds and are interested to develop these new drugs to the market.

FCUP 7

Cyanobacterial bioactive metabolites for anticancer drug discovery: characterization of new compounds and molecular mechanisms in physiologically relevant 3D cell culture

Table 2 – Cyanobacterial derived drugs for cancer treatment on the different phases of clinical trials. Adapted from Mayer, A. Marine Pharmaceutical: The Clinical Pipeline. Available online: http://marinepharmacology.midwestern.edu/clinical_pipeline.html (accessed 20 October 2019).

Compound Name	Marine Organism	Chemical Class	MolecularTarget	Cancer treatment	Company
PHASE III CLINICAL STATUS					
Enfortumab Vedotin	Mollusk/ cyanobacterium	ADC (MMAE)	Nectin-4 & microtubules	Tumors Neoplasms Metastatic urothelial cancer	SeattleGenetics
PHASE II CLINICAL STATUS					
AGS-16C3F	Mollusk/cyanobacterium	ADC (MMAF)	ENPP3 & microtubules	Renal cell carcinoma	Agensys astellas Leading Light for Life
Tisotumab Vedotin	Mollusk/ cyanobacterium	ADC (MMAE)	Tissue Factor & microtubules	Ovary cancer Cervix cancer Endometrium cancer Bladder cancer Prostate cancer (CRPC) Cancer of head and neck (SCCHN) Esophagus cancer Lung cancer (NSCLC)	Genmab
GSK2857916	Mollusk/ cyanobacterium	ADC (MMAF)	BCMA	Multiple myeloma	gsk GlaxoSmithKline
Ladiratuzumab vedotin (SGN-LIV1A)	Mollusk/cyanobacterium	ADC (MMAE)	LIV-1 & microtubules	Breast cancer	SeattleGenetics

FCUP | 8
Cyanobacterial bioactive metabolites for anticancer drug
discovery: characterization of new compounds and
molecular mechanisms in physiologically relevant 3D cell
culture

Telisotuzumab vedotin (ABBV-399)	Mollusk/ cyanobacterium	ADC (MMAE)	c-Met	Solid tumors	abbvie
Pinatuzumab vedotin	Mollusk/ cyanobacterium	ADC (MMAE)	CD22	Follicular Lymphoma Diffuse large B-Cell lymphoma	Genentech
Enapotamab vedotin (HuMax-AXL)	Mollusk/ cyanobacterium	ADC (MMAE)	Axl RTK	Ovarian cancer Cervical cancer Endometrial cancer	Genmab
RC-48	Mollusk/ cyanobacterium	ADC (MMAE)	HER2	Urothelial carcinoma Advanced cancer Gastric Cancer HER2 Overexpressing Gastric Carcinoma Advanced breast cancer Solid tumors	RemeGen
CAB-ROR2 (BA-3021)	Mollusk/ cyanobacterium	ADC (MMAE)	ROR2	Solid Tumor Non Small Cell Lung Cancer, Triple Negative Breast Cancer Soft Tissue Sarcoma	bicatla
CX-2029	Mollusk/ cyanobacterium	ADC (MMAE)	CD71	Solid Tumor Head and Neck Cancer Non Small Cell Lung Cancer Pancreatic Cancer Diffuse Large B Cell Lymphoma	abbvie CytomX

W0101	Mollusk/ cyanobacterium	ADC (MMAE)	IGF-R1	Advanced or Metastatic Solid Tumors	
PHASE I CLINICAL STATUS					
ABBV-085	Mollusk/ cyanobacterium	ADC (MMAE)	LRRC15	Solid tumors	
ASG-67E	Mollusk/ cyanobacterium	ADC (MMAE)	CD37 & microtubules	Refractory Lymphoid Malignancy Relapsed Lymphoid Malignancy	
ASG-15ME	Mollusk/ cyanobacterium	ADC (MMAE)	SLITRK6 & microtubules	Metastatic Urothelial Cancer	
ARX-788	Mollusk/ cyanobacterium	ADC (MMAE)	HER2 & microtubules	Breast Cancer, Gastric Cancer	
SGN-CD48A	Mollusk/ cyanobacterium	ADC (MMAE)	CD48 & microtubules	Multiple Myeloma	
XMT-1536	Mollusk/ cyanobacterium	ADC (Dolaflexin)	NaPi2b & microtubules	Solid tumors	
ALT-P7	Mollusk/ cyanobacterium	ADC (MMAE)	HER2 & microtubules	Breast cancer Gastric cancer	
PF-06804103	Mollusk/cyanobacterium	ADC (Auristatin variant)	HER2	Breast Neoplasms Stomach Neoplasms Esophagogastric Junction Neoplasm Carcinoma Non-small-cell Lung	
ZW-49	Mollusk/cyanobacterium	ADC (Auristatin variant)	HER2	HER2-expressing Cancers	

U. PORTO
FACULDADE DE CIÊNCIAS
UNIVERSIDADE DO PORTO

FCUP 10
Cyanobacterial bioactive metabolites for anticancer drug discovery: characterization of new compounds and molecular mechanisms in physiologically relevant 3D cell culture

Cyanobacteria are carbon-fixing, gram negative photosynthetic prokaryotic organisms that ubiquitously inhabit Earth and have an oxygenic photosynthetic system responsible for the original primitive oxygenic atmosphere[25]. They have an internal system of membranes responsible for both photosynthetic electron transport and respiration. Their morphology varies from unicellular to filamentous species, and they can live either in colonial communities or as free-living system[26-28]. On the recent years, several works cite cyanobacteria as a potential source for new compounds with different applications[29], from UVR-protective metabolites to nutraceuticals of food supplements[28, 30-31], from an alternative source of energy[32] to bioplastics[33] and antifouling properties on paints[34], from antimalarial[35], antimicrobial[36] to anticancer drugs[37-40]. The capacity to produce diverse secondary metabolites is one of the reasons for the long survival of these organisms in Earth's history. These organisms encode in their DNA for non-ribosomal synthetases (NRPSs), polyketide synthases (PKSs)[25, 41-42] and ribosomally synthesized and post translationally modified peptides (RiPPs)[43], which make them particularly prolific producers of secondary metabolites. The analysis of cyanobacterial genomes regarding these clusters of genes opened a window for the search of new compounds, but also for the discovery of new enzymes[44] that could help in the biosynthesis of new compounds.

Examples of successfully anticancer compounds originated from cyanobacteria were already described before, as the example of Brentuximab vedotin, but some other have also been isolated along the years, such as Apratoxin D[45] or Symplocamide A[46] that have been proven to have cytotoxic effects on cells. Frequently, these new compounds have their bioactivity assessed by viability assays, but their specific mechanisms of action unknown[47]. Moreover, their cytotoxic effects are assessed on cancer cell lines growing in monolayers and after this, they go for animal testing, without an intermediate step, sucha as the usage of *in vitro* 3D advanced model testing[48]. It is estimated that 85% of the preclinical anticancer agents fail throughout the clinical trials pipeline because of the current preclinical models do not replicate the diversity of the tumour biology[49]. Either from high toxicity rates not previously accessed[50], lack of safety or efficacy[51], several issues may contribute to this failure and the usage of more complex *in vitro* models that better represent the *in vivo* tumour have been described as one way to successfully put a new drug on the market[52-54].

The LEGE Culture collection – LEGE CC (http://lege.ciimar.up.pt/) is a collection of microorganisms at the Laboratory of Blue Biotechnology and Ecotoxicology (BBE),

FCUP 11
Cyanobacterial bioactive metabolites for anticancer drug
discovery: characterization of new compounds and
molecular mechanisms in physiologically relevant 3D cell
culture

University of Porto that hosts more than 1000 strains of cyanobacteria and microalgae (updated number) from different environments[55], several of them unique among the (phylogenetic) diversity of the group. The strains were isolated mainly from the Portuguese coast but also from other locations around the world, such as Morocco, Australia, Brazil, Dominican Republic and Cabo Verde. In the last decade there were several compounds that were isolated from this collection by our working group: nocuolin A, portoamides, hierridins and bartolosides.

1.2.1. Nocuolin A

Nocuolin A was firstly isolated and chemically characterized by Voráčová[56], reported as the first natural compound with an azole ring with N-N-O linkage (**Figure 1**). It was isolated from the strain *Nostoc* sp. CCAP 1453/38, although it was further identified on two more genera (*Nodularia* sp. and *Anabaena* sp.) and the biosynthetic mechanism was proposed. Voráčová reported apoptotic effects on HeLa cell line cultured in monolayer and cytotoxic effects on other cancer cell lines. Additionally, in a bioassay-guided fractionation approach in the BBE laboratory at CIIMAR, nocuolin A was also isolated from *Nodularia* sp. LEGE 06071, a filamentous cyanobacteria from the Nostocales Order, collected in Vouga estuary, Ria de Aveiro, Portugal (http://lege.ciimar.up.pt/culture/*Nodularia*-sp-lege-06071/)[37] due to their strong cytotoxic activity. Methanolic extracts of this cyanobacteria strain were previously known to be toxic against *Artemia salina* nauplii (LC_{50} of 17.81 mg mL^{-1}) and inducing morphological alterations on the development of *Paracentrotus lividus* pluteus larva (lower length and abnormal development of the larvae at the three tested concentrations 6.25 mg ml^{-1} , 3.12 mg ml^{-1} and 1.56 mg ml^{-1})[57], being the Nostocales order previously reported as a promising considering secondary metabolites isolation[58].
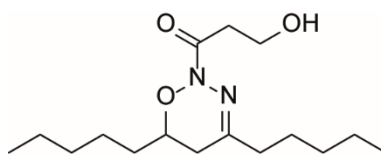
Figure 1- Nocuolin A chemical structure.

1.2.2. Portoamides A and B

U.PORTO
FACULDADE DE CIÊNCIAS
UNIVERSIDADE DO PORTO

FCUP 12
Cyanobacterial bioactive metabolites for anticancer drug
discovery: characterization of new compounds and
molecular mechanisms in physiologically relevant 3D cell
culture

Portoamides are a group of cyclic peptides isolated from the cyanobacterial strain *Phormidium* sp. LEGE 05202 (previously *Oscillatoria* sp. LEGE 05292). From this group of compounds four analogues were found (A, B, C and D), however, only portoamides A and B (**Figure 2**) revealed bioactive properties, namely the allelopathic effects against *Chlorella vulgaris* and cytotoxic effects against the lung cancer cell line H460[59]. A recent paper revealed that a mixture of portoamides A and B have antifouling properties against *Mytilus galloprovincialis* larvae[34].
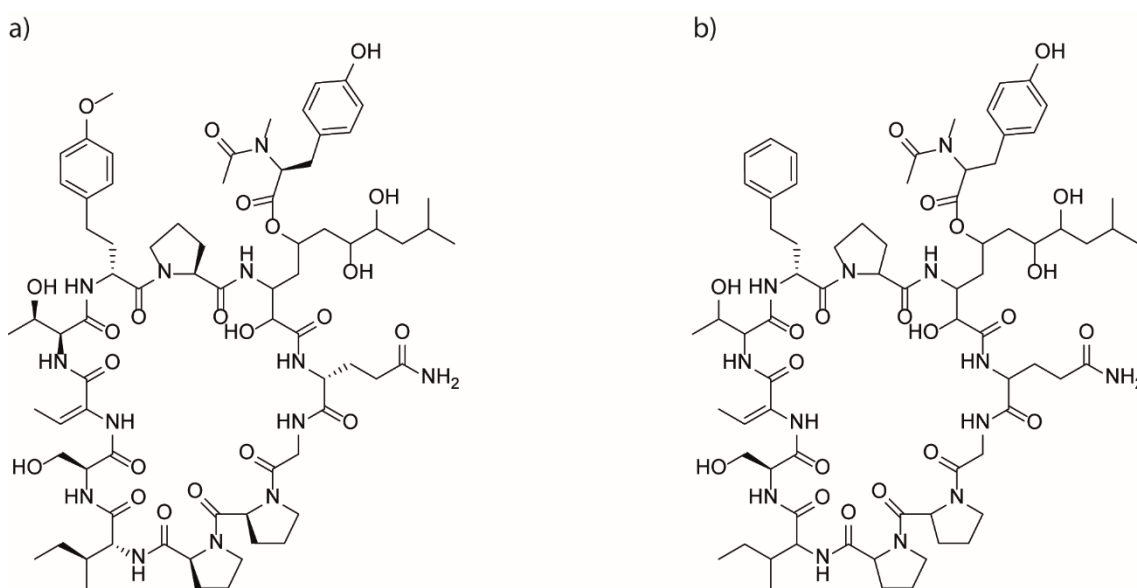
Figure 2- Structure of a) portoamides A; b) portoamides B.

1.2.3. Hierridins

Hierridins are a group of simple alkylresorcinols that were reported firstly in 1992, isolated from the lichen *Ramalina hierrensis*. In 1998 hierridin B was isolated from the cyanobacteria *Phormidium ectocarpi* strain SAG 60.90 and exhibit antiplasmodial activity[60-61]. Only in 2013, hierridin B and its homolog hierridin C (**Figure 3**) were discovered from the picocyanobacterium *Cyanobium* sp. LEGE 06113[35, 62], collected from the Portuguese Atlantic coast.
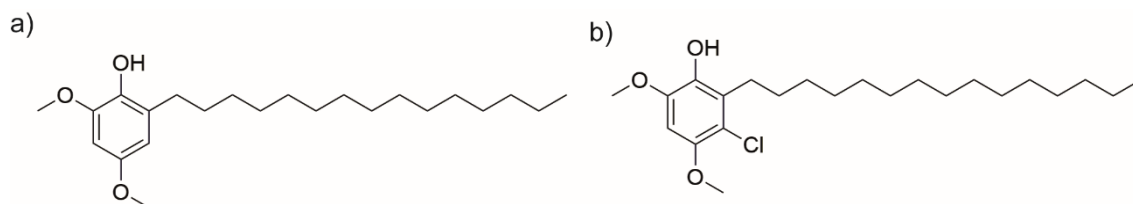
Figure 3 –Chemical structure of a) hierridin B. b) hierridin C.

The cytotoxic activity of hierridin B was assessed on a panel of cancer cell lines (hepatocellular carcinoma (HepG2), colon adenocarcinoma (HT-29), osteosarcoma (MG63), colon adenocarcinoma (RKO), neuroblastoma (SHSY5Y), breast adenocarcinoma (SKBR3), breast ductal carcinoma (T47D)) and on a normal prostate epithelium cell line (PNT2). However, cytotoxicity was exclusively observed on the HT-29 colon adenocarcinoma cell line with an IC_{50} of 100.2 µM[62]. The exploration of its mode of action suggested that hierridin B reduced strongly the mitochondrial activity, and induced a cell cycle arrest, which led finally to cell death. Furthermore, an effect was observed on VDAC1 protein expression, which might disturb the formation of mitochondrial channels[63]. Hierridin C did not reveal any cytotoxicity against the cell lines tested (MG-63, HepG2, HT-29, SH-SY5Y, RKO, T47D, colon adenocarcinoma (CaCo2) and PNT2) however, its antiplasmodial activity was more potent in comparison to its homolog (hierridin C IC_{50} 1.5 ± 0.1µM against 3D7 strain of *Plasmodium falciparum* and IC50 2.3 ± 0.7µM against Dd2 strain and hierridin B IC_{50} 2.1 ± 0.1µM against 3D7 strain and IC50 2.3 ± 0.1µM against Dd2 strain)[35, 64].

1.2.4. Bartolosides

A group of four bartolosides (A, B C and D), which belong also to the chemical class of alkylresorcinols, but that have two alkyl chains[65] (**Figure 4**), were originally isolated from two phylogenetically distant cyanobacteria *Nodosilinea nodulosa* LEGE 06102 and *Synechocystis salina* LEGE 06155. Bartoloside A had an IC_{50} of 21 µM against the colon adenocarcinoma cell line HT-29 and no cytotoxic effects were detected on SH-SY5Y, T47D, PC-3, RKO, HepG2 and MG-63 cell lines. Bartoloside B had an IC_{50} of 9.5 µM against the PC-3 and for the remaining previous list of cell lines the cytotoxicity was always higher than 12.5 µM. Bartoloside C and D had no cytotoxic effects[66].
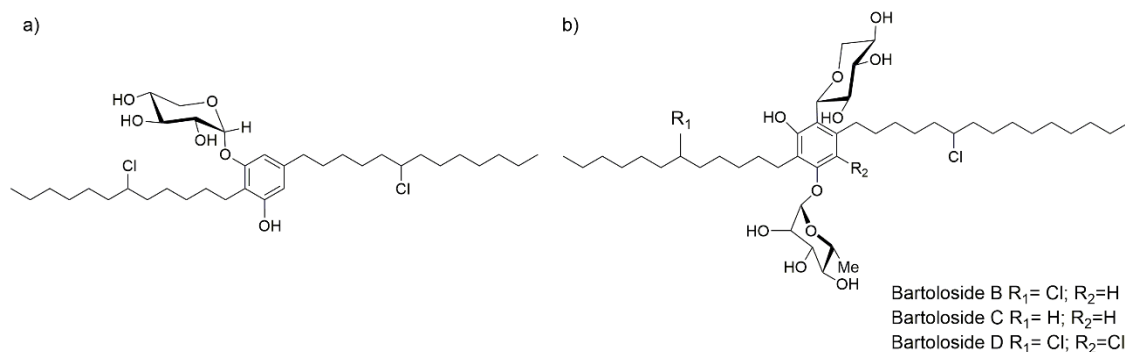
Figure 4 - Chemical structures of a) bartoloside A. b) bartoloside B, C and D skeleton.

Later, seven homologues of bartoloside A were isolated from the strain *Synechocystis salina* LEGE 06099 and their biological activity was assessed against several cancer cell lines, but no relevant cytotoxicity was observed ($IC_{50} > 20\mu M$)[67].

2. Cancer

There is no clear status about the incidence of cancer in plants or invertebrates, both because these organisms often have short lifetimes or difficulties on the characterization of tissue masses as cancer occurred[68-69], even though genetic alterations, namely in *Drosophila melanogaster* are reported of great importance to study cancer development[70]. Yet, cancer has been reported throughout the spectrum of vertebrates from the simplest such as lampreys[71] to humans. Additionally, cancer neither seems to be a recent problem, since the first records of neoplasms were recorded from the Devonian period (350 million years ago) on a fossil of the fish *Phanerosteon mirabile*[71-72]. The first diagnose of cancer on human dates from 1300-1500 BC in the Ancient Egypt based on the manuscripts discovered by Edwin Smith and George Ebers[73]. Among the description of cancers and the recognition of the lack of pharmacological treatment, some surgical procedures are mentioned as the solution for the disease. Among the Ancient Greek, Hippocrates, the father of medicine, introduced the term "karcinos" (to describe ulcerating and non-healing lumps) that evolves to the word "Cancer"[73].

Nowadays, according to the World Health Organization, cancer is the first or second leading cause of death worldwide before the age of 70 (**Figure 5**), with a particular incidence on developed countries[74].

FCUP 15
Cyanobacterial bioactive metabolites for anticancer drug
discovery: characterization of new compounds and
molecular mechanisms in physiologically relevant 3D cell
culture
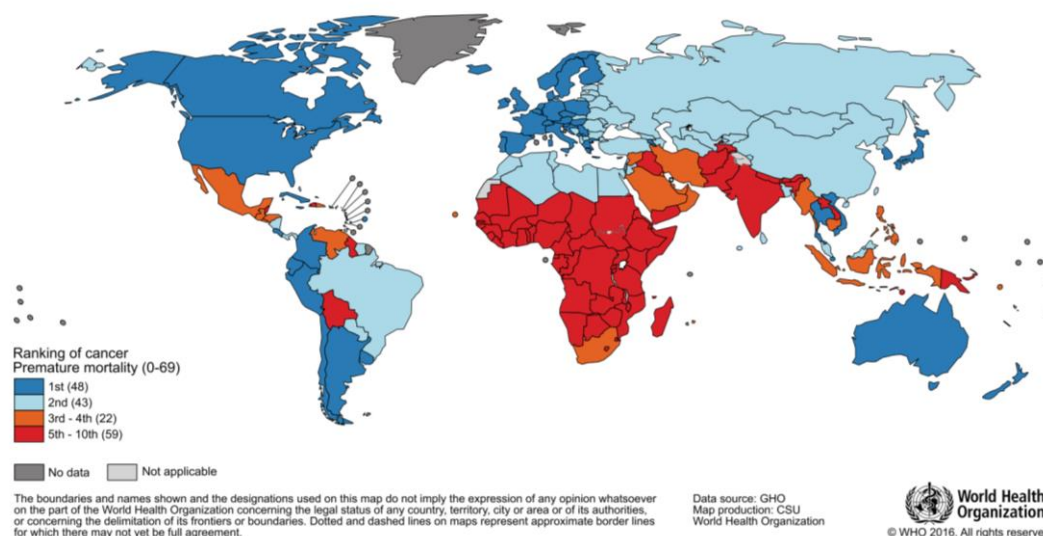
Figure 5 - Global Map represent the National Ranking of Cancer as a Cause of Death at Ages Below 70 Years in 2015. The numbers of countries represented in each ranking group are included in the legend. Source: World Health Organization[74].

In the United States alone, almost 2 million of new cases of cancer and more than 500 000 cancer deaths in 2019[75]. In Europe, the incidence of new cancers predicted for 2018 was over 4 million and the predicted cancer-related deaths could almost reach 2 million, representing 20% of cancer deaths worldwide (**Figure 6**).
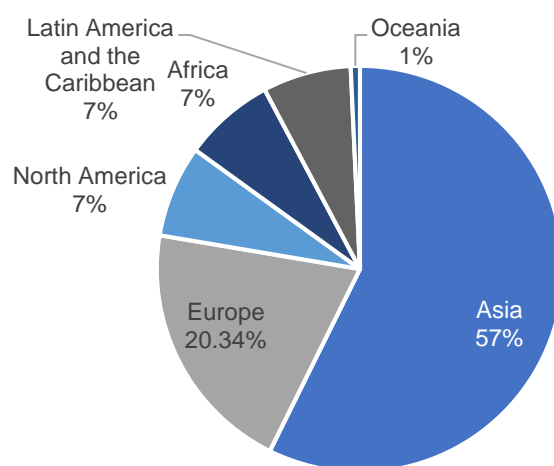
Figure 6 - Estimated age-standardized (ASR) mortality rates worldwide in 2018, for both sexes, all ages. Data source: GLOBOCAN 2018 (http://gco.iarc.fr).

In Portugal, the cancer with highest incidence is breast cancer, however the most mortal cancer is lung cancer with survival rates of around 15% (**Figure 7**).

FCUP 16
Cyanobacterial bioactive metabolites for anticancer drug
discovery: characterization of new compounds and
molecular mechanisms in physiologically relevant 3D cell
culture
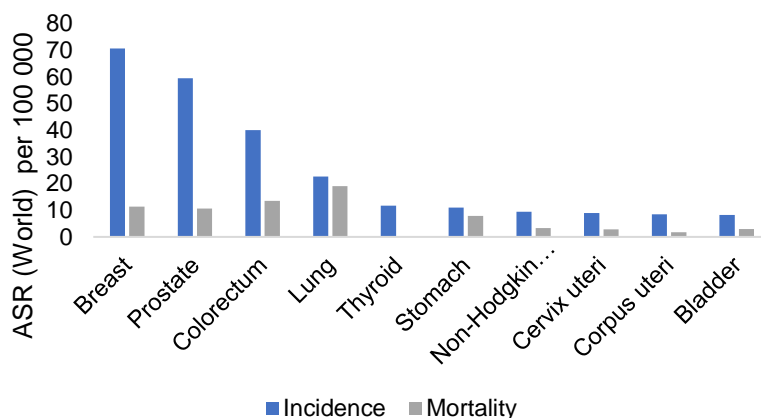
Figure 7 - Estimated age-standardized (ASR) incidence (blue) and mortality (gray) rates (World) in 2018, Portugal, both sexes, all ages. Data source: GLOBOCAN 2018 (http://gco.iarc.fr).

Cancer is considered a complex disease where cells abnormally divide out of control frequently invading nearby tissues[76]. This characteristic results from the dynamics changes of the cell genome which often leads to mutations, overexpression of oncogenes and inhibition of tumour suppression genes. These genomic alterations lead to dysregulation of proteins and signalling pathways translating into to a self-sufficiency proliferative signalling of the cancer cells accompanied with dysregulation of cellular energetics. These cells also show insensitivity to anti-growth signalling that often become unrecognizable to the immune system, avoiding this way their destruction. Cancer cells endow genetic instability and high mutation rates which results on the increasing resistance to cell death with limitless replicative potential, capacity to induce angiogenesis and opportunistic advantage over pro-inflammatory response of the immune system to growth and invade, finally resulting in metastasis[77-78].

The localization of cancers does not define the type of cancer *per se* but rather the type of cell from which it develops. Citing the National Cancer Institute dictionary of cancer terms (https://www.cancer.gov/), Carcinoma is a cancer that begins on skin or epithelial cells (tissue that covers internal organs); Sarcoma is a cancer that origins on bone, cartilage, fat or other connective tissue or supportive tissue, but also on muscle and blood vessels; Leukaemia starts in blood-forming tissue, such as bone narrow; Lymphoma and multiple myeloma are cancers related with abnormal cells of the immune system; central nervous system cancers are cancers that begin on brain and spinal cord tissues.

FCUP 17
Cyanobacterial bioactive metabolites for anticancer drug
discovery: characterization of new compounds and
molecular mechanisms in physiologically relevant 3D cell
culture

2.1. Cancer metabolism

As briefly referred before, cancer cells accumulate genomic mutations that lead to significant alterations in their metabolism and confers them characteristics such as high survival rates and indefinite proliferation in comparison to normal tissue cells. These metabolic reprogramming on tumour tissues are the hallmarks of cancer success[78] and include deregulated uptake of glucose and amino acids, the usage of different modes of nutrient acquisition, NADPH production based on glycolysis/ tricarboxylic acid cycle (TCA) intermediates, alterations in metabolite-driven gene regulation, increasing demand for nitrogen, and metabolic interactions within the microenvironment[79-80].

The two main sources of carbon in cells are glucose and glutamine, and only with these carbon sources the cancer cells are capable to assemble new macromolecules, necessary for growth and proliferation. Glucose and glutamine oxidation allow the cells to reduce NAD^+ and $FADH^+$ to NADH and $FADH_2$, which intermediate the electron transfer to the electron transport chain in mitochondria (OXPHOS) and generate the cell energy form ATP (**Figure 8**). Otto Warburg described an increasing consumption of glucose in tumours in comparison to non-proliferating cells[81]. This reprogramming of a metabolic pathway describes the switch of cancer cells to aerobic glycolysis (which in healthy cells should only be increased under hypoxia - "Pasteur effect"[82-83]), producing lactate and the glycolytic intermediates that are further used by proliferative cells on anabolic processes[84]. In addition to this up-regulation of glycolysis, glutaminolysis is also find increased, being glutamate also a carbon source for TCA and yet its metabolites serve as building blocks for *de novo* biosynthesis of macromolecules[85-86] necessary for cell proliferation, as purines or pyrimidines, as well as non-essential amino acids.
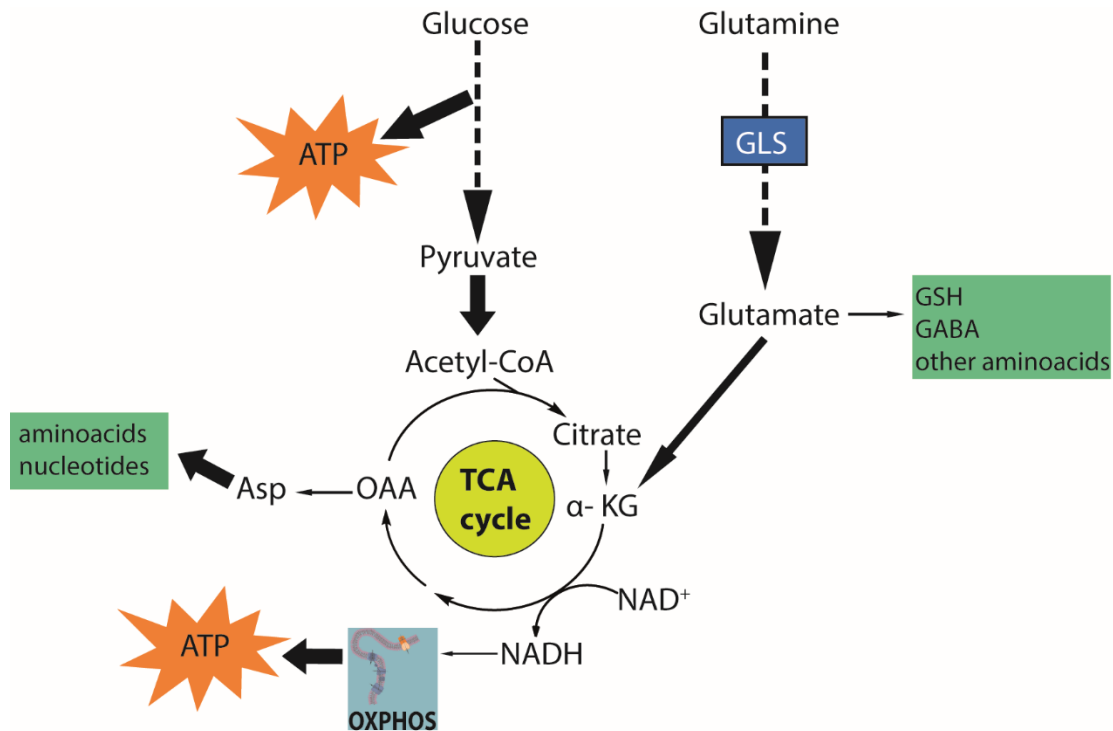
Figure 8 - Interconnection between glucose metabolism and glutamine metabolism. ATP – adenosine triphosphate; GLS – glutaminase; TCA cycle – tricarboxylic acid cycle; ETC – electron transport chain; OAA- oxaloacetate; Asp, aspartate; α- KG, α-ketoglutarate; GSH - glutathione; GABA- γ-Aminobutyric acid.

In this sense, glycolysis it is not increased in order to produce ATP in cancer cells, but rather to support macromolecular synthesis. In fact, several works showed that ATP is not limiting for cell growth, but necessary for maintenance of cell homeostasis on proliferating cells[84, 87], such as redox control. Otto Warburg erroneously concluded that mitochondria activity and aerobic glycolysis was disrupted in cancer cells, and these would confer them a higher resistance[83, 88]. Later on, and in accordance to the role of glycolysis as a supporter of biosynthesis rather than ATP producer, it was shown that cancer cells rely on functional mitochondria and OXPHOS in order obtain their higher energy requirements[89]. For each molecule of glucose, glycolysis produces 2 ATP molecules while from two pyruvate molecule (OXPHOS fuel, direct product of glycolysis), the OXPHOS yields 26 ATP molecules[90].

2.2. Tumour microenvironment

The resilience of cancer cells is a result not only of the metabolic reprogramming, but also from organization of these cells in aggregates or tumours, which give to these structures resistance to chemotherapy[91-92].

FCUP | 19
Cyanobacterial bioactive metabolites for anticancer drug
discovery: characterization of new compounds and
molecular mechanisms in physiologically relevant 3D cell
culture

On a normal tissue, almost all cells are connected by the extracellular matrix within a small distance from a blood vessel, and in this condition, it has easy access to oxygen, nutrients, metabolites, growth factors. On a tumour, cancer cells have often higher rates of proliferation, and grow more rapidly than the blood capillaries, and as a result, tumours can have areas with low vascularization[92]. Distance between cancer cells and blood stream (>100μm)[91] are the reasons why drugs often do not equally penetrate the tumours. Cell-cell interactions and adhesion[93] are also reason for tumour resistance. The microenvironment within the tumour differs from normal cells: cells in tumours experience hypoxia, extracellular acidosis, nutrient deprivation and suffer metabolic changes, which often interfere with the efficiency of anticancer treatment[91, 94-99].

2.2.1. Tumour vasculature

Tumour vasculature plays an important role regarding the efficacy of anticancer treatments. Often, tumours have poor and disorganized distribution of blood capillaries, which in addition can be structurally abnormal, tortuous and dilated, with uneven diameter and excessive branches and shunts[100-102]. These deformities have effects on blood flow and fluid pressure, leading to the unequal distribution of oxygen[103-104], nutrients and lack of metabolites exchange[80, 83, 91, 96]. The same way, in chemotherapy drugs fails to reach all the tumour regions efficiently[91, 96, 105].

2.2.2. Hypoxia, acidosis and nutrient deprivation

The deficient vascularization creates areas in tumours, where cells are under hypoxic conditions. However, cancer cells demand higher amounts of oxygen in order to proliferate in comparison to normal cells. In hypoxic conditions, cancer cells arrest their growth under the stimulation of HIF-1α, which is dependent on p53 induction[106]. Among the consequences of hypoxia and HIF family induction are the induction of vascularization[100, 107-108] and recruitment of fibroblasts to cancer-associated fibroblasts, supporting in this manner the metastasis formation[109].

With the metabolic switch towards glycolysis in cancer cells there is an accumulation of reductive agents, such as pyruvate, glutathione (GSH) that inhibits mitochondria respiration chain, leading to a hypoxic and reduced cellular environment[80, 110]. Moreover, the increasing amounts of lactate as glycolytic product, results in an interstitial acidification, which leads to tumour promotion, formation of cell clusters and cell migration[80, 94-95]. Beyond the correlation of the accumulation of lactate in tumours and the incidence of evasive metastasis[111-112] there is also the concern about the effectiveness

FCUP 20
Cyanobacterial bioactive metabolites for anticancer drug
discovery: characterization of new compounds and
molecular mechanisms in physiologically relevant 3D cell
culture

of drugs under acidic conditions[98], because they are usually studied under physiological pH (≈7.4). Some studies showed already that despite some drugs might actually have a better effect on an acidic environment[113], some others might be ineffective, unless they are at neutral pH[114].

The inefficacy of nutrient diffusion in tumours[115] allows these cells to acquire new programming of metabolic pathways in order to overcome nutrient deprivation and keep proliferating[116-117]. Contradicting Warburg effect that firstly considered that mitochondria would be impaired in cancer cells[81, 83, 88, 118], glucose absence induces p53 activation that will regulate a re-structuring of mitochondria oxidative phosphorylation chain in order to use another sources, such as pyruvate or glutamine, to keep producing ATP and guarantee cell viability[117, 119]. Moreover, under starvation, there is an integrated stress response that reduces the general translational processes (e.g. eIF2α phosphorylation or PERK activation) and activates the transcription of genes[120], such as asparagine synthase, which is now known as important regulator of amino acid homeostasis, anabolic metabolism and metastasis formation[121-123].

As described above, hypoxic and nutrient deprived environment triggers several responses from cells to overcome those difficulties from alteration of transcriptional and cellular signalling, as well as redox balance, imposing a pressure to the microenvironment, shaping the metabolic state of the cells, culminating in a more aggressive state of the cancer, resistant to treatment and metastatic.

3. Cancer treatment

3.1.1.   Chemotherapeutic drugs and their mechanisms

Until early 20th century, the only treatment for cancer was the fully removal of tumours. All other cancers, where surgery was not possible, were eventually lethal. Only in 1940's, the first chemotherapy trials begun with the use of nitrogen mustards to treat a patient with non-Hodgkins lymphoma and anti-folates to treat lymphoblastic lymphoma. Then, in 1955 the National Cancer Institute was founded in the United States of America, and an advent of new tests and compounds began[124] (**Figure 9**).

1942
• Nitrogen mustard is used to treat non-Hodgkin's lymphoma and induced tumour regression

1948
• Antifolates sucessfully induced remission in acute lymphoblastic leukaemia

1955
• National Chemotherapy Program starts under the National Cancer Institute

1958
• The first solid tumour is cured with chemotherapy treatment - methotrexate

1978
• FDA approves cisplatin for the treatment of ovarian cancer, a drug that would prove to have activity across a broad range of solid tumours

1972
• Cure rates were increased with the aplication of chemotherapy after surgical removal (adjuvant chemotherapy)

1965
• Combination of chemotherapics is used to treat lymphoblastic leukaemia in children

1959
• FDA approves the alkylating agent cyclophosphamide

1989
• The National Cancer Institute introduces "disease orientated" screening using 60 cell lines derived from different tumours

1992
• FDA approves Paclitaxel (Taxol) which becomes the first "blockbuster" oncology drug

2001
• FDA approves imatinib mesylate (Glivec) for chronic myelogenous leukaemia

2004
• FDA approves bevacizumab (Avastin) the first clinically proven anti-angiogenic agent for the treatment of colon cancer

Future
• Genomic editing using CRISPR/Cas9 technology?

2010
• Introduction of immune checkpoints inhibitors for the treatment of advanced and metastatic tumors

Figure 9- Chronological evolution of chemotherapy and anticancer drug discovery.

Depending on their activities against cancer cells, chemotherapeutical drugs can be considered as alkylating agents, antimetabolites, topoisomerase I and II inhibitors, mitosis inhibitors, mitochondrial inhibitors, immunotherapeutic anticancer agents, and molecular targeted anticancer agents[125].

Alkylating agents

These were the first chemotherapeutical compounds. Alkylating compounds cause DNA single-strand breaks (monofunctional agents, interacts with only one DNA base) or

causing crosslinks between the DNA strands (bifunctional agents, interacts with more than one biomolecule)[126]. This results in general DNA damage, affecting DNA, RNA and eventually protein synthesis leading to apoptosis. These effects are not specific to cancer cells, and hence affect acutely high replicating cells. Cancer cells are high proliferative cells, but also other healthy tissues, such as bone narrow, which can be irremediably affected by such treatments, and develop mechanisms of resistance to alkylating drugs[127-131].

Antimetabolites

Antimetabolite drugs are compounds that inhibit one or more enzymes impairing the normal functioning of certain metabolic pathway within the cell[132]. Antimetabolite drugs are often folic acid antagonists, pyrimidine and purine analogues. Folates metabolism is essential for synthesis of thymidine or methionine, essential for DNA or protein synthesis[133-134]. Cells are then arrested at S-phase of the cell cycle and undergo further apoptosis[132]. Folic derivatives are also used as immunosuppressants and anti-inflammatory drugs[135].

Topoisomerase I and II inhibitors

The topoisomerase I and II inhibitors are often natural compounds, isolated mainly from plants and microorganisms, and among these are antibiotics, which additionally possessed anticancer properties[1]. Topoisomerases are enzymes responsible for the over winding or under winding of DNA, and whenever they are inhibited, the DNA double strand breaks, which in turns arrests cell cycle, preventing cells to undergo mitosis[6-7, 136] with further apoptosis.

Mitosis inhibitors

Most of the known natural products belong to this group, such as vinka alkaloids or taxanes. Mitosis inhibitors can be characterized as three main types: mitotic entry drugs & spindle poisons, mitotic checkpoints inhibitors and mitotic exit inhibitors.

Mitotic entry or spindles poisons arrests cell cycle at G2 or prometaphase, eventually ending up with apoptosis[137]. Some examples of mitotic entry and spindle poisons are Vinka alkaloids, which inhibit the correct formation of microtubules, and taxanes, which stabilize microtubules avoiding their breakdown[1, 4, 138].

Mitotic checkpoints inhibitors cause aneuploidy (abnormal number of chromosomes), which can either be arrested at S1 phase or undergo cell death.

Finally, inhibiting mitotic exit the cell remains indefinitely at metaphase, eventually suffering mitotic cell death[137].

Mitochondrial inhibitors

The importance of energy balance in cancer cells was already referred above. Mitochondria play a main role on cell survival, particularly in cancer cells[139]. Although it was described before that cancer cells rewire their metabolism towards glycolysis, the fact is that hypoxic and glucose poor areas of the tumour still depend on mitochondria to produce ATP, even with very low amounts of oxygen[78-80, 89, 140]. As so, targeting mitochondrial ATP production would induce the cell death of these areas of the tumour[141-143]. A subset of tumours types was identified, which have improved reactive oxygen species detoxification and higher requirements of mitochondrial energy[144]. By limiting mitochondrial ATP production, glycolysis will not be enough to fulfil the energy requirements of these type of cells. Finally, targeting mitochondrial respiration *per se* might not be enough to eradicate a cancer, but, in synergy with glycolysis inhibitors[145-146], the outcome of such treatment can be improved.

The mitochondrial oxidative phosphorylation system (OXPHOS) is the aerobic pathway of cells to produce ATP, a process in which electrons produced by the TCA cycle are transferred down the five mitochondrial respiratory complexes: the complexes I–IV are located in the tubular membranes of mitochondrial cristae and complex V (ATP synthase) localises to cristae bends[147] (**Figure 10**).
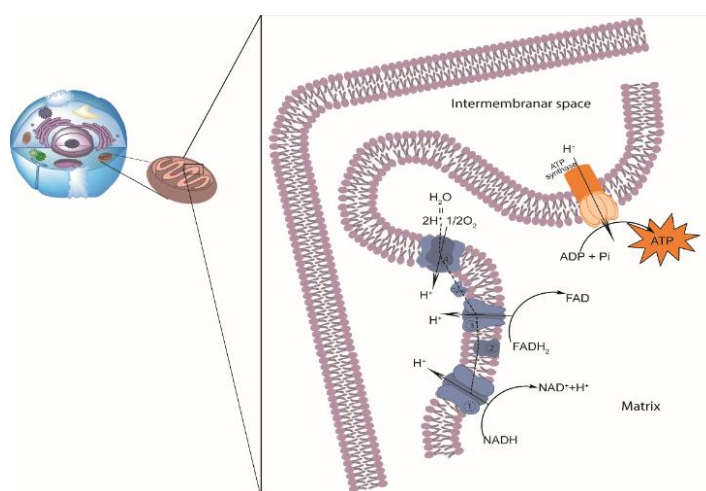
Figure 10 -The structure of electron transport chain of mitochondria. Dashed line is the electron pathway. Complexes I-IV are numbered (1-4) and complex V is ATP synthase.

FCUP 24
Cyanobacterial bioactive metabolites for anticancer drug
discovery: characterization of new compounds and
molecular mechanisms in physiologically relevant 3D cell
culture

The inhibition of any of these complexes will disrupt mitochondrial respiration and decrease the ATP production by the cell. For instance, metformin inhibits mitochondrial complex I that was originally used with diabetic patients, whereas other studies further showed anticancer effectiveness[79, 141, 145-146]. Other mechanisms of action can involve the inhibition of ROS scavengers[148-149], alteration of mitochondrial membrane polarization[150-152], inhibition of the nucleotide transporters, any targets on TCA impairing mitochondrial biosynthetic production[79, 141, 149], but also targeting other proteins whose secondary effects lie on the dysregulation of mitochondria functioning[153-156].

Immunotherapeutic anticancer agents

Immunotherapeutic drugs for treating cancer were developed in the end of the 19th century by William Bradley Coley, after observing that infecting tumours with *Streptococcus pyogenes* led to their shrinkage[157]. The conclusion was that the infection stimulated the immune system to fight not only the infection, but also the tumour. Nowadays, the usage of immune system stimulants for anticancer treatments include cytokines (interferon-α and interleukin-2), general non-specific immune system stimulation such as Bacillus Calmette-Guérin vaccine (BCG)[158-159], dendritic cells that can activate T cells (Sipuleucel-T)[160-161] or antibodies as Ipilimumab, a monoclonal antibody against cytotoxic T lymphocyte (CTLA4)[162-163] or avelumab that targets programmed cell death ligand[162, 164].

Molecular targeted therapies

The treatment of cancer suffered an evolution on the past decade, whereas the use of traditional chemotherapies (chemotherapies that act on all rapidly dividing normal and cancerous cells) was overstepped by selective therapies. Targeted therapies which works by targeting specific genes, proteins, or the tissue environment that are vital for a tumour maintenance and development, such as mitochondria respiration[142-143, 153] or proteasome deubiquitination[165-167]. However, although the target mechanism is more effective on cancer cells, general toxicity has always been an issue on the development of new cancer treatments[168]. The recent advance of combining molecular targeted therapies with a ligand target deliver, such as antibodies or substrates (folic acid, for instance)[169-171], allows small molecules with high cytotoxicity and target specificity be directed to cancer cells, reducing general toxicity. This was the strategy behind the development of the first anticancer compound derived from a cyanobacterial compound, Bretuximab vedotin[17, 20].

4. Advanced models for anticancer drug discovery

In the past decades, there has been an effort to increase the efficacy of tests and therapeutically procedures before advancing to animal testing, in particular for ethical reasons. Furthermore, there is also a need to reduce costs and time-consuming procedures on the research of new drugs. Pharmaceutical companies were the first to enhance the combination of new technologies to improve the knowledge and establish robust methods for high-throughput screening of new drugs[48, 172-173].

4.1. Multicellular spheroids

Three-dimensional culture systems (spheroids) for anticancer drugs development are a promising technique, by combining new technological approaches[97, 174-180]. Previously and still mostly used today, cell-based screening for new drugs are performed in the traditional cell culture, grown as monolayer cultures. However, frequently, compounds tested and developed in *in vitro* conditions fail in the next step of drug development, namely at animal testing stages[142, 181]. Among the systemic aspects, many of those failures are related to the form and morphology of tumours, which differs from the monolayer cells. For that reason, the use of spheroids is advantageous, since it mimics many characteristics of real solid tumours[182-185].

In 3D-culture of cancer cells systems (spheroids of cancer cells), the cells located on the periphery evidence the same active proliferative activity as the tumour cells adjacent to blood capillaries *in vivo* (**Figure 11a**). The innermost cells become quiescent and the core of the spheroid is necrotic (observable in spheroids larger than 400- 500 µm). This concentric rearrangement is similar to the morphology of *in vivo* tumours, micro metastases, avascular tumour microregions or inter-capillary tumour regions[186]. This conformation keeps up with inward gradients of nutrients and oxygenation, which is higher in the periphery and lower in the core. In contrast, the catabolites concentration decreases from the outer parts of the tumour to the inner (**Figure 11b**). These micromilieu and cellular physiological differences influence the phenotype of the cells and their sensitivity to drugs [187-188]. Another advantage of using spheroids for drug tests relies on the fact that cell-to-cell and cell-to-matrix interactions are suitable of being analysed, once they are present in this type of culture and absent in monolayer cultures. The 3D spheroid structure can also give new insights regarding both modelling of drug

delivery, pathophysiological gradients, penetration, binding and bioactivity of drugs [187-188].

a)

b)
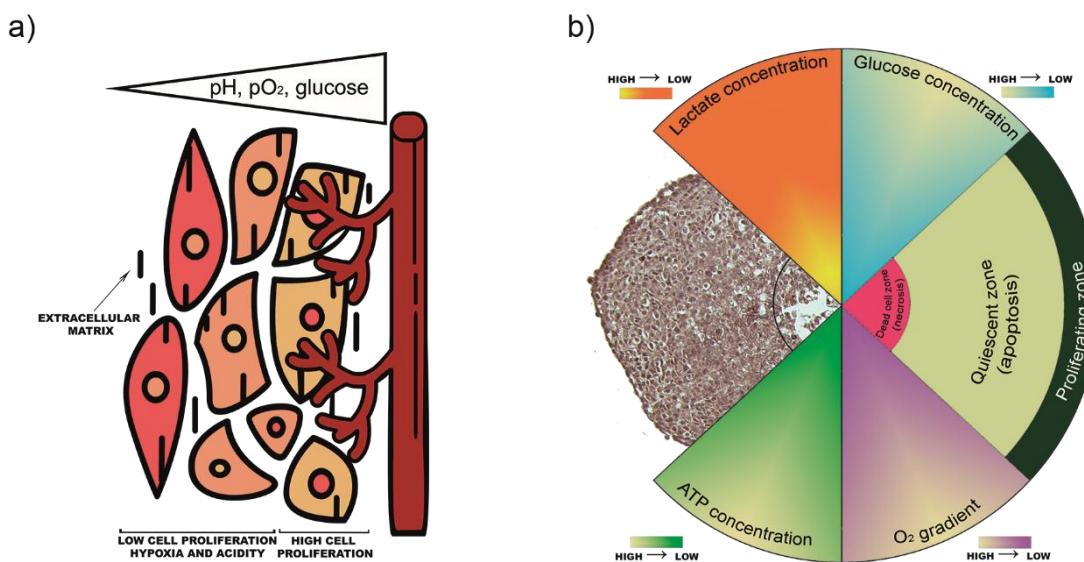
Figure 11 - Tumour microenvironment. a) Diagrammatic representation of tumour cells surrounding a capillary. b) Scheme of a spheroid morphology and physiology, with the different status of lactate, glucose, ATP and oxygen, as well as differentiation of the spheroid cell layers.

The different responses to drug exposures can be related to the location of the cells in the spheroid microenvironment. Different techniques are available to evaluate the drug response, such as viability tests, molecular markers, confocal microscopy, histological techniques, protein expression, among others.

4.2. Zebrafish embryo

Although the mouse model still is the preferential model for cancer research, it is not new that zebrafish (*Danio rerio*) has gained some visibility in the past few years[189-192]. Zebrafish indubitably emerged as an interesting model for genetics and developmental biology research in the 1960's, because of the transparent embryos that develop outside the progenitor and the high genetic conservation of vertebrates organs which allows a good comparison with humans[193-194]. Also, the production and maintenance of these animals is easy, cheap and from a pair of progenitors, hundreds of offspring eggs hatch, embryogenesis is complete at 5 days post fertilization and they keep transparency up to one month[190, 195]. Zebrafish embryos have long been used as toxicological model, and among all the reasons already mentioned above, they have the capacity to absorb chemicals through water[192, 196]. Already in 1965, it was shown that exposure of zebrafish to carcinogenic compounds resulted in the formation of tumours[197].

FCUP 27
Cyanobacterial bioactive metabolites for anticancer drug
discovery: characterization of new compounds and
molecular mechanisms in physiologically relevant 3D cell
culture

As the zebrafish full genome became available online https://www.ncbi.nlm.nih.gov/genome?term=danio%20rerio, the conservation of many genes with humans was shown, in particular genes that are essential in the development and control of diseases, such as cancer[190, 195]. Examples of these genes are tumour suppressor gene p53[198] and phosphatase and tensin homolog (pten)[199], which are crucial on the development of cancers. It became routine procedure to manipulate zebrafish genome to induce overexpression or knockdown of genes (either from zebrafish or using heterologous expression) involved in cancer progression and resistance[190, 195, 198, 200-201]. The CRISPR/Cas9 tool has also been recently applied, opening a new ocean of genetic editing on zebrafish, enhancing the possibility of mimicking human diseases and further improve the pipeline for drug discovery[202].

Another common approach are zebrafish xenographs, by injection of cancer cells, specifically marked, that produce a tumour or migrate within the animal body and are traceable under microscopy[201, 203]. As previously described, recognition of cancer diversity is one of the causes of new anti-drugs failure on clinical trials it has been recognized that profiling candidate therapeutics can increase the efficacy of chemotherapies treatments. It has been successfully employed in mice[49]; however these organisms take long to develop the tumours and the sample quantity required from the patient makes this technique hard to employ[204]. Zebrafish embryos are then suggested as an emergent model for patient-derived xenograft using tumour from primary or metastatic human cancers after collection from surgery and biopsy, not only for treatment of *in vivo* tumours profiling but also as a new strategy to speed up drug discovery[204-205]. Altogether, the benefits of using zebrafish is recognizable as a high throughput model for drug discovery, either using lethality, angiogenesis inhibitors, toxicological malformations, xenographs or specific gene mutants in order to screen chemical libraries[203, 206-207].

4.3. Stem Cells

Beside the microenvironment constrains, cancer stem cells (CSC) within the tumour exhibit high tumorigenic properties, which together with the self-renewal and differentiation capability can contribute to the resistance, metastasis[107] and relapse of cancer after chemotherapy treatment[208-209]. Since tumours can originate from normal stem cells, having similar signalling pathways and similar self-renewal mechanisms[210] these cells are important models for the search of new compounds with very specific

FCUP | 28
Cyanobacterial bioactive metabolites for anticancer drug
discovery: characterization of new compounds and
molecular mechanisms in physiologically relevant 3D cell
culture

targets, especially directed to CSC[113, 209, 211]. Some natural compounds demonstrated efficacy towards critical CSC mechanisms, such as salinomycin[113, 212], piperine[213] or curcumin[214], among others[215-216]

Also, the genetic diversity of culturable stem cells is low and there has been an effort of increasing the diversity of these pluripotent cells in order to have a better clinical representation of the different populations worldwide. This diversity of stem cells can serve different purposes, from research to treatment of diseases, since that genetic variances can influence an individual drug response[217].

OBJECTIVES

FCUP | 30
Cyanobacterial bioactive metabolites for anticancer drug
discovery: characterization of new compounds and
molecular mechanisms in physiologically relevant 3D cell
culture

FCUP   31
Cyanobacterial bioactive metabolites for anticancer drug
discovery: characterization of new compounds and
molecular mechanisms in physiologically relevant 3D cell
culture

The interest in marine blue technology is a growing phenomenon worldwide, which can be an open window for emerging ideas to promote economy. In this line, marine organisms have been explored as producers of new bioactive compounds.

The possibility of working with the cyanobacterial strains at LEGE Culture Collection (LEGE-CC) at the Laboratory of Blue Biotechnology and Ecotoxicology (BBE), in CIIMAR at University of Porto, allowed to have access to the huge potential of these organisms to produce new anticancer compounds. Previous work already denoted promising cytotoxic activity of some cyanobacterial strains on routine 2D cell culture, and new compounds were successfully isolated, such as nocuolin A, portoamides, hierridins and bartolosides. The focus of this thesis was to assess the potential activity of these isolated cyanobacterial compounds on physiologically relevant 3D cell culture and to elucidate their mechanisms of action. With this approach we focused on the following aspects:

a) Growth of marine cyanobacteria strains for the re-isolation of the known compounds characterized at BBE laboratory.

b) Use of 3D cell culture to analyse the anticancer potential on this advanced model.

c) Characterization of the molecular mechanism of the isolated compounds, using cellular and molecular methods such as flow cytometry, phenotypic alterations through light and fluorescence microscopy, proteomics and mRNA expression.

d) Perform an exploratory approach a new methodology to shorten the search of new and relevant cyanobacterial compounds, applying the 3D culture system and MS/MS data through molecular networking.

Part of the presented work was performed in collaboration and in the laboratories of Professor Stig Linder from the Karolinska Institute and Linköping University in Sweden, due to his large experience in 3D culture of cancer cells and cancer drug development.

The first scientific paper of the present thesis explores the cytotoxic activity of nocuolin A on non-cancer and cancer cells cultured as both monolayer and three-dimensional culture systems (3D) and unveiled its mode of action. The disturbance of mitochondrial respiration with more acute effects on cancer cells, a unique mode of action not related with known pathways from other compounds on C-Map database[218]. The second and third papers explore the activity of a mixture of portoamides A and B (3:1) on several cell lines, carcinogenic and non-carcinogenic cultured in monolayer[38], and further

FCUP | 32
Cyanobacterial bioactive metabolites for anticancer drug
discovery: characterization of new compounds and
molecular mechanisms in physiologically relevant 3D cell
culture

assessment of their activity on colon cell line HCT116 cultured in 3D followed by activity against zebrafish larvae and the immortalized normal cell line RPE-1[hTERT]. Exploitation of the previous results concerning mitochondria membrane hyperpolarization and ATP production impairment is here explored as well as portoamides capacity to permeabilized spheroids cell layers showing a generalized toxicity, verified also on zebrafish larvae.

On the fourth manuscript the potential activity of hierridins and bartolosides A, B and C was assessed on 3D cultured HCT116 cells. The last chapter of the present thesis describes a study for an integrative screening methodology to search for new cyanobacterial cytotoxic compounds using 3D culture systems along with metabolite profiling. This methodology aims to easier sieve the most promising compounds based on the biological activity in a relevant model system and presence of unique molecular mass peaks in active fractions.

FCUP | 33
Cyanobacterial bioactive metabolites for anticancer drug
discovery: characterization of new compounds and
molecular mechanisms in physiologically relevant 3D cell
culture

RESULTS

FCUP 34
Cyanobacterial bioactive metabolites for anticancer drug
discovery: characterization of new compounds and
molecular mechanisms in physiologically relevant 3D cell
culture

Antiproliferative effects of the natural oxadiazine nocuolin A are associated with impairment of mitochondrial oxidative phosphorylation

Sousa ML, Preto M, Vasconcelos V, Linder S and Urbatzka R (2019)

FCUP   36
Cyanobacterial bioactive metabolites for anticancer drug
discovery: characterization of new compounds and
molecular mechanisms in physiologically relevant 3D cell
culture

Antiproliferative Effects of the Natural Oxadiazine Nocuolin A Are Associated With Impairment of Mitochondrial Oxidative Phosphorylation

Maria Lígia Sousa [1,2], Marco Preto [2], Vítor Vasconcelos [1,2], Stig Linder [3,4] and Ralph Urbatzka [2]*

[1] Faculty of Sciences of University of Porto, Porto, Portugal, [2] Interdisciplinary Centre of Marine and Environmental Research, Porto, Portugal, [3] Department of Oncology and Pathology, Cancer Centre Karolinska, Karolinska Institute, Stockholm, Sweden, [4] Department of Medical and Health Sciences, Linköping University, Linköping, Sweden

Natural products are interesting sources for drug discovery. The natural product oxadiazine Nocuolin A (NocA) was previously isolated from the cyanobacterial strain *Nodularia* sp. LEGE 06071 and here we examined its cytotoxic effects against different strains of the colon cancer cell line HCT116 and the immortalized epithelial cell line hTERT RPE-1. NocA was cytotoxic against colon cancer cells and immortalized cells under conditions of exponential growth but was only weakly active against non-proliferating immortalized cells. NocA induced apoptosis by mechanism(s) resistant to overexpression of BCL family members. Interestingly, NocA affected viability and induced apoptosis of HCT116 cells grown as multicellular spheroids. Analysis of transcriptome profiles did not match signatures to any known compounds in CMap but indicated stress responses and induction of cell starvation. Evidence for autophagy was observed, and a decrease in various mitochondrial respiration parameter within 1 h of treatment. These results are consistent with previous findings showing that nutritionally compromised cells in spheroids are sensitive to impairment of mitochondrial energy production due to limited metabolic plasticity. We conclude that the antiproliferative effects of NocA are associated with effects on mitochondrial oxidative phosphorylation.

Keywords: natural products, cyanobacteria, spheroids, colon cancer, anti-cancer drugs, mitochondria, autophagy

FCUP 38

Cyanobacterial bioactive metabolites for anticancer drug discovery: characterization of new compounds and molecular mechanisms in physiologically relevant 3D cell culture

INTRODUCTION

Historically, natural products were the primary source of drugs for medical preparations (1, 2). Despite the gradually abandonment of natural products by big pharma companies since the era of antibiotics discovery (3), natural products have returned into the focus as one of the most interesting sources for drug discovery (2, 4). Cyanobacteria are versatile microorganisms, adapted to many different environments and, as such, developed the capacity of producing secondary metabolites to overcome exogenous challenges (5–7). Their potential to produce secondary metabolites is already recognized with interesting biotechnological applications as bioplastics (8) or pharmaceuticals (9), and with anticancer (10, 11), antifouling (12, 13), antibiotics (14), or antiprotozoal activities (15, 16). Our own group showed that pico-cyanobacteria produce bioactive compounds that target cancer cells via different modes of actions (17). Hierridin B induced cell death probably via inhibition of mitochondrial activity and mitochondrial pores (18), while cytotoxic activity of portoamides was associated with disturbance of energy metabolism, and alterations in mitochondrial structure, and function (19). In the marine clinical pipeline (http://marinepharmacology.midwestern.edu/clinPipeline.htm), many compounds derived from cyanobacteria are in the different phases of clinical trials, and one compound (brentuximab vedotin) is already in clinical use for the treatment of malignant lymphoma and Hodgkin's disease (11).

Monolayer cell cultures are commonly used as model to screen for cytotoxic activity of new extracts or isolated compounds in cancer cell lines; however those culture conditions do not represent well the complexity of a tumor environment, namely the tumor hypoxic core, the highly prolific outer layer and the quiescent inner core, nutrient deprivation, penetration impair of the compounds, and often the limitation of their effects *in vivo* (20). The use of multicellular spheroids (MTS) as physiologically relevant models is assumed to decrease the risk of *in vivo failures* regarding the phenotypic screening of new compounds and the assessment of their effects (21). MTS are geometrically well-defined, which allows the direct relation with structure and function, and to discriminate the morphological zones of the tumor (necrotic, quiescent, and proliferative) (20, 22). Another advantage of MTS is the possibility to understand how compounds may act on the quiescent cells of the inner core, similar to chemoresistant cells, which is one of the main reasons of failure of cancer treatment (23).

Nocuolin A (NocA) was isolated from the cyanobacterial strains *Nostoc*, *Nodularia*, and *Anabaena* by Vorácová et al (24) and also chemically characterized. This compound has an unusual structure, a natural azole ring with N-N-O linkage and was found to induce apoptotic effects in the HeLa cell line and cytotoxic effects on other cancer cell lines (24). Using a bioassay-guided fractionation procedure, NocA was re-isolated from the cyanobacterial strain *Nodularia* sp. LEGE 06071 based on its cytotoxic activities in cancer cell lines (own unpublished data). The aim of the present work was to analyse the biological activity of NocA on colon cancer cells, and to evaluate its molecular mechanism of action. The effects of NocA on this type of cancer cells were not previously evaluated. Besides its high frequency to cause cancer death (25), this cell type offers the possibility to study its comparative cytotoxic activity on monolayer cultures and MTS. Next generation sequencing was used as an unbiased approach to generate hypotheses about altered cellular signaling pathways. In order to test those hypotheses, functional assays focused on effects on cell survival, apoptosis, cell cycle, autophagy, mitochondrial respiration, and ER stress. The cytotoxic activity of NocA and functional assays were compared between cells grown as monolayer culture or as MTS in order to get insights into its potential effects on solid tumors.

METHODS

Cyanobacteria Culture

The cyanobacterial strain LEGE 06071 was grown from the LEGE CC culture (26) of CIIMAR, Porto, Portugal. Cyanobacteria were cultured under standard conditions using Z8 medium supplemented with 20 µg L^{-1} vitamin B$_{12}$ (27). Cultures were maintained at 25℃, under a light: dark cycle of 14:10 h, provided by cool white fluorescent tubes 10 µmol m^{-2} s^{-1}. Cyanobacteria were harvested by centrifugation following by freeze-drying biomass.

Nocuolin A Isolation

The initial extract was obtained from 39.2 g of lyophilized biomass of *Nodularia* sp. LEGE 06071, using a warm mixture of CH_2Cl_2: MetOH (2:1) yielding 8 g crude organic extract. The first fractionation was performed with a Vacuum-Liquid Chromatography (VLC) with a stationary phase of Silica Gel 60 (0.015–0.040, Merk KGaA). The mobile phase was a mixture of increasing polarity from 10% of EtOAc in hexane to 100% EtOAc to 100% MeOH. The samples were dissolved in methanol in a concentration of 1 mg ml^{-1} and analyzed by LC/MS on a Thermo Scientific LTQ Orbitrap XL spectrometer with a gradient from 20% MeCN (aq) to 100% MeCN (aq) for 20 min followed by isocratic condition at 100% MeCN for 10 min with a flow rate of 1 mL min^{-1}. Fractions having NocA presence on the mass-spectrum [(M–H+) 299 (m/z)]; (M+Na+) = 321 (m/z); (2M+H+) = 597 (m/z); (2M+Na+) = 618(m/z) and tR = 6.44 min) were pooled together following a flash chromatography with crescent polarity solvents. The mobile phase was a mixture of increasing polarity from 40% of EtOAc in Hexanes to 100% EtOAc to 50% MeOH. Monitoring of the composition of the collected fraction was carried out using Thin Layer Chromatography (TLC), Silica Gel 60 F254 (Merk) under UV light with 254 and 366 nm. The TLC plates were also stained using Phosphomolybdic Acid Staining (PMA) at ∼40°C and samples were pooled according to their TLC profile. Nine samples were then prepared for verification by LC-MS analysis as described before. Finally, NocA was isolated with a Waters HPLC System composed by a 1,525 binary pump and a UV- VIS detector, using a Synergi Fusion-RP column (4 μ 250 × 10 mm, 80 A) and a gradient elution program of 60–100% MeCN in 20 min, followed by 35 min at the same eluent composition, before returning to 60% MeCN in 5 min (flow = 3 mL/min). The abundance of NocA was checked by LC-MS and its purity accessed with ^{1}H Nuclear Magnetic Resonance (NMR), BRUKER AVANCE III 400 MHz, 9.4 Tesla spectrometer equipped with a 5 mm cryoprobe. The NMR spectra were processed with Mnova software v8.0 (Mestrelab Research, S.L.).

Cell Culture

The human colon carcinoma cell line HCT116^{wt} and breast cancer cell line MCF7^{wt} were obtained from the American Type Culture Collection, Manassas, VA, USA. The normal epithelial cell line hTERTRPE-1 (28) was obtained from Clontech (Palo Alto, CA) and HCT116 with red nucleus (red mKate2 fluorescent protein) was previously established using IncuCyte® NucLight Red Cell Labeling and according to manufacturer's instructions. HCT116 mutated cell lines (overexpression of BCL2, BCL2XL, MCL1) (29), and HCT116$^{pTRAFNrf2/HIF}$ were provided by Prof Elias Arnér from Karolinska Institute, Sweden. All cell lines were sub-cultivated and grown in supplemented medium as recommended by the providers. All HCT116 colon carcinoma cell lines were maintained in McCoy's 5A modified medium, MCF-7 was grown in Dulbecco's Modified Eagle Medium (DMEM) supplemented with Glutamax^{TM} (Gibco, Massachusetts, USA) and hTERT RPE-1 was grown in Dulbecco's Modified Eagle Medium: Nutrient Mixture F-12 (DMEM/F12) supplemented with Glutamax^{TM} (Gibco, Massachusetts, USA). All media were also supplemented with 10% fetal bovine serum (Biochrom, Berlin, Germany), 1% of penicillin/streptomycin (Biochrom, Berlin, Germany), and 0.1% of Amphotericin B (GE Healthcare, Little Chafont, United Kingdom), and all cells lines incubated at 37°C in 5% CO_2.

Generation of MTS

After confirming a pre-confluent growth (over 80%) on a monolayer culture, the cells were detached from the plates by trypsinisation and collected. Two hundred microliter of medium containing 50,000 cells are added on each well of a 96 well-plate (U-round bottom ultra-low attachment, Corning). Then 190 µl of medium was added, so that top of the well should form a drop, resulting of the excess of medium. Elevating the lid from the plate with plasticine on the corners, the plate was firmly putted upside down resulting in a drop by superficial tension on each well. The plate was then incubated over 24 h with shaking (300 rpm) under 37°C and humidified atmosphere with 5% of CO_2. On the next day, the plate was flipped back to the normal position. The excess of medium (190 µl) was removed and then the newly formed spheroids were incubated for 5 days.

Glucose/Galactose Assay

For the Glucose/Galactose assay HCT116[wt] cells were seeded at 3.3×10^4 cells mL^{-1} in 96 well-plates and after 24 h they were changed to glucose (25 mM) or galactose (10 mM) conditioned media, respectively, as described previously by Eakins et al. (30) and exposed to NocA at concentrations up to 10 µM over 48 h. After that period, MTT assay was performed as described below.

Viability Analyses

Cells were seeded at 3.3×10^4 cells mL^{-1} in 96 well-plates and after 24 h exposed to NocA concentrations up to 10 µM and kept in the incubator for 48 h. After the exposure, 3-(4,5- dimethylthiazol-2-yl)-2,5-diphenyltetrazolium bromide) (MTT) was added at a final concentration of 0.05 mg ml^{-1} per well for 3 h. The formation of formazan crystals was visually evaluated by microscopy, dissolved in DMSO and absorbance measured at 550 nm on a GEN5TM-Multi-detection Microplate Reader (Biotek, Bad Friedrichshall, Germany). All compounds tested in this work were dissolved in dimethylsulphoxide (DMSO) (Sigma, USA). A maximum final concentration of 0.5% DMSO was reached in cell cultures; control wells received solvent only. Suforhodamide B colorimetric assays was also performed in HCT116 cell line cultured and exposed at the same conditions and the viability assay was performed according to Vichai and Kirtikara (31). The size development of MTS was followed after exposure for 48 h in the IncuCyte-FLR 20X phase contrast/fluorescence microscope (Essen Instruments, Ann Arbor, MI). Images of spheroids were taken every 4 h, and spheroids area was measured every 24 h aided by Incucyte ZOOM Live-Cell Analysis System (Essen Instruments, Ann Arbor, MI).

Incucyte Analysis of Nrf2 and HIF

For analysis of Nrf2 and HIF, a HCT116 cell line transformed with a pTRAF[Nrf2/HIF] plasmid were cultured as described before. NocA was tested on a concentration-response assay (up to 10 µM) and incubated on an Incucyte ZOOM Live-Cell Analysis System (Essen Instruments, Ann Arbor, MI). For the duration of 48 h, Nrf2 activity was read at λex = 585 nm, emission filter: 635 nm, and auranofin (2 µM) was used as a positive control to confirm Nrf2 activity and HIF activity was read λex = 460 nm, emission filter: 524 nm using VLX600 (32) as positive control, at a concentration of 6 µM.

Autophagy Staining

HCT116 cells were seeded on a top of sterile cover slide and let adhere for 24 h. Then, cells were exposed to IC$_{90}$ concentration of NocA (7 µM) over 6 and 18 h. At the end of the exposure, cells were stained with 80 µM of monodansylcadaverine (MDC) for 10 min at 37°C in the dark. The slides were then mounted and visualized on a fluorescent microscope Leica DM6000B under DAPI filter and images were analyzed with Cell Profiler software https://cellprofiler.org/. MTS were also stained with MDC at 80 µM for 10 min at 37°C, 5% CO_2 in the dark and then visualized under the same fluorescent microscope.

Determination of Apoptosis by ELISA

Following drug exposure, caspase-cleaved keratin-18 (K18- Asp396) was determined following the instructions of the manufacturer using the M30-Cytodeath ELISA developed for detection of soluble caspase-cleaved keratin 18 (VLVBioPeviva AB, BrommaStockholm, Sweden).

Western Blot

Cells were collected in RIPA buffer (150 mM NaCl, 50 mM Tris, pH 7.4, 1% Nonidet P-40, 0.1% SDS, 0.5% sodium deoxycholate) supplemented with protease and phosphatase inhibitors. The protein concentration of cellular extracts was determined by Pierce Coomassie Plus (Bradford) Assay Reagent. SDS-PAGE was performed on pre-casted acrylamide gels NuPAGE^{TM} 4–12% Bis-Tris Protein (Invitrogen^{TM}) using the

NuPage system and loading 20 µg of proteins per lane. After electrophoresis, proteins were transferred to nitrocellulose membranes and incubated for 1 h at room temperature in PBS-Tween with 5% non-fat dry milk. Protein loading was assessed by red Ponceau staining of the membranes. Primary antibodies were used according to the manufacturer instructions, LC3 (#2775) (1:1,000), Phospho-eIF2 α (Ser51) (#9721) (1:1,000), and eIF2 α (#9722) (1:1,000), all antibodies were from Cell Signaling Technology (Danvers, MA, USA). Antibody to β-actin (#A5316) was from Sigma-Aldrich (St Louis, MO, USA) (1:5,000). Membranes were incubated with primary antibodies dilutions in 5% w/v BSA, 1x TBS, 0.1% Tween-20 overnight at 4°C, followed by appropriate HRP- conjugated secondary antibodies. Secondary Anti-rabbit IgG HRP-linked (#7074) and Anti-mouse IgG, HRP-linked Antibody (#7076), (Cell Signaling Technology, Danvers, MA, USA) were diluted at 1:5,000 in 5% non-fat milk and incubated 1 h at room temperature. Antibody staining was visualized by the Clarity Western ECL Substrate (BioRad) on a BioRad Molecular Imager Gel Doc^{TM} XR+ with Image Lab^{TM} Software.

ATP Determination

ATP levels were determined according to Mitochondrial ToxGloTM Assay kit (Promega, Madison, WI). HCT116 cells were seeded at a density 2.0×10^5 cells mL^{-1} in a 96-well plate, overnight incubation 37°C, 5% CO2 to allow the adhesion of the cells. Then, cellular ATP levels were determined relative to vehicle-treated control cells after 2 h exposure period to seven concentrations of NocA (up to 10 µM, with 1:2 dilutions). Cytotoxicity reagent from the kit was added and fluorescence measured at 485 nmEx/520–530 nmEm. Following, ATP detection reagent was added, and luminescence measured on a SparkR multimode microplate reader (Tecan).

Mitochondrial Respiration

HCT116 cells with a density of 6×10^4 cells ml^{-1} of were seeded on a XF24-plate containing blank controls. The Seahorse XF analyzer was used as indicated by the manufacturer (Seahorse Bioscience). Before the measurements, medium was replaced with 500 µL of Seahorse XF base medium (200 mM L-glutamine, 1 mM pyruvate, 2.5 M glucose, pH 7.4) at 37°C without CO$_2$ for 1 h. Oxygen consumption rate (OCR) values were measured by XF24 Extracellular Flux Analyzer. The assessment of Mitochondrial activity was performed using a Seahorse XF Cell Mito Stress Test Kit (Seahorse Bioscience). All experiments were performed in triplicates and were repeated three times.

Flow Cytometry

For cell cycle analysis, HCT116 cells were seeded at a density of 5×10^5 cells ml^{-1} in 24 well-plates and exposed to Paclitaxel 100 nM (33), NocA 2.5 µM, and NocA 1.25 µM for 24 and 48 h. After exposure, cells were collected, fixed in 70% ethanol and stored at −20°C. On the day of the analysis, the cells were collected again and resuspended in 100 µl of PI/RNAse staining buffer (BD Pharmingen^{TM}, USA) for 40 min. Then 400 µl of PBS was added and cells were analyzed on a BD FACSCanto^{TM} II flow cytometer. Cells were gated on the basis of the forward (FSC) and side scatter (SSC) profiles and were analyzed with a BD FACSCanto II equipment (Bekton Dickinson) and 10,000 events per sample were collected. For apoptosis, cells were seeded as described for cell cycle analysis, but the cells were lived stained with 5 µl of FITC Annexin V (Immunotools, Germany) and 10 µl Propidium Iodide (PI) at 50 µg ml^{-1} freshly prepared in 100 µl PBS Ca^{2+} binding buffer for 20 min. Four hundred microliter of binding buffer was added before analysis on a BD Accuri 6 Flow Cytometer. Ten thousand events, gated based on FSC and SSC, were collected on FL1/FL3 channels. For mitochondrial depolarization analysis, HCT 116 cells were seeded at a density of 5×10^5 cells ml^{-1} in 6 well-plates and exposed with 7 µM of NocA over 6 h. Cells were incubated with 25 nM TMRE (Invitrogen) for 30 min and changes in mitochondrial membrane potential (OW) were monitored in an Gallios Flow Cytometer, cells gated according to FSC And SSC profile, and 60,000 events were collected on FL2 channel per sample (34). Data analysis of flow cytometry data was performed using FlowJo v10 (FlowJo LCC, Ashland, OR, USA).

RNA Extraction

MCF-7 cells were cultured as described by Lamb et al. (35). After exposure, cells were washed with PBS, and total RNA was prepared using RNeasy miniprep kit (Qiagen, Chatsworth, CA) with a removal of DNA contamination step by DNAse I digestion (BioRad Laboratories, USA). The quantification of RNA was determined on a Biotek, HT Synergy reader using a Take3^{TM} multi-volume plate, and the quality of RNA was verified on an 1% agarose gel. Then, the samples were sent to GATC Biotech AG (Konstanz, Germany) for RNA sequencing. Single-end samples were aligned to the reference Human genome hg19.chronly/GRC37, UCSC with Gencode v19, and Ensembl 75 annotations. Of a total of 55,850,897 reads on control sample, 99% were mapped and from 62,514,401 on NocA 99.1% of NocA reads were mapped.

Bioinformatic Analysis of RNAseq

As main NGS results, a list of genes (19,976) was obtained and its number of reads corrected for sequence length bias. For analysis of C-Map, the 150 most up-regulated genes (maximum absolute fold ranging 159.36 to 5.12) and 150 most down-regulated genes (absolute minimum fold ranging -3.51 to -208.33) were inserted. A query on C-Map (https:// clue.io/l1000-query) (36) should retrieve a list of perturbagens that can be used to find similar compounds, gene knock- down, gene over-expression, and C-Map classes with similar expressing signatures to NocA. The C-Map classes with connectivity score (τ) higher than 90 were selected, as having significant relevance (36). Gene-set enrichment analysis (GSEA) was performed for the complete gene list using GSEA software (37) with 1,000 permutations on the gene set, and default values for other parameters. The gene set was selected from MSigDB C5 collection: Gene Ontology (GO) gene sets (http://www.broadinstitute.org/gsea/msigdb/ collections.jsp). The enriched GO Pathways with nominal values (the statistical significance of the enrichment score) lower than 0.005 were exported to Cytoscape 3.6.0 and an enrichment analysis map was constructed (38, 39).

Statistical Analysis

The IC$_{50}$ values were calculated from dose-response curves of NocA after transforming the data to log scale and normalization, defining 0% of viability as the positive control and the 100% of viability the solvent control. A non-linear regression choosing a variable slope with four parameters was performed and IC$_{50}$ calculated on the inflection point. Data was retrieved from three independent experiments with $\geq$3 replicates each. ATP levels obtained by the Mitochondrial ToxGlo^{TM} Assay kit were transformed to a log scale and normalized defining 0% of viability as positive control and 100% viability as solvent control, and ATP minimum values 0% with the mito-toxicant CCCP at 10 µM, and untreated wells as 100% ATP values. Error bars of the graphs represent the standard deviation. Apoptosis analysis from flow cytometry assay, Seahorse results and morphological alterations of spheroids imaged on IncuCyte were analyzed with a two- way ANOVA followed by a Bonferroni Multi comparison *post hoc*-test. Flow Cytometry were performed in triplicates counting 10,000 events on each sample, whereas Seahorse was analyzed with $n = 6$ over three independent experiments, and IncuCyte with $n = 6$. Western blot statistical analysis was performed using protein bands signal of three independent experiments with a one-way ANOVA followed by Bonferroni Multicomparison *post- hoc*-test. Results from M30-Cytodeath ELISA and fluorescence staining of spheroids were analyzed with one-way ANOVA followed by Dunnett's Multiple Comparison Test, using three independent assays with each in triplicates. For all analyses, the confidence interval was 95%, where $^*p < 0.05$; $^{**}p < 0.01$; $^{***}p < 0.001$. Error bars of the graphs represent the standard deviations.

RESULTS

NocA Shows Antiproliferative Effects on HCT116 Colon Cancer Cells in Monolayer and Spheroid Cultures

Nocuolin A (NocA) was isolated from the cyanobacterial strain LEGE 06071 and the purity estimated to ~99% by LC-MS (**Supplementary Figure 1**) and ^{1}H-NMR analysis (**Supplementary Figure 2**). Under conditions of exponential cell proliferation, NocA had similar antiproliferative activities on HCT116 colon cancer cells and immortalized human hTERT-RPE-1 epithelial cells using the MTT assay (IC$_{50}$ values of 1.35± 0.96 and 1.2 ± 0.6 µM, respectively). Since proliferating normal cells are sensitive to cancer therapeutic agents, we also examined the effects of NocA on hTERT-RPE-1 cells under non-proliferating conditions (**Supplementary Figure 3B**), using confluent and contact inhibited hTERT-RPE-1 cultures (40). When confluent cultures of hTERT-RPE-1 cells were exposed to NocA, an IC$_{50}$ value of >10 µM was observed (**Supplementary Figure 3A**). The multicellular tumor spheroid (MTS) model is of intermediate complexity between *in vivo tumors* and monolayer cell cultures. The response of HCT116 MTS to different concentrations of NocA was evaluated using an IncuCyte® instrument. NocA showed a disaggregation of the outer cell layers in particular at concentrations >5 µM (**Figure 1** and **Supplementary Figure 4**) leading to an increase of the spheroid size. Additionally, a loss of fluorescence signal of HCT116 red nucleus MTS indicated reduced viability in the outer layer of the spheroid (**Supplementary Movies**).

FIGURE 1 | Representative IncuCyte images of HCT116^{wt} spheroids. Top image represents a spheroid in the beginning (0h) and at the end of the experiment (72h), without exposure to NocA while the bottom images represent a spheroid exposed to 20 µM of NocA. Quantitative analysis is shown on Supplementary Figure 4 derived from 3 independent experiments in triplicates.
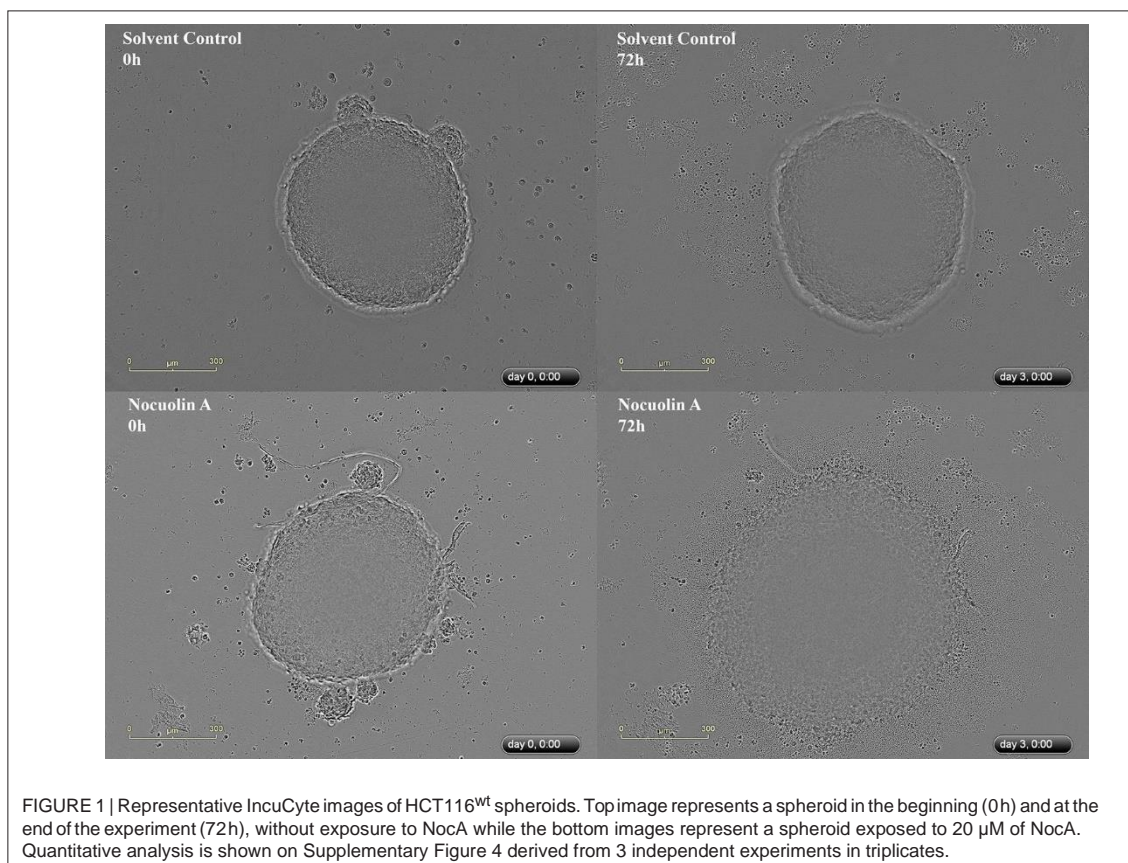
NocA Induced Apoptosis of Colon Cancer Cells in Both Monolayer and Spheroid Cultures

To examine the mechanism of antiproliferative effects, we first analyzed whether the cell cycle was affected using propidium iodide staining and flow cytometry. No effect on the cell cycle was evident after 24 or 48 h

of exposure to NocA (**Supplementary Figure 5**). We next investigated possible induction of apoptosis using annexin V/propidium iodide staining and flow cytometry (**Figure 2A**). This analysis demonstrated that apoptosis occurred in cells exposed to NocA for 48 h. Apoptosis was observed at a concentration close to the IC_{50} suggesting that apoptosis was the underlying mechanism for antiproliferative effects. Significant apoptosis was not observed after 24 h exposure (**Figure 2B**).

BCL2 family proteins are instrumental to apoptosis involving the mitochondrial pathway (29, 41). HCT116 cells overexpressing the genes BCL2, MCL1, or BCL2XL proteins were exposed to increasing concentrations of NocA for 48 h. However, cell viability was not significantly affected by overexpression of these proteins (**Table 1**). We next examined whether NocA would induce apoptosis in HCT116 MTS (**Figure 2D**). An endogenous caspase-cleavage product (CK18-DALD396, ccCK18) was assessed using the M30-Apoptosense[R] enzyme- linked immunosorbent assay method (21). Increased levels of ccCK18 were observed at concentrations ≥2.5 µM (**Figure 2C**).

Drugs that induce apoptosis of tumor cells, commonly induce an oxidative stress response (42). We examined the response to NocA using a HCT116 reporter cell line where antioxidant/electrophile response element (ARE/EpRE) are under the control of the Nrf2 promoter (43). No effect of NocA was observed over 48h of exposure (**Supplementary Figure 6**), which indicated no induction of oxidative stress.

HCT116 monolayer culture - 48h
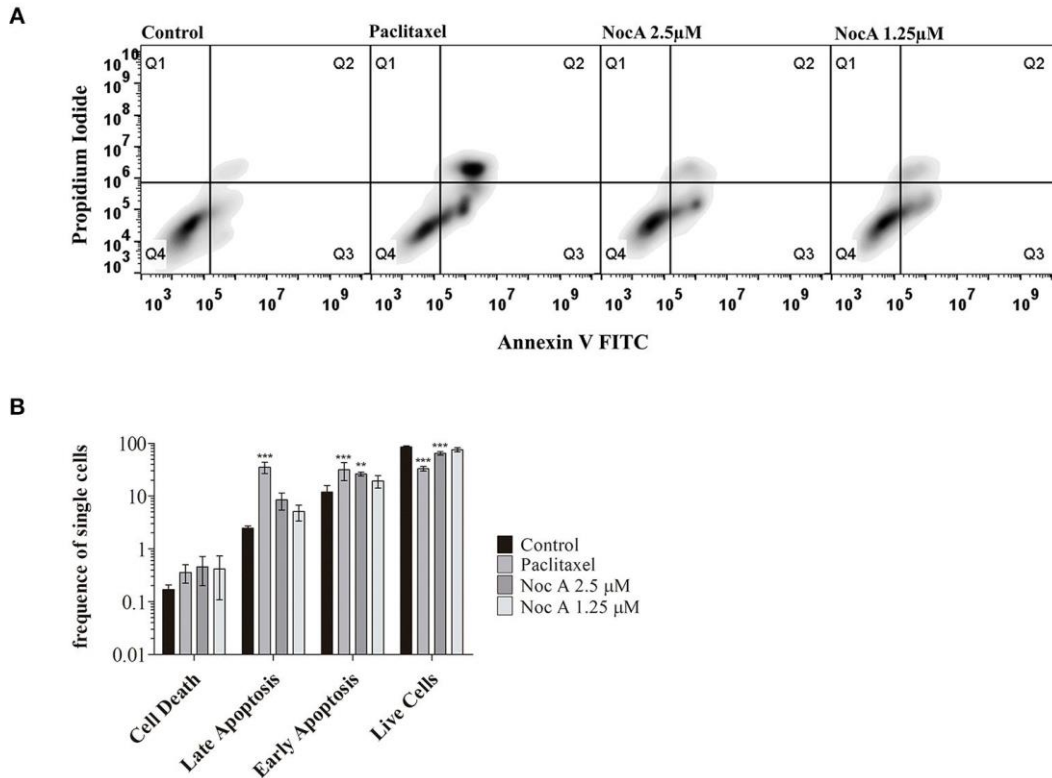
HCT116 MTS culture - 48h
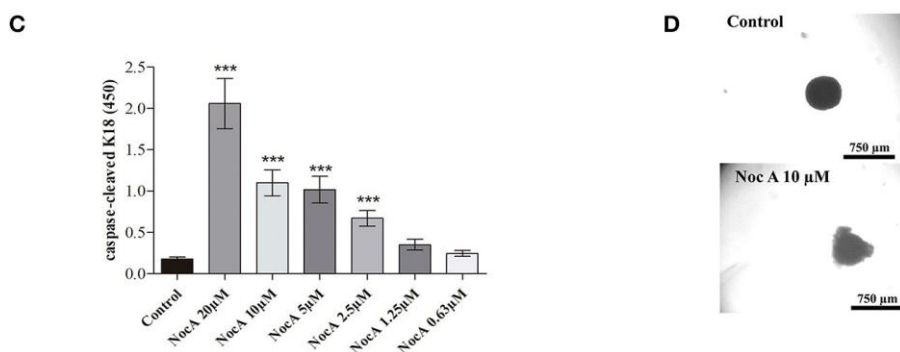
FIGURE 2 | Analysis of apoptosis on monolayer culture and multicellular spheroids (MTS). (A) Apoptosis analysis of monolayer culture HCT116 cells using flow cytometry with Annexin V and Propidium iodide staining. (B) Quantifications of flow cytometry results. Apoptosis is observed after 48 h at 2.5 μM. ***$p < 0.001$; **$p < 0.01$. Ten thousand cells per gated replicate were counted, $n = 3$. (C) M30 CytoDeathTM ELISA absorbance readings on HCT116 MTS exposed to NocA up to 20 μM. High absorbance values represent higher levels of caspase cleaved K18. Two independent assays were performed, $n = 3$. (D) Bright field images of MTS after 48 h of exposure, being the top image a control and the bottom image an MTS exposed to Noc A at 10 μM; ***$p < 0.001$.

Analysis of Transcriptome Profiles Shows a Complex Response

To generate hypotheses regarding the mechanism of action of NocA, we examined transcriptome signatures from drug-treated cells (35). The Connectivity Map database (Broad Institute) is based mainly on the MCF7 breast cancer cell line and we first established that NocA shows antiproliferative activities in this cell line (IC$_{50}$ of 1.6 µM ± 0.6) (**Supplementary Figure 3C**). The transcriptome profile was determined after 6 h exposure of MCF7 cells to 7 µM NocA and signatures with connectivity score (τ) higher than 90 were selected (35, 36, 44). These gene set signatures were rank-ordered by similarity of differentially- expressed gene sets of MCF7 and, in addition, by similarity of a summary connectivity score across nine cell lines (A375, A549, HCC515, HEPG2, HT29, MCF7, PC3, HA1E, VCAP) (**Table 2**).

The query comparing connectivity with the summary across the nine cell lines on the database demonstrated five CMap pharmacological classes with strong connectivity score, similar to the classes obtained for MCF cell line analysis (IKK inhibitor, protein synthesis inhibitor, ATPase inhibitor, PKC activator, T-type calcium channel blocker). The exceptions were T-type calcium channel blocker, which only appeared with connectivity for MCF7 cell analysis, and BCL inhibitor, which only had strong connectivity on the summary across all the cell lines (**Table 3**).

A Gene Set Enrichment Analysis by using the transcriptome data demonstrated the enrichment of 79 GO terms for NocA treated cells compared to the solvent control (**Supplementary Table 1**). Major cluster of cellular dysregulations were identified and belonged to the immune response, stress response, sterol biosynthesis, response to starvation, and endoplasmic reticulum stress. According to the number of enriched genes and difference in read frequencies, the most enriched GO terms were organized in clusters to facilitate the visualization of the data by Cytoscape software (**Figure 3**). We conclude from these data that the response to NocA is complex and is characterized by an expected general stress response but also response to starvation and endoplasmic reticulum stress.

TABLE 1 | IC$_{50}$ for NocA cytotoxic activity in colon cancer cell line HCT116^{wt} and HCT116 mutated cell lines, BCL family proteins overexpression, and MCF7^{wt} cell line.

Cell line	IC$_{50}$ [µM] mean ± SD
HCT116^{wt}	1.3 ± 0.9
HCT116$^{BCL2+/+}$	1.2 ± 0.4
HCT116$^{BCL2XL+/+}$	1.6 ± 0.6
HCT116$^{MCL1+/+}$	1.9 ± 0.6
MCF7^{wt}	1.6 ± 0.6

Viability was analyzed by MTT assay after 48 h of exposure with n > 4 in three independent assays.

Evidence of Autophagy Induction

Based on the finding of response to starvation in the GSEA analysis raised the possibility that NocA may induce autophagy. The LC3B-II protein expression of cells exposed to NocA at concentrations of 1.25–2.5 µM was significant increased after 18 h of exposure (**Figures 4A, B**). Induction of LC3B-II was also after observed 24 and 48 h of exposure of MTS to NocA (**Figures 4D, E**). Monodansylcadaverine (45) is a stain of autophagic compartments, and fluorescence intensity after 18 h of exposure to NocA was increased in HCT116 cells in monolayer cultures and on MTS after 48 h of exposure (**Figures 4C, F**). These results, although preliminary, led to the hypothesis that NocA has a negative effect on cell metabolism.

NocA Induced a Decrease in Cellular ATP and Mitochondrial Respiration

In order to directly examine whether NocA result in a metabolic insufficiency, intracellular ATP concentrations were determined. Decreases of ATP were indeed detected with increasing concentrations of NocA, after 2 h of exposure to concentrations as low as 0.16 µM NocA. The decreases in ATP occurred prior

to induction of cytotoxicity and were similar in amplitude to those induced by the mitochondrial uncoupler CCCP (**Figure 5C**).

The pronounced metabolic effect by NocA raised the possibility that the compound acts as a mitochondrial toxin. Cells cultured in glucose free medium (supplemented with galactose) showed an increase of sensitivity to NocA, supporting the idea of mitochondrial toxicity (**Table 4**). Mitochondrial respiration rates were measured using a Seahorse Extracellular Flux Analyzer. Cells were exposed to different concentrations of NocA and oxygen consumption rates were recorded over 6 h (**Figure 5A**). The basal respiration, ATP production, and non-mitochondrial respiration were decreased by 7 and 2.5 µM NocA, while maximal respiration was only reduced by 7 µM NocA (**Figure 5B**). The same analysis was performed with confluent RPE-1 hTERT cells exposed to 7 µM NocA, and similar effects were observed (**Figure 5D**) on basal respiration, maximal respiration but ATP production was not significantly reduced (**Figure 5E**).

The cationic lipophilic fluorochrome dye TMRE (tetramethylrhodamine, ethyl ester) staining of HCT116 cells indicative of depolarization of the mitochondrial membrane, did not show any differences between solvent control and cells exposed to 7 µM NocA (**Supplementary Figure 7**).

TABLE 2 | Detailed list of connections of transcriptome of MCF7 cells exposed to NocA to reference perturbagens of C-Map MCF7 cell line.

Rank	Score (τ)	Name	Compounds	Target
MCF7				
10.00	98.94	Vesicular Transport		COPA; COPB2
22.00	98.37	IKK inhibitor	Withaferin-a; IKK-16; IKK-2-inhibitor-V; BX-795; TPCA-1	
35.00	97.50	Protein synthesis inhibitor	Brefeldin-a; puromycin; homoharringtonine; emetine; cycloheximide; cephaeline	
44.00	96.89	ATPase inhibitor	Strophanthidin; digitoxin; cyclopiazonic-acid; digoxin; cinobufagin; cymarin; bufalin; ouabain; proscillaridin; digitoxigenin	
133.00	90.74	PKC activator	Prostratin; phorbol-12-myristate-13-acetate	
137.00	90.59	T-type calcium channel blocker	Penfluridol; dichlorobenzamil; KB-R7943	

Score (τ) stands for the fraction of reference gene sets with a greater similarity to the perturbagen.

TABLE 3 | Detailed list of connections of transcriptome of MCF7 cells exposed to NocA to reference perturbagens of C-Map summary across the cell lines available in the database (A375, A549, HCC515, HEPG2, HT29, MCF7, PC3, HA1E, VCAP).

Rank	Score (τ)	Name	Compound
9 CELL LINES			
1.00	99.02	Protein synthesis inhibitor	Emetine; cycloheximide; homoharringtonine; cephaeline; verrucarin-a; brefeldin-a; puromycin
4.00	98.13	ATPase inhibitor	Cinobufagin; bufalin; ouabain; proscillaridin; digoxin; digitoxin; strophanthidin; cymarin; cyclopiazonic-acid; digitoxigenin
12.00	97.47	PKC activator	Prostratin; ingenol; phorbol-12-myristate-13-acetate
20.00	96.58	IKK inhibitor	BX-795; IKK-2-inhibitor-V
28.00	95.20	BCL inhibitor	ABT-737; obatoclax

Score (τ) stands for the fraction of reference gene sets with a greater similarity to the perturbagen.

FIGURE 3 | Gene Set Enrichment Analysis mapped clustered with Cytoscape. Clusters represent different responses of exposed cells to NocA. Node sizes represent the number of genes and darken of the color increases with significance (FDR Q-value Cut-off = 0.1; P-value Cut-off = 0.005).

Monolayer culture HCT116 wt

A

6h exposure   18h exposure

Solv Ctrl | NocA 2.5µM | NocA 1.25µM | Solv Ctrl | NocA 2.5µM | NocA 1.25µM

LC3B-II

βActin

B

C

18h

Solvent Control | Nocuolin A

50 µm | 50 µm

MTS culture HCT116 wt

D

24h exposure   48h exposure

Solv Ctrl | NocA 10µM | Solv Ctrl | NocA 10µM

LC3B-II

βActin

E

F

48h

Solvent Control | Nocuolin A

100 µm | 100 µm

FIGURE 4 | Evidence of autophagy induction on monolayer cell culture of HT116 and multicellular systems (MTS). (A) Western blot of HCT116 cells exposed to NocA at 2.5 and 1.25 µM for 6 and 18 h with detection of LC3-B (B). (C) MDC staining of autophagic compartments on HCT116[wt] monolayer cultured cells exposed to NocA 7 µM over 18 h. (D) Western blot of MTS of HCT116 cells exposed to NocA at 10 µM for 24 and 48 h with detection of LC3B-II. (E) LC3B-II quantification. (F) MDC staining of MTS exposed to NocA 7 µM over 48 h. Three independent assays, ***$p < 0.001$; **$p < 0.01$.

FIGURE 5 | Seahorse analysis of cellular respiration. (A) Oxygen consumption rates by HCT116[wt] cells over 6 h in response to exposure to NocA at 1.25, 2.5, and 7 µM. (B) Mitochondrial key parameters—Basal respiration, ATP production, Maximal Respiration—calculated after addition of sequential kit reagents (Oligomycin, FCCP, Antimycin A, and Rotenone) from Seahorse XF Cell Mito Stress Test, Kit ***$p < 0.001$. (C) Dose-response for glucose-free (galactose supplemented) HCT116[wt] cells treated with NocA and CCCP and respective cell viability after 2 h of exposure (according to Mitochondrial ToxGlo[TM] Assay kit). $1 = Log (10\,\mu M)$ to $-0.81 = Log (0.16\,\mu M)$. (D) Comparison of Oxygen consumption rates between HCT116[wt] and RPE-1 hTERT cells in response to 6 h exposure to NocA at 7 µM. (E) Mitochondrial key parameters—Basal respiration, ATP production, Maximal Respiration- calculated after using Seahorse XF Cell Mito Stress Test Kit on RPE-1 hTERT and HCT116[wt] exposed to NocA 7 µM for 6 h. ***$p < 0.001$; **$p < 0.01$, $n > 5$, 3 independent assays.

TABLE 4 | IC50 comparison between HCT116[wt] cells grown in DMEM and glucose-free DMEM, supplemented with galactose.

Cell line	Medium	IC50 (µM)
HCT116	Glucose	1.3 ± 0.9
	Galactose	0.4 ± 0.07

DISCUSSION

Oxadiazoles and oxadiazines have recently attracted attention due to the exhibition of potential anticancer properties (46–49). We here report that the oxadiazine NocA shows antiproliferative activity on colon cancer cells grown as monolayer cultures and also on MTS. Conventional cancer therapeutic drugs show overall poor efficacy on MTS, a phenomenon which is believed to be reflected in limited efficacy of drugs to act on tumor masses *in vivo*. NocA induce significantly apoptosis on MTS at a concentration (2.5 µM) which is only 2-fold higher than the concentration of IC$_{50}$ *in vitro*. Cisplatin has been reported to induce apoptosis at concentrations >10-fold that of its IC$_{50}$ on monolayer cells (21). The use of cell lines overexpressing BCL2 family proteins revealed that the mechanism of cell death induction is independent of these proteins. Whereas, proliferating HCT116 cancer cells and proliferating RPE-1-hTERT immortalized cells showed similar degrees of sensitivity to NocA, non- proliferating RPE-1-hTERT were less sensitive. These findings are likely to be explained by higher metabolic demands by proliferating cells.

Transcriptome profiling can be used to generate hypotheses with regard to the mechanism of action of compounds (35, 36, 44). The molecular signature of NocA was complex, showing the alteration of a number of cellular responses such as vesicular transport, cellular response to inflammation, protein synthesis inhibitors

FCUP | 51
Cyanobacterial bioactive metabolites for anticancer drug
discovery: characterization of new compounds and
molecular mechanisms in physiologically relevant 3D cell
culture

and ATPase inhibition. Although the strong connectivity of the hits obtained for the described C-Map classes, these pharmacological classes are very distinct, and rather unspecific mechanisms, and did not point to a clear mode of action. The Gene Enrichment Analysis and Gene Ontology (GSEA) analysis indicated stress responses, including endoplasmic reticulum (ER) stress, and also autophagy, which we selected for the following analyses. ER stress was analyzed by p-EIF2α protein expression (50), but no upregulation was observed, which would indicate ER stress (data not shown). The increased expression of the autophagy marker LC3B- II as well as increased MDC staining of monolayer cells and MTS suggested evidence for the induction of autophagy. Future experiments should focus on the extent of autophagy and the analysis of the autophagic flux (51). Here, the indication of autophagy led us to speculate that treatment with NocA may interfere with cellular energy production. Our data confirmed this hypothesis, showing decreases in basal mitochondrial oxygen consumption rates and a rapid decrease in cellular ATP levels. These findings suggest that NocA is a mitochondrial toxin targeting the mitochondrial function of colon cancer cells without alteration of the mitochondrial membrane potential. These results obtained for both HCT116 and RPE-1 reinforce the previous idea that cancer cells are more susceptible to NocA than normal non-proliferating cells due to the higher energy requirements and proliferating characteristics. In contrast, the cyanobacterial compounds hierridin B and portoamides AB isolated by our lab targeted mitochondrial function by manipulation of mitochondrial membrane potential (18, 19).

Targeting bioenergetic balance of cancer cells is attracting significant attention as a strategy to treat cancer (52, 53). The concept of targeting mitochondria was proposed by Lan Bo Chen in the 1980s (54, 55) and was later described also by Fantin et al. (56). More recently, the interest in mitochondria as therapeutic targets have increased due to the demonstration of increased mitochondrial function in cancer stem cells (57) and the finding that quiescent tumor cells are dependent on oxidative phosphorylation (32, 52, 58). The finding that NocA is effective on MTS is consistent with the effects on mitochondrial OXPHOS. Quiescent cells in hypoxic and nutritionally compromised microenvironments in MTS are expected to show a limited metabolic plasticity and to be production, i.e., OXPHOS (52). The increased sensitivity to glucose starvation observed during NocA treatment is consistent with a state of decreased metabolic plasticity and vulnerability of energy production.

We conclude that the antiproliferative mechanism of NocA is likely to be due to mitochondrial inhibition. Whether NocA can be developed as anticancer compound is unclear. Future studies should focus on systemic toxicity of NocA, as well as on evaluation of cancer selectivity and pharmacological factors such as metabolism and distribution.

DATA AVAILABILITY

This manuscript contains previously unpublished data. The name of the repository and accession number are not available.

AUTHOR CONTRIBUTIONS

MS, VV, SL, and RU contributed to the conceptualization of the research. MS, MP, SL, and RU contributed to the formal analysis. RU and VV contributed to the funding acquisition. MS, MP, VV, SL, and RU contributed to the investigation and the development of methodology and validated the work. SL and RU provided supervision of the work. MS, SL, and RU wrote the original paper.

FUNDING

FCUP 52

Cyanobacterial bioactive metabolites for anticancer drug discovery: characterization of new compounds and molecular mechanisms in physiologically relevant 3D cell culture

REFERENCES

1. Harvey AL. Natural products in drug discovery. Drug Discov Today. (2008) 13:894–901. doi: 10.1016/j.drudis.2008.07.004

2. Kim K-W, Roh JK, Wee H-J, Kim C. Natural Product Anticancer Drugs. Cancer Drug Discovery: Science and History. Dordrecht: Springer Netherlands (2016). p. 113–34. doi: 10.1007/978-94-024-0844-7_6

3. Carter GT. Natural products and Pharma 2011: strategic changes spur new opportunities. Nat Prod Rep. (2011) 28:1783–9. doi: 10.1039/c1np00033k

4. Harvey AL, Edrada-Ebel R, Quinn RJ. The re-emergence of natural products for drug discovery in the genomics era. Nat Rev Drug Discov. (2015) 14:111– 29. doi: 10.1038/nrd4510

5. Brito Â, Gaifem J, Ramos V, Glukhov E, Dorrestein PC, Gerwick WH, et al. Bioprospecting portuguese atlantic coast cyanobacteria for bioactive secondary metabolites reveals untapped chemodiversity. Algal Res. (2015) 9:218–26. doi: 10.1016/j.algal.2015.03.016

6. Osswald J, Rellán S, Gago A, Vasconcelos V. Toxicology and detection methods of the alkaloid neurotoxin produced by cyanobacteria, anatoxin-a. Environ Int. (2007) 33:1070–89. doi: 10.1016/j.envint.2007.06.003

7. Ehrenreich IM, Waterbury JB, Webb EA. Distribution and diversity of natural product genes in marine and freshwater cyanobacterial cultures and genomes. Appl Environ Microbiol. (2005) 71:7401–13. doi: 10.1128/AEM.71.11.7401-7413.2005

8. Balaji S, Gopi K, Muthuvelan B. A review on production of poly βhydroxybutyrates from cyanobacteria to produce bio plastics. Algal Res. (2013) 2:278–85. doi: 10.1016/j.algal.2013.03.002

9. Singh RK, Tiwari SP, Rai AK, Mohapatra TM. Cyanobacteria: an emerging source for drug discovery. J Antibiotics. (2011) 64:401–12. doi: 10.1038/ja.2011.21

10. Katz J, Janik JE, Younes A. Brentuximab Vedotin (SGN-35). Clin Cancer Res.(2011) 17:6428–36. doi: 10.1158/1078-0432.CCR-11-0488

11. de Claro RA, McGinn K, Kwitkowski V, Bullock J, Khandelwal A, Habtemariam B, et al. U.S. food and drug administration approval summary: brentuximab vedotin for the treatment of relapsed hodgkin lymphoma or relapsed systemic anaplastic large-cell lymphoma. Clin Cancer Res. (2012) 18:5845–9. doi: 10.1158/1078-0432.CCR-12-1803

12. Dahms H-U, Ying X, Pfeiffer C. Antifouling potential of cyanobacteria: a mini-review. Biofouling. (2006) 22:317–27. doi: 10.1080/08927010600967261

13. Almeida JR, Correia-da-Silva M, Sousa E, Antunes J, Pinto M, Vasconcelos V, et al. Antifouling potential of Nature-inspired sulfated compounds. Sci Rep. (2017) 7:42424. doi: 10.1038/srep42424

14. Bui HTN, Jansen R, Pham HTL, Mundt S. Carbamidocyclophanes A– E, chlorinated paracyclophanes with cytotoxic and antibiotic activity from the vietnamese cyanobacterium Nostoc sp. J Nat Prod. (2007) 70:499–503. doi: 10.1021/np060324m

15. Linington RG, Edwards DJ, Shuman CF, McPhail KL, Matainaho T, Gerwick WH. Symplocamide a, a potent cytotoxin and chymotrypsin inhibitor from the marine cyanobacterium Symploca sp. J Nat Prod. (2008) 71:22–7. doi: 10.1021/np070280x

16. Simmons TL, Engene N, Ureña LD, Romero LI, Ortega-Barría E, Gerwick L, et al. Viridamides A and B, lipodepsipeptides with antiprotozoal activity from the marine cyanobacterium oscillatoria nigro-viridis. J Nat Prod. (2008) 71:1544–50. doi: 10.1021/np800110e

17. Freitas S, Martins R, Campos A, Azevedo J, Osório H, Costa M, et al. Insights into the potential of picoplanktonic marine cyanobacteria strains for cancer therapies – cytotoxic mechanisms against the RKO colon cancer cell line. Toxicon. (2016) 119:140–51. doi: 10.1016/j.toxicon.2016.05.016

18. Freitas S, Martins R, Costa M, Leão P, Vitorino R, Vasconcelos V, et al. Hierridin B isolated from a marine cyanobacterium alters VDAC1, mitochondrial activity, and cell cycle genes on HT-29 colon adenocarcinoma cells. Marine Drugs. (2016) 14:158. doi: 10.3390/md14090158

19. Ribeiro T, Lemos F, Preto M, Azevedo J, Sousa ML, Leão PN, et al. Cytotoxicity of portoamides in human cancer cells and analysis of the molecular mechanisms of action. PLoS ONE. (2017) 12:e0188817. doi: 10.1371/journal.pone.0188817

20. Sutherland RM. Cell and environment interactions in tumor microregions: the multicell spheroid model. Science. (1988) 240:177–84. doi: 10.1126/science.2451290

21. Herrmann R, Fayad W, Schwarz S, Berndtsson M, Linder S. Screening for compounds that induce apoptosis of cancer cells grown as multicellular spheroids. J Biomol Screen. (2008) 13:1–8. doi: 10.1177/1087057107310442

22. Weiswald L-B, Bellet D, Dangles-

Marie V. Spherical cancer models in tumor biology. Neoplasia. (2015) 17:1–15. doi: 10.1016/j.neo.2014.12.004

23. Hernlund E, Olofsson MH, Fayad W, Fryknäs M, Lesiak-Mieczkowska K, Zhang X, et al. The phosphoinositide 3-kinase/mammalian target of rapamycin inhibitor NVP-BEZ235 is effective in inhibiting regrowth of tumour cells after cytotoxic therapy. Eur J Cancer. (2012) 48:396–406. doi: 10.1016/j.ejca.2011.11.013

24. Voráčová K, Hájek J, Mareš J, Urajová P, Kuzma M, Cheel J, et al. The cyanobacterial metabolite nocuolin a is a natural oxadiazine that triggers apoptosis in human cancer cells. PLoS ONE. (2017) 12:e0172850. doi: 10.1371/journal.pone.0172850

25. L. Siegel R, D. Miller K, Jemal A. Cancer statistics, 2018. CA Cancer J Clin.(2018) 68:7–30. doi: 10.3322/caac.21442

26. Ramos V, Morais J, Castelo-Branco R, Pinheiro Â, Martins J, Regueiras A, et al. Cyanobacterial diversity held in microbial biological resource centers as a biotechnological asset: the case study of the newly established LEGE culture collection. J Appl Phycol. (2018) 30:1437–51. doi: 10.1007/s10811-017-1369-y

27. Kotai J. Instructions for Preparation of Modified Nutrient Solution Z8 for AlgaeNorwegian. Institute for Water Research, Blindern (1972).

28. Jiang X-R, Jimenez G, Chang E, Frolkis M, Kusler B, Sage M, et al. Telomerase expression in human somatic cells does not induce changes associated with a transformed phenotype. Nat Genet. (1999) 21:111–4. doi: 10.1038/5056

29. Wang X, Mazurkiewicz M, Hillert E-K, Olofsson MH, Pierrou S, Hillertz P, et al. The proteasome deubiquitinase inhibitor VLX1570 shows selectivity for ubiquitin-specific protease-14 and induces apoptosis of multiple myeloma cells. Sci Rep. (2016) 6:26979. doi: 10.1038/srep26979

30. Eakins J, Bauch C, Woodhouse H, Park S, Bevan S, Dilworth C, et al. A combined *in vitro* approach to improve the prediction of mitochondrial toxicants. Toxicol *In vitro*. (2016) 34:161–70. doi: 10.1016/j.tiv.2016.03.016

31. Vichai V, Kirtikara K. Sulforhodamine B colorimetric assay for cytotoxicity screening. Nat Protocols. (2006) 1:1112–6. doi: 10.1038/nprot.2006.179

32. Zhang X, Fryknäs M, Hernlund E, Fayad W, De Milito A, Olofsson MH, et al. Induction of mitochondrial dysfunction as a strategy for targeting tumour cells in metabolically compromised microenvironments. Nat Commun. (2014) 5:3295. doi: 10.1038/ncomms4295

33. Shi J, Orth JD, Mitchison T. Cell type variation in responses to antimitotic drugs that target microtubules and kinesin-5. Cancer Res. (2008) 68:3269–76. doi: 10.1158/0008-5472.CAN-07-6699

34. Brnjic S, Mazurkiewicz M, Fryknäs M, Sun C, Zhang X, Larsson R, et al. Induction of tumor cell apoptosis by a proteasome deubiquitinase inhibitor is associated with oxidative stress. Antioxid Redox Signal. (2014) 21:2271–85. doi: 10.1089/ars.2013.5322

35. Lamb J, Crawford ED, Peck D, Modell JW, Blat IC, Wrobel MJ, et al. The connectivity map: using gene-expression signatures to connect small molecules, genes, and disease. Science. (2006) 313:1929–35. doi: 10.1126/science.1132939

36. Subramanian A, Narayan R, Corsello SM, Peck DD, Natoli TE, Lu X, et al. A next generation connectivity map: L1000 platform and the first 1,000,000 profiles. Cell. (2017) 171:1437–52.e17. doi: 10.1016/j.cell.2017.10.049

37. Subramanian A, Tamayo P, Mootha VK, Mukherjee S, Ebert BL, Gillette MA, et al. Gene set enrichment analysis: a knowledge-based approach for interpreting genome-wide expression profiles. Proc Natl Acad Sci USA. (2005) 102:15545–50. doi: 10.1073/pnas.0506580102

38. Shannon P, Markiel A, Ozier O, Baliga NS, Wang JT, Ramage D, et al. Cytoscape: a software environment for integrated models of biomolecular interaction networks. Genome Res. (2003) 13:2498–504. doi: 10.1101/gr.1239303

39. Merico D, Isserlin R, Stueker O, Emili A, Bader GD. Enrichment map: a network-based method for gene-set enrichment visualization and interpretation. PLoS ONE. (2010) 5:e13984. doi: 10.1371/journal.pone.0013984

40. Pitaval A, Tseng Q, Bornens M, Théry M. Cell shape and contractility regulate ciliogenesis in cell cycle–arrested cells. J Cell Biol. (2010) 191:303–12. doi: 10.1083/jcb.201004003

41. Gross A, McDonnell JM, Korsmeyer SJ. BCL-2 family members and the mitochondria in apoptosis. Genes Dev. (1999) 13:1899–911. doi: 10.1101/gad.13.15.1899

42. Herr I, Debatin K-M. Cellular stress response and apoptosis in cancer therapy.Blood. (2001) 98:2603–14. doi: 10.1182/blood.V98.9.2603

43. Johansson K, Cebula M, Rengby O, Dreij K, Carlström KE, Sigmundsson

K, et al. Cross talk in HEK293 cells between Nrf2, HIF, and NF-κB activities upon challenges with redox therapeutics characterized with single-cell resolution. Antioxid Redox Signal. (2015) 26:229–46. doi: 10.1089/ars.2015.6419

44. Lamb J. The connectivity map: a new tool for biomedical research. Nat Rev Cancer. (2007) 7:54–60. doi: 10.1038/nrc2044

45. Vázquez CL, Colombo MI. Chapter 6 assays to assess autophagy induction and fusion of autophagic vacuoles with a degradative compartment, using monodansylcadaverine (MDC) and DQ-BSA. In: Klionsky DJ, editor. Methods in Enzymology Vol. 452. Academic Press (2009). p. 85–95.

46. Bajaj S, Asati V, Singh J, Roy PP. 1,3,4-Oxadiazoles: an emerging scaffold to target growth factors, enzymes and kinases as anticancer agents. Eur J Med Chem. (2015) 97:124–41. doi: 10.1016/j.ejmech.2015.04.051

47. Zhang X-M, Qiu M, Sun J, Zhang Y-B, Yang Y-S, Wang X-L, et al. Synthesis, biological evaluation, and molecular docking studies of 1,3,4-oxadiazole derivatives possessing 1,4-benzodioxan moiety as potential anticancer agents. Bioorg Med Chem. (2011) 19:6518–24. doi: 10.1016/j.bmc.2011.08.013

48. Mohareb RM, Schatz J. Anti-tumor and anti-leishmanial evaluations of 1,3,4- oxadiazine, pyran derivatives derived from cross-coupling reactions of β- bromo-6H-1,3,4-oxadiazine derivatives. Bioorg Med Chem. (2011) 19:2707–13. doi: 10.1016/j.bmc.2011.02.051

49. Carbone M, Li Y, Irace C, Mollo E, Castelluccio F, Di Pascale A, et al. Structure and cytotoxicity of phidianidines A and B: first finding of 1,2,4- Oxadiazole system in a marine natural product. Org Lett. (2011) 13:2516–9. doi: 10.1021/ol200234r

50. Kimball SR. Eukaryotic initiation factor eIF2. Int J Biochem Cell Biol. (1999) 31:25–9. doi: 10.1016/S1357-2725(98)00128-9

51. White E. Deconvoluting the context-dependent role for autophagy in cancer.Nat Rev Cancer. (2012) 12:401–10. doi: 10.1038/nrc3262

52. Zhang X, de Milito A, Olofsson M, Gullbo J, D'Arcy P, Linder S. Targeting mitochondrial function to treat quiescent tumor cells in solid tumors. Int J Mol Sci. (2015) 16:27313–26. doi: 10.3390/ijms161126020

53. Di Virgilio F, Sarti AC, Falzoni S, De Marchi E, Adinolfi E. Extracellular ATP and P2 purinergic signalling in the tumour microenvironment. Nat Rev Cancer. (2018) 18:601–18. doi: 10.1038/s41568-018-0037-0.

54. Bernal S, Lampidis T, McIsaac R, Chen L. Anticarcinoma activity *in vivo* of rhodamine 123, a mitochondrial-specific dye. Science. (1983) 222:169–72. doi: 10.1126/science.6623064

55. Sun X, Wong JR, Song K, Chen LB. Anticarcinoma activity of a novel drug, 3-ethyl-3'-methyl-thiatellucarbocyanine iodide (Te), a tellurium-containing cyanine targeted at mitochondria. Clin Cancer Res. (1996) 2:1335–40.

56. Fantin VR, Berardi MJ, Scorrano L, Korsmeyer SJ, Leder P. A novel mitochondriotoxic small molecule that selectively inhibits tumor cell growth. Cancer Cell. (2002) 2:29–42. doi: 10.1016/S1535-6108(02)00082-X

57. Viale A, Pettazzoni P, Lyssiotis CA, Ying H, Sánchez N, Marchesini M, et al. Oncogene ablation-resistant pancreatic cancer cells depend on mitochondrial function. Nature. (2014) 514:628–32. doi: 10.1038/nature13611

58. Wenzel C, Riefke B, Gründemann S, Krebs A, Christian S, Prinz F, et al. 3D high-content screening for the identification of compounds that target cells in dormant tumor spheroid regions. Exp Cell Res. (2014) 323:131–43. doi: 10.1016/j.yexcr.2014.01.017

Conflict of Interest Statement: The authors declare that the research was conducted in the absence of any commercial or financial relationships that could be construed as a potential conflict of interest.

Supplementary material

The Supplementary Material for thisarticle can be found online at: https://www.frontiersin.org/articles/10.3389/fonc. 2019.00224/full#supplementary-material
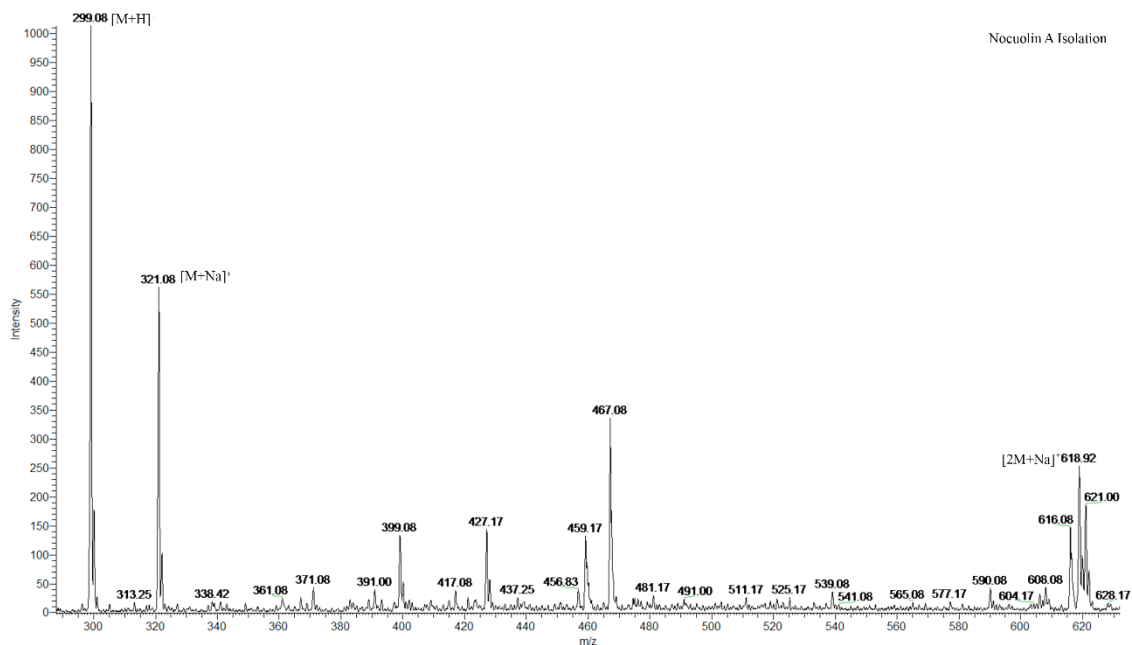
Supplementary figure 1 – HRMS spectra of Nocuolin A isolation.
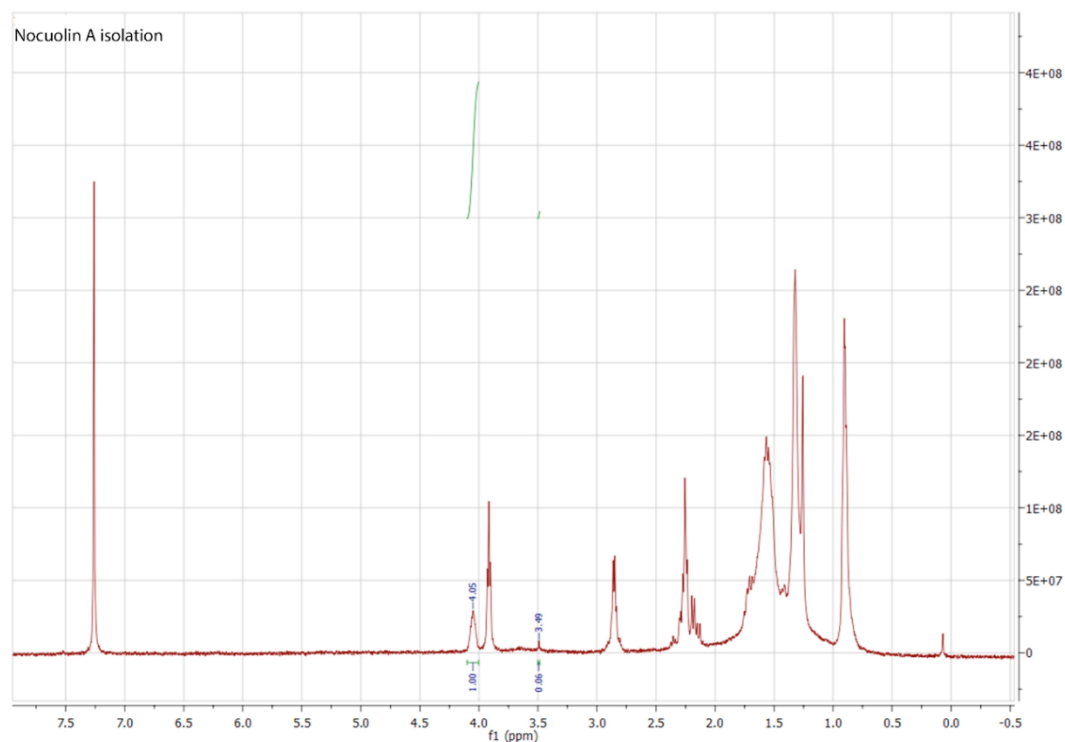
Supplementary figure 2 - 1H NMR (400 MHz) spectra of Nocuolin A isolation in chloroform-d.

MTT viability assay

a)

HCT116 non confluent vs confluent

HCT116[wt] non confluent
IC50= 1.5 μM ± 0.32

HCT116[wt] confluent
IC50= 5.0 μM ± 1.6

RPE-1 confluent vs non confluent

RPE-1[hTERT] non confluent
IC_{50} = 1.7μM ± 0.6

RPE-1[hTERT] confluent
IC_{50} > 10 μM

b)   **MCF7 cell line**

$IC_{50} = 1.6\ \mu M \pm 0.6$
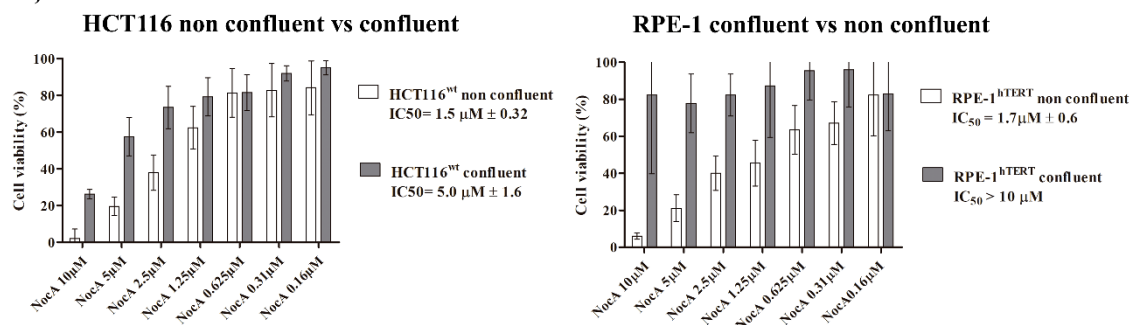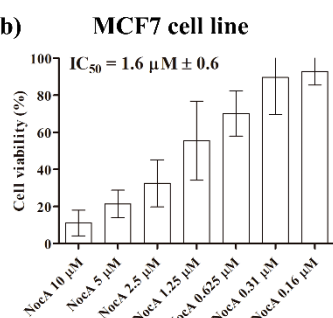
c)   **Sulforhodamine assay HCT116 cell line**

$IC_{50} = 1.9\ \mu M \pm 0.7$
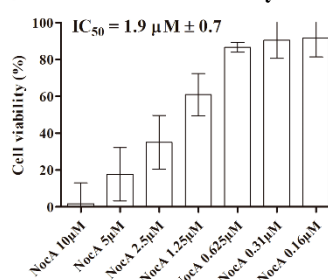
Supplementary figure 3 – Viability assays performed on the cell lines studied. Panel a) MTT viability assay performed on Monolayer HCT116 cell line and RPE-1 hTERT cell line. Left graph shows HCT116 cell cultured exhibited 80% confluence at the end of the experiment on control wells (non-confluent culture) in comparison with HCT116 cell culture at 100% confluence at the end of the experiment (confluent culture). n>3, two independent assays where the confluent and non-confluent assay were performed simultaneously. Right graph with the same assay performed on monolayer hTERT-RPE-1 cell line. n>4, three independent assays. Panel b) IC50 on MCF7 cell line based on MTT assay. n= 8, 3 independent experiments. c) Sulforhodamine viability assay confirming the MTT assay results. n>3, two independent assays.
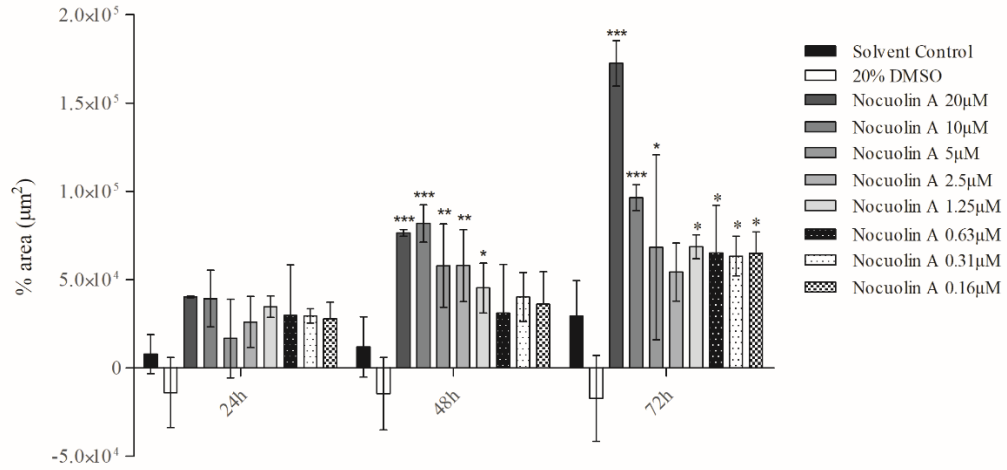
Supplementary Figure 4 - Alteration of MTS size during exposure to NocA over 72h. The measurement was performed based on the images retrieved from the IncuCyte™ ZOOM Analysis System (Essen BioScience, Inc.). The increasing size of the spheroid reveals a disaggregation of the structure due to cell death. n>3. This assay was repeated using HCT116 with red nucleus with n=6. Error bars stand for standard deviation. * $p<0.05$; ** $p<0.01$; *** $p<0.001$.
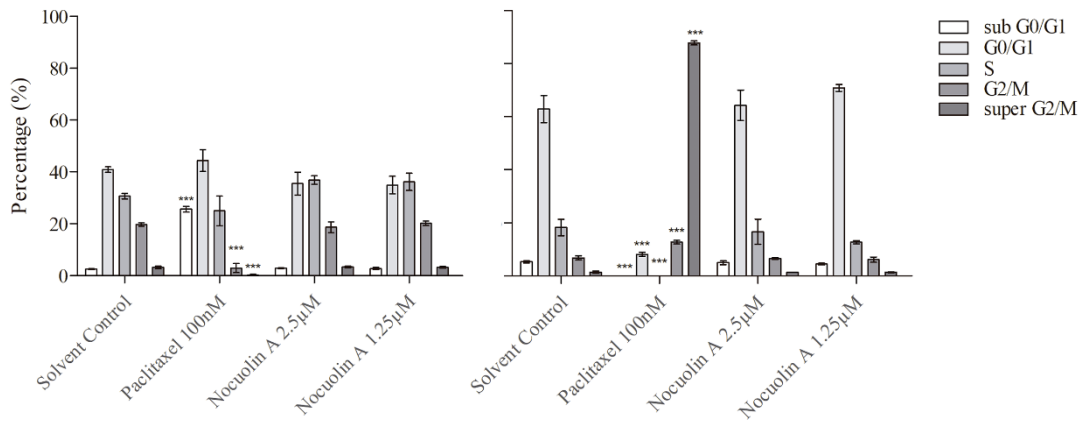
Supplementary figure 5 - Cell Cycle statistics. No significant alterations were observed on cells exposed to NocA. Error bars represent standard deviation. (*** $p<0.01$), at 24h or 48h. 10 000 events counted per gated replicate, n=3.
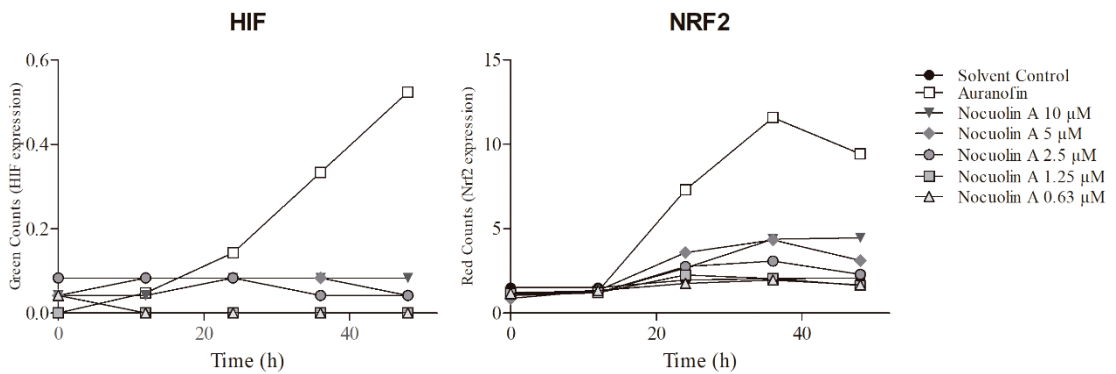
Supplementary figure 6 - NocA does not induce Nrf2 or HIF expression on HCT116 over 48h of exposure. a) Auranofin was used as positive control. b) VLX600 was used as positive control. Graphs generated by IncuCyte™ ZOOM Analysis System (Essen BioScience, Inc.). n=8.

Workspace Annotation	Count
Solvent Control	*48838*
FCCP	48030
Nocuolin A	48538
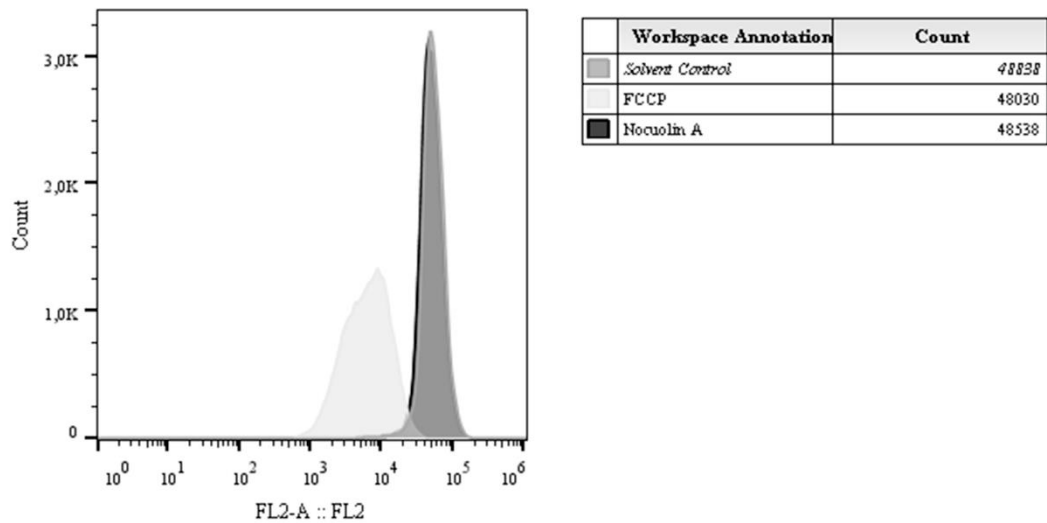
Supplementary figure 7 – TMRE flow cytometry fluorescence on polarized mitochondria. FCCP as positive control. No significant alterations on fluorescence were observed on cells exposed to NocA 7µM for 6h. 60 000 events per sample, n=2.

Supplementary table 1 - Go Terms and respective Genes ID responsible to its enrichment.

Cluster	Go Term	N.º of genes	Genes ID
Immune Response	GO_RESPONSE_TO_BACTERIUM	243	PPM1D|HLA-E|RPL39|IGHA1|HIST1H2BG|HIST1H2BJ|HIST1H2BK|HIST1H2BI|HLA-A|HIST1H2BF|HIST2H2BE|HIST1H2BC|CAV1|SEH1L|PRKCD|IL8|FCER1G|PDE4B|SYK|S100A9|XBP1|STAT5B|DAB2IP|FOS|TH|EIF2AK2|OPTN|ERAP1|RNF5|CCL2|LITAF|TLR2|NFKBIA|WASL|NFKBIB|ZC3H12A|IL27RA|VLDLR|SCARB1|ABCA1|IGHE|CCL5|CCL20|BYSL|ICAM1|IRAK1|RELA|IRAK2|PPARD|CCL3|APP|IKBKB|PRB3|PTGER3|HLA-B|P2RY2|LEAP2|LYN|PAWR|CD47|LYST|NFKB1|CD160|PLA2G2A|ANKRD1|EDN1|ANXA3|PTGER4|RAB14|HDAC2|VGF|TNIP2|JAK2|MUC5B|ANKRD17|MAPK9|BAIAP2L1|SOCS3|COCH|FN1|MR1|CEBPB|SNX3|TRAF6|ROMO1|DEFB119|VIL1|PLAC8|DROSHA|PYCARD|SERPINB9|FUCA2|TMF1|UPF1|BAIAP2|IRF3|FAS|ISG15|IL6|MAVS|TBK1|NOD1|TICAM1|CASP8|NOD2|PRKCE|TNFAIP3|MAPKAPK2|BCL10|RPS6KA3|TLR5|TNFRSF10B|MAPKAPK3|SLC11A1|JUN|PLA2G6|NFKB2|TNFRSF1A|NFKBIL1|TNFRSF18|HNRNPA0|TNFRSF21|IL1B|HLA-DRB5|TNFRSF10C|CXCL5|S100A14|CXCL1|NOTCH1|C5AR1|TNF|F3|IL23A|IL6R|ADAM17|CXCL2|RELT|LTBR|AKT1|CXCL3|TNFRSF10A|PTAFR|HMGB2|SERPINE1|HCK|CCR7|F2R|HLA-DRB1|EDNRA|TNFRSF8|PTGES|ASS1|HDAC5|CITED1|MYD88|TNFRSF11A|RIPK2|RBPJ|SRC|LIAS|CPEB1|ABL1|ALAD|CMPK2|IL18|CTR9|TGFB1|MAPK8|SRR|MAPK14|CXCL16|BCR|ABR|SPON2|AKIRIN2|MGST2|ENTPD2|NCL|OTUD5|RARA|CDC73|NRF1|PALM3|PTGER2|MALT1|ADAM9|FZD5|PRPF8|CASP3|GFI1|GCH1|SOCS1|TRIB1|CCRN4L|PTPN22|CD80|SHPK|DUSP10|ERBB2IP|PLSCR4|PELI1|NR1D1|FMO1|MTDH|SBNO2|MGST1|LOXL1|PAF1|TNFRSF11B|B2M|TSPO|THBD|NR1H3|FER|JUND|PTGFR|IRF5|CASP9|PROS1|GNG12|TFAP2A|IFNAR1|JUNB|HNRNPM|CNP|MAOB|KCNJ8|PLCG2|MAPK1|HSF1|PRDX3|CDK19|CYP1A1|TIMP4|ADH5|OGT|CYP1A2|BCL3|FOXP1|COMT|RAB1A|SIRT2|ADM
	GO_INFLAMMATORY_RESPONSE	205	HFE|SEH1L|IL8|FCER1G|PIK3CD|SYK|S100A9|EMR2|HRH1|STAT5B|GAL|DAB2IP|FOS|NFE2L2|CCL2|TLR2|ZC3H12A|CCL5|CCL20|RXRA|LIPA|ICAM1|APOL2|RELA|IRAK2|CCL26|RPS6KA5|CCL3|IKBKB|LYN|NFKB1|STAT3|CSF1R|TNIP2|CCL4|CCL22|FN1|CEBPB|RPS6KA4|ITCH|PYCARD|FFAR2|HYAL1|FAS|IL6|IKBKG|TBK1|NOD1|TICAM1|CLEC7A|CASP4|TNFAIP3|MAPKAPK2|TLR5|TNFRSF10B|TNIP1|SLC11A1|NFKB2|TNFRSF

			1A|REL|ALOX15|THBS1|TNFRSF18|HNRNPA0|ANO6|TNFRSF21|HMGB1|IL17RE|NFRKB|IL1B|PRKCZ|HLA-DRB5|ACVR1|RARRES2|TNFRSF10C|CYP4F11|SLC7A2|CXCL5|PLA2G4C|NOTCH1|CXCL1|AGER|C5AR1|LTA4H|TNF|AOX1|C3AR1|F3|IL23A|NMI|SMAD1|ITGB6|BLNK|IL6R|NFKBID|RASGRP1|SIGIRR|CSF1|EPHX2|CXCL2|RELT|LTBR|CXCL3|AKT1|TNFRSF10A|PTAFR|HMGB2|ABCF1|ADAM8|LXN|CCR7|HCK|PARP4|CCR1|CAMK1D|HMOX1|MGLL|HNRNPK|SERPINF2|UCN|F2R|HLA-DRB1|F2RL1|SNAP23|CTNNBIP1|EIF2AK1|RAC1|SERPINA1|PNMA1|AFAP1L2|PRKD1|TNFRSF8|NFX1|OGG1|NFE2L1|TOLLIP|PLAA|PRDX5|PTGES|IL4R|ADORA1|TFRC|ASS1|PXK|ECM1|ATRN|F12|MAP2K3|CYP26B1|GPR68|NAIP|HDAC5|CD97|IL1RAP|NUPR1|MYD88|F8|S1PR3|IGFBP4|B4GALT1|GSDMD|SDC1|SPHK1|NFATC4|MMP25|TNFRSF11A|SEMA7A|ANXA1|NDST1|RIPK2|RBPJ|PLSCR1|UNC13D|HDAC4|KRT16|CCR3|BCL6|XCR1|TPST1|CXCR4|BMPR1B|CCRL2|F11R|CHST1|POLB|LIAS|NOX1|ELF3|IL18|IL17C|TGFB1|BMP6|IL1RN|IL17D|SP100|AIMP1|SCG2|SPP1|C5|BMP2|TNFRSF11B|PARK7|KDM6B|GATA3|RELB
	GO_RESPONSE_TO_MOLECULE_OF_BACTERIAL_ORIGIN	180	TNFRSF18|HNRNPA0|TNFRSF21|IL1B|TNFRSF10C|CXCL5|S100A14|CXCL1|NOTCH1|C5AR1|TNF|F3|IL8|PDE4B|ADAM17|CXCL2|RELT|LTBR|XBP1|AKT1|CXCL3|PTAFR|TNFRSF10A|STAT5B|HMGB2|SERPINE1|HCK|CCR7|DAB2IP|FOS|TH|EIF2AK2|F2R|EDNRA|TNFRSF8|PTGES|ASS1|HDAC5|CCL2|CITED1|LITAF|TNFRSF11A|TLR2|RIPK2|SRC|NFKBIA|LIAS|NFKBIB|CPEB1|ABL1|ALAD|CMPK2|IL18|CTR9|MAPK8|TGFB1|SRR|ZC3H12A|MAPK14|BCR|CXCL16|ABR|SPON2|AKIRIN2|VLDLR|MGST2|ENTPD2|SCARB1|NCL|ABCA1|OTUD5|RARA|CDC73|NRF1|PALM3|PTGER2|CCL5|MALT1|ADAM9|CCL20|BYSL|FZD5|ICAM1|PRPF8|IRAK1|CASP3|GFI1|RELA|GCH1|IRAK2|SOCS1|PPARD|TRIB1|CCRN4L|CCL3|PTPN22|CD80|IKBKB|SHPK|DUSP10|ERBB2IP|PTGER3|P2RY2|PLSCR4|PELI1|LYN|PAWR|NR1D1|FMO1|NFKB1|MTDH|SBNO2|ANKRD1|MGST1|EDN1|PTGER4|LOXL1|HDAC2|TNIP2|JAK2|PAF1|TNFRSF11B|B2M|MAPK9|TSPO|THBD|SOCS3|NR1H3|FER|FN1|CEBPB|JUND|TRAF6|PTGFR|IRF5|CASP9|PROS1|GNG12|TFAP2A|PYCARD|IFNAR1|JUNB|UPF1|HNRNPM|FAS|IRF3|CNP|IL6|MAOB|KCNJ8|PLCG2|MAPK1|HSF1|PRDX3|CYP1A1|CDK19|TIMP4|ADH5|OGT|TICAM1|CASP8|CYP1A2|NOD2|PRKCE|TNFAIP3|MAPKAPK2|FOXP1|BCL10|COMT|RPS6KA3|TLR5|SIRT2|TNFRSF10B|MAPKAPK3|SLC11A1|JUN|NFKB2|TNFRSF1A|NFKBIL1|ADM

FCUP 62
Cyanobacterial bioactive metabolites for anticancer drug
discovery: characterization of new compounds and
molecular mechanisms in physiologically relevant 3D cell
culture

GO_POSITIVE_REGULATION_OF_RESPONSE_TO_EXTERNAL_STIMULUS	157		BMPR2|THBS1|MAPK13|SUPT5H|SQSTM1|CALCOCO2|EPM2A|SCOC|LARP1|RALB|PIP4K2C|OSMR|SNX4|PUM1|GPRC5B|VAMP8|RAB12|BNIP3|LRSAM1|CLOCK|IL17RB|ZP3|PIP4K2B|ZC3HAV1|ATG7|FKBP1B|NPY5R|USF1|ANO6|WDFY3|HMGB1|DAPK2|AMBRA1|IL1B|KIAA1324|RAB3GAP1|WAC|VEGFB|PUM2|RARRES2|ADORA2B|BNIP3L|CXCL12|NDEL1|CXCL5|DDX60|S100A14|SNW1|CXCL1|CALR|RAB3GAP2|AGER|C5AR1|PAFAH1B2|TNF|PIP4K2A|C3AR1|PDGFB|F3|IL8|IL23A|FCER1G|SWAP70|F7|CD74|IL6R|ADAM17|CSF1|S100A9|CXCL2|VEGFC|EDN2|CXCL3|FIGF|STAT5B|IL17RA|ADAM8|RPS19|SERPINE1|CCR7|CCR1|CAMK1D|GAS6|CXCL14|SERPINF2|TRPV4|ITGA2|PTK2B|F2RL1|EDNRA|RAC1|VEGFA|ADAM10|PRKD1|HSPB1|F12|CCL2|PRKCA|TNFRSF11A|TLR2|RIPK2|CREB3|IL18|TGFB1|BMP6|TIAM1|FGF18|BECN1|SH3GLB1|AKT2|SMAD3|STX3|ARTN|PRKD2|CCL5|PPM1F|STX4|MET|FGFR1|MEGF8|DSCAM|SCG2|CCL26|CCL3|PTGER3|SASH1|CD47|SLIT2|PLA2G2A|PTGER4|JAK2|IL6ST|ANKRD17|CCL4|THBD|SIRT1|PARK7|FN1|TRAF6|FFAR2|IL6|TBK1|CDK19|NOD1|SPTLC2|NOD2|TRIM13|BRAF|SPTLC1|NRP1|ATG5|TNIP1|SEMA5A|LPAR1|ULK1|GBA|TNFRSF1A
GO_CELLULAR_RESPONSE_TO_BIOTIC_STIMULUS	101		IL1B|TXNIP|HSPA5|TNF|IL8|PDE4B|SYK|WFS1|MUS81|FBXO18|SLX4|XBP1|AKT1|PTAFR|HMGB2|SERPINE1|HCK|DAB2IP|EIF2AK3|ASS1|CCL2|HDAC5|LITAF|TLR2|RIPK2|SRC|DDIT3|NFKBIA|NFKBIB|CPEB1|ABL1|IL18|CMPK2|CTR9|TGFB1|MAPK8|ZC3H12A|MAPK14|CXCL16|SPON2|VLDLR|ENTPD2|SCARB1|NCL|ABCA1|RARA|CDC73|TP53|CCL5|ADAM9|CCL20|FZD5|BYSL|PRPF8|ICAM1|IRAK1|GFI1|RELA|IRAK2|PPARD|PTPN22|CCL3|CD80|SHPK|PTGER3|P2RY2|PLSCR4|LYN|NR1D1|NFKB1|MTDH|ANKRD1|SBNO2|TNIP2|PAF1|B2M|TSPO|MAPK9|NR1H3|FN1|CEBPB|TRAF6|PYCARD|HNRNPM|UPF1|IRF3|IL6|PPP1R15B|MAPK1|GSK3B|ATG10|CDK19|OGT|TICAM1|PRKCE|CLEC7A|TNFAIP3|APAF1|TLR5|SIRT2|NFKBIL1
GO_REGULATION_OF_LEUKOCYTE_MIGRATION	84		THBS1|BCR|CYP19A1|ABR|CCL28|CCL5|CCL20|ICAM1|CCL3|ZP3|FADD|TNFRSF18|PTGER3|ANO6|C5|PADI2|HMGB1|PAWR|LYN|DAPK2|MPP1|IL1B|SLIT2|LGALS3|VEGFB|RARRES2|MIA3|CXCL12|PTGER4|CXCL5|S100A14|ADA|CXCL1|CALR|CCL4|C5AR1|TNF|C3AR1|IL23A|IL8|SWAP70|F7|CD74|IL6R|ADAM17|ITGA2B|PYCARD|CSF1|CXCL2|VEGFC|EDN2|CXCL3|IL6|PTAFR|PLCB1|FIGF|ADAM8|SERPINE1|CCR7|CCR1|CAMK1D|HMOX1|GAS6|CXCL14|MADCAM1|TRPV4|ITGA2|PTK2B|F2RL1|EDNRA|KITLG|RAC1|VEGFA|ADAM10|ADORA1|ECM1|CCL2|ANXA1|CREB3|HOXA7|APOD|WASL|P2RY12|STK10

GO_CELL_CHEMOTAXIS	79	CXCL16|CCL28|CCL5|CCL20|SCG2|CCL26|CCL3|ANO6|HMGB1|C5|IL1B|TGFB2|LYST|LGALS3|EDN1|CXCL12|CXCL5|CXCL1|PRKCD|CCL4|C5AR1|CCL22|PDGFB|IL8|GBF1|FCER1G|PDE4B|PIK3CD|IL6R|SYK|PREX1|S100A9|FFAR2|CXCL2|EMR2|NUP85|EDN2|PIP5K1C|IL6|CXCL3|HRH1|HMGB2|ADAM8|IL17RA|RPS19|CCR7|VAV1|CCR1|VAV3|GAS6|CXCL14|RAC1|VEGFA|LEF1|SBDS|CORO1A|TRPM4|PIP5K1A|ARHGEF16|BCAR1|ENG|CCL2|EPHA2|NRP1|BIN2|EGR3|RHOG|PARVA|RAB13|SEMA5A|NR4A1|DOCK4|HBEGF|TNFRSF11A|ELMO2|ANXA1|LPAR1|ARRB2|CXCR4	
GO_CYTOKINE_ACTIVITY	73	IL18|IL17C|TGFB1|TIMP1|BMP8B|CXCL16|CTF1|BMP6|CMTM8|CCL28|THNSL2|AREG|IL1RN|TNFSF13B|TNFSF10|BMP8A|IL17D|BMP4|CCL5|SP100|CMTM4|CCL20|AIMP1|TXLNA|TGFB3|SCG2|CMTM3|GDF15|CCL26|CRLF1|IL7|CCL3|LTB|SPP1|IL32|BMP1|INHBE|HMGB1|C5|LIF|IL1B|TGFB2|IL11|BMP2|BMP7|EDN1|GRN|CXCL12|INHBB|CXCL5|TNFRSF11B|CMTM7|CXCL1|CCL4|TNF|CCL22|IL8|IL23A|CSF1|CXCL2|IL6|CXCL3|CXCL14|KITLG|VEGFA|CCL2|TNFSF9|CMTM6|NAMPT|SECTM1|FAM3C|INHA|GDF11	
GO_POSITIVE_REGULATION_OF_CHEMOTAXIS	72	BMPR2|TGFB1|THBS1|TIAM1|FGF18|AKT2|SMAD3|STX3|ARTN|PRKD2|CCL5|PPM1F|STX4|MET|FGFR1|MEGF8|DSCAM|SCG2|CCL3|ANO6|HMGB1|DAPK2|IL1B|SLIT2|VEGFB|RARRES2|CXCL12|CXCL5|S100A14|CALR|CXCL1|CCL4|C5AR1|PDGFB|C3AR1|FN1|F3|IL8|IL23A|SWAP70|F7|CD74|IL6R|ADAM17|CSF1|CXCL2|VEGFC|EDN2|CXCL3|IL6|FIGF|SERPINE1|CCR7|CCR1|CAMK1D|GAS6|CXCL14|TRPV4|ITGA2|PTK2B|F2RL1|EDNRA|RAC1|VEGFA|ADAM10|PRKD1|HSPB1|CCL2|NRP1|SEMA5A|LPAR1|CREB3	
GO_CELL_ACTIVATION_INVOLVED_IN_IMMUNE_RESPONSE	71	STXBP3|EIF2AK4|ICAM1|MLH1|NR4A3|NBN|VAMP8|CCL3|ERCC1|TSC1|EOMES|LIG4|HMGB1|LYN|MSH2|SBNO2|ANXA3|PTGER4|RNF8|RNF168|RC3H1|EXOSC6|ADA|EXO1|GBF1|FCER1G|SWAP70|PIK3CD|RORA|SYK|RASGRP1|PYCARD|IL6|PLCG2|PTK2B|F2RL1|SNAP23|TICAM1|SEMA4A|PRKCE|ATP7A|CLEC7A|GATA3|BCL3|HSPD1|LEF1|STAT6|RORC|BATF|ZFPM1|RELB|FOXP1|CORO1A|RC3H2|PI4K2A|LAT2|GATA2|PLA2G3|ITFG2|LFNG|NOTCH2|RAB27A|LGALS1|SLC11A1|LCP1|RPS6|PSEN1|DLL1|UNC13D|C8ORF4|ABL1	
GO_ADAPTIVE_IMMUNE_RESPONSE_BASED_ON_SOMATIC_RECOMBINATION_OF_IMMUNE_RECEPTORS_BUILT_FROM_IMMUNO	69	IL18|TGFB1|IGHA1|SLA2|BTN3A2|IGHE|MASP2|C8G|CTSH|MLH1|ICAM1|CD46|HLA-DQB1|NBN|JAG1|HRAS|DLG1|EMP2|SUSD4|ZP3|ERCC1|GNL1|CTSC|HMGB1|LIG4|C5|DENND1B|BTN3A3|MSH2|HLA-DRB5|CD8A|CADM1|CD55|RNF8|RNF168|EXOSC6|MICB|PRKCD|EXO1|C3AR1|SWAP70|FCER1G|TRAF6|CD74|RORA|ADAM17|FAS|IL6|HLA-	

FCUP | 64

Cyanobacterial bioactive metabolites for anticancer drug discovery: characterization of new compounds and molecular mechanisms in physiologically relevant 3D cell culture

GLOBULIN_SUPERFAMILY_DOMAINS		DRB1|RFTN1|SEMA4A|GATA3|HSPD1|BCL3|LEF1|CLU|STAT6|RORC|BATF|IL4R|FOXP3|RELB|BCL10|IRF7|RAB27A|SLC11A1|UNC13D|BCL6|NFKB2
GO_RESPONSE_TO_INTERLEUKIN_1	66	ZC3H12A|VLDLR|CCL5|IL1R1|CCL20|BYSL|ICAM1|IRAK1|SOX9|RELA|IRAK2|CCL26|RPS6KA5|CCL3|PPP4C|IKBKB|RBMX|PTGER3|P2RY2|PAWR|EGR1|NFKB1|PSMB9|ANKRD1|EDN1|PTGER4|TNIP2|RC3H1|MAPK9|CCL4|CCL22|FN1|CEBPB|IL8|TRAF6|RPS6KA4|KLF2|RORA|HSPA9|PYCARD|NKX3-1|HYAL1|UPF1|FAS|IL6|PLCB1|FIGF|DAB2IP|CCL2|TAF9|CITED1|IGBP1|MYD88|PRKCI|PRKCA|YTHDC2|AES|CREBBP|SPHK1|HNMT|TNFRSF11A|ANXA1|RIPK2|SRC|MTHFR|HDAC4
GO_POSITIVE_REGULATION_OF_LEUKOCYTE_MIGRATION	64	THBS1|CCL5|CCL20|ICAM1|CCL3|ZP3|FADD|TNFRSF18|ANO6|PTGER3|HMGB1|DAPK2|PAWR|IL1B|LGALS3|VEGFB|RARRES2|MIA3|CXCL12|PTGER4|CXCL5|S100A14|CXCL1|CALR|CCL4|C5AR1|TNF|C3AR1|IL23A|IL8|SWAP70|F7|CD74|IL6R|ADAM17|PYCARD|ITGA2B|CSF1|CXCL2|VEGFC|EDN2|IL6|CXCL3|PTAFR|FIGF|ADAM8|SERPINE1|CCR7|CCR1|CAMK1D|GAS6|CXCL14|MADCAM1|TRPV4|ITGA2|PTK2B|F2RL1|EDNRA|KITLG|RAC1|VEGFA|ADAM10|CCL2|CREB3
GO_REGULATION_OF_B_CELL_ACTIVATION	55	PPP2R3C|MMP14|NDFIP1|TGFB1|NFATC2|CDKN1A|APLF|BCL2|ATM|IL27RA|CD81|SUPT6H|IGHA1|PCID2|SLC39A10|MZB1|ATP11C|TNFSF13B|TCF3|UNG|WHSC1|SLA2|IGHE|PTPN6|AHR|PKN1|ID2|CASP3|BANK1|PAXIP1|CDKN2A|THOC1|IL7|TNFRSF21|PAWR|PELI1|LYN|TNIP2|ADA|RC3H1|CD74|SYK|XBP1|FAS|IL6|STAT5B|VAV3|TICAM1|NOD2|STAT6|TNFAIP3|FOXP3|BCL6|INHA|IRS2
GO_REGULATION_OF_LEUKOCYTE_CHEMOTAXIS	52	THBS1|CYP19A1|CCL5|CCL3|ANO6|PADI2|HMGB1|C5|LYN|DAPK2|IL1B|MPP1|SLIT2|VEGFB|RARRES2|CXCL12|CXCL5|S100A14|CXCL1|CALR|C5AR1|CCL4|C3AR1|IL23A|IL8|SWAP70|F7|CD74|IL6R|ADAM17|CSF1|CXCL2|VEGFC|EDN2|IL6|CXCL3|FIGF|SERPINE1|CCR7|CCR1|CAMK1D|GAS6|CXCL14|TRPV4|PTK2B|F2RL1|EDNRA|RAC1|VEGFA|ADAM10|CCL2|CREB3
GO_HUMORAL_IMMUNE_RESPONSE	50	BCL2|HLA-E|RPL39|SPON2|IGHA1|HIST1H2BG|HIST1H2BJ|HIST1H2BK|HIST1H2BI|HLA-A|HIST1H2BF|HIST2H2BE|HIST1H2BC|IGHE|MASP2|C8G|CD46|HLA-DQB1|IL7|SUSD4|ZP3|APP|TNFRSF21|C5|HLA-DRB5|CD55|B2M|NOTCH1|EXO1|TNF|BLNK|IL6|TRAF3IP2|TFE3|ST6GAL1|MNX1|PAX

			5|CFD|YTHDF2|TFEB|CD83|HLA-DRB1|BST2|GATA3|BCL3|CLU|CCL2|RBPJ|PLA2G6|ADM
GO_MYELOID_LEUKOCYTE_ACTIVATION	49		TGFB1|STXBP3|CCL5|ADAM9|NR4A3|VAMP8|CCL3|HMGB1|LYN|SBNO2|ANXA3|SLC7A2|PRKCD|IL8|TRAF6|FCER1G|JMJD6|PIK3CD|SYK|PYCARD|PREX1|RASGRP1|CSF1|LTBR|EDN2|SNAP23|F2RL1|TICAM1|ADAM10|PRKCE|CLU|BATF|RELB|FOXP1|NDRG1|LCP2|CRTC3|PI4K2A|LAT2|GATA2|TGFBR2|PLA2G3|DHRS2|RHOH|SLC11A1|PSEN1|JUN|RBPJ|TNFSF9
GO_CELLULAR_RESPONSE_TO_INTERLEUKIN_1	48		ZC3H12A|DAB2IP|VLDLR|CCL5|IL1R1|CCL20|BYSL|ICAM1|IRAK1|SOX9|RELA|IRAK2|CCL26|RPS6KA5|CCL3|PPP4C|IKBKB|RBMX|PTGER3|P2RY2|PAWR|CCL2|EGR1|NFKB1|PSMB9|ANKRD1|EDN1|PTGER4|TNIP2|RC3H1|MAPK9|CCL4|CCL22|FN1|IL8|CEBPB|TRAF6|RPS6KA4|KLF2|RORA|HSPA9|PYCARD|NKX3-1|HYAL1|UPF1|FAS|IL6|PLCB1
GO_REGULATION_OF_CYTOKINE_BIOSYNTHETIC_PROCESS	47		HMOX1|THBS1|UBE2J1|TICAM1|HSPB1|TNFRSF8|GATA3|BCL3|CCL20|IGF2BP1|FOXP3|RELA|MAPKAPK2|ZNF287|ZFPM1|LAG3|GLMN|ASB1|EREG|MAST2|IRF1|LTB|MAP2K5|CD276|BCL10|CD80|ERRFI1|CEBPG|MAP2K3|RNF128|IGF2BP2|TRIB2|IL1B|NFKB1|KLF4|INHBB|TNF|CEBPB|NMI|TRAF6|SYK|SIGIRR|IL6|PTAFR|STAT5B|INHA|TBK1
GO_POSITIVE_REGULATION_OF_LEUKOCYTE_CHEMOTAXIS	46		CCR1|CAMK1D|GAS6|CXCL14|THBS1|TRPV4|PTK2B|F2RL1|EDNRA|RAC1|VEGFA|ADAM10|CCL5|CCL3|ANO6|HMGB1|CCL2|DAPK2|IL1B|VEGFB|RARRES2|CXCL12|CXCL5|S100A14|CXCL1|CALR|C5AR1|CCL4|C3AR1|IL23A|IL8|SWAP70|F7|CD74|IL6R|ADAM17|CSF1|CXCL2|VEGFC|CREB3|EDN2|IL6|CXCL3|FIGF|SERPINE1|CCR7
GO_MYELOID_LEUKOCYTE_MIGRATION	44		VAV3|RAC1|VEGFA|CCL5|CCL20|SCG2|CCL26|CCL3|CCL2|DAPK2|TGFB2|IL1B|LGALS3|EDN1|CCL4|C5AR1|JAGN1|CCL22|TNFRSF11A|PDGFB|ANXA1|GBF1|IL8|FCER1G|PDE4B|MITF|PIK3CD|IL6R|SYK|PREX1|S100A9|IRAK4|EMR2|EDN2|NUP85|CXCL3|PIP5K1C|IL6|HRH1|STAT5B|IL17RA|RPS19|CCR7|VAV1
GO_GRANULOCYTE_MIGRATION	34		VAV3|VEGFA|CCL5|CCL20|SCG2|CCL26|CCL3|CCL2|DAPK2|IL1B|TGFB2|LGALS3|EDN1|C5AR1|CCL4|CCL22|JAGN1|IL8|ANXA1|GBF1|FCER1G|PDE4B|PIK3CD|SYK|PREX1|S100A9|IRAK4|EMR2|EDN2|PIP5K1C|CXCL3|HRH1|IL17RA|VAV1
GO_POSITIVE_REGULATION_OF_MYELOID_LEUKOCYTE_DIFFERENTIATION	34		CCR1|OGT|FOS|CA2|RIPK1|RUNX1|ACIN1|CD101|CTNNBIP1|ATP6AP1|KITLG|TMEM64|CASP8|HAX1|GNAS|TESC|RB1|PPARGC1B|CCL5|LEF1|ID2|TRIB1|FADD|GPR68|CREB1|KLF10|LIF|CSF1R|PRKCA|TNF|IL23A|TRAF6|JUN|CSF1

GO_POSITIVE_REGULATION_OF_B_CELL_ACTIVATION		32	VAV3|PPP2R3C|MMP14|TGFB1|CDKN1A|NFATC2|BCL2|CD81|IGHA1|PCID2|SLC39A10|TICAM1|ATP11C|TCF3|TNFSF13B|UNG|NOD2|WHSC1|IGHE|STAT6|PAXIP1|IL7|PELI1|TNIP2|ADA|CD74|BCL6|SYK|XBP1|IL6|STAT5B|IRS2
GO_RESPONSE_TO_ANTIBIOTIC		31	SKIL|CYP1A1|CDKN1B|UQCRFS1|PLA2G4F|PPP2CB|SLC9A1|CASP8|TP53|CASP3|HSP90AA1|EP300|CCL2|IL1B|HSPA5|PPP1R15A|JAK2|SOD1|CASP9|MDM2|JAK1|HYAL1|ID1|UROS|IL6|HMBS|CYB5R4|RAB10|RSRC1|ZC3H8|ENDOG
GO_ACUTE_INFLAMMATORY_RESPONSE		30	HNRNPK|SERPINF2|HFE|CTNNBIP1|EIF2AK1|SERPINA1|IL1RN|GATA3|OGG1|ICAM1|PTGES|APOL2|TFRC|ASS1|F12|ANO6|IL1B|NUPR1|STAT3|F8|ACVR1|B4GALT1|FN1|CEBPB|F3|PLSCR1|IL6R|SIGIRR|IL6|STAT5B
GO_T_CELL_ACTIVATION_INVOLVED_IN_IMMUNE_RESPONSE		28	F2RL1|SEMA4A|ATP7A|EIF2AK4|GATA3|BCL3|LEF1|STAT6|RORC|ICAM1|BATF|ZFPM1|RELB|FOXP1|RC3H2|TSC1|EOMES|HMGB1|PTGER4|RC3H1|RAB27A|SLC11A1|LCP1|RPS6|PSEN1|FCER1G|RORA|IL6
GO_POSITIVE_REGULATION_OF_CYTOKINE_BIOSYNTHETIC_PROCESS		25	HMOX1|THBS1|TICAM1|TNFRSF8|HSPB1|BCL3|CCL20|MAPKAPK2|RELA|ZFPM1|GLMN|EREG|IRF1|LTB|CD80|BCL10|CD276|CEBPG|IL1B|TNF|TRAF6|SYK|PTAFR|STAT5B|TBK1
GO_CHEMOKINE_RECEPTOR_BINDING		25	CXCL14|CXCL16|CCL28|CCL5|CCL20|CCL26|CCL3|C5|CCL2|STAT3|CXCL12|CXCL5|S100A14|CXCL1|CCL4|CCL22|IL8|CNIH4|ITCH|YARS|JAK1|CCRL2|CXCL2|CREB3|CXCL3
GO_REGULATION_OF_GRANULOCYTE_CHEMOTAXIS		23	CAMK1D|CCL2|DAPK2|MPP1|THBS1|IL1B|SLIT2|TRPV4|RARRES2|EDNRA|S100A14|RAC1|CXCL1|C5AR1|C3AR1|IL23A|IL8|CCL5|CD74|CSF1|CXCL2|CXCL3|CCR7
GO_CHEMOKINE_MEDIATED_SIGNALING_PATHWAY		21	CCR1|CCL2|PTK2B|CXCL12|CXCL5|CXCL1|CCL4|CCL22|IL8|CCL5|CCL20|CCR3|XCR1|CXCR4|CCRL2|CXCL2|CIB1|CXCL3|CCL26|CCL3|CCR7
GO_CD4_POSITIVE_ALPHA_BETA_T_CELL_ACTIVATION		21	HMGB1|PTGER4|RC3H1|SEMA4A|CEBPB|ATP7A|GATA3|BCL3|RORA|LEF1|STAT6|RORC|BATF|FOXP3|ZFPM1|BRAF|IL6|RELB|FOXP1|STOML2|RC3H2
GO_T_CELL_DIFFERENTIATION_INVOLVED_IN_IMMUNE_RESPONSE		20	EOMES|HMGB1|PTGER4|RC3H1|SEMA4A|FCER1G|ATP7A|GATA3|BCL3|LEF1|RORA|STAT6|RORC|BATF|ZFPM1|RELB|IL6|FOXP1|RC3H2|TSC1

	GO_CHEMOKINE_ACTIVITY	17	C5|CCL2|CXCL14|CXCL16|CXCL12|CXCL5|CCL28|CXCL1|CCL4|CCL22|IL8|CCL5|CCL20|CXCL2|CCL26|CXCL3|CCL3
	GO_ANTIMICROBIAL_HUMORAL_RESPONSE	17	HLA-E|RPL39|SPON2|IGHA1|HIST1H2BG|B2M|HIST1H2BJ|HIST1H2BK|HIST1H2BI|HLA-A|HIST1H2BF|HIST2H2BE|HIST1H2BC|BCL3|PLA2G6|ADM|APP
Response to Starvation	GO_CELLULAR_RESPONSE_TO_EXTERNAL_STIMULUS	185	PPM1D|BMPR2|DEPDC5|CDKN1A|HFE|GLUL|WDR59|MAX|RRAGB|AKR1C3|SRD5A1|NPRL3|WRN|EIF2AK4|MAP1LC3B|RALB|ZFYVE1|FOSL1|WNT4|FBXO22|GCN1L1|PRKAA1|SLC38A2|COL1A1|RNF152|RRAGC|BNIP3|GLRX2|UCP2|CAV1|WDR24|FADD|ATG7|USF1|USP33|RRAGA|IL1B|KIAA1324|SEH1L|ADORA2B|HSPA5|ADNP|MAG|CYP24A1|CASP8AP2|ITGB1|NCOA1|MDM2|CRADD|KCNJ4|CDKN2B|IGF2|SIPA1|LTBR|XBP1|CCNE1|AKT1|HABP4|TNFRSF10A|NR4A2|BAK1|ATP2B1|FZD1|PIM1|BAG3|BRIP1|EIF2S1|HMOX1|KIF26A|GAS6|TXN2|USF2|SLC9A1|ATP1A1|FOS|EIF2AK2|ITGA6|CHMP1A|ITGA2|EIF2AK3|CBS|VDR|MAP2K4|EDNRA|PDK2|RAC1|MAP3K2|PRDM4|MTPN|NPPA|TNFRSF8|RPTOR|NUDT1|ATF4|CNN2|PPP1R9B|SKP2|HDAC7|ASNS|SRF|HSPA8|BHLHA15|NFE2L2|TBL2|MYD88|MTOR|PPP1R15A|GSDMD|SPHK1|FOLR1|ATF3|HDAC4|PMAIP1|PIK3C3|PIK3R4|ATG14|RRP8|MAPK8|ZC3H12A|BCL2|UPP1|MTMR3|IMPACT|BMP6|VLDLR|SLC2A1|PICK1|BECN1|SH3GLB1|MYBBP1A|NUAK2|CPEB4|TP53|BMP4|CCL5|ICAM1|SOX9|IRF1|TSC1|LYN|PAWR|NFKB1|ANKRD1|GADD45A|PTGER4|INHBB|SIRT1|FAS|GSK3B|CTSB|MAP3K1|CASP8|CTNNB1|CASP2|AIFM1|BCL10|SLC39A4|COMT|NPRL2|KLF10|DNAJC15|TLR5|SIRT2|FADS1|ATG5|TNFRSF10B|GAS2L1|DSC2|PPARG|FOXO1|ULK1|JUN|CADPS2|GBA|GABARAPL1|SREBF1|RRAGD|PDK4|SREBF2|MIOS|TNFRSF1A|DAP|GABARAPL2|MAP3K14|EHMT2
	GO_RESPONSE_TO_STARVATION	111	PPM1D|BMPR2|DEPDC5|CDKN1A|SLC18A2|HFE|GLUL|WDR59|MAX|RRAGB|AKR1C3|SRD5A1|ZFP36|NPRL3|ADSSL1|WRN|EIF2AK4|BDH1|MAP1LC3B|RALB|ZFYVE1|HDDC3|WNT4|FBXO22|PRKAA1|GCN1L1|SLC38A2|RNF152|RRAGC|TBC1D5|UCP2|CAV1|WDR24|ATG7|AACS|USP33|RRAGA|KIAA1324|SEH1L|HSPA5|XBP1|EIF2S1|GAS6|EIF2AK2|EIF2AK3|ATF4|ASNS|HSPA8|BHLHA15|NFE2L2|TBL2|PPP1R15A|SPHK1|DDIT3|ATF3|PMAIP1|PIK3C3|PIK3R4|ATG14|RRP8|ZC3H12A|BCL2|UPP1|MTMR3|IMPACT|VLDLR|SLC2A1|PICK1|BECN1|SH3GLB1|MYBBP1A|NUAK2|CPEB4|TP53|INHBB|SIRT1|SLC39A4|COMT|NPRL2|KLF10|DNAJC15|ACADS|HMGCL|SIRT2|FADS1|DHODH|ATG5|GAS2L1|DSC2|PPARG|BCAS3|GNPAT|ULK2|FOXO1|ULK1|JUN|CADPS2|GBA|GABARA

			PL1|SREBF1|RRAGD|PDK4|SREBF2|LRP11|MIOS|DAP|OXCT1|ADM|GABARAPL2|ACAT1|EHMT2
	GO_CELLULAR_RESPONSE_TO_STARVATION	91	PPM1D|PIK3R4|BMPR2|ATG14|DEPDC5|RRP8|CDKN1A|ZC3H12A|BCL2|HFE|UPP1|MTMR3|GLUL|IMPACT|WDR59|VLDLR|MAX|SLC2A1|RRAGB|PICK1|AKR1C3|BECN1|SRD5A1|SH3GLB1|MYBBP1A|NPRL3|NUAK2|CPEB4|WRN|EIF2AK4|TP53|MAP1LC3B|RALB|ZFYVE1|WNT4|FBXO22|PRKAA1|GCN1L1|SLC38A2|RNF152|RRAGC|UCP2|CAV1|WDR24|ATG7|USP33|RRAGA|KIAA1324|SEH1L|INHBB|HSPA5|SIRT1|XBP1|EIF2S1|GAS6|EIF2AK2|EIF2AK3|ATF4|ASNS|HSPA8|BHLHA15|SLC39A4|COMT|NPRL2|NFE2L2|KLF10|DNAJC15|TBL2|SIRT2|FADS1|ATG5|PPP1R15A|GAS2L1|DSC2|SPHK1|FOXO1|JUN|CADPS2|GBA|ATF3|GABARAPL1|SREBF1|RRAGD|PDK4|SREBF2|MIOS|DAP|GABARAPL2|PMAIP1|EHMT2|PIK3C3
	GO_MONOSACCHARIDE_TRANSPORT	34	SESN2|HK2|SLC2A13|STXBP3|EZR|FABP5|KLF15|YES1|SLC23A1|SORBS1|SLC2A1|EDNRA|G6PC3|DRD1|BRAF|PPARD|TSC1|EDN1|VIL1|HK1|PLS1|SLC2A10|M6PR|SLC2A4|SLC26A5|SLC2A6|SLC2A12|AKT1|STXBP4|SLC23A2|SLC37A4|SORT1|HNF1A|SLC2A8
	GO_NUCLEOTIDE_SUGAR_METABOLIC_PROCESS	30	GNPNAT1|SLC35A3|UGDH|MGAT1|FUT8|CSGALNACT1|GMDS|RENBP|GUK1|PGM3|GALT|UXS1|GMPPB|GNE|UGP2|TGDS|PMM1|UGGT2|UAP1L1|GFPT1|NAGK|SLC35D1|MPI|UGGT1|DPM1|TSTA3|GFPT2|EXTL2|UAP1|DPAGT1
	GO_CELLULAR_RESPONSE_TO_GLUCOSE_STARVATION	28	PIK3R4|ATG14|RRP8|ZC3H12A|BCL2|UPP1|MTMR3|EIF2AK3|IMPACT|VLDLR|SLC2A1|PICK1|BECN1|SH3GLB1|MYBBP1A|NUAK2|CPEB4|ATF4|TP53|ASNS|PRKAA1|BHLHA15|NFE2L2|TBL2|HSPA5|XBP1|PMAIP1|PIK3C3
	GO_GLUTAMATE_RECEPTOR_BINDING	26	FUS|SHANK2|DNM3|GNAS|HOMER1|CTNNB1|FLOT2|OPHN1|IL1R1|CALM1|FLOT1|GRIN1|NETO2|CANX|DLG4|CALM3|DLG1|SHANK3|ESR1|SYNDIG1|DLG2|DLG3|RAB4A|HOMER2|GSK3B|DRD2
ER Stress	GO_RESPONSE_TO_ENDOPLASMIC_RETICULUM_STRESS	191	RNF185|FBXO6|ALOX15|THBS1|SRPX|USP13|TMEM67|MAP3K5|SELK|UFC1|EEF2|TMBIM6|ATP2A1|ITPR1|STT3B|SEL1L|EIF2AK4|OS9|TXNDC11|HM13|UBE2J2|FBXO2|FLOT1|PDIA4|RNF139|UBE2G2|NRBF2|PSMC6|PIK3R2|VAPB|EP300|CREB3L2|ERN1|LMNA|ANKZF1|DNAJB9|HERPUD1|PREB|TATDN2|HSPA5|ATXN3|CALR|ARFGAP1|ERO1L|ATP6V0D1|IL8|ACADVL|EDEM1|CTH|SRPR|HSP90B1|WFS1|STC2|CCND1|VCP|XBP1|DNAJB11|SEC63|BAK1|SRPRB|UFD1L|STUB1|EIF2S1|KLHDC3|AMFR|DAB2IP|PARP16|EIF2AK2|DERL2|EIF2AK3|HDGF|DERL1|TLN1|BAX|FKBP14|SDF2L1|DNAJC3|PPP2R5B|ATF4|RNF5|CXXC1|SERP1|ASNS|DDX11|GFPT1|HYOU1|PTPN1|MBTPS2|TPP1|WIPI

FCUP 69
Cyanobacterial bioactive metabolites for anticancer drug
discovery: characterization of new compounds and
molecular mechanisms in physiologically relevant 3D cell
culture

			1|BHLHA15|CUL7|ADD1|EDEM3|NFE2L2|CCL2|CREB3L1|ATF6|TBL2|PDIA6|RHBDD1|PPP1R15A|ASNA1|TOR1A|MBTPS1|C19ORF10|ZBTB17|TSPYL2|DDIT3|SEC61A2|ATF3|CTDSP2|AARS|PARK2|YIF1A|SEC61G|CREB3|SEC61A1|SEC61B|SEC62|EXTL3|PMAIP1|BCL2|TP53|CEBPB|PPP1R15B|GSK3B|ATG10|ERLIN2|ATP2A2|TTC23L|PPP2CB|UBQLN1|PSMC2|UBE2J1|UBE2K|UBXN8|TRIM25|FOXRED2|USP19|TMEM129|BBC3|UFM1|DNAJB2|CASP4|COL4A3BP|PSMC4|TRAF2|DNAJC10|UBA5|UBXN4|PSMC1|TRIM13|MAN1B1|AUP1|BRSK2|AIFM1|ERLEC1|TMEM33|TMX4|APAF1|PDIA3|BCL2L11|FAF2|NCK2|TMUB1|SCAMP5|TNFRSF10B|TMX3|UFL1|JKAMP|CHAC1|MARCH6|UBE4B|PML|JUN|ERP44|P4HB|PLA2G6|DDRGK1|BAG6|TARDBP|TMX1|PIK3R1|ERP27|PSMC3|TRIB3|UBQLN2|KIAA0368|AGR2|NPLOC4
GO_RESPONSE_TO_TOPOLOGICALLY_INCORRECT_PROTEIN	128		FBXO6|THBS1|TMBIM6|STT3B|UBE2J2|VAPB|EP300|CREB3L2|ERN1|LMNA|ANKZF1|DNAJB9|HERPUD1|PREB|TATDN2|HSPA5|ATXN3|CALR|ARFGAP1|ERO1L|ATP6V0D1|IL8|ACADVL|EDEM1|CTH|SRPR|HSP90B1|WFS1|STC2|CCND1|VCP|XBP1|DNAJB11|SEC63|BAK1|SRPRB|UFD1L|STUB1|EIF2S1|KLHDC3|AMFR|DAB2IP|PARP16|EIF2AK2|DERL2|EIF2AK3|HDGF|DERL1|TLN1|BAX|FKBP14|SDF2L1|HSPA2|DNAJC3|HSPB1|PPP2R5B|HSP90AB1|ATF4|RNF5|MANF|CXXC1|HSPD1|CLU|SERP1|TOR1B|ASNS|DNAJB1|RNF126|HSPA1L|DDX11|HSPA8|GFPT1|HSPA4|HYOU1|DNAJB4|PTPN1|SERPINH1|MBTPS2|HSP90AA1|TPP1|WIPI1|MFN2|BHLHA15|DNAJA1|CUL7|F12|ADD1|HSPH1|EDEM3|DNAJB5|NFE2L2|HERPUD2|CCL2|HSPA4L|CREB3L1|ATF6|TBL2|HDAC6|PDIA6|RHBDD1|PPP1R15A|ASNA1|TOR1A|MBTPS1|PACRG|C19ORF10|ZBTB17|TSPYL2|DDIT3|SEC61A2|ATF3|CTDSP2|AARS|PARK2|YIF1A|SEC61G|CREB3|SEC61A1|SEC61B|SEC62|EXTL3|TMEM129|DNAJB2|UBXN4|FAF2|JKAMP|CHAC1|ERP44
GO_CELLULAR_RESPONSE_TO_TOPOLOGICALLY_INCORRECT_PROTEIN	95		VAPB|EP300|CREB3L2|ERN1|LMNA|ANKZF1|DNAJB9|HERPUD1|PREB|TATDN2|HSPA5|ATXN3|CALR|ARFGAP1|ERO1L|ATP6V0D1|IL8|ACADVL|EDEM1|CTH|SRPR|HSP90B1|WFS1|STC2|CCND1|VCP|XBP1|DNAJB11|SEC63|BAK1|SRPRB|UFD1L|STUB1|EIF2S1|KLHDC3|AMFR|DAB2IP|PARP16|EIF2AK2|DERL2|EIF2AK3|HDGF|DERL1|TLN1|BAX|FKBP14|SDF2L1|DNAJC3|PPP2R5B|ATF4|RNF5|CXXC1|SERP1|ASNS|RNF126|DDX11|GFPT1|HYOU1|PTPN1|MBTPS2|TPP1|WIPI1|BHLHA15|CUL7|ADD1|EDEM3|NFE2L2|CCL2|CREB3L1|ATF6|TBL2|HDAC6|PDIA6|RHBDD1|PPP1R15A|ASNA1|TOR1A|MBTPS1|PACRG|C19ORF10|ZBTB17|TSPYL2|DDIT3|SEC61A2|ATF3|CTDSP2|AARS|PARK2|YIF1A|SEC61G|CREB3|SEC61A1|SEC61B|SEC62|EXTL3

GO_RESPONSE_TO_AMINO_ACID	78	RRAGB|EEF2|TMBIM6|NRF1|CPEB4|CCL5|ICAM1|CASP3|RELA|SOCS1|COL1A1|RRAGC|RRAGA|LYN|EDN1|PTGER4|TNF|CEBPB|XBP1|FAS|HMBS|IL6|GSK3B|CDKN1B|HNRNPK|CAPN2|ASCL1|BCL2L1|ZNF354A|RPTOR|DNMT3A|ABCG2|OGG1|LAMTOR1|ZEB1|DRD1|ASNS|COL6A1|UBR2|MGMT|TYMS|GLRB|COL16A1|ASS1|CTGF|EGFR|PDGFC|AIFM1|NEURL|UBR1|GSS|CREB1|NAIP|SLC38A9|CCL2|GLRA3|HNRNPD|COL3A1|COL5A2|TIMP3|MTOR|IPO5|LAMTOR2|UFL1|GSN|COL4A1|SH3BP4|PEMT|FOLR1|LAMTOR3|RAPGEF3|MTHFR|CPEB3|RRAGD|AARS|CPEB1|PIK3C3|ALAD
GO_GOLGI_ORGANIZATION	76	UBXN2A|GAK|GOLGA2|TMED5|TMED2|SYNE1|GBF1|BAG5|ATL2|OPTN|LMAN1|TBC1D20|FBXW8|COG7|COG4|CSNK1D|YWHAZ|ATL3|PRKD1|ARFGEF1|CDK1|HACE1|SEC23IP|DYNC2H1|ARHGAP21|OBSL1|RAB2A|GCC2|GOLGA5|ARL1|CDC42|SURF4|GOLPH3|RAB7L1|UBXN2B|TJAP1|HTT|TMED10|BHLHA15|USP6NL|CUL7|VTI1A|VRK1|CSNK1A1|GORASP1|RAB1A|COG1|PRMT5|GOLPH3L|PLEKHM2|VMP1|DNAJC28|NSFL1C|COG2|BCAS3|TMED9|CLASP1|ATP8B2|DYM|ZW10|ARHGEF7|VCPIP1|ATP8B1|GOLGB1|ATP8B3|STK25|COG3|CLASP2|PDCD10|MYO18A|KIFC3|BLZF1|PLK3|STX17|NPLOC4|VAMP4
GO_IRE1_MEDIATED_UNFOLDED_PROTEIN_RESPONSE	45	KLHDC3|HDGF|TLN1|FKBP14|DNAJC3|PPP2R5B|CXXC1|SERP1|DDX11|GFPT1|HYOU1|PTPN1|TPP1|WIPI1|CUL7|ADD1|ERN1|LMNA|DNAJB9|PDIA6|PREB|TATDN2|HSPA5|ASNA1|ARFGAP1|C19ORF10|ATP6V0D1|ZBTB17|TSPYL2|ACADVL|EDEM1|SEC61A2|SRPR|CTDSP2|WFS1|YIF1A|SEC61G|XBP1|DNAJB11|SEC61A1|SEC63|SEC61B|SEC62|SRPRB|EXTL3
GO_DEMETHYLATION	41	CYP1A1|KDM1A|KDM6B|KDM5C|KDM3A|KDM1B|KDM4B|ALKBH3|PHF8|CYP51A1|KDM4D|KDM4A|JHDM1D|CYP1A2|ARID5B|TET2|CYP2D6|CYP3A5|PPME1|TDG|POR|APEX1|ALKBH1|CYP2C8|TET3|UBE2B|TET1|JMJD6|KDM3B|FTO|JMJD1C|ALKBH2|KDM2B|KDM5A|KDM5B|KDM2A|PHF2|KDM6A|ALKBH5|KDM4C|ALKBH4
GO_INTRINSIC_APOPTOTIC_SIGNALING_PATHWAY_IN_RESPONSE_TO_ENDOPLASMIC_RETICULUM_STRESS	31	DAB2IP|BCL2|MAP3K5|SELK|UBE2K|BAX|TMBIM6|ATP2A1|ITPR1|BBC3|ATF4|CASP4|TRAF2|DNAJC10|BRSK2|AIFM1|APAF1|ERN1|TNFRSF10B|PPP1R15A|CHAC1|ERO1L|CEBPB|PML|DDIT3|BAG6|XBP1|TRIB3|BAK1|GSK3B|PMAIP1

	GO_DEMETHYLASE_ACTIVITY	30	CYP1A1|KDM1A|KDM6B|JARID2|KDM5C|KDM3A|KDM1B|KDM4B|ALKBH3|PHF8|CYP51A1|KDM4D|KDM4A|JHDM1D|CYP1A2|ARID5B|JMJD6|KDM3B|FTO|JMJD1C|ALKBH2|KDM2B|KDM5A|KDM5B|KDM2A|PHF2|KDM6A|ALKBH5|KDM4C|ALKBH4
	GO_ER_NUCLEUS_SIGNALING_PATHWAY	29	EIF2S1|EIF2A|ATP2A2|SCAP|EIF2AK3|INSIG1|ATF4|TP53|ASNS|MBTPS2|INSIG2|NFE2L2|CCL2|LMNA|ATF6|HERPUD1|HSPA5|CALR|MBTPS1|IL8|DDIT3|ATF3|HSP90B1|WFS1|XBP1|PPP1R15B|GSK3B|ATG10|ERLIN2
	GO_NEGATIVE_REGULATION_OF_RESPONSE_TO_ENDOPLASMIC_RETICULUM_STRESS	28	DERL2|UBE2J1|TMBIM6|DNAJC3|OS9|HYOU1|PTPN1|UBE2G2|ERLEC1|CREB3L1|NCK2|HERPUD1|PPP1R15A|OPA1|PARK7|GRINA|GNB2L1|USP14|WFS1|USP25|BFAR|PARK2|SVIP|UBAC2|CREB3|XBP1|UBXN1|PPP1R15B
	GO_REGULATION_OF_TYROSINE_PHOSPHORYLATION_OF_STAT3_PROTEIN	26	IL18|PPP2R1A|INPP5F|CTF1|NF2|VEGFA|SOCS1|CRLF1|LIF|STAT3|PTK6|CSF1R|PTGER4|HDAC2|JAK2|ARL2BP|IL6ST|HES1|SOCS3|STAP2|GHR|IL23A|FGFR3|PTPN2|IL6R|IL6
	GO_PROTEIN_DEALKYLATION	24	KDM1A|PPME1|KDM6B|KDM5C|KDM3A|KDM1B|KDM4B|UBE2B|PHF8|KDM4D|KDM4A|JHDM1D|ARID5B|JMJD6|KDM3B|JMJD1C|KDM2B|KDM5A|KDM5B|KDM2A|PHF2|KDM6A|KDM4C|ALKBH4
	GO_REGULATION_OF_ENDOPLASMIC_RETICULUM_UNFOLDED_PROTEIN_RESPONSE	24	ERN1|DAB2IP|BCL2L11|NCK2|PPP1R15A|HSPA5|BAX|TMBIM6|POMT2|SDF2L1|POMT1|BBC3|SDF2|PTPN2|GNB2L1|WFS1|BFAR|PIK3R1|PTPN1|XBP1|PPP1R15B|BAK1|AGR2|TMEM33
	GO_PROTEIN_LOCALIZATION_TO_GOLGI_APPARATUS	23	OPTN|NRAS|VPS13A|COG7|CSNK1D|IFT20|PAQR3|ATP9B|GBF1|GCC1|PACS1|SORL1|ARFRP1|OBSL1|GCC2|ARL1|VPS13D|GOLPH3|VPS13C|GOLGA4|RAB6A|TRIP11|RAB33B
	GO_HISTONE_DEMETHYLASE_ACTIVITY	22	KDM1A|KDM6B|JARID2|KDM5C|KDM3A|KDM1B|KDM4B|PHF8|KDM4D|KDM4A|JHDM1D|ARID5B|JMJD6|KDM3B|JMJD1C|KDM2B|KDM5A|KDM5B|KDM2A|PHF2|KDM6A|KDM4C
	GO_REGULATION_OF_ENDOPLASMIC_RETICULUM_STRESS_INDUCED_INTRINSIC_APOPTOTIC_SIGNALING_PATHWAY	22	CREB3L1|BCL2L11|NCK2|HERPUD1|EIF2AK3|OPA1|TMBIM6|SIRT1|PARK7|BBC3|SERINC3|ERP29|GRINA|DDIT3|PTPN2|WFS1|PARK2|HYOU1|CREB3|PTPN1|XBP1|PMAIP1

	GO_POSITIVE_REGULATION_OF_TYROSINE_PHOSPHORYLATION_OF_STAT3_PROTEIN	21	IL18|LIF|STAT3|PTK6|CTF1|CSF1R|HDAC2|PTGER4|JAK2|ARL2BP|IL6ST|VEGFA|HES1|SOCS3|STAP2|IL23A|GHR|FGFR3|IL6R|IL6|CRLF1
	GO_POSITIVE_REGULATION_OF_TRANSCRIPTION_FROM_RNA_POLYMERASE_II_PROMOTER_IN_RESPONSE_TO_STRESS	18	NFE2L2|CREB3L1|ATF6|MAPK7|HSPA5|NOTCH1|VEGFA|CEBPB|TP53|RBPJ|ATF4|DDIT3|KLF2|ATF3|GCN1L1|XBP1|MBTPS2|CHD6
	GO_PROTEIN_EXIT_FROM_ENDOPLASMIC_RETICULUM	18	FAF2|DERL2|HERPUD1|RANGRF|RHBDD1|LMAN1|DERL1|TMED9|TMEM129|SEL1L|HM13|HSP90B1|SURF4|VCP|SEC61B|AUP1|UFD1L|NPLOC4
	GO_ENDOPLASMIC_RETICULUM_TO_CYTOSOL_TRANSPORT	17	FAF2|DERL2|HERPUD1|RHBDD1|DERL1|NOL3|TMEM129|SEL1L|HM13|HSP90B1|VCP|SEC61B|AUP1|CCL3|UFD1L|FKBP1B|NPLOC4
Sterol Biosynthesis	GO_ALCOHOL_BIOSYNTHETIC_PROCESS	74	DHCR7|CYB5R3|HMGCS1|MVK|MVD|ACLY|INSIG1|HMGCR|PMVK|AKR1C3|CYP51A1|HSD17B7|IDI2|MSMO1|LBR|NSDHL|CYB5R1|SQLE|FDFT1|PRKAG2|AKR1B1|GGPS1|G6PD|EBP|PRKAA1|ARV1|FDPS|INSIG2|C14ORF1|DHCR24|CNBP|IDI1|DPAGT1|NUS1|PARK7|IMPA1|SAMD8|PTAFR|ACHE|PLCG2|SLC44A1|SGMS1|SCP2|CHKA|SGMS2|IPMK|LPIN2|GOT1|FABP5|AGPAT6|IMPA2|SLC44A3|LPIN1|ACER2|SPTLC2|LPCAT2|ABHD3|SPHK2|CACNA1H|CEPT1|SLC27A1|CDS1|CYP2R1|ISYNA1|CHPT1|ACER3|SLC44A2|IMPAD1|LPIN3|SPTLC1|PHOSPHO1|SPHK1|PEMT|GBA
	GO_STEROL_METABOLIC_PROCESS	71	CEL|CEBPA|DHCR7|ABCG1|CYB5R3|SNX17|HMGCS1|LRP5|MVK|CYP19A1|MVD|OSBPL5|ACLY|HDLBP|INSIG1|CYP46A1|HMGCR|VLDLR|SOAT1|PMVK|SCARB1|CYP51A1|LDLRAP1|HSD17B7|ABCA1|IDI2|CUBN|MSMO1|CAT|LBR|NSDHL|PTCHD2|CYB5R1|NPC2|SQLE|CYP4V2|STARD3|FDFT1|RXRA|PRKAG2|NPC1|GGPS1|G6PD|LIPA|EBP|FDX1|PRKAA1|APOL2|ARV1|CLN8|FDPS|FDXR|INSIG2|PPARD|C14ORF1|APOBR|DHCR24|APOE|CNBP|LDLR|IDI1|APP|ERLIN2|SCAP|SORL1|MBTPS2|MBTPS1|SREBF1|SREBF2|TRERF1|EBPL

	GO_STEROID_BIOSYNTHE TIC_PROCESS	67	HSD17B6|DHCR7|HSD17B12|CYB5R3|ACOX2|HMGCS1|HSD17B11|MVK|HINT2|MVD| CYP19A1|SRD5A3|ACLY|INSIG1|HMGCR|CYP46A1|PMVK|AKR1C3|CYP51A1|SCARB 1|SRD5A1|HSD17B7|IDI2|MSMO1|LBR|NSDHL|CYB5R1|SQLE|FDFT1|STARD3|PRKAG 2|AKR1B1|GGPS1|G6PD|WNT4|FDX1|EBP|PRKAA1|ARV1|FDXR|FDPS|INSIG2|C14ORF 1|DHCR24|CNBP|IDI1|TSPO|SCP2|CACNA1H|CYP2R1|SLC27A2|HSD3B7|SDR42E1|PRL R|STARD5|ACBD3|HSD11B2|MED1|HSD17B14|SLC27A5|HSD17B8|PBX1|ADM|ACOT8| HSD17B4|TRERF1|AKR1B15
	GO_STEROL_BIOSYNTHET IC_PROCESS	30	DHCR7|CYB5R3|HMGCS1|MVK|MVD|ACLY|INSIG1|HMGCR|PMVK|CYP51A1|HSD17 B7|IDI2|MSMO1|LBR|NSDHL|CYB5R1|SQLE|FDFT1|PRKAG2|GGPS1|G6PD|EBP|PRKA A1|ARV1|FDPS|INSIG2|C14ORF1|DHCR24|CNBP|IDI1
	GO_ISOPRENOID_BIOSYN THETIC_PROCESS	19	CYP1A1|HMGCS1|MVK|PDSS1|MVD|BCMO1|DPAGT1|ISPD|HMGCR|NUS1|PMVK|CO Q2|RDH10|IDI2|PDSS2|FDFT1|GGPS1|FDPS|IDI1
Stress Response	GO_RESPONSE_TO_HYDR OGEN_PEROXIDE	81	BCL2|MAP3K5|IMPACT|EEF2|AREG|CAT|DUSP1|PPP5C|AKR1B1|ADAM9|FOSL1|RPS3 |MB|CASP3|NR4A3|PRKAA1|HBB|RELA|COL1A1|BNIP3|PCGF2|GLRX2|KLF6|STK24|F KBP1B|NET1|EP300|LDHA|ECT2|KPNA4|KLF4|MAPK7|EZH2|TXNIP|HDAC2|APTX|MS T4|ADA|ZNF277|SIRT1|AGER|PRKCD|PARK7|SOD1|PLEKHA1|F3|CBX8|SETX|RHOB|K LF2|FXN|PPIF|MDM2|FAS|IL6|PPP1R15B|BAK1|GSK3B|PRDX3|HMOX1|KDM6B|SLC8 A1|PPP2CB|PTK2B|CDK1|STAT6|TNFAIP3|AIFM1|NFE2L2|APEX1|HDAC6|SDC1|SPHK 1|FOXO1|ANXA1|JUN|DDIT3|SRC|STK25|PDCD10|ABL1
	GO_PATTERN_RECOGNITI ON_RECEPTOR_SIGNALIN G_PATHWAY	73	PIK3R4|IRAK1|RELA|IRAK2|FADD|IKBKB|TNIP2|S100A14|TRAF6|ITCH|HSP90B1|UBE 2D3|FFAR2|SCARA3|IRAK4|BIRC3|IRF3|UNC93B1|DDX58|MAVS|COLEC12|IKBKG|TB K1|UBE2D1|FAM105B|UBE2D2|CTSB|TAB2|TAB3|RIPK1|MAP3K1|CTSK|UBB|NOD1|TI CAM1|CASP8|UBE2N|RFTN1|NOD2|PRKCE|CLEC7A|HSPD1|CTSS|MAP2K6|BIRC2|LG MN|TNFAIP3|TAB1|MAPKAPK2|IKBKE|UBC|ITGAM|RPS27A|BCL10|TRAF3|IFIH1|UB A52|RPS6KA3|LSM14A|TANK|TLR5|TRIM5|MYD88|MAP3K7|CNPY3|TNIP1|IRF7|MAP KAPK3|CYLD|TLR2|RIPK2|NFKBIA|PIK3C3
	GO_HOMOPHILIC_CELL_A DHESION_VIA_PLASMA_ MEMBRANE_ADHESION_ MOLECULES	64	PVRL1|PCDHB4|RET|PCDHB3|CDH24|PCDHB2|PCDHB13|PCDHB10|PCDHB14|MPZL2| PCDHB16|PCDHB11|PCDHB9|NPTN|CDH3|CDHR3|DSCAM|CDH2|CDH18|CDH12|CDH 1|PCDH19|PCDHA4|PCDHB12|CELSR2|CDH26|PCDHGA1|CADM1|PCDH10|CELSR1|PT PRT|SDK2|AMIGO1|ITGB1|DSCAML1|PVRL2|AMIGO2|IGSF9B|SMAGP|SDK1|PVRL4|P CDH8|CELSR3|ROBO1|CDH8|PCDH9|ROBO2|PVRL3|PKD1|CADM4|PCDH17|PTPRM|P

			CDH7|FAT4|IGSF9|DSG2|DSC2|PCDH1|CLSTN1|FAT1|CLSTN2|PIK3CB|CLSTN3|CDHR2
GO_DNA_PACKAGING_COMPLEX	60		HIST1H2BG|HIST1H2BJ|HIST1H2BK|HIST1H2BI|HIST1H2BF|HIST2H2BE|HIST1H2BC|NCAPG|HIST1H4K|HIST1H3E|HIST1H2AC|HIST1H2BO|H2AFY|HIST1H3G|H2AFV|HIST1H2BL|HIST1H2AL|HIST1H4J|H2AFZ|H1FX|HIST4H4|KAT6A|HIST1H3D|H2AFX|NCAPD2|NCAPH|HIST1H3A|HIST1H3C|HIST1H1E|ANKRD32|KAT6B|HIST1H3B|HIST1H2BD|HIST1H2BH|SMC4|HIST1H2AH|H3F3B|H2AFY2|HIST1H4H|HIST1H4E|HIST1H4D|SHPRH|HIST1H2AG|SMC2|HIST1H3H|H2AFJ|HIST1H3J|HIST1H2BN|HIST3H2BB|HIST1H1D|HIST1H1C|HIST1H1B|HIST1H3F|H1F0|HP1BP3|MPHOSPH8|HIST1H4C|HIST3H2A|HIST1H2AK|HIST1H2AE
GO_TOLL_LIKE_RECEPTOR_SIGNALING_PATHWAY	57		PIK3R4|IRAK1|IRAK2|FADD|IKBKB|TNIP2|S100A14|TRAF6|HSP90B1|UBE2D3|IRAK4|SCARA3|BIRC3|IRF3|UNC93B1|COLEC12|IKBKG|TBK1|UBE2D1|UBE2D2|CTSB|TAB2|TAB3|RIPK1|MAP3K1|CTSK|UBB|TICAM1|CASP8|RFTN1|PRKCE|HSPD1|CTSS|BIRC2|LGMN|TAB1|MAPKAPK2|IKBKE|UBC|ITGAM|RPS27A|BCL10|TRAF3|UBA52|RPS6KA3|TANK|TLR5|MYD88|MAP3K7|CNPY3|TNIP1|IRF7|MAPKAPK3|TLR2|RIPK2|NFKBIA|PIK3C3
GO_POSITIVE_REGULATION_OF_NEURON_DEATH	54		ATM|MAP3K5|TP53|CASP3|CCL3|APOE|IKBKB|PAWR|TGFB2|AGER|CASP9|TFAP2A|GSK3B|EIF2S1|EPHA7|ZNF746|NQO1|BAX|ATF2|ASCL1|MAP2K7|FBXW7|BBC3|CTNNB1|DAXX|ATF4|TP53BP2|SRPK2|FOXO3|CLU|DDIT4|CDK5R1|ELK1|CDC42|CASP2|PIN1|AIMP2|MAP3K11|CDK5|UBE2M|AIFM1|CDC34|PICALM|NF1|GRIK2|MCL1|BCL2L11|MTOR|JUN|DDIT3|HDAC4|PARK2|PMAIP1|ABL1
GO_I_KAPPAB_KINASE_NF_KAPPAB_SIGNALING	52		SNIP1|PTPLAD1|REL|NKIRAS1|IRAK2|IKBKB|NFKB1|TNIP2|TNF|TRAF6|BIRC3|IKBKG|TBK1|DAB2IP|TAB2|TAB3|RIPK1|UBB|TICAM1|BCL3|BIRC2|TRAF2|TAB1|IKBKE|RELB|UBC|RPS27A|BCL10|UBA52|TANK|MAP3K7|RBCK1|TLR2|NLRC3|RIPK2|ERC1|PRDX4|ROCK1|IRAK1BP1|NFKB2|ZNF268|SHARPIN|TIFA|AZI2|TRIP6|ZNF675|TNFRSF1A|NKIRAS2|NFKBIL1|ROCK2|MAP3K14|TRADD
GO_RESPONSE_TO_OSMOTIC_STRESS	46		ICOSLG|SLC12A6|SERPINB6|STK39|MARVELD3|PCP4|TRPV4|TH|ANXA7|ITGA2|MAPK13|PTK2B|DDX3X|SLC2A1|TSC22D3|MAP7|BAX|RAC1|SORD|AKT2|ATF2|NFAT5|MAP2K7|HSP90AB1|CCL5|PKN1|RELB|HSP90AA1|ERRFI1|FMO1|TSPO|HNMT|TNF|MYLK|SLC2A4|CAB39|AQP9|OXSR1|KMO|ARHGEF2|KCNMA1|LRRC8A|TSC22D2|PLK3|PDPK1|PKD2

	GO_REGULATION_OF_NF_KAPPAB_IMPORT_INTO_NUCLEUS	28	IL18|ZC3H12A|BCL3|IL1B|BMP7|NOL3|CCDC22|RBCK1|SPHK1|LITAF|TNF|CYLD|TLR2|IL23A|EDA|RHOA|PPM1B|NFKBIA|PRDX1|ZNF268|PSMD10|G3BP2|FAF1|TRIP6|PPM1A|FBXW11|NFKBIB|C8ORF4
	GO_TUMOR_NECROSIS_FACTOR_RECEPTOR_BINDING	18	TRAP1|TRAF4|TRIM37|TRAF1|ERAP1|STAT1|CASP8|TNF|TNFSF13B|TNFSF10|TRAF6|EDA|TRAF2|TNFSF9|LTB|TRAF3|FADD|TRADD
	GO_RESPONSE_TO_IMMOBILIZATION_STRESS	15	CYP1A1|TFF1|GAL|SLC8A1|FOS|TH|BRD1|PTK2B|KEAP1|PTGER4|PPP1R15A|PPARG|HNMT|CYP1A2|LRP11

Supplementary Videos can be visualized at https://www.frontiersin.org/articles/10.3389/fonc.2019.00224/full#supplementary-material

Supplementary material video 1 – Spheroid made of HCT116 cells with red nucleus exposed to NocA at 10μM, for 48h and reinforcement at same concentration for another 48h.

Supplementary material video 2 –Spheroid made of HCT116 cells with red nucleus over 48h with solvent control of NocA and change of medium and respective solvent control concentration of NocA for another 48h.

FCUP | 76
Cyanobacterial bioactive metabolites for anticancer drug
discovery: characterization of new compounds and
molecular mechanisms in physiologically relevant 3D cell
culture

Cytotoxicity of portoamides in human cancer cells and analysis of the molecular mechanisms of action

Ribeiro T, Lemos F, Preto M, Azevedo J, **Sousa ML**, Leão PN, Campos, A, Linder, S, Vitorino, R, Vasconcelos, V, Urbatzka, R. (2017)

FCUP | 78
Cyanobacterial bioactive metabolites for anticancer drug
discovery: characterization of new compounds and
molecular mechanisms in physiologically relevant 3D cell
culture

Cytotoxicity of portoamides in human cancer cells and analysis of the molecular mechanisms of action

Tiago Ribeiro[1], Filipa Lemos[1], Marco Preto[1], Joana Azevedo[1], Maria Lígia Sousa[1], Pedro N. Leão[1], Alexandre Campos[1], Stig Linder[2,3], Rui Vitorino[4,5], Vitor Vasconcelos[1,6], Ralph Urbatzka[1]*

1 CIIMAR, Interdisciplinary Center of Marine and Environmental Research, Porto, Portugal, **2** Department of Oncology-Pathology, Karolinska Institute, Stockholm, Sweden, **3** Department of Medical and Health Sciences, Faculty of Health Sciences, Linköping University, Linköping, Sweden, **4** Department of Medical Sciences, Institute of Biomedicine–iBiMED, University of Aveiro, Aveiro, Portugal, **5** Department of Physiology and Cardiothoracic Surgery, Faculty of Medicine, University of Porto, Porto, Portugal, **6** FCUP, Faculty of Science, Department of Biology, University of Porto, Porto, Portugal

* rurbatzka@ciimar.up.pt

Abstract

Portoamides are cyclic peptides produced and released by the cyanobacterial strain *Phormidium sp.* presumably to interfere with other organisms in their ecosystems ("allelopathy"). Portoamides were previously demonstrated to have an antiproliferative effect on human lung carcinoma cells, but the underlying mechanism of this activity has not been described. In the present work, the effects of portoamides on proliferation were examined in eight human cancer cell lines and two non-carcinogenic cell lines, and major differences in sensi- tivities were observed. To generate hypotheses with regard to molecular mechanisms of action, quantitative proteomics using 2D gel electrophoresis and MALDI-TOF/TOF were performed on the colon carcinoma cell line HT-29. The expression of proteins involved in energy metabolism (mitochondrial respiratory chain and pentose phosphate pathway) was found to be affected. The hypothesis of altered energy metabolism was tested in further experiments. Exposure to portoamides resulted in reduced cellular ATP content, likely due to decreased mitochondrial energy production. Mitochondrial hyperpolarization and reduced mitochondrial reductive capacity was observed in treated cells. Furthermore, alterations in the expression of peroxiredoxins (PRDX4, PRDX6) and components of proteasome sub- units (PSB4, PSA6) were observed in portoamide-treated cells, but these alterations were not associated with detectable increases in oxidative stress. We conclude that the cytotoxic activity of portoamides is associated with disturbance of energy metabolism, and alterations in mitochondrial structure and function.

RESEARCH ARTICLE

Introduction

Natural compounds have been an important source of new drugs for the treatment of many diseases [1]. Cyanobacteria are known to produce a plentitude of secondary metabolites whose potential applications range from industrial to biomedical. For example, poly-β- hydroxybutyrate is used for the production of bioplastics [2] and compounds like the veraguamides have revealed cytotoxicity against human cancer cell lines [3]. The most famous example of a cyanobacterial anticancer drug is brentuximab vedotin, a synthetic compound with its origin from a cyanobacterial metabolite, which passed the U.S. FDA (US Food and Drug Administration) approval for clinical use. Brentuximab vedotin targets CD30 and microtubules and is used for the treatment of anaplastic large T-cell systemic malignant lymphoma and Hodgkin's disease [4]. Our own group demonstrated that picocyanobacteria have the capacity to induce cytotoxicity in human cancer cells via different modes of actions [5] and that hierridin B, a metabolite from the marine cyanobacterium *Cyanobium sp*. decreased mitochondrial activity and function [6]. Portoamides were previously isolated from the cyanobacteria *Phormidium* sp. LEGE 05292 from the Blue Biotechnology and Ecotoxicology Culture Collection (LEGE CC, http://www.ciimar.up.pt/legecc/), due to its allelopathic effect upon the alga *Chlorella vulgaris* [7]. Portoamides A and B individually reduced the viability of the non-small lung carcinoma cell line H460, and interestingly, stronger cytotoxicity was observed for the mixture of the two compounds [7].

In this work, the cyanobacterial strain *Phormidium sp*. LEGE 05292 was grown under standard conditions in order to isolate portoamides A and B (designated portoamides in the following sections). The aim of the study was to expand the analysis of cytotoxicity of portoamides to eight human carcinogenic and two non-carcinogenic cell lines using the MTT assay. Following these results, the most sensitive cell line was selected for analyses of the molecular mechanisms underlying the observed cytotoxicity. Proteomics was applied as a non-targeted approach using 2D gel electrophoresis and protein identification by MALDI-TOF/TOF to gain insights into altered cellular pathways. In order to complement the proteomics data, a quantitative analysis of fluorescently labeled nuclei, cytoplasm and mitochondria was per- formed using the CellProfiler [8] software to detect cellular alterations and phenotypic anchors. Hypotheses generated by proteomics were further tested by functional assays for oxidative stress, ROS production, redox potential, ATP level and mitochondrial (Glu/Gal) toxicity assessment.

Results and discussion

Isolation and purification of portoamides

Phormidium sp. LEGE 05292 was grown for eight months, and the total lyophilized biomass obtained was 5.35 g. Portoamides A and B (30.0 mg) were isolated by column chromatography followed by HPLC-PDA, and their presence confirmed by LC/MS with a relative proportion of A to B of 3:1 based on the PDA spectrum (S1 Fig). This naturally occurring and defined mixture of both portoamides was used for exposure of cells and called portoamides throughout the document.

Effect of portoamides on the proliferation of different cell lines

The effects of portoamides (78 ng/mL—10 μg/mL) on the proliferation of eight human carcinogenic and two non-carcinogenic cell lines were examined using the MTT assay. Portoamides were dissolved in 0.5% dimethyl sulfoxide (DMSO), a solvent concentration that did not affect the proliferation of any of the cell lines tested. Portoamides did not affect the viability of lung carcinoma (A549), hepatocellular carcinoma (HepG2), breast ductal carcinoma (T-47D) and neuroblastoma (SHSY-5Y) cells at the concentrations tested. In contrast, portoamides showed antiproliferative effects in the cell lines of colon carcinoma (RKO, HCT116), colon-rectal adenocarcinoma (HT-29) and osteosarcoma (MG-63), and the non-carcinogenic cell lines of human brain capillary endothelial cells (hCMEC/D3) and keratinocytes (HaCa) (Table 1). HT-29 was the most sensitive cell line (IC50: 1.5 μg/mL) and chosen for further

FCUP 81
Cyanobacterial bioactive metabolites for anticancer drug
discovery: characterization of new compounds and
molecular mechanisms in physiologically relevant 3D cell
culture

experiments. The exposure concentrations of 0.5 μg/mL (IC15) and 1.0 μg/mL (IC25) were selected to analyze the HT-29 cells at the phase of initial loss of viability.

Membrane-active agents and other generally toxic compounds are not expected to show variations in IC_{50} between different cell lines. Variations in sensitivities in the NCI_{60} cell line panel to different drugs has been used as an indicator for selection of drugs for further testing [9]. The difference in sensitivity to portoamides between the tested cell lines (cytotoxic, non- cytotoxic) indicated the potential to induce cytotoxicity via specific molecular targets. The non-carcinogenic cell lines (hCMEC/D3, HaCaT) are characterized by infinite cell division. HaCaT keratinocytes are described as clonogenic, but not tumorigenic [10], and have mutations in the p53 gene [11]. Future work should test portoamides on human primary cells or stem cells in order to analyze their potential toxicity on normal cells.

Potential reasons for selective cytotoxicity of portoamides in different cell lines were analyzed with the help of available scientific databases, which contain genomic and proteomic data regarding the expression of many genes/proteins in different human cell lines or primary human tissues, as well as sequence variants for genes/proteins. By focusing on the two strongest induced proteins in our data set (NDUFS3 and TALDO1), a search was performed on the Human Protein Atlas (http://www.proteinatlas.org/), the NCI-60 Proteome Database (http://129.187.44.58:7070/NCI60/main/index), and the Colorectal Cancer Atlas (http://www.colonatlas.org/). However, on the basis of available data, no differences could be observed that would argue for different cell selectivity. Future works should focus on a detailed target deconvolution, which would enable a comparison between the different selectivity in human cell lines.

Table 1. Viability assays for eight human cancer cell lines, and two non-carcinogenic cell lines. Viability assays were performed for eight human cancer cell lines, and two non-carcinogenic cell lines treated for 48 h with portoamides. IC_{50} values are derived from triplicates per plate, and from at least two independent assays. Portoamides did not affect the viability of lung carcinoma (A549), hepatocellular carcinoma (HepG2), breast ductal carcinoma (T-47D) and neuroblastoma (SHSY-5Y) cells at the concentrations tested.

Cell Lines	IC_{50} (μg/mL) Mean ± SD	IC_{50} (μmol/L)
MG-63	9.2 ± 8.3	6.03
HCT116	5.2 ± 1.2	3.38
RKO	4.6 ± 3.8	3.02
HT-29	1.5 ± 1.3	0.98
hCMEC/D3	5.5 ± 0.5	3.61
HaCaT	4.3 ± 1.1	2.82

https://doi.org/10.1371/journal.pone.0188817.t001

Evaluation of proteomic alteration after exposure to portoamides

Drugs generally induce phenotypic changes that are useful indicators of their mechanisms of action [12]. We examined here the effects of portoamides on the proteome of HT-29 cells using 2D gel electrophoresis and mass spectrometry. The expression of 30 protein spots was observed to differ between control and treated cells. Seventeen proteins could be identified (57%), presented in Table 2, and were up regulated. Their relative position on polyacrylamide gel is shown in Fig 1.

The quantitative proteomic analyses pointed out to interesting alterations in the expression of cytoplasmic and mitochondrial proteins, and on signaling processes. The proteins with the highest rate of alterations were involved in the mitochondrial respiratory chain (NADH dehydrogenase from the mitochondrial complex I, NDUFS3) and in the pentose phosphate pathway (PPP) (transaldolase, TALDO). The strong increase of NDUFS3 at both exposure concentrations revealed alterations of mitochondrial metabolism and energy production. Higher activity of NDSUF3 accompanied by a rise in the production of ROS is one of several causes of cellular oxidative stress, which can induce apoptosis [13], also known as ROS dependent apoptosis. Compounds such as retinoic acid induced the activity of the mitochondrial respiratory chain via NDUFS3, which led to cytotoxicity in cancer cells, overproduction of ROS and loss of mitochondrial function [14]. TALDO is the rate-limiting enzyme of the non-oxidative branch of PPP, which ensures the formation of ribose-5-phosphate for nucleotide (DNA, RNA) biosynthesis and of NADPH for neutralization of ROS [15]. TALDO deficiency in mice led to the depletion of NADPH and GSH, loss of mitochondrial transmembrane potential and

mitochondrial mass, and was linked to many clinical diseases such as male infertility, chronic liver diseases and hepatic carcinoma [15]. The action of TALDO varied in a cell-type specific manner, but in Jurkat cells the overexpression of TALDO accelerated NADPH turnover and increased cellular sensitivity to apoptosis induced by hydrogen peroxide or nitric oxide [16], and elevated the mitochondrial membrane potential [15]. Furthermore, two subunits of the proteasome (PSA6_HUMAN e PSB4_HUMAN) were increased in both portoamide exposure groups in comparison with the solvent control. The proteasome is a key component in the response to cellular stress, but also in the regulation of the cell cycle and of apoptosis. Two peroxiredoxins were increased, peroxiredoxin-4 (PRDX4) and peroxiredoxin-6 (PRDX6), two important anti-oxidant enzymes and scavengers of ROS, as well as GST1, an enzyme responsible for protein modification related with cellular redox variations [17]. Summarizing, the proteomics results, two main hypotheses can be generated that were tested in the following experiments; (1) portoamides induce oxidative stress that may lead to ROS induced apoptosis, (2) portoamides affect energy metabolism and in particular mitochondrial activity/function.

FCUP | 83
Cyanobacterial bioactive metabolites for anticancer drug
discovery: characterization of new compounds and
molecular mechanisms in physiologically relevant 3D cell
culture

Table 2. Identification of differentially expressed spots from HT-29 cells exposed to portoamides by MALDI-TOF/TOF. The Table 2 indicates the spot number (SPP), protein name, mean intensity and standard deviation (SD), the protein accession number, protein score and the matched peptides obtained by MS and by MS/MS, of the different protein spots of the solvent control and portoamides treatment.

SPP	Protein Name	0.5% DMSO (mean ± SD)	0.5 µg/mL portoamides (mean ± SD)	Fold (x)	1.0 µg/mL portoamides (mean ± SD)	Fold (x)	Acession Number	Gene	Protein Score	Matched Peptides	
										MS	MS/MS
304	Eukaryotic translation initiation factor 6	1705.4 ± 508.7	2774.4 ± 1314.2	1.6	3176.3 ± 717.7	1.9	IF6_HUMAN	EIF6	232	6	3
1323	14-3-3 protein zeta/ delta	224.6 ± 161.8	1427.2 ± 263.0	6.4	451.1 ± 395.7	2.0	1433Z_HUMAN	YWHAZ	171	6	3
1305	14-3-3 protein beta/ alpha	4887.4 ± 1804.0	7209.3 ± 3226.9	1.5	9801.3 ± 1574.4	2.0	1433B_HUMAN	YWHAB	228	15	3
1401	14-3-3 protein epsilon	4373.6 ± 1582.3	6207.2 ± 1851.9	1.4	6381.5 ± 627.7	1.5	1433E_HUMAN	YWHAE	310	16	4
2503	Serine/arginine-rich splicing factor 1	—	—		615.1 ± 333.3		SRSF1_HUMAN	SRSF1	57	7	2
2902	Keratin. type I cytoskeletal 19	—	11439.0 ± 1326.8		10723.1 ± 4165.0		K1C19_HUMAN	KRT19	128	10	1
3408	UMP-CMP kinase	210.5 ± 130.0	715.5 ± 117.0	3.4	—		KCY_HUMAN	CMPK1	112	11	3
3719	Spermidine synthase		—		106.9 ± 83.5		SPEE_HUMAN	SRM	73	8	1
4308	Proteasome subunit beta type-4 precursor	18.9 ± 13.0	123.7 ± 59.8	6.5	98.9 ± 76.7	5.2	PSB4_HUMAN	PSMB4	96	5	1
4349	Peroxiredoxin-4	25.9 ± 3.1	202.5 ± 166.3	7.8	196.9 ± 94.2	7.6	PRDX4_HUMAN	PRDX4	103	6	2
4509	NADH dehydrogenase [ubiquinone] iron- sulfur protein 3. mitochondrial	4.6 ± 7.0	49.1 ± 44.1	10.7	43.2 ± 41.4	9.4	NDUS3_HUMAN	NDUFS3	79	9	1
4616	Glutathione S-transferase omega- 1	30.6 ± 12.9	40.3 ± 31.1	1.3	82.5 ± 55.4	2.7	GSTO1_HUMAN	GSTO1	64	7	1
4709	Transaldolase	31.5 ± 22.6	519.3 ± 232.7	16.5	944.2 ± 932.8	30.0	TALDO_HUMAN	TALDO1	153	11	2
5302	Peroxiredoxin-6	2146.3 ± 498.9	3147.3 ± 635.3	1.5	2975.9 ± 405.5	1.4	PRDX6_HUMAN	PRDX6	135	7	2

5303	Proteasome subunit alfa type-6	—	437.8 ± 395.0		—		PSA6_HUMAN	PSMA6	168	7	3
5813	28S ribossomal protein S22. mitochondrial	125.9 ± 57.7	—		239.5 ± 75.3	1.9	RT22_HUMAN	MRPS22	49	8	1
9707	Heterogeneous nuclear ribonucleoprotein A1	—	590.7 ± 178.8		301.4 ± 0.0		ROA1_HUMAN	HNRNPA1	80	14	-

FCUP 85
Cyanobacterial bioactive metabolites for anticancer drug
discovery: characterization of new compounds and
molecular mechanisms in physiologically relevant 3D cell
culture
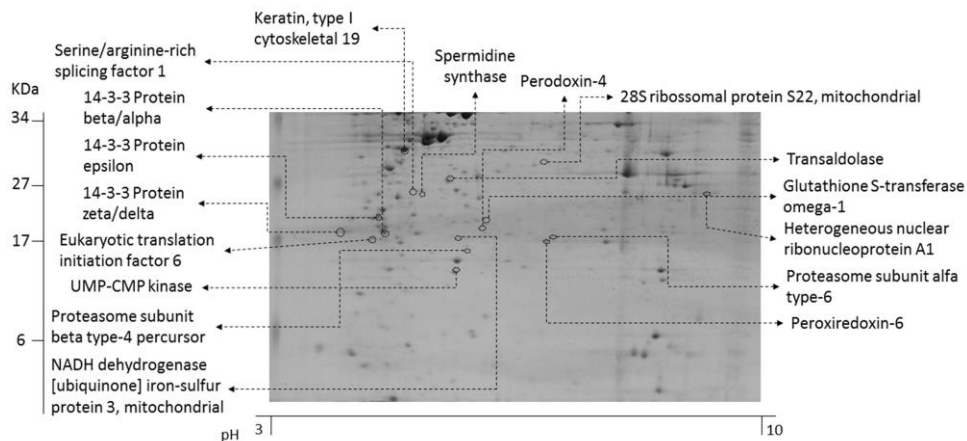
Fig 1. Polyacrylamide gel (12.5%) with indication of the position of the proteins identified by MALDI-TOF/TOF from the HT-29 cell line.
https://doi.org/10.1371/journal.pone.0188817.g001

Portoamides do not induce oxidative stress

The increases in TALDO, NDUFS3, GSTO1, PRDX4 and PRDX6 were all consistent with the generation of oxidative stress in exposed cells. We therefore examined ROS levels in portoamide-treated HT-29 cells using the redox-sensitive probe DCFDA. DCFDA fluorescence increased after treatment with tert-Butyl hydroperoxide (TBHP) but did not, however, increase in portoamide exposed cells (Fig 2). We also used a reporter gene assay based on the antioxidant/electrophile response element (ARE/EpRE) known to be stimulated by the transcription factor Nrf2. Nrf2 is stabilized and translocated to the nucleus under condition of oxidative stress. The reporter has previously been demonstrated to respond to conditions of oxidative stress [18]. Whereas the thioredoxin reductase inhibitor auranofin induced strong increases in Nrf-2 reporter activity, no effect was observed using portoamides (Fig 3). These findings do not support the concept that portoamides induce oxidative stress.
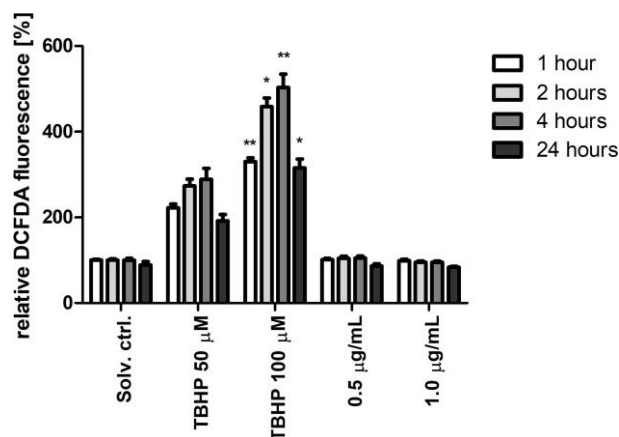
Fig 2. Detection of cellular ROS production using DCFDA reagent after exposure to portoamides (0.5 µg/mL and 1.0 µg/mL) and positive controls (tert-Butyl hydroperoxide, TBHP at 50 µM and 100 µM). Values are shown relative to the respective solvent control (DMSO 0.5%) of each time period (1, 2, 4, 24 hours). Statistically significant differences between the respective solvent control and the treatment groups are indicated by asterisks (Kruskal-Wallies, Dunn's test, * = p<0.05, ** = p<0.01).
https://doi.org/10.1371/journal.pone.0188817.g002

FCUP 86
Cyanobacterial bioactive metabolites for anticancer drug
discovery: characterization of new compounds and
molecular mechanisms in physiologically relevant 3D cell
culture

Fig 3. Nrf2 activity in HCT116 cells transfected with the plasmid pTRAF. HCT116 cells were cultured at different concentrations of portoamides, the solvent control was 0.3% DMSO, and fluorescent signals were analyzed with the Incucyte ZOOM software. Statistically significant differences between the solvent control and the treatment groups are indicated by asterisks (One-Way ANOVA, Dunnett's test, ******* = p<0.001.

https://doi.org/10.1371/journal.pone.0188817.g003

Decreased mitochondrial reductive activity in portoamide-treated cells

The reductive capacity of mitochondria can be assessed by determining reduction of resazurin (oxidized form: 7-hydroxy-3H-phenoxazin-3-1-10-oxide) to resorufin (Alamar Blue assay) [19]. Significant decreases in reductive capacity were observed after four hours of exposure of HT-29 cells to 5 and 10 µg/mL of portoamides (Fig 4). Metabolic activity may also be determined using tetrazolium dyes (MTT assay), widely used as viability assay. Tetrazolium reduction occurs in mitochondria but is mainly due to NAD(P)H-dependent oxidoreductases situated in the cytosolic compartment of the cell [20]. Interestingly, no alterations in tetrazolium dye reduction were observed in cells after four hours of exposure to portoamides (Fig 4), suggesting that mitochondrial reductive capacity was selectively affected, under conditions in which no cytotoxicity was present. Results indicated that the redox potential was more oxidative compared to the solvent control. More oxidative redox potentials are typical for cells undergoing apoptosis and several protein redox switches exist as for p53, HIF1α or Bax [21].
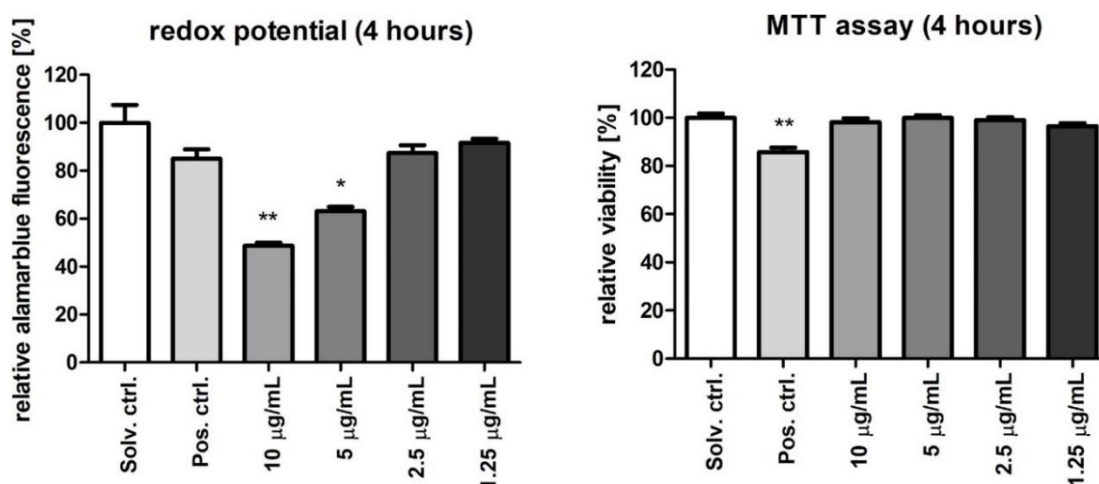
Fig 4. Evaluation of cellular redox status using the alamar blue assay (left panel) and viability by MTT (right panel). Values are shown relative to solvent control (DMSO 0.5%) after exposure to portoamides for 4 hours. Statistically significant differences between the solvent control and the treatment groups are indicated by asterisks (Kruskal-Wallies, Dunn's test, ***** = p<0.05, ****** = p<0.01). DMSO 20% was used as a positive control.

https://doi.org/10.1371/journal.pone.0188817.g004

Portoamides decreased cellular ATP levels, and were not mito-toxic

The proteome analysis indicated effects of portoamides on HT-29 mitochondrial metabolism. In order to

FCUP | 87
Cyanobacterial bioactive metabolites for anticancer drug
discovery: characterization of new compounds and
molecular mechanisms in physiologically relevant 3D cell
culture

provide more data on the potential alteration of mitochondrial activity, glucose or galactose conditioned media were applied, which are known as a cellular switch, where cells either rely on glycolysis and oxidative phosphorylation (OXPHOS) or solely on OXPHOS, respectively, to generate ATP, and hence energy [22,23]. In glucose media, energy can be produced via glycolysis or OXPHOS. However, since oxidation of galactose to pyruvate yields no net ATP, galactose-containing media reveal the importance of mitochondrial OXPHOS for energy production. ATP levels were significantly reduced after four hours exposure to 5 and 10 µg/mL portoamides in both glucose and galactose media (Fig 5); but a higher level of ATP was present in glucose media. These results suggest that the effect of portoamides was primarily at the level of mitochondrial energy production.

Next, the effects of portoamides on cell proliferation/cell viability were examined in glucose- or galactose-containing media. Mitochondrial dysfunction in response to 24 hour exposure to many different known mito-toxic compounds led to higher cytotoxicity in galactose conditioned media compared to glucose media [22]. A stronger anti-proliferative effect is expected for mito-toxic compounds in galactose-containing medium, since compensatory glycolysis cannot be activated. Portoamides reduced proliferation under both conditions (Fig 6), which demonstrated that portoamides were not mito-toxic.
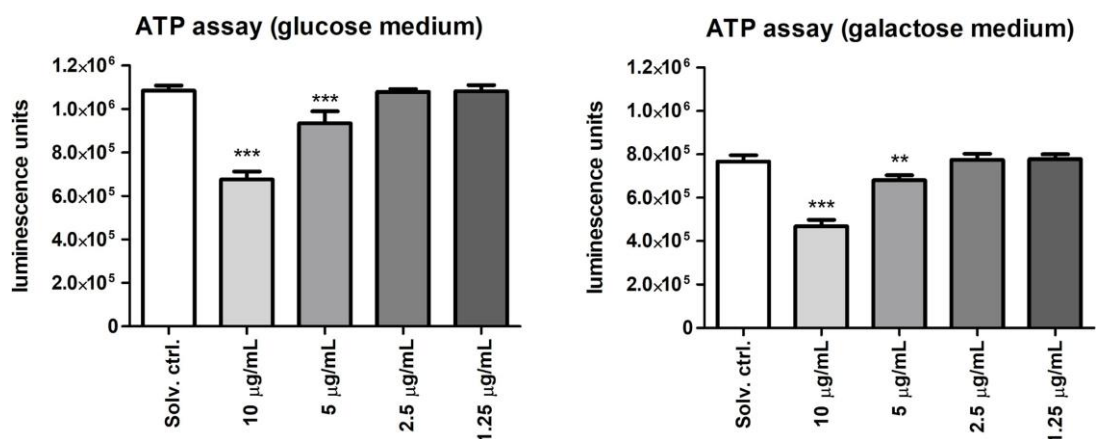
Fig 5. Quantification of ATP levels using selective media conditions. ATP levels were measured in HT-29 cells cultured in glucose (25 mM) and galactose (10 mM) conditioned media, which are known as a cellular switch, where cells either rely on glycolysis and oxidative phosphorylation or solely on oxidative phosphorylation, respectively. Results are expressed in luminescence units, and statistically significant differences between the solvent control and the treatment groups are indicated by asterisks (One-Way ANOVA, Dunnett's test, ** = p<0.01, *** = p<0.001).
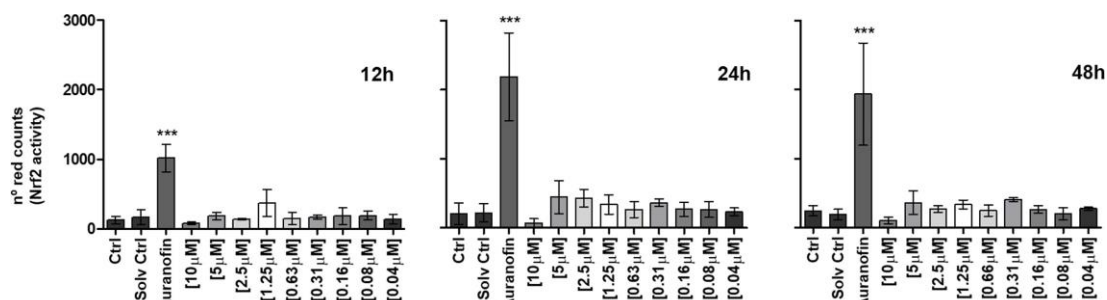
https://doi.org/10.1371/journal.pone.0188817.g005
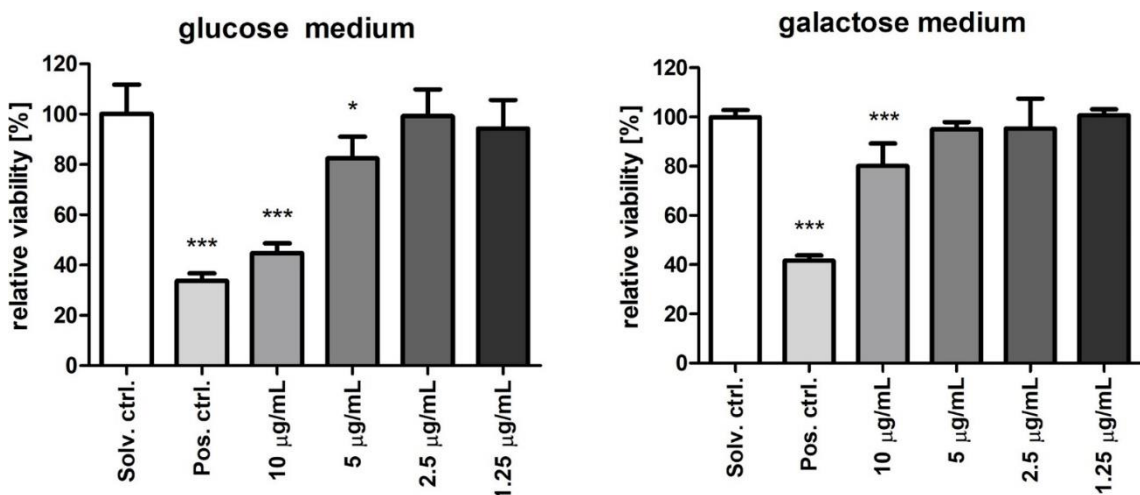
Fig 6. Mito-toxicity evaluation using MTT on selective media. Values are represented relative to the solvent control (DMSO 0.5%) for HT-29 cells cultured in glucose (25 mM) and galactose (10 mM) conditioned media, which

are known as cellular switch, where cells either rely on glycolysis and oxidative phosphorylation or solely oxidative phosphorylation, respectively. HT-29 cells were exposed to four different portoamide concentrations, using DMSO 20% as a positive control. Statistically significant differences between the solvent control and the treatment groups are indicated by asterisks (One-Way ANOVA, Dunnett's test, * = p<0.05, *** = p<0.001).
https://doi.org/10.1371/journal.pone.0188817.g006

Portoamides affect mitochondrial morphology

We next examined the effect of portoamides on mitochondria using principal component analysis of 40 different parameters recorded after staining with the membrane potential-dependent dye MitoTracker CMXRos (Fig 7, S1 Dataset). Factors that contributed mainly (> 0.85) to PC1 were related to intensity measurements, while parameters related to size and shape contributed mainly (> 0.85) to PC2. Two parameters were chosen for further statistical analysis (contributing either to PC1 or PC2), and mean fluorescence intensity and mean radius were increased in the 1.0 µg/mL portoamide treatment relative to the solvent control, while the same parameters were diminished in the 0.5 µg/mL portoamide treatment (p < 0.001). Since uptake of the Mito- Tracker CMXRos is dependent on the membrane potential, increased fluorescence intensity suggests increased activity or hyperpolarization of the mitochondrial membrane.

The above described increase of mitochondrial fluorescence intensity and the mean radius in the portoamide-treated cells provides support for alterations in mitochondrial activity (in line with NDUFS3). Another cyanobacterial metabolite, hierridin B, targeted mitochondrial activity in HT-29 cells, but in the opposite way to portoamides, by strongly reducing the mitochondrial fluorescence intensity and increasing level of VDAC1, protein responsible for formation of mitochondrial channels [6]. The heterodimer of 14-3-3 ε (YWHAE) and 14-3-3 z (YWHAZ) was originally described as a mitochondrial import stimulating factor [24] and accordingly both proteins were increased in portoamide-exposed cells, which may be related to the observed increase of mitochondrial size. The 14-3-3 protein family is described to control the mitochondria membrane permeability. High concentrations of 14-3-3γ subunits opposed the development of the mitochondria permeability transition pore (MPTP), which led to the swelling of the mitochondria [25]. However, the family of 14-3-3 proteins are keys proteins in many signaling pathways, amongst other in apoptosis and cell proliferation [26], which makes the interpretation of observed profiles difficult.

Conclusion

We conclude that portoamides show differential toxicities in some carcinogenic and non-carcinogenic cell lines, suggesting specific mechanisms of action. Data showed that portoamides exposure in the most sensitive cell line HT-29 affected mainly mitochondrial metabolism (NDUFS3, 14-3-3 proteins, ATP level, redox potential) and various indicators of mitochondrial size and shape. Portoamides did not, however, induce oxidative stress, increase ROS or mitotoxicity. Mitochondrial bioenergetics is required for tumorigenesis [27,28], and drugs that compromize mitochondrial metabolism are expected to be particularly effective in cell populations residing in poorly vascularized areas. Poor oxygen and nutrient availability in such areas lead to limited tumor metabolic plasticity and sensitivity to inhibition of mitochondrial function [29,30].
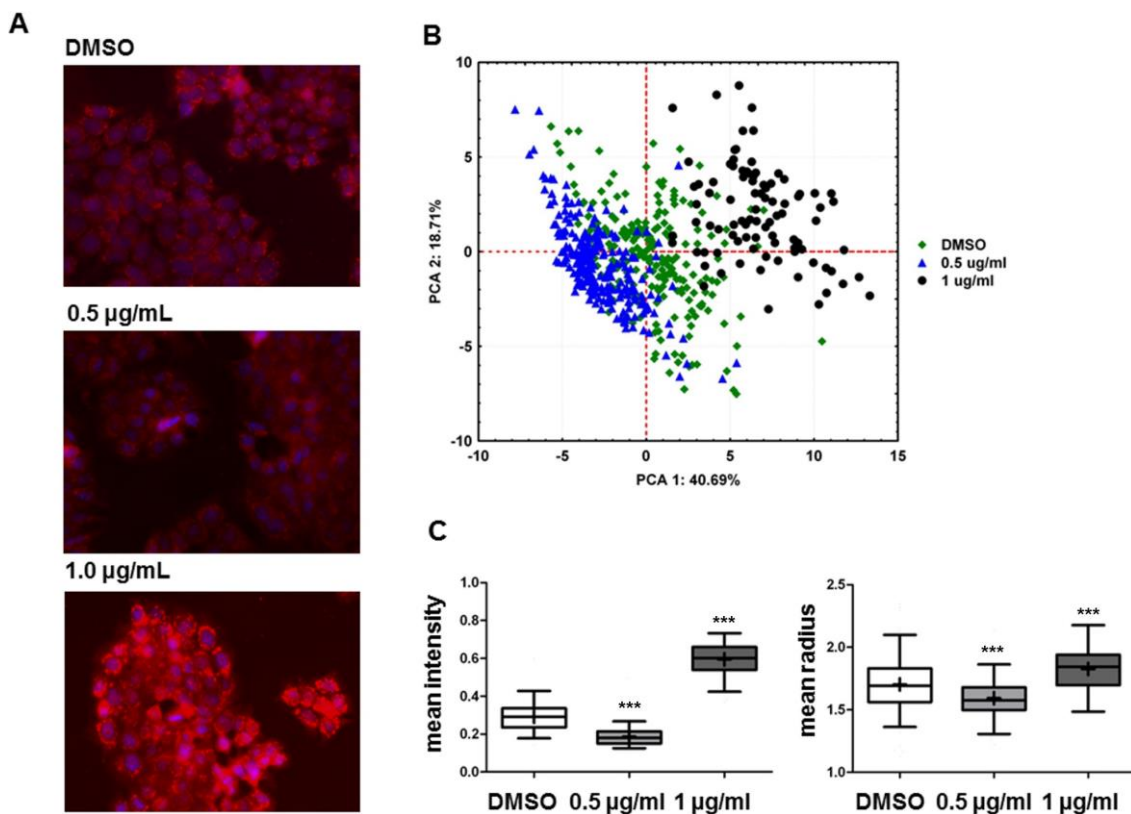
Fig 7. Quantitative analysis of fluorescence microscopy by CellProfiler software. A) Overlay of two fluorescent channels: blue, nucleus (HO- 33342); red, mitochondria (MitoTracker). B) Principal component analysis of 40 mitochondrial parameters (object intensity, size and shape of objects) discriminated between treatments (portoamides 0.5 μg/mL, 1 μg/mL) and solvent control (DMSO). Factors that contributed mainly (> 0.85) to PC1 were related to intensity measurements (IntegratedIntensityEdge, LowerQuartileIntensity, MaxIntensityEdge, MaxIntensity, MeanIntensityEdge, MeanIntensity, MedianIntensity, MinIntensityEdge, MinIntensity, StdIntensityEdge, UpperQuartileIntensity), while parameters related to size and shape (AreaShape_Area, AreaShape_MaxFeretDiameter, AreaShape_MaximumRadius, AreaShape_MeanRadius, AreaShape_MedianRadius, AreaShape_MinFeretDiameter, AreaShape_MinorAxisLength, AreaShape_Perimeter) contributed mainly (> 0.85) to PC2. C) Detailed analysis of two mitochondrial parameters, mean fluorescence intensity and mean radius, are shown. Data are represented as box-whisker plots and statistically significant differences between the solvent control and the treatment groups are indicated by asterisks (Kruskal-Wallies, Dunn's test, ******* = p<0.001). https://doi.org/10.1371/journal.pone.0188817.g007

The effects of portoamides on mitochondria were unexpected, characterized by increased mitochondrial polarization and decreased ATP production. Similar phenomena have, however, been reported in the literature [31] and attributed to the inhibition of F0F1-ATPase or adenine nucleotide transporter (ANT) activity under conditions of normal dislocation of protons from mitochondria. This will be expected to result in an elevated proton gradient and a drop in ATP levels. Finally, ROS will not necessarily be elevated under conditions of normal electron transport chain function.

FCUP 90
Cyanobacterial bioactive metabolites for anticancer drug
discovery: characterization of new compounds and
molecular mechanisms in physiologically relevant 3D cell
culture

Speculating on a potential mechanism (Fig 8), we propose that the energy metabolism is disrupted by portoamide exposure. Acute exposure experiments (4 hours) pointed to a more oxidative redox potential and decreased ATP level. Longer exposure time (48 hours) revealed a cellular response to generate more energy by increased mitochondrial electron transport chain (NDUFS3) and pentose phosphate pathway (TALDO).
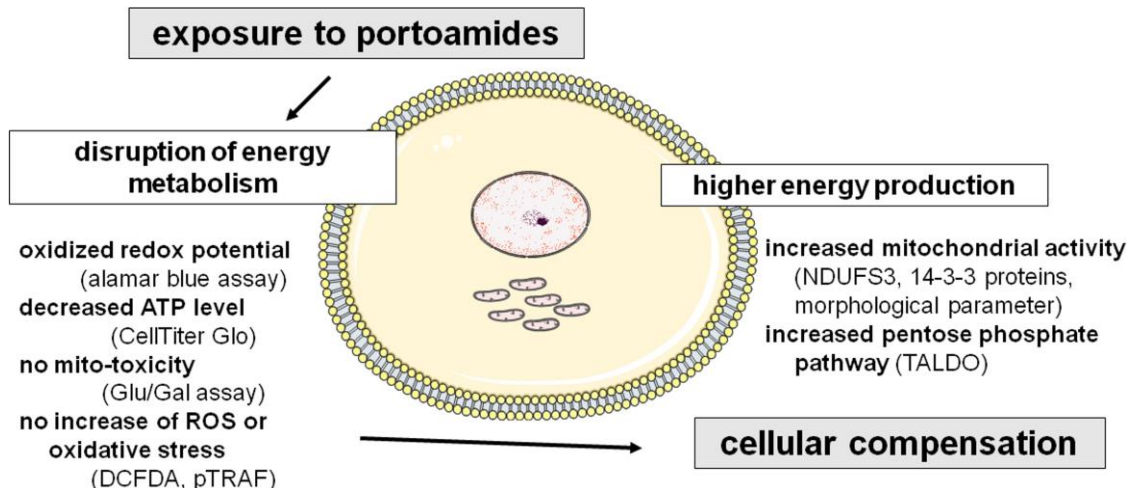
Fig 8. Predicted mechanism of action of portoamides in HT-29 colon adenocarcinoma cells, based on all experimental data.
https://doi.org/10.1371/journal.pone.0188817.g008

Experimental section

Growth of *Phormidium sp.* LEGE 05292

Phormidium sp. LEGE 05292 was obtained from the Blue Biotechnology and Ecotoxicology Culture Collection (LEGE CC) and grown under standard conditions to obtain sufficient quantity of biomass as previously described [7].

Isolation and purification of portoamides A and B

The purification of portoamides A and B was performed as previously described [7], using 5.0 g (dry mass) of *Phormidium sp*. LEGE 05292 biomass with slight alterations as detailed below. The fraction eluted at 100% methanol (MeOH) was purified and qualitatively analyzed on a HPLC (Alliance e2695) linked to a PDA 2998 detector and an automatic fraction collector III from Waters (Waters, Milford, Massachusetts, USA). The software Empower 2 (Chromatogra- phy Data Software) was used for data interpretation. The chromatographic column, XB-C18 Aeris PEPTIDE (150 mm × 4.6 mm i.d, 3.6 μm, Phenomex, Torrance, California, USA), was kept at 35˚C, and the solvents were acetonitrile and ultra-pure water, both acidified with 0.1% trifluoroacetic acid (TFA) with a flux of 0.8 mL/min. The PDA ranged from 210 to 280 nm at 254 nm and a resolution of 1.2 nm. For the purification, 500 μL was injected in 0.1% MeOH, and separated by a gradient of MeOH from 50% to 100% in 35 minutes. The mixture of por- toamides A and B eluted between tR = 13–15 min. For the analytic method, 20 μL were injected and separated by isocratic elution with 65% of MeOH acidified with 0.1% TFA.

Monitoring of the portoamides A and B mixture by Liquid Chromatography–Mass Spectrometry (LC-MS)

The collected portoamides A and B mixture was lyophilized and re-suspended in 100% aceto- nitrile (ACN) for LC-MS analysis. The sample was injected in the liquid phase chromatograph (Finningan, Surveyor) linked to a Mass Spectrometry detector (MS LCQ Fleet Ion Trap) equipped with an electronic ionization source, both from Thermo Finningan (Thermo Scien- tific, San Jose, California, USA). For data

acquisition and analysis, the software Xcalibur ver- sion 2 (Thermo Scientific) was used. Nitrogen served as nebulizer gas (80) and auxiliary gas (20), both in arbitrary units. The capillary potential was 22kV and the temperature of the metallic capillary was 350˚C. The spray voltage was 5.5 kV and 120V for the tubular lens. The chromatographic column used was the Hypersil GOLD (100 × 4.6 mm, 5 μL) (Thermo Scientific). The elution was done with acidified solvents with 0.1% formic acid in a flow of 0.8 mL/ min with the following gradient: 40 minutes 80% H_2O / 20% ACN; 8 minutes 100% ACN; 7 minutes 80% H_2O / 20% ACN. The injection volume was 20 μL in a partial loop. The samples were injected in both positive and negative modes, in full scan (200–2000 m/z).

Cell culture

The human cell lines HT-29, SH-SY5Y and T-47D were obtained from Sigma-Aldrich (St. Louis, Missouri, USA). A549, MG-63, RKO, HepG2 and HaCaT human cell lines were obtained from the American Type Culture Collection (ATCC) (Manassas, Virginia, EUA). The hCMEC/D3 cells were kindly donated by Dr. P. O. Courad (INSERM, France). All cell lines with the exception of SH-SY5Y were grown in Dulbecco Modified Eagle Medium (DMEM) from Gibco (Thermo Fisher Scientific, Waltham, Massachusetts, USA) supplemented with 10% fetal bovine serum (Bio- chrom, Berlin, Germany), 1% penicillin/streptomycin (Biochrom) at 100 IU/mL and 10 mg/mL, respectively, and 0.1% amphotericin (GE Healthcare, Little Chafont, United Kingdom). The cell line SH-SY5Y was grown in a 1:1 mix of the Eagle´s Minimum Essential Medium (MEM) with F12 Nutrient Mixture (HAM´s) medium, both from Life Technologies (Thermo Fisher Scientific), supplemented as described above, plus 1% of non-essential amino acids. Cells were grown in an incubator at 37˚C and 5% CO_2.

Cell viability evaluation by MTT

The MTT assay (3-(4,5-dimethylthiazol-2-yl)-2,5-diphenyltetrazolium bromide) was used to assess the cytotoxicity of different concentrations of portoamides on the studied cell lines as described in [5]. Cells were seeded in 96-well plates at 1 x 10^4 cells/cm^2 and the final exposure concentrations of portoamides ranged from 78 ng/mL to 10μ/mL. Based on the molarity of the portoamides (A = 1532 g/mol and B = 1502 g/mol) and the relative proportion (3:1), a molar mass of 1525 g/mol was attributed to the portoamides, and IC_{50} values converted to μmol/L (Table 1).

Exposure of HT-29 to portoamides

For proteomics, HT-29 cells were seeded in 6-well plates at a density of 1.3 x 10^5 cells/cm^2 for 24 hours before experiments. Then, the medium was replaced by fresh DMEM medium with: DMSO 0.5% (solvent control); 2) 0.5 μg/mL portoamides; and 3) 1 μg/mL portoamides. Six replicates per group were exposed for 48 hours. For fluorescence microscopy, HT-29 cells were seeded at a concentration of 1.3 × 10^5 cells/cm^2 in a 24-well plate (Orange Scientific, Braine-l'Alleud, Belgium) on a sterile glass cover slip, and three replicates were done per group.

Protein extraction

After exposure, cells were washed two times with PBS, before 600 μL of trypsin (Life Technolo- gies, Thermo Fischer Scientific) was added per well. Cells were transferred to 2 mL microcen- trifuge tubes and centrifuged at 3000 ×g for 5 minutes. The supernatant was removed and solubilization buffer (7 M Urea, 2M Thiourea, 4% CHAPS, 65 mM Dithiothreitol (DTT) and 0.8% ampholytes (v/v), all from Sigma-Aldrich) was added (80 μL per 15 mg of cell pellet).

Each tube was vortexed for two periods of 20 seconds, placed on ice for 30–45 minutes, before centrifugation at 16000 ×g for 20 minutes at 4˚C. The supernatants were collected, and protein content quantified with the Bradford method according to the instructions of the manufacturer (Bradford Protein Assay, Bio-Rad, Hercules, California, USA). Samples were stored at -20˚C until analysis.

Two-dimensional gel electrophoresis (2DGE)

The Isoelectric focusing (IEF) of each sample was done based on [5] using immobilized pH gradient (IPG) strips (pH 3–10, 17cm) (BioRad). For SDS-PAGE electrophoresis, 12.5% poly- acrylamide gels were used in cooled vertical electrophoresis unit (Hoefer, SE900, Massachu- setts, USA) connected to a power supply (Hoefer, PS600). Six gels were run simultaneously with constant amperage of 480 mA for six hours. After electrophoresis, gels were fixed for 24 hours in a 200 mL solution of MeOH (40% v/v) (Merck, New Jersey, USA) and acetic acid (10% v/v) (Panreac, Barcelona, Spain) per gel. Each gel was stained for 24 hours with Coomassie Blue as described in [32]. After staining, each gel was washed with distilled water, and stored in 200 mL of ammonium sulfate (20% p/v). Images of the gels were acquired using Quantity One (BioRad) and the densitometer GS-800 (Bio-Rad), image analysis with the PDQuest 2D analysis software (BioRad) as described in [5].

Protein identification by mass spectrometry

Differentially expressed spots were excised from the gels, washed, dehydrated, digested in tryp- sin (Promega, Madison, Wisconsin, USA), desalted and concentrated with 10 μl C18 reverse- phase tips (Pierce, Thermo Fisher Scientific) and spotted in duplicate on a MALDI plate, as described in [5]. Peptide mass spectra were obtained on a MALDI-TOF/TOF mass spectrometer (4800 Proteomics Analyzer, Applied Biosystems Europe) in the positive ion reflector mode. Spectra were obtained in the mass range between 800 and 4500 Da with ca. 1500 laser shots.

For each sample spot, a data dependent acquisition method was created to select the six most intense peaks, excluding those from the matrix, trypsin autolysis, or acrylamide peaks, for sub- sequent MS/MS data acquisition. Spectra were processed and analyzed by the Global Protein Server Workstation (Applied Biosystems), which uses internal MASCOT software (v2.1.0 Matrix Science, London, UK) on searching the peptide mass fingerprints and MS/MS data.

Swiss-Prot nonredundant protein sequence database (October 2014) was used for all searches under taxonomy *Homo sapiens*. Database search parameters were as follows: carbamidomethy- lation and propionamide of cysteine as a variable modification, oxidation of methionine, and the allowance for up to two missed tryptic cleavages. The peptide mass tolerance was 25 ppm and fragment ion mass tolerance was 0.3 Da. Positive identifications were accepted up to 95% of confidence level.

Morphological evaluation by fluorescence microscopy

After 48 hours exposure, cells were stained with 5 μg/mL Hoechst 33342 (HO-33342) (Sigma- Aldrich), 2 μg/mL Acridine Orange (AO) (Sigma-Aldrich), 500 nM Mitotracker Red CMXRos (Life Technologies) in PBS for 10 minutes at 37°C, fixed in 4% paraformaldehyde (VWR, Rad- nor, Pennsylvania, USA) for 10 minutes and then mounted on microscope slides (Fluoro- Mount, Sigma-Aldrich). Cells were observed under a fluorescence microscope Olympus BX41 (Olympus America Inc., Melville, New York, USA) with fixed excitation times for each fluores- cence channel (blue, green, red; 80 ms, 25 ms, 10 ms, respectively). Selected parameters were automatically quantified by the software CellProfiler [8]. The following modules were included in the pipeline: object intensity (19 parameters), size and shape of objects (21 parameters). A complete list of parameters can be found on the manual of CellProfiler (available at http://cellprofiler.org/).

Evaluation of oxidative stress with pTRAF transformed cells

We acknowledge the gift of the pTRAF plasmid from Elias Arnér, Division of Biochemistry, Department of Medical Biochemistry and Biophysics, Karolinska Institutet, Stockholm, Swe- den. Colorectal carcinoma cell line HCT116 transformed with a pTRAF plasmid [18,33] were cultured in Dulbecco's modified Eagle's (DMEM) supplemented with 10% fetal bovine serum at 37°C in 5% CO_2, 1% of penicillin/streptomycin and 0.1% of amphotericin B (Biochrom, United Kingdom). Cells were seeded in 96-well culture plates at a 1.0 x10^4 cells/cm^2, and adhe- sion allowed for 24 hours. Portoamides were tested on a concentration-response assay (up to 10 μM) and incubated on an Incucyte1 ZOOM Live-Cell Analysis System (Essen Instru- ments, Ann Arbor, MI). For the duration of 48h, Nrf2 activity was read at λex = 585 nm, emis- sion

filter: 625–705 nm, and auranofin (6 µM) was used as a positive control to confirm Nrf2 activity [18].

Detection of cellular reactive oxygen species (ROS)

Cells were seeded in a black-sided 96-well plate at 7.5×10^4 cells/cm^2 and allowed to attach overnight. Afterwards, cells were washed with PBS and stained with 25 µM 2',7'–dichloro- fluorescin diacetate (DFCDA) (Sigma-Aldrich) in PBS for 45 minutes in the dark at 37˚C. Cells were then washed with PBS and treated with portoamides (0.5 µg/mL and 1.0 µg/mL) for 1, 2, 4 and 24 hours. DMSO at 0.5% was the solvent control and tert-butyl hydrogen per- oxide (TBHP) at 50 µM and 100 µM the positive controls. Fluorescence was measured at 485 nm excitation and 535 nm emission at a Fluoroskan Ascent CF (MTX Lab Systems, Florida, USA).

Evaluation of cellular redox status using the AlamarBlue assay

Cells were seeded in a 96-well plate at 1.8×10^4 cells/cm^2, allowed to attach overnight and exposed to a gradient of portoamide concentrations from 80 ng/mL to 10 µg/mL in 1:2 dilu- tion steps. DMSO at 0.5% was the solvent control and DMSO at 20% was the positive control. After 1 hour, 10 µL of AlamarBlue (Thermo Fischer Scientific) was added to each well and fur- ther incubated for 3 hours (total exposure time 4h). Fluorescence was read at 530 nm excita- tion and 590 nm emission in a multimode microplate reader (Biotek, HT Synergy).

Quantification of ATP levels using glucose and galactose conditioned media conditions

Cells were seeded at 3.6×10^4 cells/cm^2 in complete DMEM medium and after 24 hours changed to glucose (25 mM) or galactose (10 mM) conditioned media as described in [22]. After 6 hours pre-incubation, cells were exposed for 4 hours to four portoamide concentra- tions (1.25–10 µg/mL). 100 µL of CellTiter-GLo1 Reagent (Promega) was added to each well and mixed on an orbital shaker for 2 minutes. The plate was incubated at room temperature for 10 minutes in the dark and luminescence read in a multimode microplate reader (Biotek, HT Synergy) at 1 sec integration time, and gain of 125.

Cytotoxicity evaluation using glucose and galactose selective medium conditions

Cells were seeded at 3.6×10^4 cells/cm^2 in complete DMEM medium and after 24 hours changed to glucose (25 mM) and galactose (10mM) conditioned media as previously described. After 6 hours pre-incubation, cells were exposed to a concentration gradient of por- toamides from 78 ng/mL to 10 µg/mL for 24 hours. The MTT assay was then performed as described before.

Statistical analyses

The IC$_{50}$ values were calculated from dose-response curves of portoamides on each cell line with a nonlinear regression choosing a variable slope with four parameters. The range was defined by 0% of viability for the highest concentration of portoamides (10 µg/mL) and by 100% viability for the solvent control (0.5% DMSO). For the fluorescence microscopy data quantified with CellProfiller, principal component analysis was performed for the 40 parame- ters of mitochondria. Factors were Kaiser normalized and Varimax rotated. Variables that contributed > 0.85 to the factor loadings of PC1 or PC2 were considered as important.

Selected parameters contributing to PC1 or PC2 were tested for normal distribution by the Kolmogorov-Smirnov test. Since data showed a non-parametric distribution, Kruskal-Wallis was applied followed by Dunn´s Multiple Comparison posthoc test. Significant differences were considered if $p < 0.05$. Data from functional assays (DCFDA, nrf2, alamar blue, ATP) were tested for normality distribution (Kolmogorov-Smirnov) and equal variances (Barthlett´s test). If such criteria were met, One-Way ANOVA was applied followed by Dunnett´s posthoc test; if criteria were not met, Kruskal-Wallis was applied followed by Dunn´s Multiple Com- parison posthoc test.

Acknowledgments

Author Contributions

Conceptualization: Pedro N. Leão, Alexandre Campos, Vitor Vasconcelos, Ralph Urbatzka.

Formal analysis: Tiago Ribeiro, Filipa Lemos, Marco Preto, Joana Azevedo, Maria Lígia Sousa, Pedro N. Leão, Alexandre Campos, Stig Linder, Rui Vitorino, Vitor Vasconcelos, Ralph Urbatzka.

Funding acquisition: Pedro N. Leão, Rui Vitorino, Vitor Vasconcelos, Ralph Urbatzka.

Investigation: Tiago Ribeiro, Filipa Lemos, Marco Preto, Joana Azevedo, Maria Lígia Sousa, Pedro N. Leão, Alexandre Campos, Stig Linder, Rui Vitorino, Vitor Vasconcelos, Ralph Urbatzka.

Methodology: Tiago Ribeiro, Filipa Lemos, Marco Preto, Joana Azevedo, Maria Lígia Sousa, Pedro N. Leão, Alexandre Campos, Stig Linder, Rui Vitorino, Vitor Vasconcelos, Ralph Urbatzka.

Supervision: Ralph Urbatzka.

Validation: Ralph Urbatzka.

Writing – original draft: Tiago Ribeiro, Filipa Lemos, Marco Preto, Joana Azevedo, Pedro N. Leão, Alexandre Campos, Rui Vitorino, Vitor Vasconcelos, Ralph Urbatzka.

Writing – review & editing: Tiago Ribeiro Maria Lígia Sousa, Stig Linder, Ralph Urbatzka.

References

1. Erwin PM, López-Legentil S, Schuhmann PW. The pharmaceutical value of marine biodiversity for anti-cancer drug discovery. Ecol Econ. 2010; 70: 445–451. https://doi.org/10.1016/j.ecolecon.2010.09.030
2. Balaji S, Gopi K, Muthuvelan B. A review on production of poly β hydroxybutyrates from cyanobacteria for the production of bio plastics. Algal Res. 2013; 2: 278–285. https://doi.org/10.1016/j.algal.2013.03. 002
3. Mevers E, Liu W-T, Engene N, Mohimani H, Byrum T, Pevzner PA, et al. Cytotoxic veraguamides, alky- nyl bromide-containing cyclic depsipeptides from the marine cyanobacterium cf. *Oscillatoria margariti- fera*. J Nat Prod. 2011; 74: 928–36. https://doi.org/10.1021/np200077f PMID: 21488639
4. Katz J, Janik JE, Younes A. Brentuximab Vedotin (SGN-35). Clin Cancer Res. 2011; 17: 6428–6436. https://doi.org/10.1158/1078-0432.CCR-11-0488 PMID: 22003070
5. Freitas S, Martins R, Campos A, Azevedo J, Osório H, Costa M, et al. Insights into the potential of pico-planktonic marine cyanobacteria strains for cancer therapies–Cytotoxic mechanisms against the RKO colon cancer cell line. Toxicon. 2016; 119: 140–151. https://doi.org/10.1016/j.toxicon.2016.05.016 PMID: 27242042
6. Freitas S, Martins R, Costa M, Leão P, Vitorino R, Vasconcelos V, et al. Hierridin B Isolated from a Marine Cyanobacterium Alters VDAC1, Mitochondrial Activity, and Cell Cycle Genes on HT-29 Colon Adenocarcinoma Cells. Mar Drugs. 2016; 14: 158. https://doi.org/10.3390/md14090158 PMID: 27589771
7. Leão PN, Pereira AR, Liu W-T, Ng J, Pevzner PA, Dorrestein PC, et al. Synergistic allelochemicals from a freshwater cyanobacterium. Proc Natl Acad Sci USA. 2010; 107: 11183–8. https://doi.org/10.1073/pnas.0914343107 PMID: 20534563
8. Carpenter AE, Jones TR, Lamprecht MR, Clarke C, Kang IH, Friman O, et al. CellProfiler: image analy- sis software for identifying and quantifying cell phenotypes. Genome Biol. 2006; 7: R100. https://doi. org/10.1186/gb-2006-7-10-r100 PMID: 17076895
9. Rabow AA, Shoemaker RH, Sausville EA, Covell DG. Mining the National Cancer Institute's tumor- screening database: Identification of compounds with similar cellular activities. J Med Chem. 2002; 45: 818–840. https://doi.org/10.1021/jm010385b PMID: 11831894
10. Boukamp P, Petrussevska RT, Breitkreutz D, Hornung J, Markham A, Fusenig NE. Normal Keratiniza- tion in a Spontaneously Immortalized. J Cell Biol. 1988; 106: 761–771. PMID: 2450098
11. Lehman TA, Modali R, Boukamp P, Stanek J, Bennett WP, Welsh JA, et al. P53 mutations in human immortalized epithelial cell lines. Carcinogenesis. 1993; 14: 833–839. https://doi.org/10.1093/carcin/14. 5.833 PMID: 8504475
12. Lamb J, Crawford ED, Peck D, Modell JW, Blat IC, Wrobel MJ, et al. The Connectivity Map: Using Gene-Expression Signatures to Connect Small Molecules, Genes, and Disease. Science. 2006; 313: 1929–1935.

https://doi.org/10.1126/science.1132939 PMID: 17008526

13. Hirst J, King MS, Pryde KR. The production of reactive oxygen species by complex I. Biochem Soc Trans. 2008; 36: 976–980. https://doi.org/10.1042/BST0360976 PMID: 18793173

14. Huang G, Chen Y, Lu H, Cao X. Coupling mitochondrial respiratory chain to cell death: an essential role of mitochondrial complex I in the interferon-beta and retinoic acid-induced cancer cell death. Cell Death Differ. 2007; 14: 327–37. https://doi.org/10.1038/sj.cdd.4402004 PMID: 16826196

15. Perl A, Hanczko R, Telarico T, Oaks Z, Landas S. Oxidative stress, inflammation and carcinogenesis are controlled through the pentose phosphate pathway by transaldolase. Trends Mol Med. 2011; 17: 395–403. https://doi.org/10.1016/j.molmed.2011.01.014 PMID: 21376665

16. Riganti C, Gazzano E, Polimeni M, Aldieri E, Ghigo D. The pentose phosphate pathway: an antioxidant defense and a crossroad in tumor cell fate. Free Radic Biol Med. 2012; 53: 421–436. https://doi.org/10.1016/j.freeradbiomed.2012.05.006 PMID: 22580150

17. Paul S, Jakhar R, Bhardwaj M, Kang SC. Glutathione-S-transferase omega 1 (GSTO1-1) acts as medi- ator of signaling pathways involved in aflatoxin B1-induced apoptosis-autophagy crosstalk in macro- phages. Free Radic Biol Med. 2015; 89: 1218–1230. https://doi.org/10.1016/j.freeradbiomed.2015.11. 006 PMID: 26561775

18. Johansson K, Cebula M, Rengby O, Dreij K, Carlström KE, Sigmundsson K, et al. Cross Talk in HEK293 Cells Between Nrf2, HIF, and NF-κB Activities upon Challenges with Redox Therapeutics Characterized with Single-Cell Resolution. Antioxid Redox Signal. 2017; 26: 229–246. https://doi.org/ 10.1089/ars.2015.6419 PMID: 26415122

19. Pagé B, Pagé M, Noel C. A new fluorometric assay for cytotoxic measurements in vitro. Int J Oncol. 1993; 3: 473–476. https://doi.org/10.3892/ijo.3.3.473 PMID: 21573387

20. Berridge M V, Herst PM, Tan AS. Tetrazolium dyes as tools in cell biology: new insights into their cellular reduction. Biotechnol Annu Rev. 2005; 11: 127–52. https://doi.org/10.1016/S1387-2656(05)11004-7 PMID: 16216776

21. Mallikarjun V, Clarke DJ, Campbell CJ. Cellular redox potential and the biomolecular electrochemical series: A systems hypothesis. Free Radic Biol Med. 2012; 53: 280–288. https://doi.org/10.1016/j. freeradbiomed.2012.04.034 PMID: 22609360

22. Eakins J, Bauch C, Woodhouse H, Park B, Bevan S, Dilworth C, et al. A combined in vitro approach to improve the prediction of mitochondrial toxicants. Toxicol Vitro. 2016; 34: 161–170. https://doi.org/10. 1016/j.tiv.2016.03.016 PMID: 27083147

23. Kamalian L, Chadwick AE, Bayliss M, French NS, Monshouwer M, Snoeys J, et al. The utility of HepG2 cells to identify direct mitochondrial dysfunction in the absence of cell death. Toxicol Vitro. 2015; 29: 732–740. https://doi.org/10.1016/j.tiv.2015.02.011 PMID: 25746382

24. Aghazadeh Y, Papadopoulos V. The role of the 14-3-3 protein family in health, disease, and drug devel- opment. Drug Discov Today. 2016; 21: 278–287. https://doi.org/10.1016/j.drudis.2015.09.012 PMID: 26456530

25. Liu D, Yi B, Liao Z, Tang L, Yin D, Zeng S, et al. 14-3-3γ protein attenuates lipopolysaccharide-induced cardiomyocytes injury through the Bcl-2 family/mitochondria pathway. Int Immunopharmacol. 2014; 21: 509–515. https://doi.org/10.1016/j.intimp.2014.06.014 PMID: 24957688

26. Freeman AK, Morrison DK. 14-3-3 Proteins: Diverse functions in cell proliferation and cancer progres- sion. Semin Cell Dev Biol. 2011; 22: 681–687. https://doi.org/10.1016/j.semcdb.2011.08.009 PMID: 21884813

27. Wallace DC. Mitochondria and cancer. Nat Rev Cancer. 2012; 12: 685–698. https://doi.org/10.1038/ nrc3365 PMID: 23001348

28. Weinberg SE, Chandel NS. Targeting mitochondria metabolism for cancer therapy. Nat Chem Biol. 2015; 11: 9–15. https://doi.org/10.1038/nchembio.1712 PMID: 25517383

29. Zhang X, Fryknäs M, Hernlund E, Fayad W, De Milito A, Olofsson MH, et al. Induction of mitochondrial dysfunction as a strategy for targeting tumour cells in metabolically compromised microenvironments. Nat Commun. 2014; 5: 3295. https://doi.org/10.1038/ncomms4295 PMID: 24548894

30. Senkowski W, Zhang X, Hägg Olofsson M, Isacson R, Höglund U, Gustafsson M, et al. Three-dimen- sional cell culture-based screening identifies the anthelminthic drug nitazoxanide as a candidate for treatment of colorectal cancer. Mol Cancer Ther. 2015; 14: 25911689. https://doi.org/10.1158/1535- 7163.MCT-14-0792 PMID: 25911689

31. Vander Heiden MG, Chandel NS, Schumacker PT, Thompson CB. Bcl-xL prevents cell death following growth factor withdrawal by facilitating mitochondrial ATP/ADP exchange. Mol Cell. 1999; 3: 159–67. https://doi.org/10.1016/s1097-2765(00)80307-x PMID: 10078199

32. Neuhoff V, Arold N, Taube D, Ehrhardt W. Improved staining of proteins in polyacrylamide gels includ- ing isoelectric focusing gels with clear background at nanogram sensitivity using Coomassie Brilliant Blue G-250 and R-250. Electrophoresis. 1988; 9: 255–262. https://doi.org/10.1002/elps.1150090603 PMID: 2466658

33. Kipp AP, Deubel S, Arnér ESJ, Johansson K. Time- and cell-resolved dynamics of redox-sensitive Nrf2, HIF and NF-κB activities in 3D spheroids enriched for cancer stem cells. Redox Biol. 2017; 12: 403– 409. https://doi.org/10.1016/j.redox.2017.03.013 PMID: 28319891

Supporting information
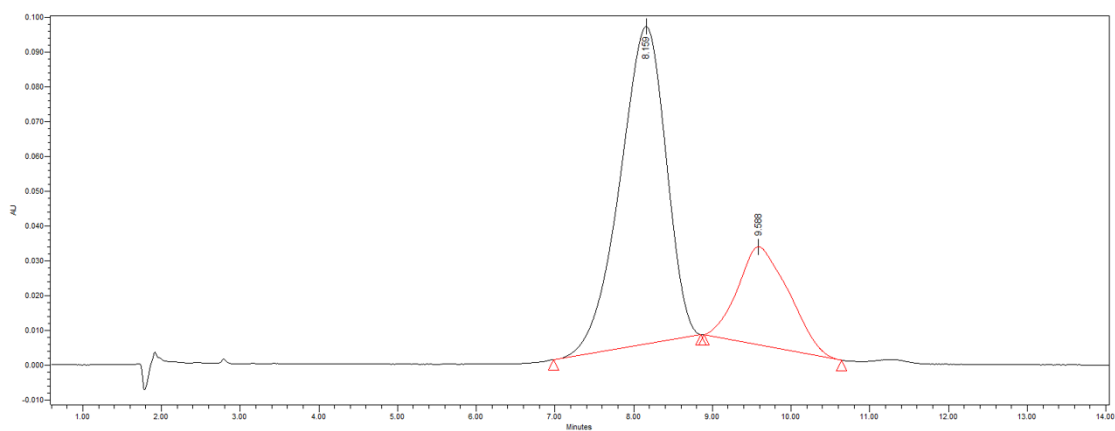
SI_Figure 1 - Relative proportions of portoamides A and B. Absorption spectra (A) obtained by the analytic method with the absorbance as function of time. The first peak represents portoamide A, while the second peak is portoamide B. The PDA spectrum (B), for each absorbance spectrum, with absorbance in the wavelength of 276.0 nm.

Supplementary information Dataset can be visualized at https://doi.org/10.1371/journal.pone.0188817.s002

SI_DataSet - Data from CellProfiler analyses. Raw data are given as derived from the CellProfiler software after analysis of fluorescent images and included 40 parameters of mitochondria used for the principal component analysis. CS, solvent control; PA, portoamides 0.5 µg/mL; PB, portoamides 1 µg/mL.

Portoamides A and B are mitochondrial toxins and induce cytotoxicity on the proliferative cell layer of *in vitro* microtumours

Published

Sousa ML, Ribeiro T, Vasconcelos V, Linder S and Urbatzka R (2019)

Portoamides A and B are mitochondrial toxins and induce cytotoxicity on the proliferative cell layer of *in vitro* microtumours

Maria Lígia Sousa [a, b], Tiago Ribeiro [a, b], Vítor Vasconcelos [a, b], Stig Linder [c, d], Ralph Urbatzka [a,*]

[a] *CIIMAR, Interdisciplinary Centre of Marine and Environmental Research, Porto, Portugal*
[b] *FCUP - Faculty of Sciences of University of Porto, Porto, Portugal*
[c] *Department of Oncology and Pathology, Cancer Centre Karolinska, Karolinska Institute, Stockholm, Sweden*
[d] *Department of Medical and Health Sciences, Linköping University, Linköping, Sweden*

ARTICLE INFO

Keywords:
Cyanobacteria
Natural compounds
Mitochondria
Spheroid

ABSTRACT

Cyanobacteria are known to produce many toxins and other secondary metabolites. The study of their specific mode of action may reveal the biotechnological potential of such compounds. Portoamides A and B (**PAB**) are cyclic peptides isolated from the cyanobacteria *Phormidium sp.* due to their growth repression effect on microalgae and were shown to be cytotoxic against certain cancer cell lines. In the present work, viability was assessed on HCT116 colon cancer cells grown as monolayer culture and as multicellular spheroids (MTS), non-carcinogenic cells and on zebrafish larvae. HCT116 cells and epithelial RPE-1[hTERT] cells showed very similar degrees of sensitivities to **PAB**. **PAB** were able to penetrate the MTS, showing a four-fold high IC$_{50}$ compared to monolayer cultures. The toxicity of **PAB** was similar at 4 °C and 37 °C suggesting energy-independent uptake. **PAB** exposure decreased ATP production, mitochondrial maximal respiration rates and induced mitochondrial membrane hyperpolarization. **PAB** induced general organelle stress response, indicated by an increase of the mitochondrial damage sensor PINK-1, and of phosphorylation of eIF2α, characteristic for endoplasmic reticulum stress. In summary, these findings show general toxicity of PAB on immortalized cells, cancer cells and zebrafish embryos, likely due to mitochondrial toxicity.

1. Introduction

Cyanobacteria are ancient photosynthetic microorganisms that inhabit ubiquitously and are recognized as prolific producers of secondary metabolites (Salvador-Reyes and Luesch, 2015) with widespread applications (Wijffels et al., 2013), from antifouling biotechnology (Dahms et al., 2006) to cancer treatment (de Claro et al., 2012; Katz et al., 2011; Newman and Cragg, 2017). Several compounds isolated from cyanobacteria, such as curacin A (Gerwick et al., 1994), dolastatin 10 and its analogue symplostatin 1 (Harrigan et al., 1998; Luesch et al., 2001), carmaphycins (Pereira et al., 2012) or cryptophycins (Golakoti et al., 1995) were initially identified as promising anticancer compounds, with very specific targets. For example, cytotoxic auristatins derivatives conjugated with antibodies (Brentuximab vedotin (Katz et al., 2011), Depatuxizumab Mafodotin (Mittapalli et al., 2019), ASG-15ME (Morrison et al., 2016), Polatuzumab vedotin (Morschhauser et al., 2019)), were successfully developed into clinical anticancer drugs or are under development in different phases of clinical trials (http://marinepharmacology.midwestern.edu/clinical_pipeline.html).

Compounds from cyanobacteria were often isolated from symbiotic (Kobayashi et al., 1994) or filamentous cyanobacteria (Tan, 2013), but picocyanobacteria also have shown antiproliferative effects on cancer cell lines with different modes of actions (Freitas et al., 2016a). Hierridin B was isolated by bioassay-guided fractionations due its selective cytotoxic activity on colon cancer cells, and decreased mitochondrial activity and function (Freitas et al., 2016b). Cyclic peptides have been identified as defence-related or toxic against other organisms. Examples of such compounds are cyclosporin (Page et al., 1986), vancomycin (Hammes and Neuhaus, 1974), tyrocidins (Mootz and Marahiel, 1997) or gramidicin S (Kondejewski et al., 1996) which were successfully used in medicine.

Portoamides A and B from the strain *Phormidium* sp. (previous *Oscillatoria* sp.) LEGE 05292 (Leão et al., 2010) were discovered due to its allelopathic effects on the microalgae *Chlorella vulgaris* (Leão et al., 2009) and its cytotoxic effects on cancer cell lines (Antunes et al., 2019; Leão et al., 2010; Ribeiro et al., 2017). Portoamides A and B are naturally produced on a proportion of 3:1 in *Phormidium* sp. and this mixture disturbed energy metabolism on the colon cancer cell line HT29 with prominent effects on mitochondria, but was not effective on other cell lines as A549 (lung carcinoma), HepG2 (hepatocellular carcinoma), T-47D (ductal carcinoma) and SHSY-5Y (neuroblastoma) at concentrations up to 6.5 μM (10 μg ml^{-1}) (Ribeiro et al., 2017). However, often such compounds with promising activities in monolayer cultures lack efficiency in advanced models of cancer as multicellular spheroids *in vitro*. The lack of effects may be related to the 3D architecture of spheroids with different gradients of oxygen, nutrients or proliferation state of cellular layers (Minchinton and Tannock, 2006; Sutherland, 1988; Weiswald et al., 2015) or to multicellular diffusion. Diffusion is controlled by biological barriers including plasma membranes, transport proteins and efflux pumps, and vesicular systems, among others (Minchinton and Tannock, 2006). 3D cell culture approaches are helpful to simulate the complexity of a solid tumor with regards to the occurrence of regions that are hypoxic and have poor nutritional status.

In the present work, we aimed to analyse the biological effects of the cytotoxic cyclic peptides mixture of Portoamides A and B on the proportion of 3:1, from now on assigned as **PAB,** on the colon cancer cell line HCT116 grown as both monolayer cells and multicellular spheroids. In order to assess **PAB** toxicity, the cytotoxicity on an epithelial cell line, and systemic toxicity on zebrafish larvae were included. The majority of the mechanistic work focused on the potential of **PAB** to alter mito-chondrial function and to act as a mitocan, which have been considered as a promising group of compounds, due to the importance of mitochondria for ATP production, cell signaling and cellular growth in tumors (He et al., 2015; Wallace, 2012). Verifying cytotoxic effects on multicellular spheroids, the uptake mechanism of **PAB** on cells was analysed. Overall, the presented research aimed to contribute to the suitability analysis of **PAB** as an anticancer molecules.

2. Experimental section

2.1. Monolayer cell culture

HCT116 cells (Sigma-Aldrich, St. Louis, USA), HCT116[BCL2+/+], HCT116[BCL2XL+/+], HCT116[MCL1+/+] and HCT116[p53 -/-] (kindly provided by Stig Linder, Karolinska Institute) were cultured on McCoy's 5 A medium (Gibco, Massachusetts, USA) supplemented with 10% of Fetal Bovine Serum (Biochrom, Berlin, Germany), 1% of penicillin/streptomycin (Biochrom, Berlin, Germany) and 0.1% of Amphotericin (GE Healthcare, Little Chafont, United Kingdom) and grown under 37ºC and 5% CO_2.

RPE-1[hTERT] cell line (Clontech, Palo Alto, USA) was cultured in Dulbecco's Modified Eagle Medium: Nutrient Mixture F-12 (DMEM/F12) from Gibco (Thermo Fisher Scientific, Massachusetts, USA) supplemented with 10% of Fetal Bovine Serum (Biochrom, Berlin, Germany), 1% of penicillin/streptomycin (Biochrom, Berlin, Germany) and 0.1% of Amphotericin (GE Healthcare, Little Chafont, United Kingdom) and grown under 37ºC and 5% CO_2.

2.2. MTT viability assay

The MTT assay (3-(4,5-dimethylthiazol-2-yl)-2,5-diphenylte-trazolium bromide) was used to evaluate monolayer cell culture viability. Cells were seeded at 33 000 cells ml^{-1} on 96 well plates and let to adhere overnight before being exposed to crescent concentrations of **PAB**, from 0.04 µM up to 10 µM over 48 h. After exposure, cells were incubated 4 h at 37ºC with 0.05 mg mL^{-1} MTT. Formazan salts formed during incubation were then dissolved with dimethyl sulfoxide (DMSO) and the absorbance read at 550 nm on a spectrophotometer GEN5™- Multi-detection Microplate Reader (Biotek, Bad Friedrichshall, Germany).

2.3. Permeabilization assay

Two 96 well plates of HCT116wt cells at 33 000 cells ml^{-1} were seeded with Dulbecco's Modified Eagle Medium (DMEM) supplemented with 10% of Fetal Bovine Serum (Biochrom, Berlin, Germany), 1% of penicillin/streptomycin (Biochrom, Berlin, Germany) and 0.1% of Amphotericin (GE Healthcare, Little Chafont, United Kingdom), 10 mM of HEPES (Sigma-Aldrich, St. Louis, USA) and adhere overnight under 37º C and 5% CO_2. They were further exposed to **PAB** at different concentrations up to 10 µM for 1 h, one plate at 37º C and the other at 4ºC. After that period, the wells were washed twice, and new medium was added. Viability was checked with MTT assay 48 h later.

2.4. Tetramethyl-rhodamine ethyl ester (TMRE) staining

The alteration of polarization of mitochondrial membrane was monitored by tetramethyl rhodamine ethyl ester (Life Technologies, USA). HCT116 wt cells were exposed for 6 h to 10 µM, 5 µM of **PAB** and a negative control Carbonyl cyanide-4-phenylhydrazone (FCCP) with 10 µM. At the end of the treatment, cells were exposed to 1 µM TMRE for 15 min and then observed under the fluorescence microscope Leica DM6000B and taken images were analysed with Cell Profiller software (Carpenter et al., 2006) followed by statistical analysis.

2.5. Mitochondrial ToxGlo assay

The Mitochondrial ToxGlo™ Assay kit (Promega, Madison, WI) was used as indicated by the manufacturer. Ten thousand cells were seeded on a 96 well plate and let to adhere overnight. The cell membrane integrity and cellular ATP levels were measured after 2 h exposure to **PAB** at concentrations of 10 µM, 5 µM, 2.5 µM, 1.25 µM, 0.625 µM, 0.3125 µM and 0.156 µM.

2.6. Seahorse mitochondrial stress test

Sixty thousand cells (optimized concentration) per well in 100 µL culture medium were plated in XF24-plate and incubated overnight. Medium was replaced with 500 µL of Seahorse XF base medium (200 mM L-glutamine, 1 mM pyruvate, 2.5 M glucose, pH 7.4) at 37º C without CO_2 for 1 h before measurements. Oxygen consumption rate (OCR) values were measured by XF24 Extracellular Flux Analyzer. The assessment of Mitochondrial activity was performed using a

Seahorse XF Cell Mito Stress Test Kit (Seahorse Bioscience).

2.7. 3D cell culture

A cell suspension of HCT116 containing 50 000 cells mL^{-1} was seeded on an Ultra-Low Attachment round bottom 96 well plate (Costar, Corning) and cells were allowed to settle for 20 min inside of the flow chamber. Then, the plate was incubated at 37 ºC, 5% of CO_2 for 5 days. After that period, the newly formed spheroids were treated for the following different experiments.

2.8. Viability assay: MTT, trypan blue, acid phosphatase and CellTiter-glo® 3D

Cells seeded on 96 well plates at 33 000 cells ml^{-1} were exposed to **PAB** (10 µM) or to model compounds, such as Etoposide (Target Mol, Boston, USA) (200 µM), Paclitaxel (Enzo Life Sciences, Lausen, Switzerland) (400 nM), Mitomycin C (Bioaustralis, New South Wales, Australia) (4 µM). After 48 h of exposure, different methodologies were applied to analyse cellular viability. (i) MTT was added to each well and the spheroid staining was controlled over the microscope. Then, the formazan salt crystals were dissolved in DMSO and absorbance was read at 550 nm on a GEN5™-Multi-detection Microplate Reader (Biotek, Bad Friedrichshall, Germany). (ii) Following the same experimental setup, Trypan Blue at 0.4% was added to each well containing a formed and treated spheroid. The staining was followed under the microscope. (iii) Acid Phosphatase assay was performed, according to Friedrich (Friedrich et al., 2007). The 96 well plate was carefully washed with PBS and then 100 µl was added of Sodium acetate buffer at 0.1 M containing p-nitrophenyl phosphate. The reaction was stopped after 2 h with 10 µLof NaOH (1 N) and the absorbance was read at 405 nm in a GEN5™-Multi-detection Microplate Reader (Biotek, Bad Friedrich- shall, Germany). (iv) The CellTiter-Glo® 3D Cell (Promega, Madison, USA) is an assay based on quantitation of the ATP as a marker for the presence of metabolically active cells. The assay was performed according to the manufacture's instructions and luminescence results were measured with a 0.3 s of integration time and gain of 100 with a GEN5™-Multi-detection Microplate Reader (Biotek, Bad Friedrich- shall, Germany).

2.9. Toxicological zebrafish embryo assay

Zebrafish embryos were raised from one day post fertilization (DPF) in egg water (60 µg mL^{-1} marine sea salt dissolved in distilled H_2O with 200 µM 1-phenyl-2-thiourea). From 3 to 5 DPF, 6 viable embryos per well were selected on a 96 well plate. Crescent concentrations of **PAB** were added to the wells and 24 h later the viable embryos were counted. A solvent control (0.1% DMSO) was included.

2.10. M30 CytoDeath ELISA

Analysis of apoptosis on spheroids were performed using M30 CytoDeath ELISA kit (Peviva AB, Bromma, Sweden), using 25 ml medium/extract and according to the manufacturer's instructions.

2.11. Western blot

Spheroids were collected and pooled according to its treatment (12 spheroids per pool), treated with RIPA buffer (150 mM NaCl, 50 mM Tris, pH 7.4, 1% Nonidet P-40, 0.1% SDS, 0.5% sodium deoxycholate) supplemented with protease and phosphatase inhibitors, and sonicated for short period to disrupt the spheroid. The solution was left on ice for 1 h and then centrifuged and protein collected and quantified by B Pierce Coomassie Plus (Bradford) Assay Reagent. SDS-PAGE was performed on pre-casted acrylamide gels NuPAGE™ 4–12% Bis-Tris Protein (Invi-troge™) using the NuPage system, loading 20 µg of proteins per sample. After electrophoresis, proteins on the gel were transferred on a Trans-Blot[R] Turbo™ Transfer System (semi-dry blot) to nitrocellulose membranes and incubated for 1 h at room temperature in PBS-Tween

with 5% non-fat dry milk. Protein loading was assessed by red pon-ceau staining of the membranes. Membranes were incubated with primary antibodies, PINK1 (H-300): sc-33796 (1: 1000), from Santa Cruz Biotechnology, Phospho-eIF2 α (Ser51) (#9721) (1: 1000), eIF2 α (#9722) (1: 000) from Cell Signaling Technologies, Antibody to β-actin (1: 5000) (# A5316) from Sigma-Aldrich (St Louis, MO, USA), diluted in PBS-Tween overnight at 4° C, followed by appropriate HRP-conjugated secondary antibodies, Anti-rabbit IgG HRP-linked (1: 3000) (#7074) and Anti-mouse HRP-linked Antibody (#7076) (1: 3000), both from Cell signaling Technologies. Antibody staining was visualized by the Clarity Western ECL Substrate (BioRad) on a BioRad Molecular Imager Gel DocTM XR+ with Image LabTM Software.

2.12. Fluorescence imaging

After exposure, spheroids were incubated with Hoechst 33342 (5 μg ml^{-1}), Propidium Iodide (5 μg ml^{-1}) (Sigma- Aldrich) and Calcein AM (Life Technologies) (3 μM) for 1 h. After fluorescent staining, the spheroids were observed under fluorescent microscope Leica DM6000B and images were analysed with Cell Profiller software (Carpenter et al., 2006) followed by statistical analysis.

2.13. Incucyte imaging

Spheroids made of HCT116 cells previously transfected with Incu-Cyte® NucLight nuclear-restricted red (mKate2) fluorescent protein were imaged on an IncuCyteFLR (Essen BioScience) over 48 h and images of each spheroid were taken every 4 h. The images were then collapsed on a short video (Supplementary Information) and spheroids areas measure with Incucyte software (IncuCyte® ZOOM) aid.

2.14. Statistical analysis

Normality of the data was studied by a Shapiro- Wilk normality test and when verified, a Student's t-test or One-way ANOVA was applied, for two variables or more, respectively, the last followed by Dunnet's multiple comparison post-test. For grouped analysis, a two-way ANOVA was applied, followed by Bonferroni Multicomparison post-test. When data did not obey to normal distribution, a Mann-Whitney or a Kruskal-Wallis test was applied followed by a Dunns post-test. Confidence interval used was 95%, where * means $p < 0.05$; ** means $p < 0.01$; ***means $p < 0.001$. Error bars of the graphs stand for Standard Deviation. All the described analysis was performed on GraphPad Prism 5 (La Jolla, CA) software.

3. Results

Loss of viability of cells exposed to **PAB** was verified in monolayer cell culture of about 50% confluence after 48 h of exposure on the cancer cell line HCT116 [wt] (Fig. 1) and the epithelial immortalized cell line RPE-1[hTERT] with similar IC$_{50}$ values, 3.38 μM and 3.36 μM, respectively (Fig. 1 and SI_Fig. 1), using MTT assay. The RPE-1[hTERT] cells exhibit proliferation inhibition when in contact with neighbouring cells (Pitaval et al., 2010), simulating better the characteristics of non-carcinogenic cells. When cultured confluent and exposed to **PAB,** a similar response was observed by MTT with an IC$_{50}$ of 2.94 0.65 (SI_Fig. 1). These results indicate that cytotoxic activity of **PAB** it is not dependent on the degree of confluence of cells, and therefore not dependent on the state of cell
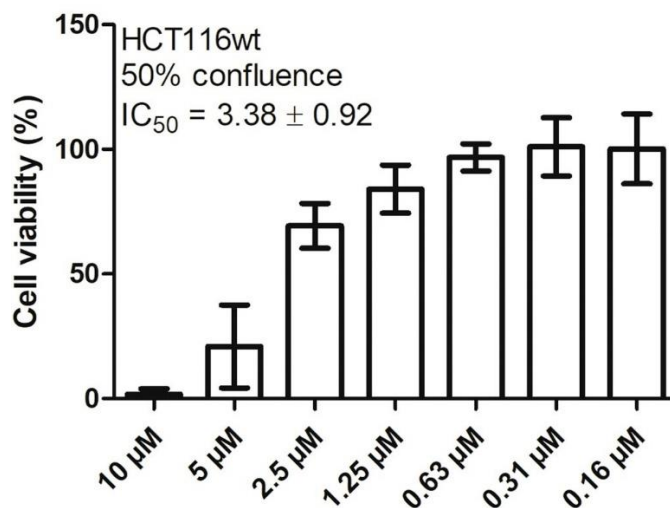
Fig. 1. Monolayer culture HCT116 wt cells viability assessment by MTT. n > 6, mean ± standard deviation, 3 independent assays proliferation.

Viability was additionally analysed on HCT116 cells cultured as multicellular spheroids (MTS), using both acid phosphatase assay (Friedrich et al., 2007; Herrmann et al., 2008) and the Cell Titer Glow 3D assay. Similar IC$_{50}$ values of 12.67 μM − acid phosphatase - (Fig. 2a) and 15.2 μM − Cell Titer Glow 3D assay - (Fig. 2b) were obtained in both methodologies. A 3-4-fold higher concentration of **PAB** was necessary to induce cell death on spheroids compared to monolayer cultures, and the different methodologies consistently demonstrated that **PAB** reduced significant the viability of spheroids. Toxicity was also assessed with zebrafish larvae at 3 DPF to 5 DPF.

FCUP 101
Cyanobacterial bioactive metabolites for anticancer drug
discovery: characterization of new compounds and
molecular mechanisms in physiologically relevant 3D cell
culture

After 24 h exposure, 100% of larvae were dead at concentrations higher than 5 µM (LC$_{50}$ ¼ 1.49 µM), while after 48 h exposure larvae were dead at concentrations higher than 0.6125 µM at 48 h (SI_Fig. 3).

MTT and trypan blue staining (SI_Fig. 2), as well as bright field and fluorescence images (Fig. 2c) revealed that the outer layer of spheroids
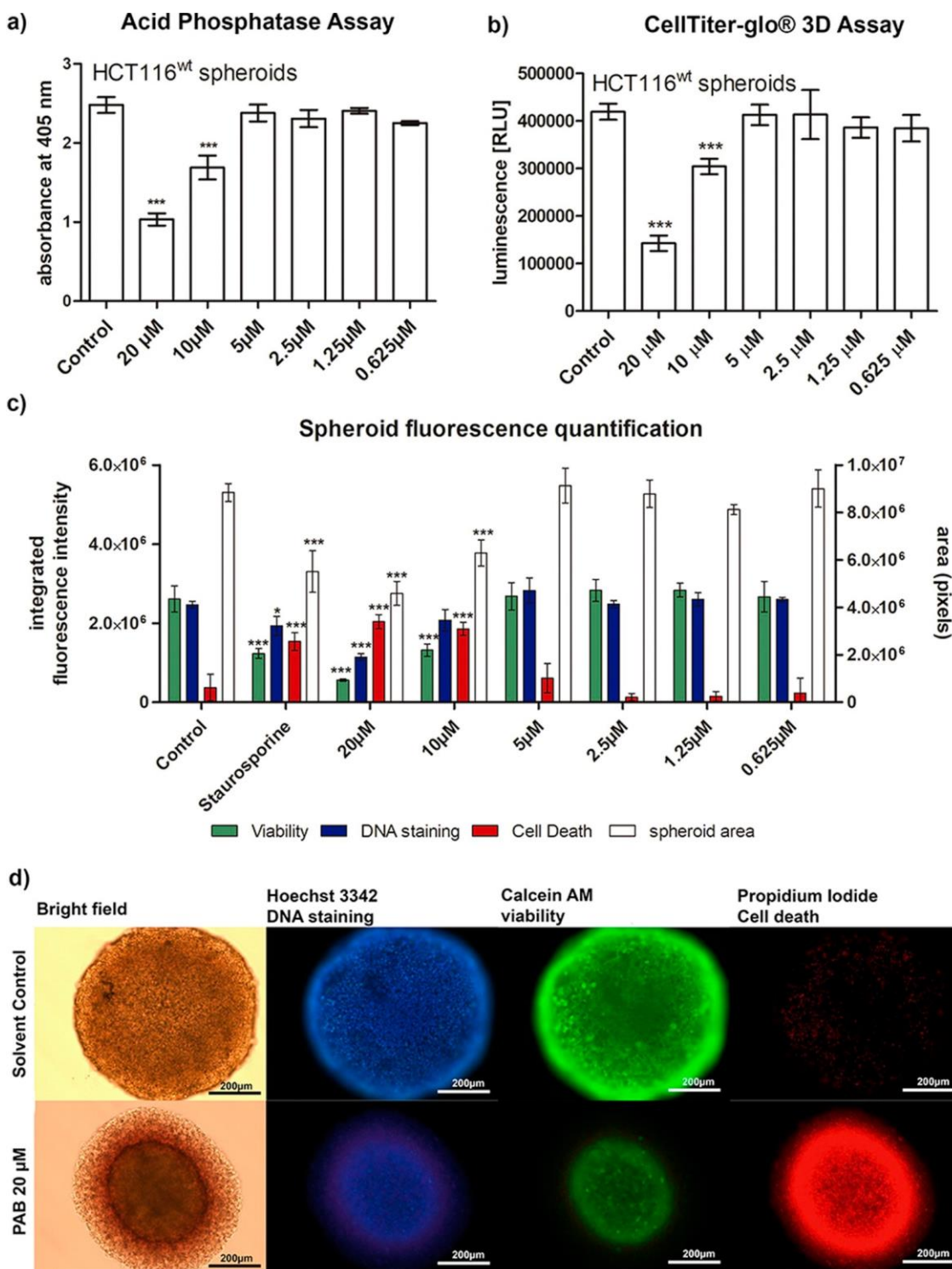
Fig. 2. Viability of HCT116 spheroids after 48 h exposure to **PAB**. a) Acid Phosphatase assay resulted in an IC$_{50}$ of 12.67 µM. b) CellTiter-glo® 3D viability assay resulted in an IC$_{50}$ value of 15.21 µM n > 3, mean±standard deviation; statistical differences to the control were indicated by *** p < 0.001. c) Quantification of fluorescence in spheroids after 48 h of exposure to **PAB**. Calcein AM (green) shows activity of cellular esterases (viability), Hoechst 33342 nuclear condensation (blue) and PI (red) dead cells (cell death). Staurosporine 500 nM was used as positive control. n = 3, mean ± standard deviation. **p < 0.01.***p < 0.001. d) Microscopy images of spheroids exposed to 20 µM **PAB** after 48 h, followed by fluorescent staining with Hoechst 33342, Calcein AM and PI general cell death. (For interpretation of the references to colour in this figure legend, the reader is referred to the Web version of this article.)

U. PORTO
FACULDADE DE CIÊNCIAS
UNIVERSIDADE DO PORTO

FCUP | 102
Cyanobacterial bioactive metabolites for anticancer drug discovery: characterization of new compounds and molecular mechanisms in physiologically relevant 3D cell culture

containing the active proliferating cells was majorly affected by **PAB.** In contrast, the inner zone of the spheroid remained alive after 48 h of exposure, at concentrations up to 20 µM. This information is particularly interesting, since this feature would not be assessed by only quantitative viability assays.

Quantification of fluorescence intensities by Cell Profiler software demonstrated that **PAB** increased PI (dead cells), decreased Calcein AM (cellular esterases, viability) and Hoechst 33342 (nuclear condensation) (Fig. 2c and SI_Fig. 5). Here, the use of fluorescent dyes for viability and cell death provided the clear information that the size of the spheroid decreased significantly, while the total area remained unchanged (Fig. 2d). **PAB** exposure led to the disintegration of the outer shell of the spheroids (bright field images), and to higher PI intensity on the outer cell layers.

Spheroids imaged on IncuCyteFLR (Essen BioScience) confirmed the observations that the outer layers lost their fluorescent signal consistent with cell death (SI_ Video 1 and 2). No alterations were verified for the size of the spheroids over the 48 h of exposure (SI_ Fig. 2).

The reduction of viability in spheroids was related to the induction of apoptosis. The M30 Cytodeath assay detects the caspase-cleaved cytokeratin 18, which can be cleaved by caspase 3, 6, 7 or 9 and therefore do not discriminate between intrinsic or extrinsic apoptosis. Here, concentrations of **PAB** ranging from 10 µM to 2.5 µM induced apoptosis (Fig. 3).

Supplementary video related to this article can be found at https://doi.org/10.1016/j.toxicon.2019.12.159

We intended to analyse further the mechanism of action of **PAB**, since viability assays do not specify the cell death mechanism. In apoptosis, cells recognize damage or irregular development and undergo a series of programmed mechanisms leading to its death without damaging surrounding healthy cells or the system (Ashkenazi, 2008). We tested HCT116 cells that overexpress different members of Bcl family genes (D'Arcy et al., 2011), which encode for anti-apoptotic mitochondrial-transmembrane proteins or knockout of p53, a key gene for apoptosis (Li et al., 2006). No alteration of sensitivity to **PAB** exposure was observed for these different strains of cells, IC_{50} values between the HCT116 wild type (3.38 µM) and HCT116 cell lines with Bcl family overexpression or p53 knockout (SI Table 1). Hence, analysed apoptotic genes are not involved in the molecular mechanism of **PAB**.

In a previous publication on HT29 cells grown as monolayers, **PAB** was suggested to induce hyperpolarization of mitochondria
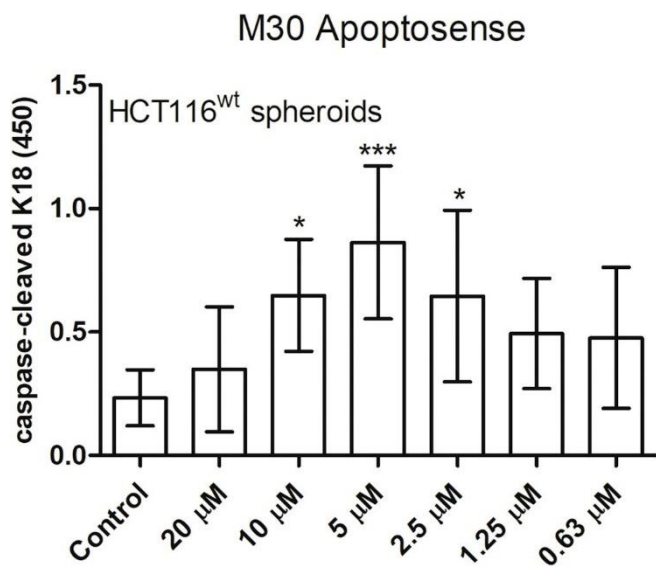
Fig. 3. M30 Apoptosense assay on spheroids exposed to **PAB** after 48 h of exposure. * p < 0.05, ** p < 0.01 and *** p < 0.001. n 6, error bars stand for standard deviation.

(Ribeiro et al., 2017). Here, effects of **PAB** were analysed on the mitochondria in wildtype HCT116 cells by focusing on the mitochondrial membrane potential, ATP level and mitochondrial respiration rates Tetramethylrhodamine Ethyl Ester (TMRE), a widely used fluorescent dye that enters the mitochondria with polarized membrane (Perry et al., 2011). HCT 116[wt] cells that were exposed to **PAB** for 6 h at the concentrations of 5 µM and 10 µM (Fig. 4f and g) and increased significantly the fluorescence intensity of the TMRE staining, which revealed a hyperpolarization of the mitochondrial membrane. Such effects have been previously observed in Jurkat cells exposed to well characterized com- pounds such as staurosporin (Scarlett et al., 2000) or camptothecin(Sanchez-Alcazar et al., 2000), followed by apoptosis. In agreement to our results, mitochondrial hyperpolarization has been reported as an event leading to cell death via apoptosis unrelated to the Bcl-2 family (Khaled et al., 2001) in an immune cell line. The hyperpolarization of the mitochondria would suggest that either Adenine nucleotide translocator or ATP synthase are impaired, leading to the efflux of protons. In support to this speculation, **PAB** in mussel plantigrade larvae reduced ATP synthase expression after 15 h of exposure at 16 µM (Antunes et al., 2019).

In order to get a better insight into effects on mitochondria, ATP level were analysed by the Mitochondrial ToxGlo assay kit and mitochondrial respiration with a Seahorse XF equipment. One of Seahorse XF features is to measure oxygen consumption rates of live cells in a multi-well plate, interrogating key cellular functions such as mitochondrial respiration. By using a Seahorse XF Cell Mito Stress Test Kit, parameters such as basal respiration, ATP production-coupled respiration or capacity can be assessed through the injection of compounds that modulate the functioning of independent steps of the mitochondrial electron transport chain. The injection of oligomycin impairs the proton pump (complex V); the FCCP injection leads to the transport of protons across the mitochondrial membrane, leading to the maximal mitochondrial respiration values; the injection of rotenone/mitomycin A impairs the complexes I and III of the electron transport chain, impairing the mitochondrial respiration. A decrease of ATP was detected in HCT116 [wt] cells with increasing concentrations of **PAB**, however, was accompanied by a decrease of cell viability at 5 and 10 µM within 2 h of exposure (Fig. 4e). The positive control CCCP (Carbonyl cyanide m-chlorophenyl hydrazine) decreased ATP content without affecting cell viability at any concentration. **PAB** exposure led to a decrease on oxygen consumption rates on HCT116 [wt] cells after 6 h of exposure (Fig. 4a). The maximum respiration was significantly reduced (Fig. 4b), but not the ATP production. This result is in accordance to Mitochondrial ToxGlo assay, which demonstrates that loss ATP production occurs in parallel to the increase of toxicity. In comparison, the respiration analysis with Seahorse XF analyser on RPE-1[hTERT] cells revealed also acute effects on respiration parameter with the same significant decrease on the maximum respiration rate (Fig. 4c), but not on ATP production (Fig. 4d). **PAB** are large cyclic peptides with molecular weights of 1532 Da (portoamide A) and 1502 Da (portoamide B) (Leão et al., 2010), which are unlikely to diffuse over cell membranes. As next, we examined whether **PAB** uptake is energy-dependent by incubating cells with **PAB** at 37º C or 4º C followed by washing out of the compounds. No significant difference in **PAB**-induced cytotoxicity was observed under these conditions (Fig. 5), suggesting that **PAB** uptake is not energy-dependent. Zebrafish assay is also consistent with this result (SI_Fig. 3), but these assays do not discard the possibility that **PAB** is attached to the cell membrane and acts on membrane proteins.

In order to analyse effects of **PAB** on mitochondria on spheroids, we measured the protein expression of PTEN-induced putative kinase 1 (PINK1), which is described to be a sensor of mitochondrial dysfunction (Kroemer et al., 2010; Narendra et al., 2010; Nunnari and Suomalainen, 2012), leading to mitophagy. PINK1 expression was increased after 48 h in response to **PAB** (Fig. 6a and b), confirming mitochondrial dysfunction in tumour spheroids. Mitochondrial function is required for cancer cell viability, and depletion of functional mitochondria impairs tumour
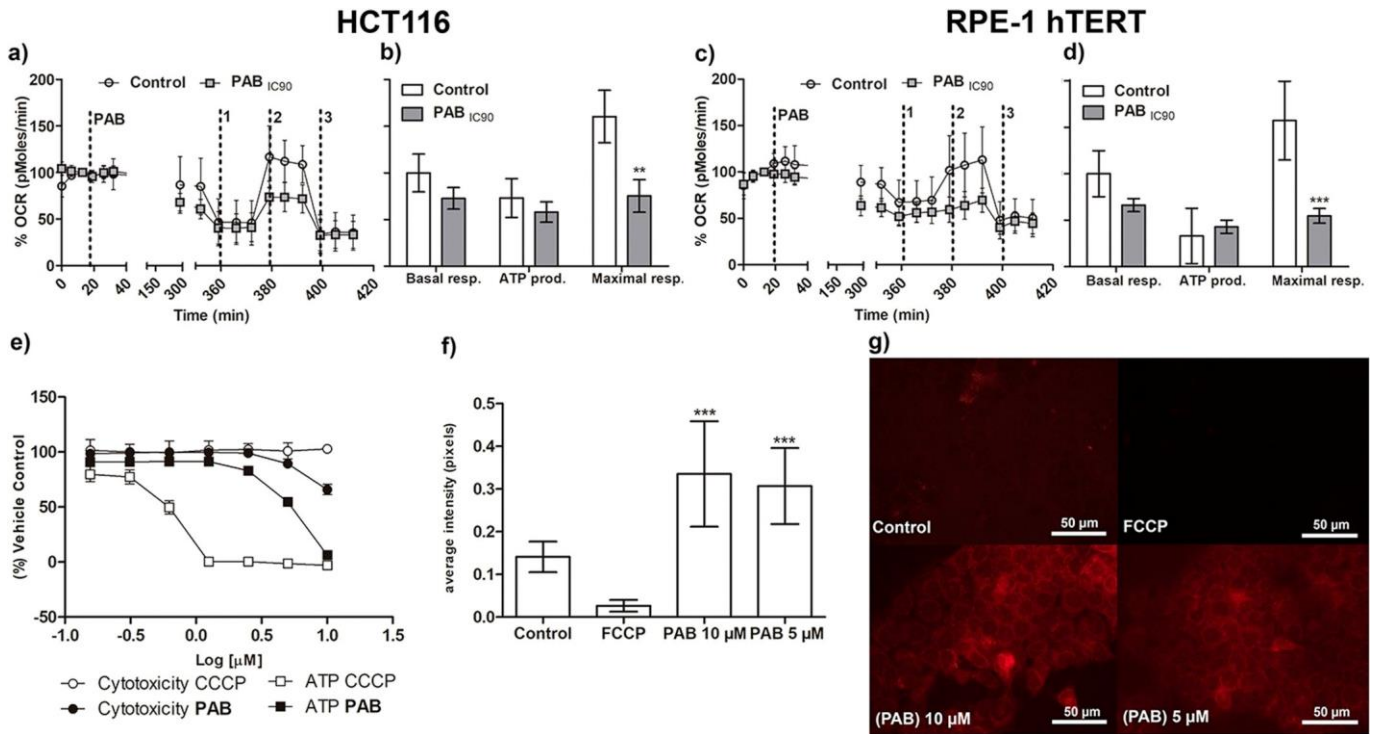
Fig. 4. Mitochondrial respiration by Seahorse XF analyser on HCT116[WT] and RPE-1[hTERT] cells exposed to **PAB**. a) HCT116[WT] oxygen consumption rates (OCR) over 6 h of exposure, followed by injection of mitochondrial stress kit reagents (1) oligomycin, (2) FCCP, and (3) Rotenone/Antimycin A. b) Quantification and statistical analysis of mitochondrial respiration parameters. c) RPE-1[hTERT] oxygen consumption rates. d) Quantification and statistical analysis of mitochondrial respiration parameters. Significant differences between treatments are indicated by ** = $p < 0.01$. *** = $p < 0.001$. n>8, mean ± SEM. e) ATP production in HCT116[wt] cells after 2 dph exposure to **PAB** at different concentrations (0.16–10 µM). CCCP is the positive control, a model compound that depolarizes the mitochondrial membrane in short periods of time. On X-axis, 1 Log (10 µM) to 0.81 Log (0.156 µM); Y-axis normalized 0% for Digitonin exposure 100% for untreated wells. n= 3, mean ± standard deviation. f) Statistical analysis of fluorescence intensity after running images on Cell Profiler software analysis. n =6, mean± standard deviation, statistical differences between treatments are shown by *** = $p < 0.001$. g) HCT116[wt] cells exposed to **PAB** at 5 µM and 10 µM followed by TMRE staining in which the increasing of fluorescence intensity indicates hyperpolarization of the mitochondrial membrane.
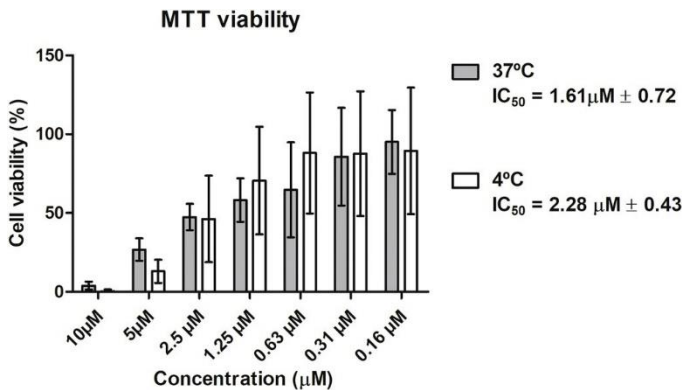
Fig. 5. Permeabilization assay. HCT116[wt] cells were exposed for 1 h to **PAB** at different temperatures followed by washouts and viability measurement after 48 h by MTT assay. n = 16, mean ± standard deviation.

cell growth (Weinberg et al., 2010). Also, a significant increase of the phosphorylation of eukaryotic initiation factor 2 (eIF2) was observed (Fig. 6 c and d), consistent with a generalized stress response related with the endoplasmic reticulum stress and protein synthesis disruption. Considering all data, **PAB** do not seem suitable for development as anticancer molecules, in particular due to the high toxicity of **PAB** on normal cells and on zebrafish larvae with effects at all tested concentrations (from 20 µM until 0.6125 µM) over 48 h. A future development for anticancer therapy would only be possible, if structural improvements would be done by medicinal chemistry, or targeted therapies are developed, such as conjugation to a high affinity targeted compound or linking the to an antibody (Chari et al., 2014) that would enable a targeted delivery of **PAB** to the cancer cells. Recently, two antibody-drug conjugates of cytotoxic molecules were approved by FDA for anti-cancer therapy, brentuximab vedotin (de Claro et al., 2012) and ado-trastuzumab (Verma et al., 2012).

4. Conclusions

In conclusion, **PAB** reduced the viability of HCT116 colon cancer cells grown as monolayer or as multicellular spheroid. **PAB** can penetrate the spheroids and its effects were more prominent on the outer layer. The uptake of **PAB** seems to be energy independent. In both cases, **PAB** disturbed the energy metabolism of cells by targeting mitochodrial function suggesting that **PAB** act as mitochondrial toxin. However, our data clearly demonstrate that **PAB** affected both carcinogenic and non-carcinogenic cells and exerted systemic toxicity on zebrafish larvae. Its future application will be dependent on a targeted transfer to cancer cells, to avoid prominent side effects.

Ethical statement

No approval by an ethics committee was not necessary for the pre- sented work, since chosen procedures are not considered animal experimentation according to the EC Directive 86/609/EEC for animal experiments, as this manuscript complies with the Elsevier Ethical Guidelines for Journal Publication.

FCUP 104
Cyanobacterial bioactive metabolites for anticancer drug
discovery: characterization of new compounds and
molecular mechanisms in physiologically relevant 3D cell
culture
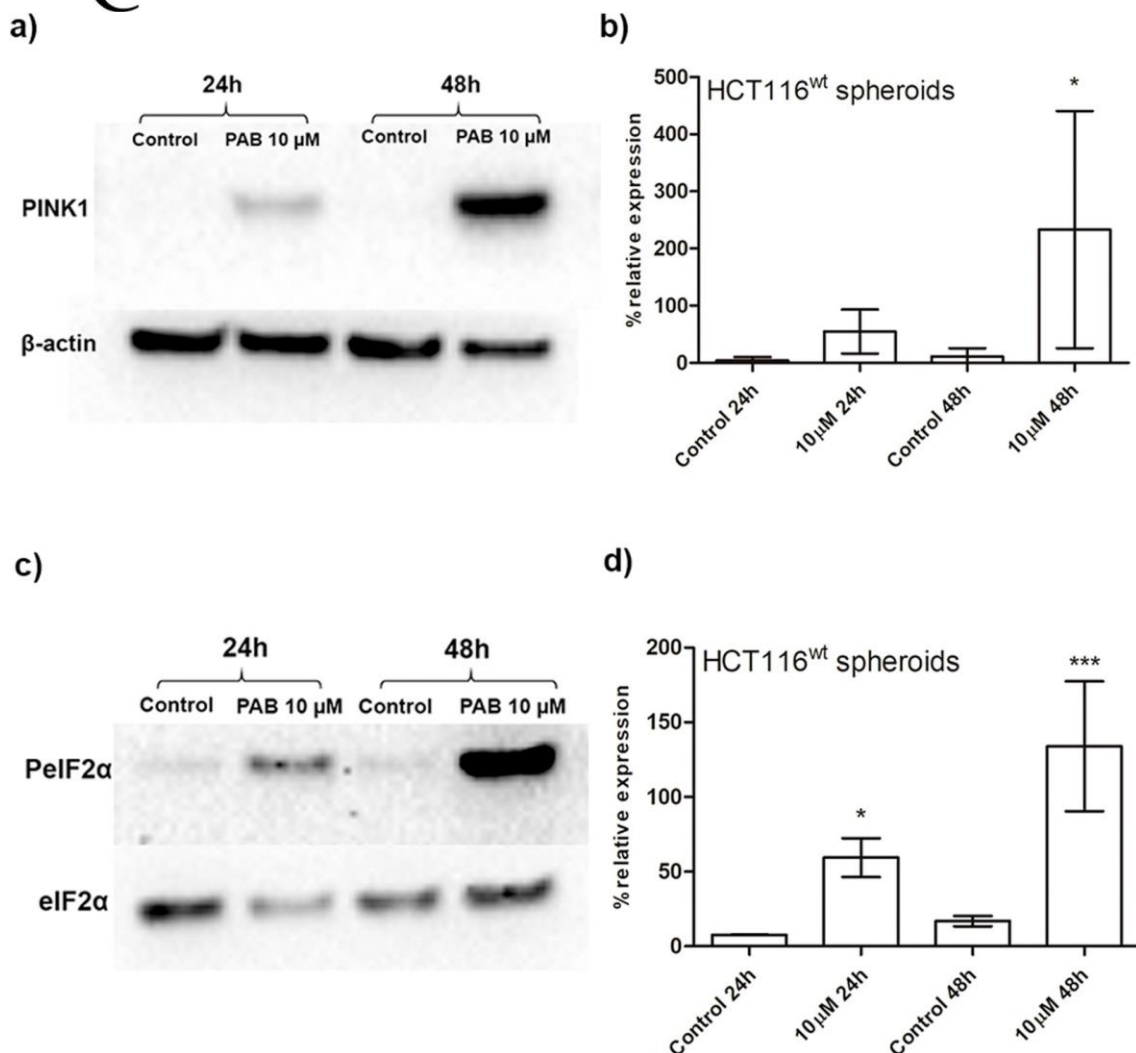
Fig. 6. PINK1 and P-eIF2α expression after exposure to **PAB** on HCT116 [wt] spheroids. a) Picture of a representative Western blot membrane of PINK1 and β-actin. b) Quantification of Western blot bands normalized by β-actin amount. c) Picture of a representative Western blot membrane of eIF2α phosphorylation and eIF2α. d) Quantification of Western blot bands normalized to eIF2α. Statistical differences to the control are indicated by * = $p < 0.05$, ** = $p < 0.01$ and *** = $p < 0.001$. n = 3, mean ± standard deviation.

Declaration of competing interest

The authors declare that there are no conflicts of interest.

Appendix A. Supplementary data

Supplementary data to this article can be found online at https://doi. org/10.1016/j.toxicon.2019.12.159.

References

Antunes, J., et al., 2019. A multi-bioassay integrated approach to assess the antifouling potential of the cyanobacterial metabolites portoamides. Mar. Drugs 17, 111. https://doi.org/10.3390/md17020111.

Ashkenazi, A., 2008. Directing cancer cells to self-destruct with pro-apoptotic receptor agonists. Nat. Rev. Drug Discov. 7, 1001. https://doi.org/10.1038/nrd2637.

Carpenter, A.E., et al., 2006. CellProfiler: image analysis software for identifying and quantifying cell phenotypes. Genome Biol. 7, R100. https://doi.org/10.1186/gb-2006-7-10-r100.

Chari, R.V.J., et al., 2014. Antibody–drug conjugates: an emerging concept in cancer therapy. Angew. Chem. Int. Ed. 53, 3796–3827. https://doi.org/10.1002/anie.201307628.

D'Arcy, P., et al., 2011. Inhibition of proteasome deubiquitinating activity as a new cancer therapy. Nat. Med. 17, 1636. https://doi.org/10.1038/nm.2536.

Dahms, H.-U., et al., 2006. Antifouling potential of cyanobacteria: a mini-review. Biofouling 22, 317–327. https://doi.org/10.1080/08927010600967261.

de Claro, R.A., et al., 2012. U.S. Food and drug administration approval summary: brentuximab vedotin for the treatment of relapsed Hodgkin lymphoma or relapsed

systemic anaplastic large-cell lymphoma. Clin. Cancer Res. 18, 5845–5849. https://doi.org/10.1158/1078-0432.ccr-12-1803.

Freitas, S., et al., 2016a. Insights into the potential of picoplanktonic marine cyanobacteria strains for cancer therapies – cytotoxic mechanisms against the RKO colon cancer cell line. Toxicon 119, 140–151. https://doi.org/10.1016/j.toxicon.2016.05.016.

Freitas, S., et al., 2016b. Hierridin B isolated from a marine cyanobacterium alters VDAC1, mitochondrial activity, and cell cycle genes on HT-29 colon adenocarcinoma cells. Mar. Drugs 14, 158. https://doi.org/10.3390/md14090158.

Friedrich, J., et al., 2007. A reliable tool to determine cell viability in complex 3-D culture: the acid phosphatase assay. J. Biomol. Screen 12, 925–937. https://doi.org/10.1177/1087057107306839.

Gerwick, W.H., et al., 1994. Structure of Curacin A, a novel antimitotic, antiproliferative and brine shrimp toxic natural product from the marine cyanobacterium lyngbya majuscula. J. Org. Chem. 59, 1243–1245. https://doi.org/10.1021/jo00085a006.

Golakoti, T., et al., 1995. Structure determination, conformational analysis, chemical stability studies, and antitumor evaluation of the cryptophycins. Isolation of 18 new analogs from Nostoc sp. strain GSV 224. J. Am. Chem. Soc. 117, 12030–12049. https://doi.org/10.1021/ja00154a002.

Hammes, W.P., Neuhaus, F.C., 1974. On the mechanism of action of Vancomycin: inhibition of peptidoglycan synthesis in gaffkya homari. Antimicrob. Agents Chemother. 6, 722–728. https://doi.org/10.1128/AAC.6.6.722.

Harrigan, G.G., et al., 1998. Symplostatin 1: A dolastatin 10 analogue from the marine cyanobacterium symploca hydnoides. J. Nat. Prod. 61, 1075–1077. https://doi.org/10.1021/np980321c.

He, H., et al., 2015. A novel bifunctional mitochondria-targeted anticancer agent with high selectivity for cancer cells. Sci. Rep. 5, 13543. https://doi.org/10.1038/srep13543.

Herrmann, R., et al., 2008. Screening for compounds that induce apoptosis of cancer cells grown as multicellular spheroids. J. Biomol. Screen 13, 1–8. https://doi.org/10.1177/1087057107310442.

Katz, J., et al., 2011. Brentuximab vedotin (SGN-35). Clin. Cancer Res. 17, 6428–6436. https://doi.org/10.1158/1078-0432.CCR-11-0488.

Khaled, A.R., et al., 2001. Interleukin-3 withdrawal induces an early increase in mitochondrial membrane potential unrelated to the Bcl-2 family: roles of intracellular pH, ADP transport and F0F1-ATPase. J. Biol. Chem. 276, 6453–6462. https://doi.org/10.1074/jbc.M006391200.

Kobayashi, M., et al., 1994. Arenastatin A, a potent cytotoxic depsipeptide from the okinawan marine sponge Dysidea arenaria. Tetrahedron Lett. 35, 7969–7972. https://doi.org/10.1016/0040-4039(94)80024-3.

Kondejewski, L.H., et al., 1996. Gramicidin S is active against both gram-positive and gram-negative bacteria. Int. J. Pept. Protein Res. 47, 460–466. https://doi.org/10.1111/j.1399-3011.1996.tb01096.x.

Kroemer, G., et al., 2010. Autophagy and the integrated stress response. Mol. Cell 40, 280–293. https://doi.org/10.1016/j.molcel.2010.09.023.

Leão, P.N., et al., 2010. Synergistic allelochemicals from a freshwater cyanobacterium. Proc. Natl. Acad. Sci. 107, 11183–11188. https://doi.org/10.1073/pnas.0914343107.

Leão, P.N., et al., 2009. Allelopathic activity of cyanobacteria on green microalgae at low cell densities. Eur. J. Phycol. 44, 347–355. https://doi.org/10.1080/09670260802652156.

Li, J., et al., 2006. Endoplasmic Reticulum Stress-induced Apoptosis: multiple pathways and activation of p53-up-regulated modulator of apoptosis (PUMA) and NOXA by p53. J. Biol. Chem. 281, 7260–7270. https://doi.org/10.1074/jbc.M509868200.

Luesch, H., et al., 2001. Isolation of dolastatin 10 from the marine cyanobacterium symploca species VP642 and total stereochemistry and biological evaluation of its analogue Symplostatin 1. J. Nat. Prod. 64, 907–910. https://doi.org/10.1021/np010049y.

Minchinton, A.I., Tannock, I.F., 2006. Drug penetration in solid tumours. Nat. Rev. Cancer 6, 583–592. https://doi.org/10.1038/nrc1893.

Mittapalli, R.K., et al., 2019. An integrated population pharmacokinetic model versus individual models of Depatuxizumab Mafodotin, an anti-EGFR antibody drug conjugate, in patients with solid tumors likely to overexpress EGFR. J. Clin. Pharmacol. https://doi.org/10.1002/jcph.1418.

Mootz, H.D., Marahiel, M.A., 1997. The tyrocidine biosynthesis operon of Bacillus brevis: complete nucleotide sequence and biochemical characterization of functional internal adenylation domains. J. Bacteriol. 179, 6843–6850. https://doi.org/10.1128/jb.179.21.6843-6850.1997.

Morrison, K., et al., 2016. Development of ASG-15ME, a novel antibody–drug conjugate targeting SLITRK6, a new urothelial cancer biomarker. Mol. Cancer Ther. 15, 1301–1310. https://doi.org/10.1158/1535-7163.MCT-15-0570.

Morschhauser, F., et al., 2019. Polatuzumab vedotin or pinatuzumab vedotin plus rituximab in patients with relapsed or refractory non-Hodgkin lymphoma: final results from a phase 2 randomised study (ROMULUS). The Lancet Haematol. https://doi.org/10.1016/S2352-3026(19)30026-2.

Narendra, D.P., et al., 2010. PINK1 is selectively stabilized on impaired mitochondria to activate parkin. PLoS Biol. 8, e1000298 https://doi.org/10.1371/journal.pbio.1000298.

Newman, D., Cragg, G., 2017. Current status of marine-derived compounds as warheads in anti-tumor drug candidates. Mar. Drugs 15, 99. https://doi.org/10.3390/md15040099.

Nunnari, J., Suomalainen, A., 2012. Mitochondria: in sickness and in health. Cell 148, 1145–1159. https://doi.org/10.1016/j.cell.2012.02.035.

Page, E.H., et al., 1986. Cyclosporin A. J. Am. Acad. Dermatol. 14, 785–791. https://doi.org/10.1016/S0190-9622(86)70094-7.

Pereira, A.R., et al., 2012. The carmaphycins: new proteasome inhibitors exhibiting an α,β-epoxyketone warhead from a marine cyanobacterium. Chembiochem 13,

810–817. https://doi.org/10.1002/cbic.201200007.

Perry, S.W., et al., 2011. Mitochondrial membrane potential probes and the proton gradient: a practical usage guide. Biotechniques 50, 98–115. https://doi.org/10.2144/000113610.

Pitaval, A., et al., 2010. Cell shape and contractility regulate ciliogenesis in cell cycle-arrested cells. J. Cell Biol. 191, 303–312. https://doi.org/10.1083/jcb.201004003.

Ribeiro, T., et al., 2017. Cytotoxicity of portoamides in human cancer cells and analysis of the molecular mechanisms of action. PLoS One 12, e0188817. https://doi.org/10.1371/journal.pone.0188817.

Salvador-Reyes, L.A., Luesch, H., 2015. Biological targets and mechanisms of action of natural products from marine cyanobacteria. Nat. Prod. Rep. 32, 478–503. https://doi.org/10.1039/C4NP00104D.

Sanchez-Alcazar, J.A., et al., 2000. Increased mitochondrial cytochrome c levels and mitochondrial hyperpolarization precede camptothecin-induced apoptosis in Jurkat cells. Cell Death Differ. 7, 1090. https://doi.org/10.1038/sj.cdd.4400740.

Scarlett, J.L., et al., 2000. Changes in mitochondrial membrane potential during staurosporine-induced apoptosis in Jurkat cells. FEBS (Fed. Eur. Biochem. Soc.) Lett. 475, 267–272. https://doi.org/10.1016/S0014-5793(00)01681-1.

Sutherland, R.M., 1988. Cell and environment interactions in tumor microregions: the multicell spheroid model. Science 240, 177. https://doi.org/10.1126/science.2451290.

Tan, L.T., 2013. Pharmaceutical agents from filamentous marine cyanobacteria. Drug Discov. Today 18, 863–871. https://doi.org/10.1016/j.drudis.2013.05.010.

Verma, S., et al., 2012. Trastuzumab emtansine for HER2-positive advanced breast cancer. N. Engl. J. Med. 367, 1783–1791. https://doi.org/10.1056/NEJMoa1209124.

Wallace, D.C., 2012. Mitochondria and cancer. Nat. Rev. Cancer 12, 685. https://doi.org/10.1038/nrc3365.

Weinberg, F., et al., 2010. Mitochondrial metabolism and ROS generation are essential for Kras-mediated tumorigenicity. Proc. Natl. Acad. Sci. 107, 8788–8793. https://doi.org/10.1073/pnas.1003428107.

Weiswald, L.-B., et al., 2015. Spherical cancer models in tumor biology. Neoplasia 17, 1–15. https://doi.org/10.1016/j.neo.2014.12.004.

Wijffels, R.H., et al., 2013. Potential of industrial biotechnology with cyanobacteria and eukaryotic microalgae. Curr. Opin. Biotechnol. 24, 405–413. https://doi.org/10.1016/j.copbio.2013.04.004.

Supplementary material
Supplementary Figure 1
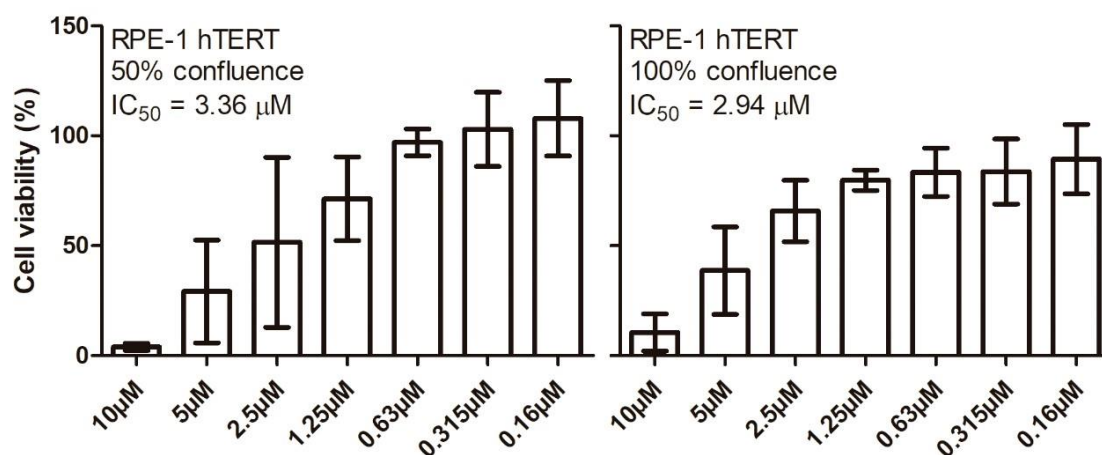
Figure 1. Monolayer culture viability. a) RPE-1hTERT cell viability assessment by MTT assay where cells were exposed to PAB under non-confluent and b) confluent culture conditions (standard). RPE-1hTERT cells viability assessment by MTT. n > 10 mean ± standard deviation.

Supplementary Figure 2

a)
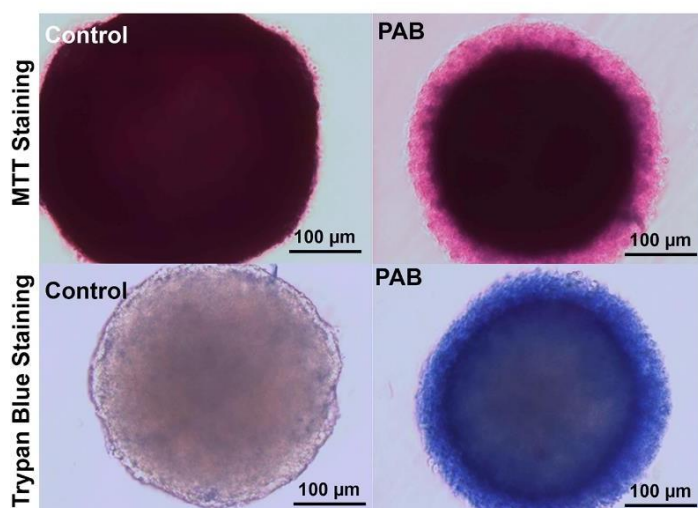
b)
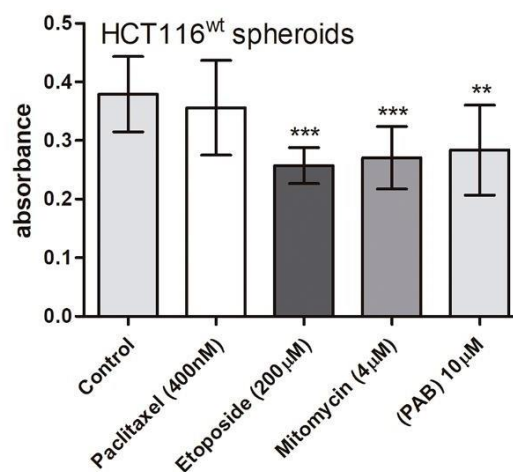
Figure 2. Viability assays of spheroids exposed to PAB for 48h. a) Microscopy observation of spheroid with MTT staining and TB staining. b) MTT viability test with **PAB** and other model compounds (Paclitaxel 400 nM; Etoposide 200 µM; Mitomycin 4 µM). Statistical differences to the control are indicated by ** = p – value < 0.01 and *** = p- value < 0.001. n=12, mean ± standard deviation.

Supplementary Figure 3
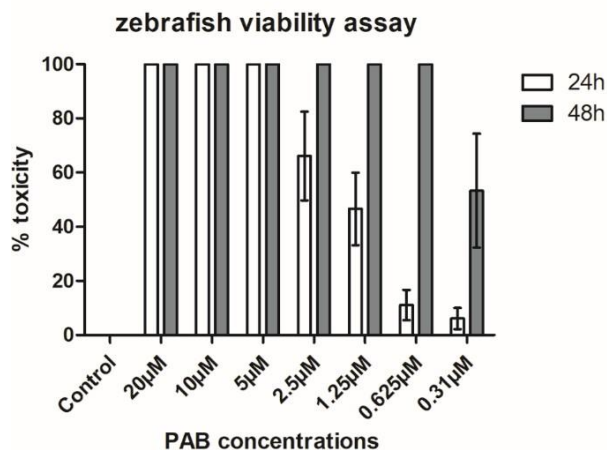
Figure 3. Zebrafish toxicological assay. Toxicity was evaluated based on the number of dead embryos after 24h and 48h. n>15, 2 independent assays.

Supplementary Figure 4
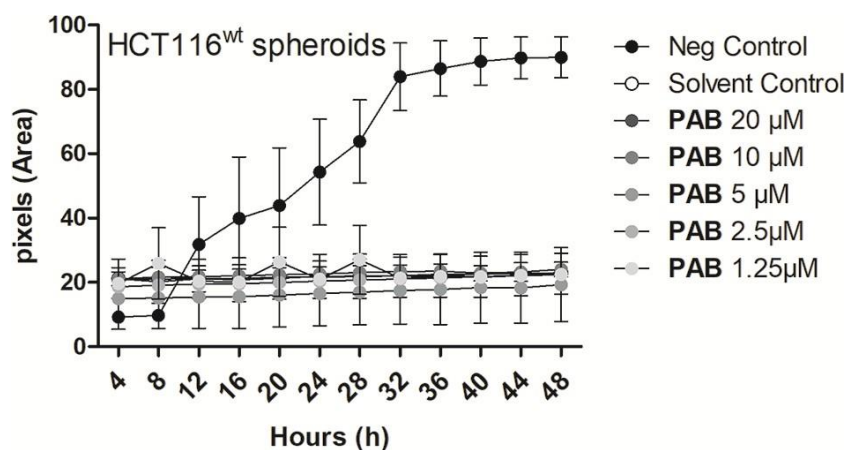
Figure 4. Graph of the total area measured on the different spheroids exposed over 48h. Negative control is 20% f DMSO. n>3. Mean ± standard deviation.

Supplementary Figure 5
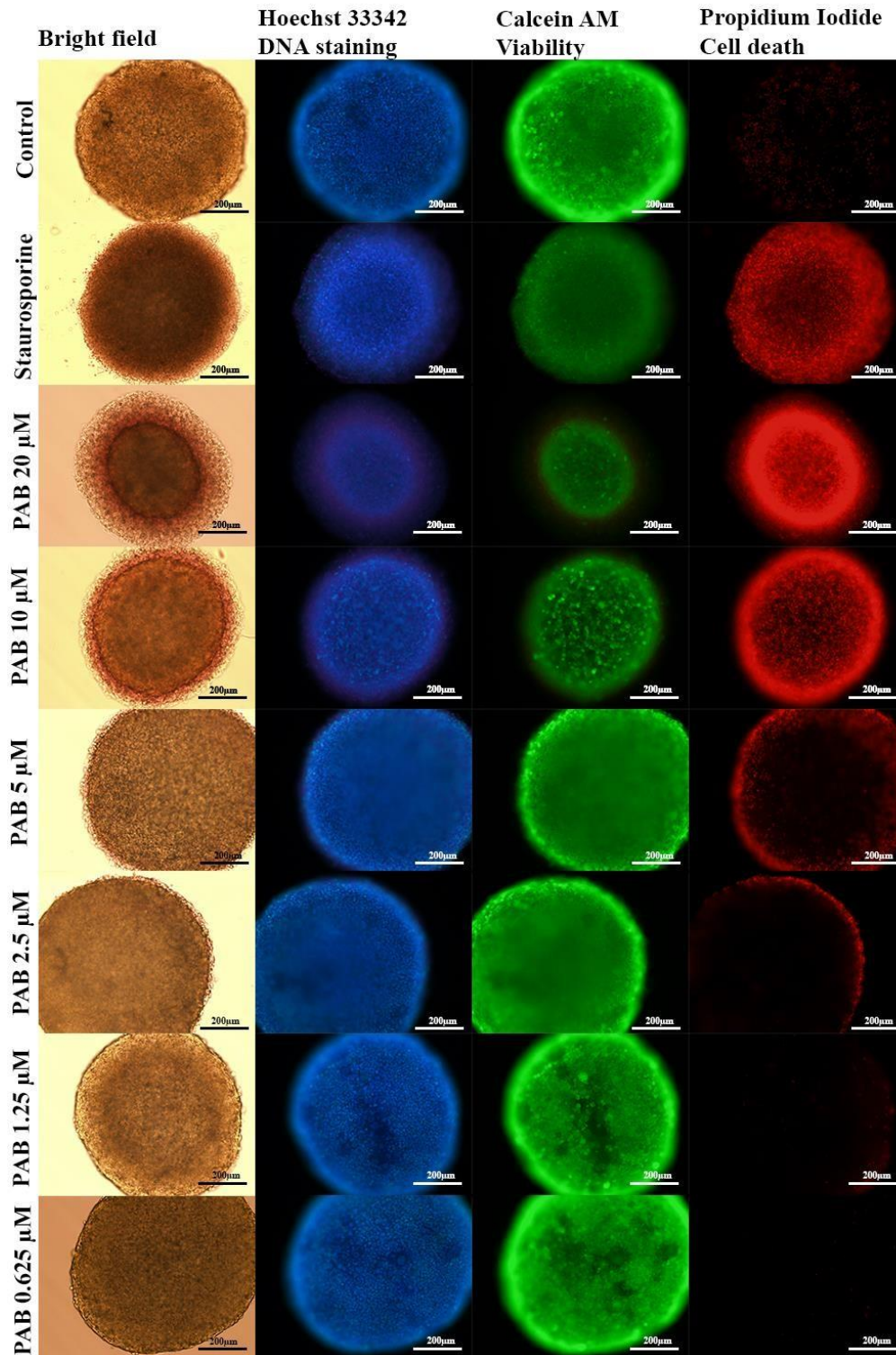
Figure 5. Microscopy images of spheroids exposed concentrations of **PAB** up to 20 µM for 48h, followed by fluorescent staining with Calcein AM (green) shows activity of cellular esterases (viability), Hoechst 33342 nuclear condensation (blue) and PI (red) dead cells (cell death). Staurosporine 500nM was used as positive control.

FCUP | 109
Cyanobacterial bioactive metabolites for anticancer drug
discovery: characterization of new compounds and
molecular mechanisms in physiologically relevant 3D cell
culture

Supplementary table 1

Table 1. IC_{50} calculated for HCT116 mutated cells, with overexpression of BCL2, BCL2XL and MCL1 genes and HCT116 mutated with p53 knock-out gene, based on MTT viability assay.

Cell line	IC_{50} (μM)
HCT116^{wt}	3.37 ± 0.92
HCT116$^{BCL2\ +/+}$	2.54 ± 0.79
HCT116$^{BCL2XL+/+}$	2.94 ± 0.56
HCT116$^{MCL1\ +/+}$	3.05 ± 0.05
HCT116$^{p53\ -/-}$	4.56 ± 0.45

FCUP 110
Cyanobacterial bioactive metabolites for anticancer drug
discovery: characterization of new compounds and
molecular mechanisms in physiologically relevant 3D cell
culture

Cytotoxicity assessment of the alkylresorcinols bartolosides A, B and C and hierridins B and C on multicellular culture systems of the colon carcinoma cell line HCT116

Manuscript in preparation

Maria Lígia Sousa, Pedro N. Leão, Rosário Martins, Stig Linder, Vítor Vasconcelos & Ralph Urbatzka (2019)

FCUP | 112
Cyanobacterial bioactive metabolites for anticancer drug
discovery: characterization of new compounds and
molecular mechanisms in physiologically relevant 3D cell
culture

Manuscript:

Cytotoxicity assessment of the alkylresorcinols bartolosides A, B and C and hierridins B and C on multicellular culture systems of the colon carcinoma cell line HCT116

Maria Lígia Sousa[1,2*], Pedro N. Leão[1], Rosário Martins[3], Stig Linder[4,5], Vítor Vasconcelos[1,2] & Ralph Urbatzka[1]

[1] CIIMAR Interdisciplinary Centre of Marine and Environmental Research, Porto, Portugal

[2] Faculty of Sciences of University of Porto, Porto, Portugal

[3] CISA- ESS Centre of Health and Environmental Research, School of Health, Porto Polytechnic, Portugal

[4] Department of Oncology and Pathology, Cancer Centre Karolinska, Karolinska Institute, Stockholm, Sweden

[5] Department of Medical and Health Sciences, Linköping University, Linköping, Sweden

*corresponding author: msousa@ciimar.up.pt

Abstract

The search for unique secondary metabolites attracts pharmaceutic interest, namely for discovery of novel and potent anticancer drugs, and cyanobacteria have been recognized as a powerful source of such compounds. Five phenolic lipids, bartoloside A (**1**) bartoloside B (**2**), bartoloside C (**3**), hierridin B (**4**) and hierridin C (**5**), previously isolated from cyanobacteria from the culture collection LEGE CC, were tested for anti-tumour activity by using three dimensional culture systems (3D) of the colon adenocarcinoma cell line HCT116. Compound **2** decreased the size of tumour spheroids at 20 µM after 48h and induced the disintegration of the outer layers of the structure. Apoptosis, oxidative stress and hypoxia were not found to be involved in the observed bioactivity. Western blot analysis suggested that **2** might interfere with protein synthesis, while **4** and **5** induced c-myc expression. In general, those cyanobacterial compounds did not reveal promising potential for the treatment of solid tumours.

FCUP | 114

Cyanobacterial bioactive metabolites for anticancer drug discovery: characterization of new compounds and molecular mechanisms in physiologically relevant 3D cell culture

Introduction

Alkylresorcinols are a group of phenolic lipids that were identified as secondary products of organisms, such as plants[1], animals, fungi, slime molds [2], bacteria and cyanobacteria[3-4] produced during normal development but also under stress conditions[1]. These lipids represent a diversified group that due to their amphiphilic physicochemical characteristics can incorporate into membrane phospholipid bilayers[3], which result in several already know bioactivities, such as bacterial inhibition, cytotoxicity, antioxidant[5], among others [3-4].

Bartolosides (**Figure 1**) are a group or halogenated dialkylresorcinols[4, 6-7] isolated from different cyanobacteria (*Nodosilinea* sp. LEGE 06102 and *Synechocystis salina* LEGE 06155). From this family of glycolipids, eleven compounds were isolated and only bartoloside A (**1**) and bartoloside B (**2**) showed low cytotoxic effects [6-7] (lowest IC_{50} for **1** was of 21µM in colon adenocarcinoma cell line (HT-29) and for **2** was 9.5 µM on the human prostate cell line PC-3)[6]. No data related to cytotoxicity of bartoloside C (**3**) was reported, despite the fact that it was isolated through a bioassay-guided fractionation using the MG-63 osteosarcoma cell line[6].

(1)

(2) R$_1$= Cl; R$_2$=H
(3) R$_1$= H; R$_2$=H
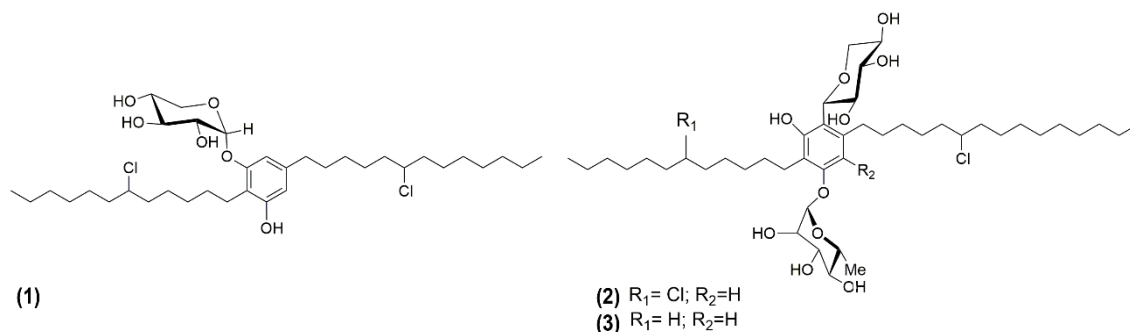
Figure 1 - Chemical structures of a) compound **1** b) Skeleton of compound **2** and **3**.

Hierridins B (**4**) and C (**5**) (**Figure 2**) are monoalkylresorcinols isolated from the cyanobacterial strain *Cyanobium* LEGE 06113, which were found to have activity against the malaria parasite *Plasmodium falciparum*[8-10]. Moreover, their cytotoxic activity was explored[8, 11], and a high IC_{50} (100.2µM)[8] of **4** was reported for the cell line HT-29 and no cytotoxicity of **5**. Interestingly, cytotoxic activity of **4** was restricted solely to HT-29 cells and not observed on the hepatocellular carcinoma HepG2, osteosarcoma MG63, colon adenocarcinoma RKO, neuroblastoma SHSY5Y, breast adenocarcinoma SKBR3, breast and ductal carcinoma T47D cell lines, or on the normal prostate epithelium cells line PNT2. An effect on mitochondrial pores was postulated, however, no indications on the reasons for cell selectivity[11].

a)

b)
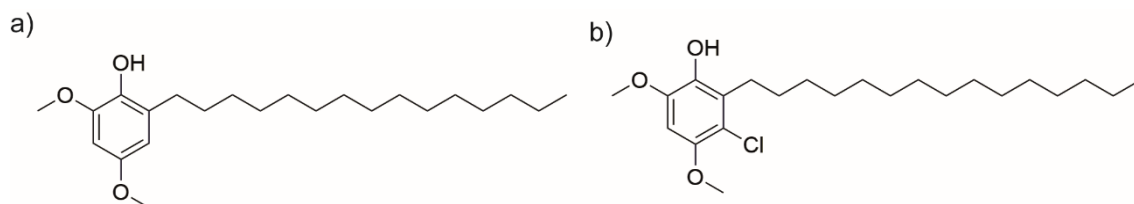
Figure 2 - Chemical structures of a) compound **4**; b) compound **5**.

Although cytotoxic effects were previously observed on the described compounds on monolayer cultures of cancer cells, we aimed to understand if their activity was effective on three dimensional (3D) structures such as spheroids. This approach focused on the biological relevance of using 3D structures, which mimics *in vivo* tumour rather than monolayer cell cultures. The cells within a tumour are not as metabolically active as in monolayer culture. The core of a tumour, or a spheroid, are necrotic, and non-proliferating, surrounded by an acidic environment rich in lactate and CO_2, low oxygen, low ATP and low glucose concentrations[12-14]. Often, these cells are responsible for the resistance to drug treatments, namely the interstitial acidification of the tumour core[15-18]. Following this knowledge, our approach aimed to understand if bartolosides and hierridins could penetrate the spheroid and have a cytotoxic effect on the 3D model, under acidic, nutrient-deprived and hypoxic conditions of the spheroid core.

Results

Evaluation of effects on a 3D cell system

HCT116 spheroids were exposed to all the compounds and alterations on tumor size were measured after 24h and 48h (**Figure 3**). Considering bartolosides, for compound **1** **(Figure 3a)** no significant alterations were observed. Compound **2** (**Figure 3b)** showed a general tendency to decrease the size of the spheroids. The decreasing size, compared to control spheroids, was significant at the higher concentration of 20 µM. In addition, the integrity of the spheroid was affected during exposure to **2** (**Figure 4a**). Even though few cell debris were visible on the controls after 24h of exposure, the cell debris around the spheroid was present at higher amount after 24h and 48h exposure to **2,** indicating a strong cell detachment. Exposure to compound **3 (Figure 3c)** did not affect spheroids area or morphology.

For hierridins, compounds **4** and **5** (**Figure 3d** and **e**) did not induce significant changes on the spheroid size or morphology, after 48h of exposure.

FCUP | 116
Cyanobacterial bioactive metabolites for anticancer drug
discovery: characterization of new compounds and
molecular mechanisms in physiologically relevant 3D cell
culture
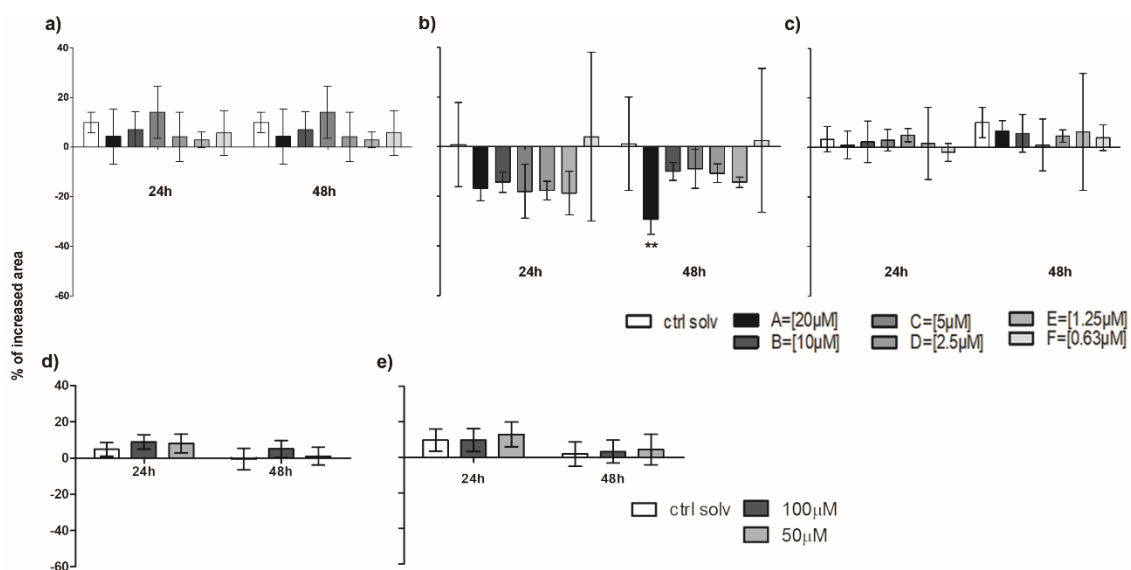
Figure 3 - Difference of area growth of the HTC116 spheroids after the 48h treatment compared to 0h. Results of exposure are shown in a) for compound **1**; b) compound **2**; c) compound **3**; d) compound **4**; e) compound **5**. Statistical differences are indicated by asterisks, ** p-value < 0.1. Each colum presents at least 6 replicates.

Cell death and Apoptosis (3D)

Since compound **2** demonstrated effects on 3D cultures, further studies were performed. Assessment of cell viability and apoptosis using the acid phosphatase assay (**Figure 4b**) and M30 CytoDeath™ ELISA kit, respectively, revealed that **2** did not alter the general spheroid viability nor activates caspase cleavage K18, which indicates the involvement of apoptosis (**Figure 4c**).

FCUP 117
Cyanobacterial bioactive metabolites for anticancer drug
discovery: characterization of new compounds and
molecular mechanisms in physiologically relevant 3D cell
culture
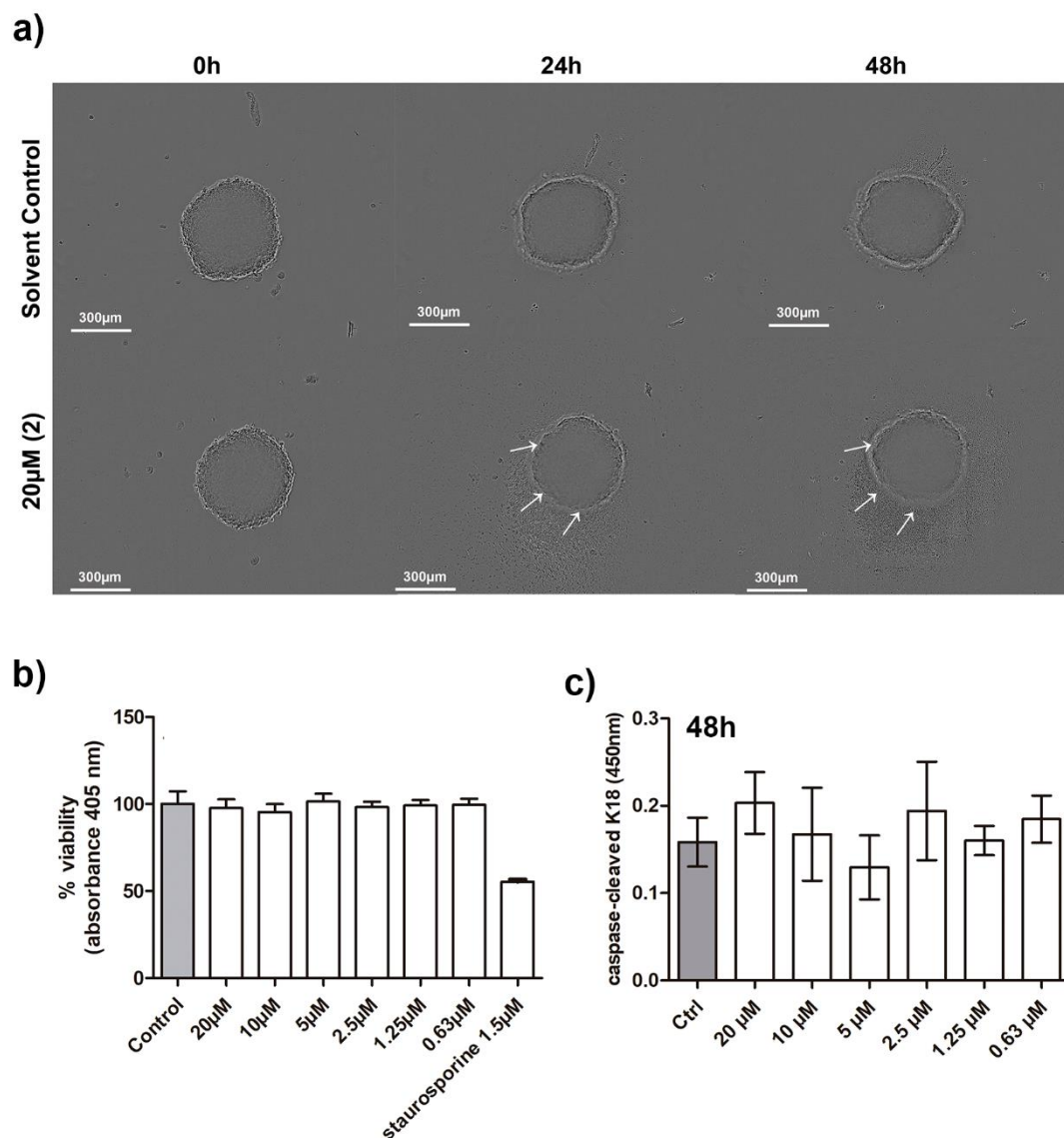
Figure 4 -a) Incucyte images representing the evolution of HCT116 spheroids of during the exposure to **2**. The spheroid exposed to high concentrations of **2** shows some cell disaggregation of the outer structure of the spheroid (arrows) after 24h and 48h exposure. b) Viability assay by acid phosphatase normalized towards the solvent control. c) M30 CytoDeathTM ELISA on HCT116 MTS exposed to 2 - 20 µM. Absorbance values represent the level of caspase cleaved K18. All assays were performed in triplicates.

Evaluation of oxidative stress and hypoxia induction (2D)

Next, we aimed to understand if an induction of oxidative stress or hypoxia may be involved in effects of compound **2** on tumour spheroids.

HCT116 pTRAF$^{Nrf2/HIF/NF-κB}$ cells were cultured in monolayer and exposed to **2** on a first approach. These cells could be cultured in 3D, however, the hypoxic signal and stress

response from the inner core of the spheroids would mask the fluorescence signal. Therefore, analyses were performed in 2D monolayer cells.

The results showed that **2** did not induce reactive oxygen species within the cells that would trigger the production of Nrf2 protein, or triggered a cell response to hypoxic conditions[19], which would result on the increased expression of HIF1α (**Figure 5a** and **b**). In this order, Nrf2 and HIF1α was not assessed in 3D culture, since the mechanistic pathway will be the same.
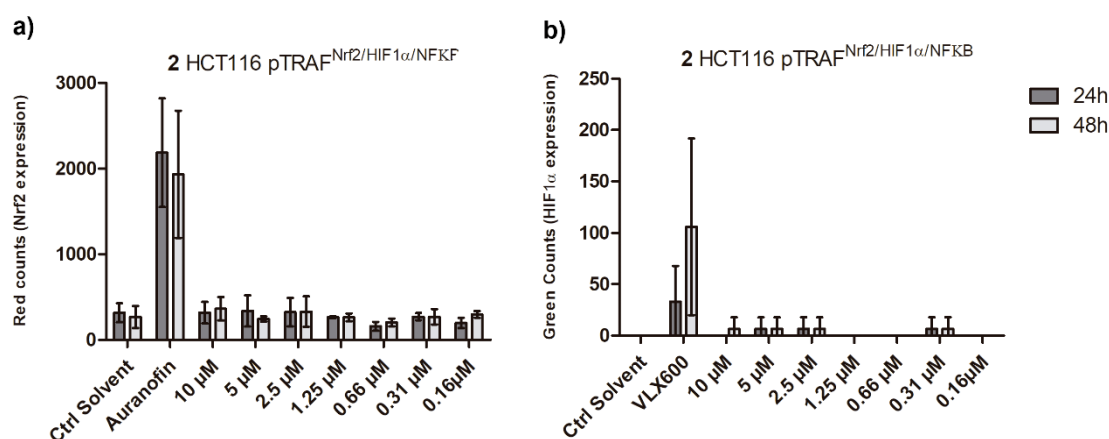
Figure 5 - Expression of HCT116 cells with pTRAF plasmid, exposed to compound **2** for 24h and 48h and cultured as monolayer cells and invubated on the Incucyte. a) Expression of Nrf2 genes and b) expression of HIF1α reporter genes. No significant changes were observed. Positive controls were at 6 μM. Error bars represent standard deviation, n ≥ 3.

*Cytotoxicity of **2** in HCT116 and in non-carcinogenic cell lines*

In order to assess if **2** would induce effects on normal cell lines, MTT assays were performed on three human cells lines, retinal cells RPE-1[hTERT], brain blood barrier endothelial cells hCMEC/D3 and keratinocyte cells HaCaT (**Figure 6b**). Those cell lines do not form spheroids (on the methods tested in our laboratory), and therefore assays were performed on monolayer cultures. No significant effects were observed on RPE-1[hTERT] and hCMEC/D3 cells, but a 10 μM exposure significantly decreased the viability of HaCaT after 48h (**Figure 6c and d**). As a comparison, the HCT116 cell line was also cultured in monolayer and no significant reduction in cell viability up to 10 μM.
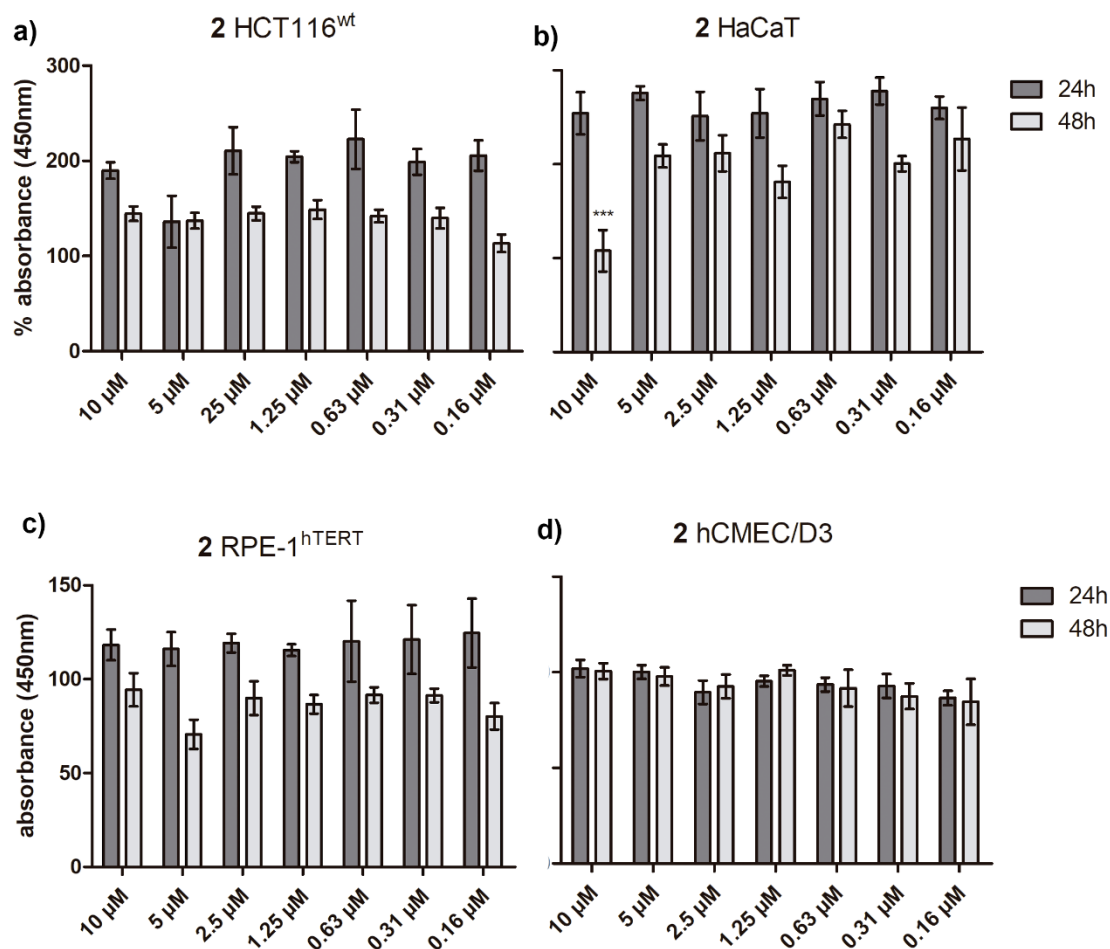
Figure 6 – Viability assays of the cell lines exposed to **2**. a) HCT116 wild type; b) normal Keratinocytes cell line HaCaT; c) normal Retinal Epithelial cell line RPE-1[hTERT]; d) normal Blood Brain Barrier cell line hCMEC/D3. Statistical differences are indicated by asterisks, *** = p-value < 0.01. error bars represent standard deviation. Assays were performed with 6 replicates.

Western blots (3D)

Cleavage of PARP protein was analysed on western blot and no cleavage was observed at the concentration of 20 µM (**Figure 7a**), which confirmed that apoptosis was not involved.

Oxidative stress was analysed in tumour spheroids by the protein levels of Nrf2 and Heme Oxygenase 1 (HMOX-1)[20]. No significant changes were observed for Nrf2, while HMOX1 did not reveal any visible bands (**Figure 7c and d**). ER stress was assessed by the analysis of the chaperone BiP and the phosphorylation of the eukaryotic initiation factor 2 subunit α (eIF2-α). The expression of eIF2-α was decreased for both treated samples (**Figure 7a**). P-eIF2-α did not show alterations after 6h, but a small decrease after 18h. No differences were observed for BiP (**Figure 7c and d**). The analysis of

FCUP | 120
Cyanobacterial bioactive metabolites for anticancer drug
discovery: characterization of new compounds and
molecular mechanisms in physiologically relevant 3D cell
culture

tumour suppressor protein p53 and p21 demonstrated no significant alterations on the expression of these proteins, and hence, no effect on the cell cycle or cell damage (**Figure 7b**).
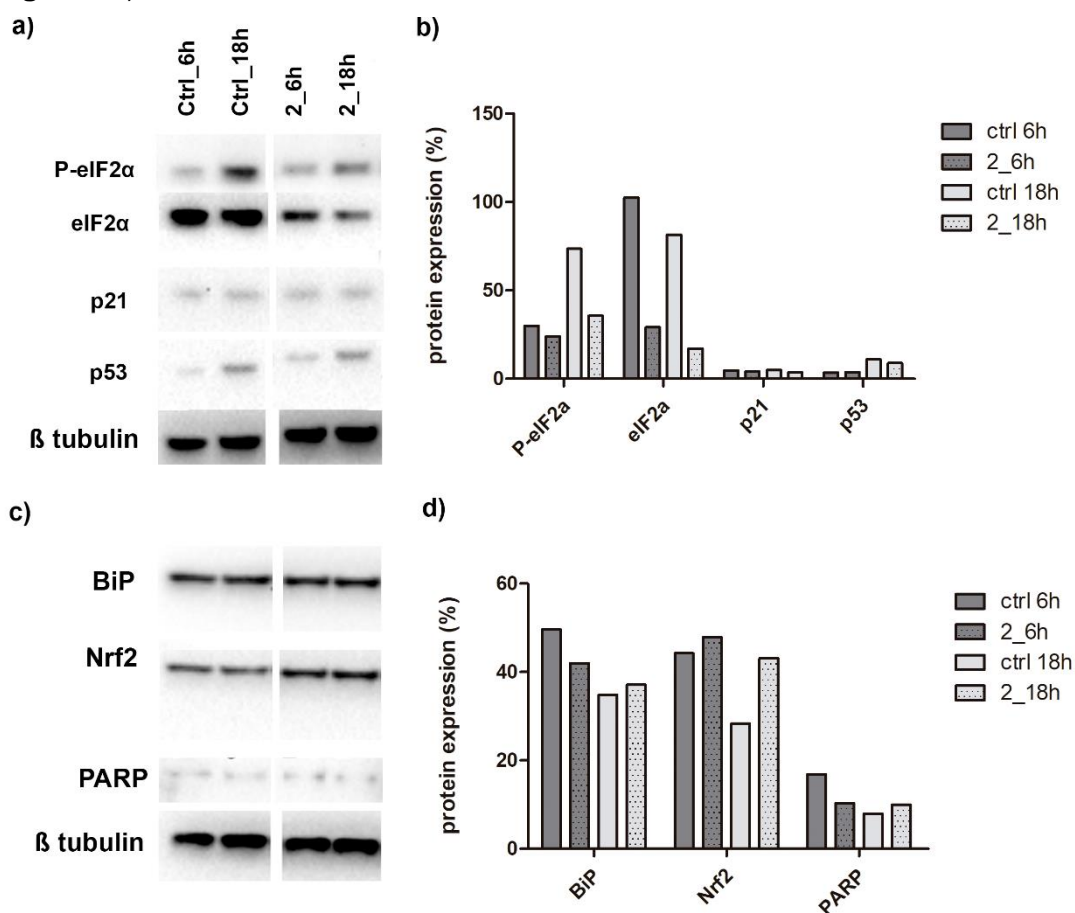
Figure 7 – Protein detection on western blot of HCT116 spheroid proteins exposed to **2** at 20 µM for 6 and 18 h for a) BiP and P-eIF2α (ER stress) and its respective control (eIF2α), Nrf2 (oxidative stress), PARP (apoptosis), and p21, p53 (cell cycle regulation) and β-tubulin was used as protein loading control. b) Relative expression of the proteins in relation to β-tubulin. n=1, where the protein observed correspond to a pool of 21 spheroids or more.

Although compounds **4** and **5** did not retrieve any significant results on spheroid size or morphology, we followed the same protocol to assess their eventual effects on some target proteins in cells. The expression was evaluated for the previously described proteins and for c-Myc, a transcriptional regulator of cell proliferation, differentiation and apoptosis[21]. An increase of c-Myc was observed after 18h of exposure to **4** and **5**, and a decrease of p53 (**Figure 8c, d** and **9c, d**). No evident alterations were visualized for the remaining tested proteins.

FCUP | 121
Cyanobacterial bioactive metabolites for anticancer drug
discovery: characterization of new compounds and
molecular mechanisms in physiologically relevant 3D cell
culture
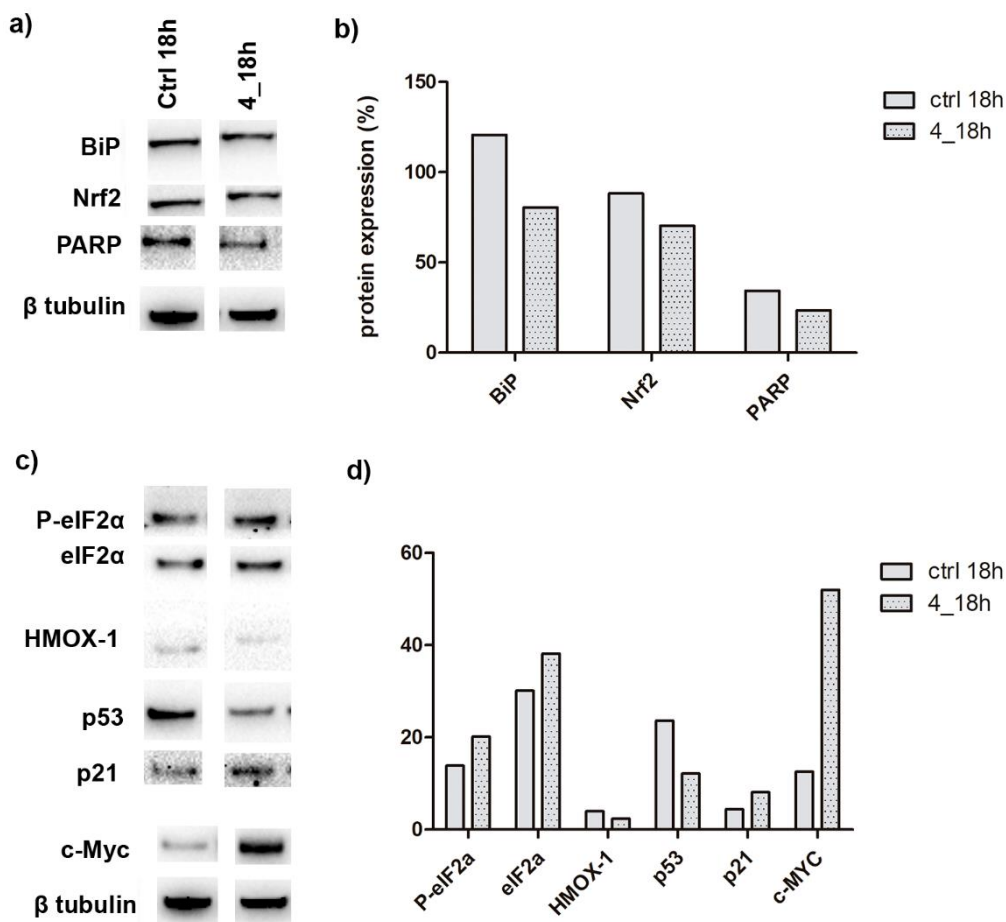
Figure 8 - Protein detection on western blot of HCT116 spheroid proteins exposed to compound **4** at 100 µM for 6 and 18 h for a) BiP and P-eIF2α (ER stress) and its respective control (eIF2α), Nrf2 and HMOX-1 (oxidative stress), PARP (apoptosis), and p21, p53 and c-Myc (cell cycle regulation). β-tubulin was detected for protein loading control. b) Relative expression of the proteins normalized by the amount β-tubulin. n=1, where the protein observed correspond to a pool of 21 spheroids or more.
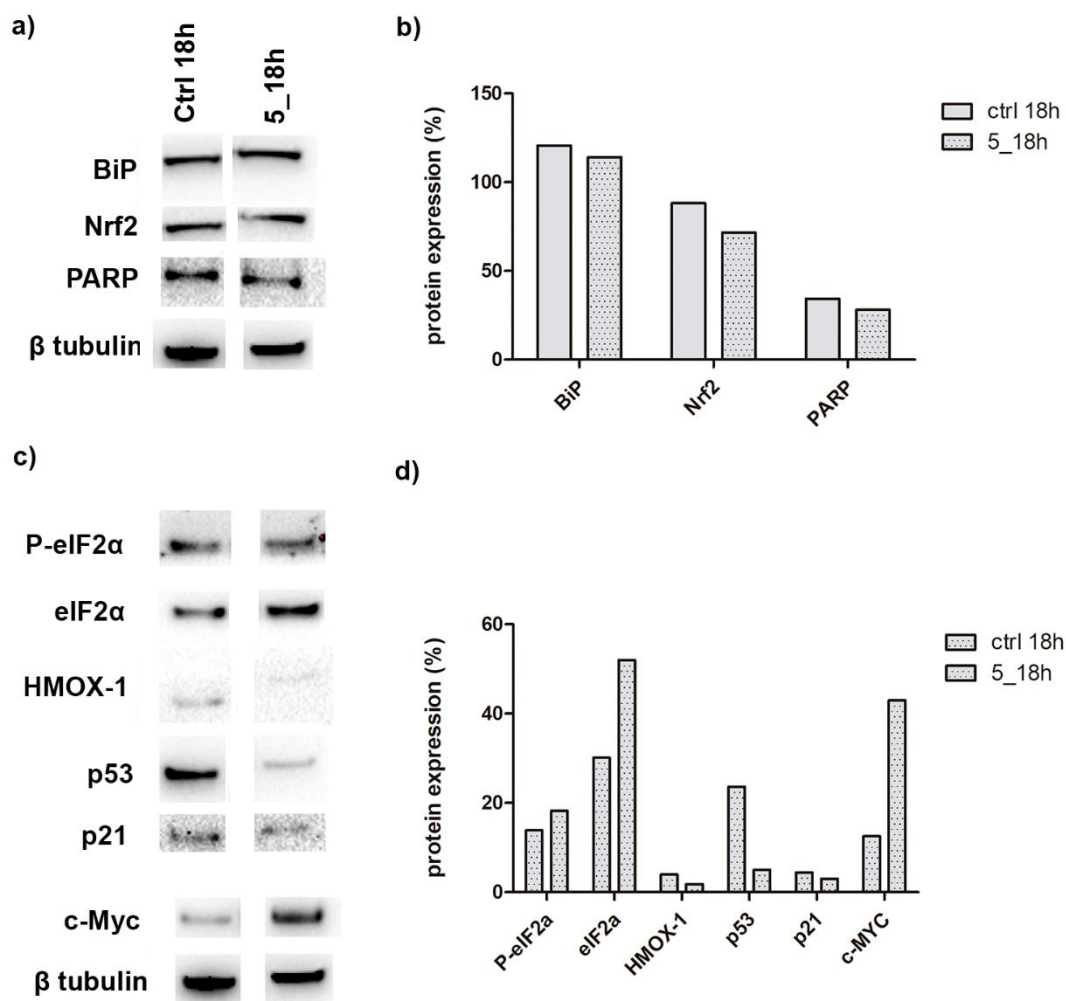
Figure 9 - Protein detection on western blot of HCT116 spheroid proteins exposed to compound **5** at 100 μM for 6 and 18 h for a) BiP and P-eIF2α (ER stress) and its respective control (eIF2α), Nrf2 and HMOX-1 (oxidative stress), PARP (apoptosis), and p21, p53 and c-Myc (cell cycle regulation). β-tubulin was detected for protein loading control. b) Relative expression of the proteins normalized by the amount β-tubulin. n=1, where the protein observed correspond to a pool of 21 spheroids or more.

Discussion

Cells growing in 3D structures such as spheroids that are subjected to a particular microenvironment, often reveal higher resistance to compounds penetration in comparison to monolayer cultured cells[22-23]. This finding is most likely due to acidic environment, hypoxia, nutrient deprivation, drug transporters, different stages of the cell cycle progression, higher expression of proteins involved in cell survival, namely proteins involved in drug metabolism that enables these cells to be more resistant to classical chemotherapeutical drugs[24]. At the same time, these structures offer a differentiated environment for cells dependent to their localization within the spheroid structure. This represents an opportunity to better understand if certain compounds, with low cytotoxicity

U. PORTO
FACULDADE DE CIÊNCIAS
UNIVERSIDADE DO PORTO

FCUP | 123
Cyanobacterial bioactive metabolites for anticancer drug discovery: characterization of new compounds and molecular mechanisms in physiologically relevant 3D cell culture

on 2D cultures, can have activities under microtumour environment, i.e., hypoxic acid environment. A previous study revealed that acidic adapted HCT116 cells were more sensitive to veterporfin or salinomycin[18]. On the present study, we tested bartolosides A, B and C (**1**, **2** and **3**) and hierridins B and C (**4** and **5**) on HCT116 spheroids, in order to understand if those compounds would have effects on a more relevant cell culture system as 3D spheroids.

Our results show that only **2** induced morphological alterations on the spheroid after 24h and 48h of exposure, decreasing tumour size in comparison to the control at 20 µM, and promoting its disintegration at the periphery. This was a preliminary indication that spheroid growth was arrested. However, the disintegration of the periphery of the spheroid did not correlate with the absence of cell death viability or apoptosis.

If we compare the structures of all the bartolosides, **2** differs from the other analogues by the presence of two sugars and two chlorines on the alkyl skeleton of the structure, which might be responsible for cell disintegration. In the past, the halogenation of a compound in specific positions of a molecule was explored to improve their biological activity without being related to a toxic electrophilic reaction between the carbon chlorine bond[25-26]. Also, the presence of two sugars on the molecule might have a good acceptance to enter the cell, due to their importance in several biological processes (molecular recognition, inflammation, adhesion). This characteristic has even been used in the industry as a potential alternative system for drug delivery[27].

When analysing if **2** could be involved on a resistance to oxidative stress mediated by Nrf2 mechanism, or hypoxia, through HIF1α activation[28], no significant alterations were observed on monolayer cells. In agreement to these results, the absence of oxidative stress induction was confirmed by Nrf2 and HMOX-1 protein expression on tumour spheroids. The western blot analysis indicated that **2** may affect protein synthesis by reducing the production of eIF2a and PeIF2a. BiP is highly expressed in cells whenever there are misfolded proteins[29-30] and phosphorylation of eIF2-α downregulates protein synthesis under stress conditions[31]. The overexpression of P-eIF2α relative to eIF2α is due to the strong decrease on eIF2α, and probably an artefact of the normalization. Since this assay was only performed once, with a pool of 21 spheroids treated in the same way, this result would need to be repeated to understand if this results from a wrong preparation of the assay or if eIF2α recycling is somehow being impaired[32-33].

The general lack of activity can be due the low penetration of the compound into the spheroids[14], as well as it permeabilization into the cells, being only possible to assess

the effects of the compound on the outer metabolic layer of the spheroid. These outer cells are the most metabolically activity and the ones in which effects are more similar to the 2D culture, even though on a spheroid the cell contact effect confers to these cells a higher resistance to treatments[34].

The approach applied to **4** and **5** was the same in bartolosides, but, as referred before, no significant morphological alterations were observed on spheroids exposed to these compounds. However, since biological activity was reported before for both compounds[4, 8-9, 11] in monolayer cultures, the search for some key proteins was assessed. No difference of effects was observed for Nrf2, HMOX-1 (oxidative stress), BiP, P-eIF2α (protein synthesis), PARP (apoptosis). c-Myc showed increased protein level. This protein was reported to inhibit p21 gene[35] in agreement with the slight p21 reduction at 18h and may be the reason for the strong reduction on p53 (**Figure 9**). These results indicate that compounds **4** and **5** can interact with spheroid cells and interfere with the regulation of their cell cycle. These results support a previously shown effect of **4** on the cell cycle arresting the cancer colon cell line (HT-29)[11]. Additionally, activity and function of mitochondria was reduced after 48h of exposure to **4**, which is in agreement with previously reported effects on mitochondrial pores[11]. C-Myc is referred in the literature as a regulator of mitochondria biogenesis and of multiple enzymes that are involved in OXPHOS[36]. Therefore, a first activity could be triggered by **4** and **5** on c-Myc, which might influence the maintenance of mitochondria structure[37].

To the best of our knowledge, this is the first indication that **5** also interferes with the normal progression of cell cycle, even though previous studies did not reveal any cytotoxicity of this compound in 2D neither the present study reveals any effects in 3D.

Summarising, exposure to a high concentration of **2** (20 μM) for 48h reduced significantly tumour spheroids size and integrity, and affected protein synthesis via eIF2α protein level. Exposure to **4** and **5** at 100 μM did not influence the morphology of spheroids, but did show an interaction with c-Myc, which provided support for a previous described effect of **4** on the mitochondrial activity in another colon cancer cell line[11].

U.PORTO

FACULDADE DE CIÊNCIAS
UNIVERSIDADE DO PORTO

FCUP | 125
Cyanobacterial bioactive metabolites for anticancer drug
discovery: characterization of new compounds and
molecular mechanisms in physiologically relevant 3D cell
culture

Methods

Re-isolation of 2 and 3

Compounds **1**, **4** and **5** were kindly provided by Sara Freitas (**1** and **4**) and Rosário Martins (**5**). Compounds **2** and **3** were re-isolated from lyophilized biomass of the strain *Synechocystis salina* LEGE 06155. An initial extract was obtained from 45 g of *Synechocystis salina* LEGE 06155, using a warm mixture of CH_2Cl_2/MeOH (2:1) yielding 8.05 g crude organic extract. The first fractionation was performed by Vacuum-Liquid Chromatography (VLC) with a stationary phase of Silica Gel 60 (0.015-0.040, Merk KGaA). The mobile phase was a mixture of crescent polarity, from 10% of EtOAc in Hexanes to 100% EtOAc to 100% MeOH. Based on the previous work[6] the resultant fractions were analysed using Liquid-Chromatography coupled to Mass Spectrometry (LC-MS). For the LC-MS analysis, the samples were dissolved in MeOH to a concentration of 1 mg ml^{-1} and analysed on a Thermo Scientific LTQ Orbitrap XL spectrometer, with a gradient from 20% MeCN (aq) to 100% MeCN (aq) for 20 min followed by isocratic separation at 100% MeCN for 10 min, with a flow rate of 1ml min^{-1}. (CEMUP - Materials Centre of the University of Porto). According to the original publication[6] **2** showed a [M-H]⁻ ion at 833.4743 *m/z* with a t_R = 26,2 min and **3** [M-H]⁻ 799.5132 *m/z* with t_R = 53,5 min. The selected fraction (G) was submitted to flash liquid chromatography using Silica Gel 60 (0.015-0.040 mm mesh) (Merk). The mobile phase was a mixture of increasing polarity, from 40% EtOAc in Hexanes to 100% EtOAc to 20% MeOH. The chromatographic fractions were then monitored by a Thin Layer Chromatography (TLC) in Silica Gel 60 F254 (Merk). For the first 80 fractions, the chamber solution was 60% EtOAc: 40% Hexane. Then the last 34 fractions were tested in a solution of 80% EtOAc: 20% MetOH. The TLC visualization was aided by UV light with 254 nm and 366 nm wavelengths. The staining was made with Phosphomolybdic Acid Staining (PMA). The fractions were then pooled according to their TLC profile to yield ten samples. Relative abundance of the compounds was assessed by the integration of the extracted ion chromatograms. The samples E16113 G7- G10 appeared to contain **2**, samples E16113 G7 – G9 contain **3**. Samples E16113G7 (118.47 mg) and E16113G8 (60,50 mg) were pooled together for further fractionation using semi-preparative High-Performance Liquid Chromatography (HPLC), on a Waters HPLC System composed by a 1525 binary pump and a UV-VIS detector, using a Synergi Fusion-RP 4u 250x10 mm, 80 A. The separation employed a solvent system of isocratic 85% MeCN to 30 min, gradient to 100% MeCN for 5 min, held 32 min on the same

FCUP | 126
Cyanobacterial bioactive metabolites for anticancer drug
discovery: characterization of new compounds and
molecular mechanisms in physiologically relevant 3D cell
culture

solvent and then returning to 85% MeCN for 5 min. This procedure afforded 12 new fractions and the abundance of the three target compounds was checked on the LC-MS and their purity inspected with ^{1}H Nuclear Magnetic Resonance (NMR). Sample E16113G78_3 (4.18 mg) corresponded to **2.** The NMR analysis confirmed the presence of the compound and its purity, about 95%. Sample E16113G78_5 (2.14 mg) contained **3,** was further fractionated by HPLC finally yielding **3** with 80% of purity.

Cell culture and viability assessment

Monolayer cell lines used on the present work were culture in Dulbecco's modified Eagle's (DMEM) with exception of the cell line RPE-1^{hTERT} which was cultured on Dulbecco's Modified Eagle Medium: Nutrient Mixture F-12 (DMEM/F12) supplemented with 200mM GlutamaxTM (Gibco, Massachusetts, USA). All media were further supplemented with 10% fetal bovine serum, 1% of Penicillin/Streptomycin and 0.1% of Amphotericin B (Biochrom, United Kindom) and incubated at 37ºC in 5% CO_2. The compounds were tested in a concentration-response assay (up to 20 µM). The viability was assessed both by Incucyte ZOOM Live-Cell Analysis System (Essen Instruments, Ann Arbor, MI) automatic measurement of cell confluence and by the reduction of the 3-(4,5-dimethylthiazole-2-yl)-2,5-diphenyl tetrazolium bromide (MTT, Sigma-Aldrich, St. Louis, MO, USA) at 24h and 48h. The cells were seeded in 96-well culture plates at a 3.3×10^4 cells ml^{-1} and the adhesion was allowed for 24h hours. After adhesion, cells were exposed to the compounds for 24h and 48h. After the treatment, the cells were incubated for 4 h with 0.2 mg ml-1 of MTT at 37ºC and 5% CO_2. The formed formazan crystals were dissolved with DMSO (dimethyl sulfoxide) and the absorbance was read at 550 nm in a GEN5TM-Multi-Detection Microplate Reader (Biotek, Bad Friedrichshall, Germany). The positive control for each experiment was the cultivation of cells with 20% of DMSO (cytotoxic concentration)[38].

Colorectal carcinoma cell line HCT116 transformed with a pTRAF plasmid (HCT116 pTRAF $^{Nrf2/HIF/NF-κB}$) (provided by Prof Elias Arnér from Karolinska Institute, Sweden) containing E2- related factor 2 (Nrf2), hypoxia-inducible factor (HIF) and nuclear factor kappa-light-chain-enhancer of activated B cell (NF-κB), which activation is monitored by a fluorescent reporter, was used to test if the compounds affect the activity of these genes[19]. Due to the limitation of the IncuCyte® ZOOM Live-Cell Analysis System it was only possible to read the Nrf2 activity at λex = 585 nm, emission filter: 635 nm, and HIF fluorescence at λex = 460 nm, emission filter: 524 nm, not being possible to assess NF-

U. PORTO
FACULDADE DE CIÊNCIAS
UNIVERSIDADE DO PORTO

FCUP | 127

Cyanobacterial bioactive metabolites for anticancer drug discovery: characterization of new compounds and molecular mechanisms in physiologically relevant 3D cell culture

κB activity. As positive controls for these experiments, the compound VLX600 at 6μM induced HIF expression[39], while Auranofin (6 μM)[19] confirmed Nrf2 activity.

Spheroids generation

After confirming a pre-confluent growth on a monolayer culture, the HCT116[wt] cells were detached from the plates and collected. 200 μl of medium containing 50 000 cells are added on each well of a 96 well-plate with U-round bottom ultralow attachment treatment (Corning). Then 190 μl of medium was added, so that top of the well should form a drop, resulting of the excess of medium. Elevating the lid from the plate with plasticine on the corners, the plate was firmly putted upside down resulting in a drop by superficial tension on each well. The plate was then incubated over 24h, with shaking (300 rpm), under 37ºC and humidified atmosphere with 5% of CO_2. After 24h the plate was flipped back to the normal position. The excess of medium (190μl) was removed and the newly formed spheroids incubated under the same atmosphere conditions for 4 days, before any compound exposure[40]. The development of the spheroids was monitored automatically over time using the Incucyte equipment.

Viability assessment and apoptosis

After the exposure, the acid phosphatase assay was performed, according to Friedrich[41]. Briefly, the 96 well plate was carefully washed with PBS followed by the addition of 100 μl of Sodium acetate buffer at 0.1M containing p-nitrophenyl phosphate (2 mg ml^{-1}). The reaction was stopped after 2h with 10 μL of NaOH (1N) and the absorbance was read at 405nm in a GEN5TM-Multi-detection Microplate Reader (Biotek, Bad Friedrichshall, Germany). For apoptosis assessment, an *in vitro* immunoassay (M30 CytoDeathTM ELISA) was applied for quantitative determination of the apoptosis associated K18Asp396 (M30), a neo-epitope that appears after caspase cleavage of K18 during early apoptosis (PEVIVA M30 Cytodeath ELISA Instructions for use)[42].

Western Blot

HCT116 spheroids were produced on 96 well plates as described before and exposed to 20 μM of compound **2** and 100 μM of compounds **4** and **5**. A minimum of 21 spheroids were cleaned with cold PBS and further collected in RIPA buffer (150 mM NaCl, 50 mM

FCUP | 128

Cyanobacterial bioactive metabolites for anticancer drug discovery: characterization of new compounds and molecular mechanisms in physiologically relevant 3D cell culture

Tris, pH 7.4, 1% Nonidet P-40, 0.1% SDS, 0.5% sodium deoxycholate) supplemented with protease and phosphatase inhibitors. Protein concentration was determined by Pierce Coomassie Plus (Bradford) Assay Reagent. SDS-PAGE was performed on pre-casted acrylamide gels NuPAGE TM 4–12% Bis-Tris Protein (Invitrogen™) using the NuPage system and loading 20 µg of proteins per lane. Gel proteins were transferred to nitrocellulose membranes and incubated for 1 h at room temperature in PBS-Tween with 5% non-fat dry milk. Protein loading was assessed by red Ponceau staining of the membranes. Primary antibodies were used according to the manufacturer instructions, BiP (#3183), Phospho-eIF2 α (Ser51) (#9721), and eIF2 α (#9722) p21Cip1 (2946S), Nrf2 (#12721), c-Myc (#5605) were all from Cell Signaling Technology, HMOX (#610713) and anti-human PARP (# 556494) from BD Bioscience, and p53 (DO-1): sc-126 from Santa Cruz Biotechnology. Antibody to β-tubulin (#T4026) was from Sigma-Aldrich (St Louis, MO, USA) (1:1000). Membranes were incubated with primary antibodies dilutions (1:1000) in 5% w/v BSA, 1x TBS, 0.1% Tween-20 overnight at 4º C, followed by appropriate HRP- conjugated secondary antibodies. Secondary Anti-rabbit IgG HRP-linked (#7074) and Anti-mouse IgG, HRP-linked Antibody (#7076), (Cell Signaling Technology, Danvers, MA, USA) were diluted at 1:5,000 in 5% non-fat milk and incubated 1h at room temperature. Antibody staining was visualized by the Clarity Western ECL Substrate (BioRad) on a BioRad Molecular Imager Gel DocTM XR+ with Image LabTM Software.

Statistical analysis

All the treatments have a minimum of an n=3. Whenever it was not possible to verify the normality of the data, a non-parametric test (Kruskal-Wallis test) was performed, and the treatments compared to the Solvent Control. When the normality of the data was verifiable, a One-way ANOVA was performed and followed by a Bonferroni Multicomparison post-test. Confidence interval used was 95%, where * means $p < 0.05$; ** means $p < 0.01$; ***means $p < 0.001$. Error bars of the graphs stand for Standard Deviation.

References

1.   Kozubek, A.; Tyman, J. H. P., Resorcinolic Lipids, the Natural Non-isoprenoid Phenolic Amphiphiles and Their Biological Activity. *Chemical Reviews* **1999,** *99* (1), 1-26.

2.   Kikuchi, H.; Ito, I.; Takahashi, K.; Ishigaki, H.; Iizumi, K.; Kubohara, Y.; Oshima, Y., Isolation, Synthesis, and Biological Activity of Chlorinated Alkylresorcinols from Dictyostelium Cellular Slime Molds. *Journal of Natural Products* **2017,** *80* (10), 2716-2722.

3.   Stasiuk, M.; Kozubek, A., Biological activity of phenolic lipids. *Cellular and Molecular Life Sciences* **2010,** *67* (6), 841-860.

4.   Martins, T. P.; Rouger, C.; Glasser, N. R.; Freitas, S.; de Fraissinette, N. B.; Balskus, E. P.; Tasdemir, D.; Leão, P. N., Chemistry, bioactivity and biosynthesis of cyanobacterial alkylresorcinols. *Natural Product Reports* **2019**.

5.   Konanykhina, I. A.; Shanenko, E. F.; Loiko, N. G.; Nikolaev, Y. A.; El-Registan, G. I., Regulatory effect of microbial alkyloxybenzenes of different structure on the stress response of yeast. *Applied Biochemistry and Microbiology* **2008,** *44* (5), 518-522.

6.   Leão, P. N.; Nakamura, H.; Costa, M.; Pereira, A. R.; Martins, R.; Vasconcelos, V.; Gerwick, W. H.; Balskus, E. P., Biosynthesis-Assisted Structural Elucidation of the Bartolosides, Chlorinated Aromatic Glycolipids from Cyanobacteria. *Angewandte Chemie International Edition* **2015,** *54* (38), 11063-11067.

7.   Afonso, T. B.; Costa, M. S.; Rezende de Castro, R.; Freitas, S.; Silva, A.; Schneider, M. P. C.; Martins, R.; Leão, P. N., Bartolosides E–K from a Marine Coccoid Cyanobacterium. *Journal of Natural Products* **2016,** *79* (10), 2504-2513.

8.   Leão, P. N.; Costa, M.; Ramos, V.; Pereira, A. R.; Fernandes, V. C.; Domingues, V. F.; Gerwick, W. H.; Vasconcelos, V. M.; Martins, R., Antitumor Activity of Hierridin B, a Cyanobacterial Secondary Metabolite Found in both Filamentous and Unicellular Marine Strains. *PLOS ONE* **2013,** *8* (7), e69562.

9.   Margarida, C.; Ivo E., S.-D.; Raquel, C.-B.; Hugo, S.; Roberta, R. d. C.; Artur, S.; Maria Paula Cruz, S.; Maria João, A.; Rosário, M.; Valentina, F. D.; Fatima, N.; Vera, C.; Vitor M., V.; Pedro, L., *Structure, Synthesis of Hierridin C and Discovery of Prevalent Alkylresorcinol Biosynthesis in Picocyanobacteria. Journal of Natural Products.* **2018**. 82 (2), 393-402.

FCUP 130
Cyanobacterial bioactive metabolites for anticancer drug
discovery: characterization of new compounds and
molecular mechanisms in physiologically relevant 3D cell
culture

10.   Papendorf, O.; König, G. M.; Wright, A. D., Hierridin B and 2,4-dimethoxy-6-heptadecyl-phenol, secondary metabolites from the cyanobacterium Phormidium ectocarpi with antiplasmodial activity. *Phytochemistry* **1998,** *49* (8), 2383-2386.

11.   Freitas, S.; Martins, R.; Costa, M.; Leão, P.; Vitorino, R.; Vasconcelos, V.; Urbatzka, R., Hierridin B Isolated from a Marine Cyanobacterium Alters VDAC1, Mitochondrial Activity, and Cell Cycle Genes on HT-29 Colon Adenocarcinoma Cells. *Marine Drugs* **2016,** *14* (9), 158.

12.   Sutherland, R. M., Cell and environment interactions in tumor microregions: the multicell spheroid model. *Science* **1988,** *240* (4849), 177.

13.   Hirschhaeuser, F.; Menne, H.; Dittfeld, C.; West, J.; Mueller-Klieser, W.; Kunz-Schughart, L. A., Multicellular tumor spheroids: An underestimated tool is catching up again. *Journal of Biotechnology* **2010,** *148* (1), 3-15.

14.   Minchinton, A. I.; Tannock, I. F., Drug penetration in solid tumours. *Nat Rev Cancer* **2006,** *6* (8), 583-592.

15.   Tannock, I. F.; Rotin, D., Acid pH in Tumors and Its Potential for Therapeutic Exploitation. *Cancer Research* **1989,** *49* (16), 4373-4384.

16.   Kolosenko, I.; Avnet, S.; Baldini, N.; Viklund, J.; De Milito, A., Therapeutic implications of tumor interstitial acidification. *Seminars in Cancer Biology* **2017,** *43,* 119-133.

17.   Trédan, O.; Galmarini, C. M.; Patel, K.; Tannock, I. F., Drug Resistance and the Solid Tumor Microenvironment. *JNCI: Journal of the National Cancer Institute* **2007,** *99* (19), 1441-1454.

18.   Pellegrini, P.; Serviss, J. T.; Lundbäck, T.; Bancaro, N.; Mazurkiewicz, M.; Kolosenko, I.; Yu, D.; Haraldsson, M.; D'Arcy, P.; Linder, S.; De Milito, A., A drug screening assay on cancer cells chronically adapted to acidosis. *Cancer Cell International* **2018,** *18* (1), 147.

19.   Johansson, K.; Cebula, M.; Rengby, O.; Dreij, K.; Carlström, K. E.; Sigmundsson, K.; Piehl, F.; Arnér, E. S. J., Cross Talk in HEK293 Cells Between Nrf2, HIF, and NF-κB Activities upon Challenges with Redox Therapeutics Characterized with Single-Cell Resolution. *Antioxidants & Redox Signaling* **2015**. 26 (6): 229-246.

20.   Araujo, J.; Zhang, M.; Yin, F., Heme Oxygenase-1, Oxidation, Inflammation, and Atherosclerosis. *Frontiers in Pharmacology* **2012,** *3* (119).

FCUP 131
Cyanobacterial bioactive metabolites for anticancer drug
discovery: characterization of new compounds and
molecular mechanisms in physiologically relevant 3D cell
culture

21.   Miller, D. M.; Thomas, S. D.; Islam, A.; Muench, D.; Sedoris, K., c-Myc and cancer metabolism. *Clinical cancer research : an official journal of the American Association for Cancer Research* **2012,** *18* (20), 5546-5553.

22.   Weiswald, L.-B.; Bellet, D.; Dangles-Marie, V., Spherical Cancer Models in Tumor Biology. *Neoplasia* **2015,** *17* (1), 1-15.

23.   Wartenberg, M.; Ling, F. C.; Müschen, M.; Klein, F.; Acker, H.; Gassmann, M.; Petrat, K.; Pütz, V.; Hescheler, J.; Sauer, H., Regulation of the multidrug resistance transporter P-glycoprotein in multicellular tumor spheroids by hypoxia-inducible factor-1 and reactive oxygen species. *The FASEB Journal* **2003**.

24.   Breslin, S.; O'Driscoll, L., The relevance of using 3D cell cultures, in addition to 2D monolayer cultures, when evaluating breast cancer drug sensitivity and resistance. *Oncotarget* **2016,** *7* (29), 45745-45756.

25.   Fenical, W.; Jensen, P. R., Developing a new resource for drug discovery: marine actinomycete bacteria. *Nature Chemical Biology* **2006,** *2* (12), 666-673.

26.   Naumann, K., Influence of chlorine substituents on biological activity of chemicals. *Journal für praktische Chemie* **1999,** *341* (5), 417-435.

27.   Zhang, Y.; Chan, J. W.; Moretti, A.; Uhrich, K. E., Designing polymers with sugar-based advantages for bioactive delivery applications. *Journal of Controlled Release* **2015,** *219*, 355-368.

28.   Osada-Oka, M.; Hashiba, Y.; Akiba, S.; Imaoka, S.; Sato, T., Glucose is necessary for stabilization of hypoxia-inducible factor-1α under hypoxia: Contribution of the pentose phosphate pathway to this stabilization. *FEBS Letters* **2010,** *584* (14), 3073-3079.

29.   Kohno, K.; Normington, K.; Sambrook, J.; Gething, M. J.; Mori, K., The promoter region of the yeast KAR2 (BiP) gene contains a regulatory domain that responds to the presence of unfolded proteins in the endoplasmic reticulum. *Molecular and Cellular Biology* **1993,** *13* (2), 877-890.

30.   Munro, S.; Pelham, H. R. B., An hsp70-like protein in the ER: Identity with the 78 kd glucose-regulated protein and immunoglobulin heavy chain binding protein. *Cell* **1986,** *46* (2), 291-300.

31.   Bogorad, A. M.; Lin, K. Y.; Marintchev, A., Novel mechanisms of eIF2B action and regulation by eIF2α phosphorylation. *Nucleic Acids Research* **2017,** *45* (20), 11962-11979.

FCUP | 132
Cyanobacterial bioactive metabolites for anticancer drug
discovery: characterization of new compounds and
molecular mechanisms in physiologically relevant 3D cell
culture

32.   Sudhakar, A.; Ramachandran, A.; Ghosh, S.; Hasnain, S. E.; Kaufman, R. J.; Ramaiah, K. V. A., Phosphorylation of Serine 51 in Initiation Factor 2α (eIF2α) Promotes Complex Formation between eIF2α(P) and eIF2B and Causes Inhibition in the Guanine Nucleotide Exchange Activity of eIF2B. *Biochemistry* **2000,** *39* (42), 12929-12938.

33.   Matts, R. L.; London, I. M., The regulation of initiation of protein synthesis by phosphorylation of eIF-2(alpha) and the role of reversing factor in the recycling of eIF-2. *Journal of Biological Chemistry* **1984,** *259* (11), 6708-6711.

34.   Olive, P. L.; Durand, R. E., Drug and radiation resistance in spheroids: cell contact and kinetics. *Cancer and Metastasis Reviews* **1994,** *13* (2), 121-138.

35.   Jung, P.; Hermeking, H., The c-MYC-AP4-p21 cascade. *Cell Cycle* **2009,** *8* (7), 982-989.

36.   Zhang, X.; Mofers, A.; Hydbring, P.; Olofsson, M. H.; Guo, J.; Linder, S.; D'Arcy, P. MYC is downregulated by a mitochondrial checkpoint mechanism *Oncotarget*, 2017, p. 90225-90237. PubMed. https://doi.org/10.18632/oncotarget.21653.

37.   Graves, J. A.; Wang, Y.; Sims-Lucas, S.; Cherok, E.; Rothermund, K.; Branca, M. F.; Elster, J.; Beer-Stolz, D.; Van Houten, B.; Vockley, J.; Prochownik, E. V., Mitochondrial Structure, Function and Dynamics Are Temporally Controlled by c-Myc. *PLOS ONE* **2012,** *7* (5), e37699.

38.   Da Violante, G.; Zerrouk, N.; Richard, I.; Provot, G.; eacute; rard; Chaumeil, J. C.; Arnaud, P., Evaluation of the Cytotoxicity Effect of Dimethyl Sulfoxide (DMSO) on Caco2/TC7 Colon Tumor Cell Cultures. *Biological and Pharmaceutical Bulletin* **2002,** *25* (12), 1600-1603.

39.   Zhang, X.; Fryknäs, M.; Hernlund, E.; Fayad, W.; De Milito, A.; Olofsson, M. H.; Gogvadze, V.; Dang, L.; Påhlman, S.; Schughart, L. A. K.; Rickardson, L.; D'Arcy, P.; Gullbo, J.; Nygren, P.; Larsson, R.; Linder, S., Induction of mitochondrial dysfunction as a strategy for targeting tumour cells in metabolically compromised microenvironments. *Nature Communications* **2014,** *5*, 3295.

40.   Sousa, M. L.; Preto, M.; Vasconcelos, V.; Linder, S.; Urbatzka, R., Antiproliferative Effects of the Natural Oxadiazine Nocuolin A Are Associated With Impairment of Mitochondrial Oxidative Phosphorylation. *Frontiers in Oncology* **2019,** *9* (224).

41.   Friedrich, J.; Eder, W.; Castaneda, J.; Doss, M.; Huber, E.; Ebner, R.; Kunz-Schughart, L. A., A Reliable Tool to Determine Cell Viability in Complex 3-D

Culture: The Acid Phosphatase Assay. *Journal of Biomolecular Screening* **2007,** *12* (7), 925-937.

42.   Herrmann, R.; Fayad, W.; Schwarz, S.; Berndtsson, M.; Linder, S., Screening for Compounds That Induce Apoptosis of Cancer Cells Grown as Multicellular Spheroids. *Journal of Biomolecular Screening* **2008,** *13* (1), 1-8.

FCUP | 134

Cyanobacterial bioactive metabolites for anticancer drug discovery: characterization of new compounds and molecular mechanisms in physiologically relevant 3D cell culture

FCUP | 135

Cyanobacterial bioactive metabolites for anticancer drug discovery: characterization of new compounds and molecular mechanisms in physiologically relevant 3D cell culture

Assessing promising bioactivity of cyanobacterial strains on a 3D *in vitro* model of solid tumours

Manuscript in preparation

Maria Lígia Sousa, Leonor Ferreira, Tim Krempel, Rosário Martins, Vítor Vasconcelos & Ralph Urbatzka (2019)

FCUP 136
Cyanobacterial bioactive metabolites for anticancer drug
discovery: characterization of new compounds and
molecular mechanisms in physiologically relevant 3D cell
culture

FCUP | 137
Cyanobacterial bioactive metabolites for anticancer drug
discovery: characterization of new compounds and
molecular mechanisms in physiologically relevant 3D cell
culture

Assessing promising bioactivity of cyanobacterial extracts on a 3D *in vitro* model of solid tumors

Maria Lígia Sousa[1,2], Leonor Ferreira[1], Tim Krempel[1], Rosário Martins[1,3], Vítor Vasconcelos[1,2] & Ralph Urbatzka[1]

[1] CIIMAR Interdisciplinary Centre of Marine and Environmental Research, Porto, Portugal

[2] Faculty of Sciences of University of Porto, Porto, Portugal

[3] CISA-ESS- Centre of Health and Environmental Research, School of Heath, Porto Polytechnic, Portugal

*corresponding author: msousa@ciimar.up.pt

Abstract

The use of advanced *in vitro* models, such as multicellular spheroid cultures (MSC) is gaining attention for cancer research and screening of bioactive compounds. In the present work, chromatographic fractions obtained from crude organic extracts of 27 cyanobacterial strains from the Portuguese coast were tested on MSC, generated from the human cell line HCT116 (colon colorectal carcinoma). MSC were incubated over 48h with these cyanobacterial fractions, and viability assessed by acid phosphatase activity and by staining with fluorescent dyes (propidium iodide for dead cells, and calcein AM for cytoplasmic esterases). Some bioactive fractions were detected, and their metabolite profiles analysed by HR-LC–MS/MS and the Global Natural Products Social Molecular Networking program (GNPS). The comparison of active and non-active fractions in this molecular networking approach allowed the identification of several unknown mass peaks (597.992 and 543.065 m/z), which could be related to the bioactivity, since they were unique in the active fractions. One cyanobacterial strain was identified as promising and should be explored in the future by mass-guided fractionation, in order to isolate the suspected mass peaks, confirm their bioactivity and elucidate their chemical structures.

FCUP | 138
Cyanobacterial bioactive metabolites for anticancer drug
discovery: characterization of new compounds and
molecular mechanisms in physiologically relevant 3D cell
culture

Introduction

Cyanobacteria are a group of gram-negative oxygen producing bacteria that convert CO_2 into biomass through photosynthesis, releasing O_2 and being responsible for the atmosphere oxidation 3 billion years ago[1]. They are well known for extensive proliferation, forming blooms and the production of toxins that often cause severe damage to humans and the ecossystems[2-3]. The capacity to produce toxins, secondary metabolites, was the main reason why cyanobacteria started to be considered promising producers of compounds with several biotechnological applications[4-8], ranging from antifouling paints[9-11] to pharmacological drugs[12-17]. The genome of cyanobacteria is organized in gene clusters containing ribosomal peptide synthase (NRPS) and/or polyketide synthase (PKS) genes, which are often responsible for the biosynthesis of secondary metabolites, such as hierridin C[18] or bartolosides[19]. Other compounds can be synthesized in the endoplamic reticulum and further post-translationally modified by RiPPs[20], as sphaerocyclamide[21].

The LEGE Culture collection – LEGE CC (http://lege.ciimar.up.pt/) contains today more than 1000 phylogenetic diverse[22] cyanobacterial and microalgae strains, most of them isolated from the Portuguese coast and rivers. Although phylogenetic diversity does not necessarily[23] reflect chemical diversity, previous works showed that this collection is promising regarding the presence of type I polyketide synthase (PKS) and non-ribosomal peptide synthetase (NRPS) genes[24]. Cyanobacteria were established as an important source for new anticancer compounds[16, 25-26]. In a previous work developed at the Blue Biotechnology and Ecotoxicology (BBE) laboratory at CIIMAR, 27 strains were used to assess the potential cytotoxicity on several cancer cell lines, both by using the crude extracts or three fractions of different polarities[17]. The fractions with interesting activity on several cancer cell lines were selected for this work, in order to assess the potential toxicity against cancer cells cultured as multicellular spheroid cultures (MSC)[27-34]. Following the bioactivity analyses, the most active fractions were identified and analysed on a HR-LC–MS/MS platform coupled to molecular networking on the Global Natural Products Social Molecular Networking program[35] (GNPS). This software clusters the metabolites with similar MS/MS fragmentation patterns, in order to better understand which strains, and fractions would be more promising regarding their chemical diversity, in comparison with similar strains with no toxicological activity against MSC.

U. PORTO
FACULDADE DE CIÊNCIAS
UNIVERSIDADE DO PORTO

FCUP | 139
Cyanobacterial bioactive metabolites for anticancer drug
discovery: characterization of new compounds and
molecular mechanisms in physiologically relevant 3D cell
culture

Methods

Samples preparation

The fractionation was performed by Costa[17] work, where from approximately 1g of dried cyanobacterial biomass an organic crude extract was obtained with CH_2Cl_2: MeOH (2:1) extraction at room temperature and 40ºC. This crude was further fractionated by a vacuum liquid chromatography using a SiOH normal phase SPE cartridge (Strata SI-1, Phenomenex) yielding fraction A (the less polar), extracted with hexane, fraction B extracted with EtOAc and fraction C (the most polar fraction), extracted with methanol[17]. These fractions were further dried and then dissolved in dimethyl sulfoxide (DMSO) at a concentration of 10 mg ml^{-1}.

Cell culture and MSC generation

The colon cancer cell line HCT116 was maintained in McCoy's 5A modified medium, supplemented with Glutamax^{TM} (Gibco, Massachusetts, USA), 10% fetal bovine serum (Biochrom, Berlin, Germany), 1% of penicillin/streptomycin (10.000 U) (Biochrom, Berlin, Germany), and 0.1% of Amphotericin B (250 µg ml^{-1}) (GE Healthcare, Little Chafont, United Kingdom), at 37 ◦ C in 5% CO2. An HCT116 cell suspension containing 50 000 cells mL^{-1} was seeded on an Ultra-Low Attachment round bottom 96 well plate (Costar, Corning) and cells were allowed to settle for 20 min inside of the flow chamber. Then, the plate was re-incubated for 5 days. After that period, the newly formed MSC were treated for 96h with the different cyanobacterial fractions at 30 µg ml^{-1} and 100 µg ml^{-1}.

Acid phosphatase

The 96 well plates with the treated MSC were carefully washed twice with PBS. Followed by the addiction of 100 µl of Sodium acetate buffer at 0.1M containing p-nitrophenyl phosphate (2 mg ml^{-1})[33]. The reaction was stopped after 2h with 10 µL of NaOH (1N) and the absorbance was read at 405 nm in a GEN5TM-Multi-detection Microplate Reader (Biotek, Bad Friedrichshall, Germany).

Fluorescence Imaging

After exposure, MSC were incubated with Hoechst 33342 (5 µg ml^{-1}), Propidium Iodide (5 µg ml^{-1}) (Sigma- Aldrich) and Calcein AM (Life Technologies) (3 µM) for 40 min, for fluorescent staining. The resulted fluorescence was observed under a fluorescent

FCUP 140
Cyanobacterial bioactive metabolites for anticancer drug
discovery: characterization of new compounds and
molecular mechanisms in physiologically relevant 3D cell
culture

microscope Leica DM6000B, and images were analyzed with Cell Profiller software[36] followed by statistical analysis.

LC MS/MS analyses and molecular networking generation

The fractions that exhibited higher effects on cell viability were fully dried and then dissolved on Methanol (MS grade) at a concentration of 1 mg ml^{-1}. A 0.020 ml aliquot of each sample was injected on into an ACE UltraCore 2.5 Super C18 (75 mm × 2.1 mm) column (Advanced Chromatography Technologies, Aberdeen, United Kingdom) on a HR-ESI-LC-MS/MS platform, composed of a Dionex Ulimate 3000 HPLC coupled to a qExactive Focus Mass spectrometer controlled by XCalibur 4.1 software (Thermo Fisher Scientific, MA, United States). The separation was performed using a gradient from 99.5 to 10% water/methanol/formic acid (95:5:0.1, v/v) to 0.5 to 90% isopropanol/methanol/formic acid (95:5:0.1, v/v) for 9.5 min and held for 6 min before returning to the initial conditions. The UV absorbance was monitored at 254 nm and a full MS scan at the resolution of 70,000 FWHM (range of 150–2000 m/z), and data dependent MS2 (ddMS2, Discovery mode) with resolution of 17,500 FWHM (isolation window used was 3.0 amu and normalized collision energy was 35).

To perform the molecular networking, the raw data files obtained from these analyses were converted to the mzML format by the MS converter (MSConvertGUI software) and imported to GNPS, for creating the molecular network using ion mass tolerance precursor of 0.01 Da and fragment ion mass tolerance at 0.04 to account for high resolution data, as indicated on the GNPS documentation. A dereplication was performed using *in silico* Peptidic Natural Product Dereplicator[37-38] and Dereplicator+: Identification of Metabolites Through Database Search of Mass Spectra[39].

The resulting molecular network was visualized with Cytoscape v3.7.2[40] and searched for clusters of m/z data that were associated only with those extracts that were previously identified as bioactive. The HR-ESI-MS/MS spectra corresponding to such data were annotated to clarify the likely masses of the compounds generating the clusters. The darker colors correspond to the active fractions (dark green for the fractions A and dark pink for the fractions C) and the lighter colors for the fractions that were previously identified as not having any activity against the MSC (once again, light green for fractions A and light pink for the fractions C). No fractions B were selected for GNPS analysis; therefore, they are not represented on the molecular network.

FCUP | 141
Cyanobacterial bioactive metabolites for anticancer drug
discovery: characterization of new compounds and
molecular mechanisms in physiologically relevant 3D cell
culture

Results and Discussion

Viability assays

The acid phosphatase assay is described in the literature as a good indicator for viability of MCS, namely for high throughput screening[33]. The hydrolysis of p-nitrophenyl phosphate by intracellular acid phosphatases in viable cells produces p-nitrophenol, which turns yellow and the absorbance is read at 405 nm and the cell viability is calculated. Here, the exposure to two different concentrations of the cyanobacteria fractions were performed, 30 µg ml^{-1} and 100 µg ml^{-1}. However, at 30 µg ml^{-1} no alterations on the viability was registered by this method; hence we re-tested the fractions at a higher concentration of 100 µg ml^{-1}. Although the decrease in cell viability was not as effective as the positive control (1.5 µM Staurosporine), we selected those fractions in which activity lowered more than 15%. Six fractions (E14058A, E14060A, E14056C, E14045A, E14044C and E14053A) had a reduced viability between 15%-20% in comparison with the solvent control (**Figure 1**).
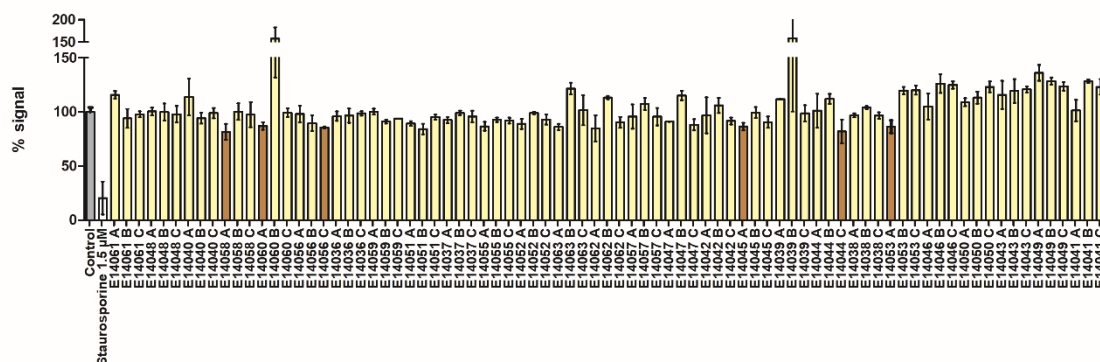
Figure 1 - Acid Phosphatase assay for 81 cyanobacterial fractions derived from 27 strains. Fractions with a reduction of signal >15% were selected for further analysis, which are here marked with a darker coloration. The current graph is normalized considering the solvent control signal as 100%. Staurosporine at 1.5 µM is the positive control. Error bars stand for standard deviation. n=3.

The cytotoxic assessment of the fractions was also performed with the staining of the MSC with Calcein AM for cell viability and Propidium Iodide for cell death, at the concentration of 30 µg ml^{-1}. Propidium enters dead cells with membrane damage while calcein AM emits fluorescence signal when hydrolysed by intracellular esterases. Hoechst staining was used as a control of fluorescence of the spheroid, since it stains nucleic acids, and is sometimes used as indicator of apoptosis due to the increase of fluorescence by nuclear condensation[34]. With this approach, the fractions E14056A and

FCUP | 142
Cyanobacterial bioactive metabolites for anticancer drug
discovery: characterization of new compounds and
molecular mechanisms in physiologically relevant 3D cell
culture

E14057A showed a decrease of Calcein staining of 11% and 30%, respectively; the fractions E14056C, E14044C and E14056A had an increase of PI staining of 27%, 10% and 14%, respectively; the fractions 14056C and 14044C had indication of increased cell death by AP and PI concordantly, while the fraction 14056A by Calcein and PI (**Figure 2**).
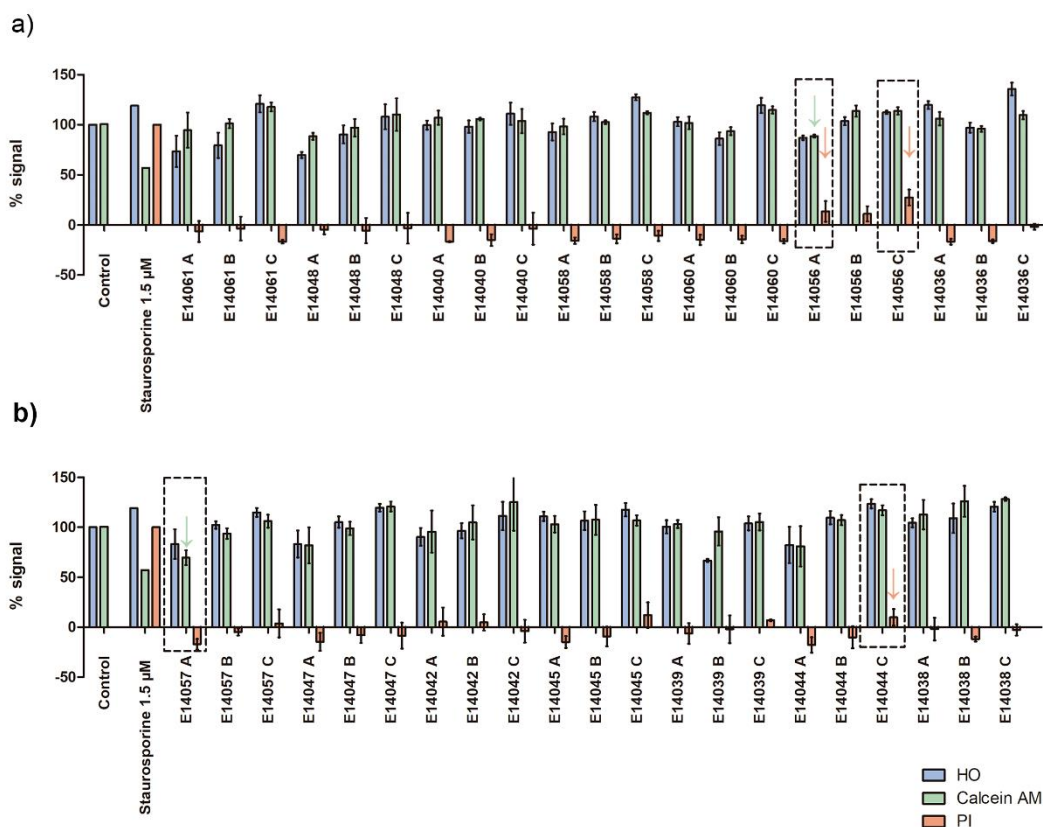
Figure 2 - Fluorescent analysis performed on MSC stained with Hoechst (HO) in blue, Calcein AM in green and Propidium Iodide (PI), in red; data are normalized considering the solvent control as 100% for HO and Calcein and for PI solvent control represents 0% while staurosporine 1.5μM represents 100%. a) Activity of the fractions E14056 A with a 11% reduction of Calcein staining against the control and 14% increasing of PI staining, and E14056 C with a 27% increasing of PI staining in comparison with the control. b) activity of the fraction E14057A with a decrease of Calcein staining of 30%, and activity of the fraction E14044C with an increase of PI staining of 10% in comparison with the control. n=3.

The lack of consistency between the PI and Calcein AM staining is probably related to the different assessments that both assays represent. PI only stains DNA when cell membranes are damaged, while calcein gives an enzymatic intracellular signal in the cytoplasm. As an example, if we look to the sample E14056C, we can observe a clear increase of PI staining but also a high increase of calcein, in comparison to the control (**Figure 3**). The impairment of the MSC growth or dead cells detachment might lead to the lack of PI staining[41]. In MSC the resilience of the cells is often higher than in individual

cells, due to their microenviroment and penetration of compounds into the MSC[42-43] might not happen. Still, calcein AM is a very potent marker for viability, but it does not confirm if the cells or, in this case, the MSC is metabolically compromised[34].
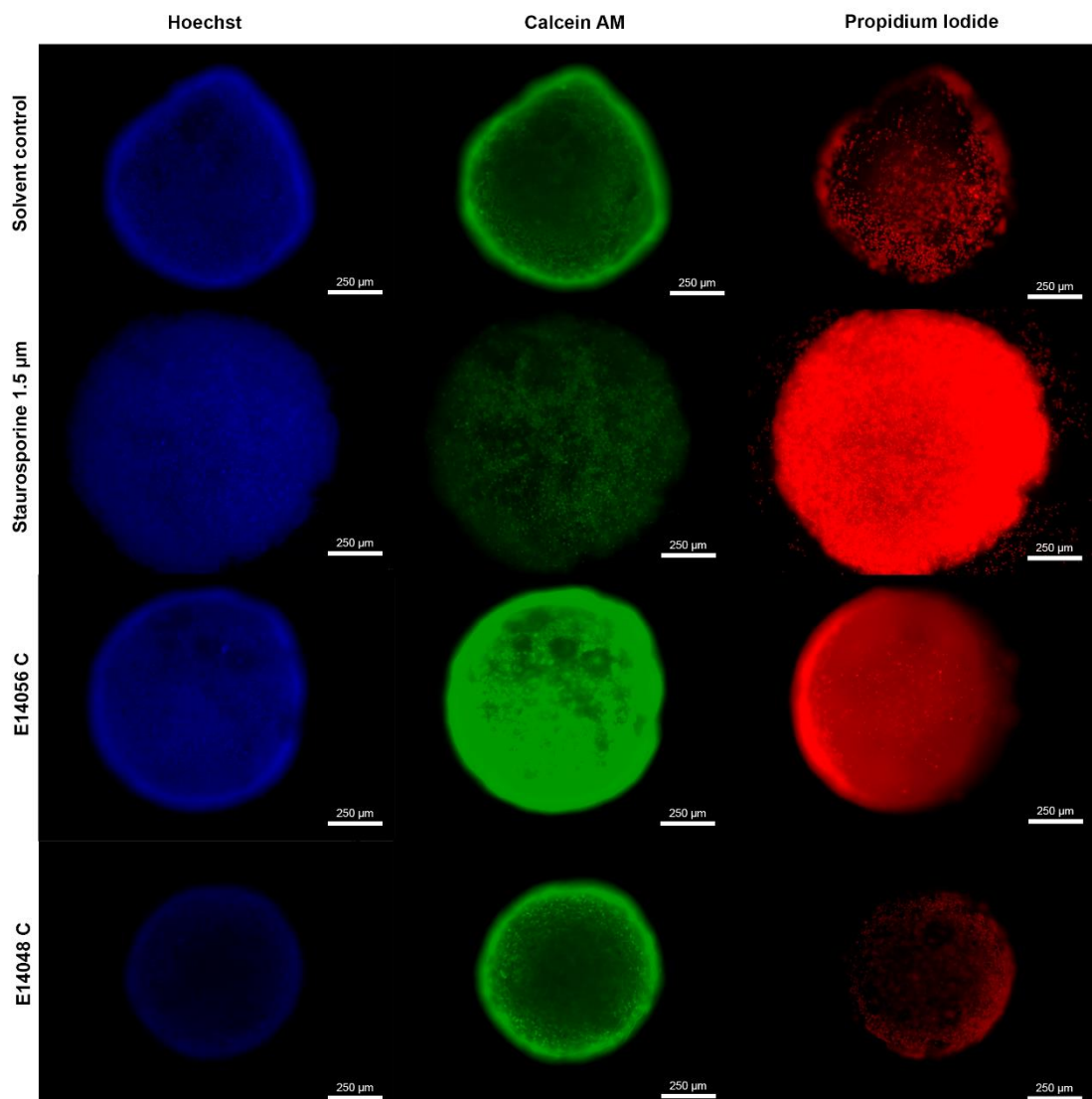
Figure 3 – Representative images of fluorescence microscopy of MSC after 96h of exposure and HO, Calcein and PI staining. First line the MSC was exposed to the solvent control, second line to the positive control Staurosporine 1.5 µM, the third line to the fraction E14056C and the fourth line to the fraction E14056C, that did not reduce general spheroid viability.

Although it is an interesting and promising approach, the present study reveals necessary improvements. The fluorescence assay approach is very sensitive when working with pure compounds[44] but when testing mixtures such as the tested fractions, the variations in fluorescence are higher within the same replicates and often insoluble compounds may precipitate on the top of MSC, not allowing the correct capture of the

FCUP | 144
Cyanobacterial bioactive metabolites for anticancer drug
discovery: characterization of new compounds and
molecular mechanisms in physiologically relevant 3D cell
culture

fluorescence (**SI_Figure 6**). Also, we cannot control if the fractions contain or not esterases inhibitors, influencing the calcein signal[45]. The acid phosphatase assay was less sensitive, only using 100µg ml^{-1} gave us enough resolution (**Figure 1**). Once again, the composition of the fractions used is unknown, therefore it is not possible at this stage to know if phosphatase inhibitors are present causing a reduction of the sensitivity of the assay.

Considering the data from acid phosphatase and fluorescence assays, the eight fractions that were more active on both assays were then selected for further analysis (**Table 1**).

GNPS analysis

The fractions that revealed a reduction of viability on MCS in the previous described assays were selected to perform a MS/MS analysis with data analysis on GNPS and Cytoscape (Table 1). The aim was to identify the secondary metabolites in the fractions and to compare active fractions to non-active fractions, in order to speculate about responsible metabolites for the bioactivity and to verify if those compounds would be novel or already known.

Table 1 - Active cyanobacteria fractions run in LC-MS/MS for further GNPS analysis

SAMPLE CODE	CYANOBACTERIAL STRAIN
E14058A	*unidentified filamentous Synechococcales* LEGE 06118
E14060A	*Nodosilinea* sp. LEGE 06009
E14056A	*Lusitaniella coriacea* LEGE 07167
E14056C	*Lusitaniella coriacea* LEGE 07167
E14057A	*Cyanobium* sp. LEGE 06113
E14045A	*Cyanobium* sp. LEGE 06139
E14044C	*Synechococcus* sp. LEGE 07172
E14053A	*Cyanobium* sp. LEGE 06026

FCUP 145
Cyanobacterial bioactive metabolites for anticancer drug
discovery: characterization of new compounds and
molecular mechanisms in physiologically relevant 3D cell
culture

As non-active fractions, samples from the same genera phylogenetically close to them were selected in order to try to eliminate metabolites from the analyses that are not related to bioactivity (**Table 2**).

Table 2 - Control cyanobacteria fractions run in LC-MS/MS for further GNPS analysis.

SAMPLE CODE	*CYANOBACTERIAL STRAIN*
14048A	*Nodosilinea* nodulosa LEGE 06102
14048C	*Nodosilinea* nodulosa LEGE 06102
14036A	unidentified filamentous *Synechococcales* LEGE 07160
14036C	unidentified filamentous *Synechococcales* LEGE 07160
14052A	*Cyanobium* sp. LEGE 06098
14052C	*Cyanobium* sp. LEGE 06098

GNPS is a web-based mass spectrometry system where we can network and search our data on a spectral library. It is then possible to identify the presence of known compounds or establish the relation between the different masses. Using further Cytoscape software[40], we can visualize that data on a network where each node (circle) represents a single consensus MS/MS spectrum for a given precursor mass, and the relation between the precursor masses (nodes) is defined by an edge (lines). The thickness of the edge is larger if the degree of similarity is higher between the nodes of MS/MS spectra.

Retrieving the data from the GNPS, 12 isolated clusters were selected from active cyanobacterial strains (**Figure 4**). The analysis of the network revealed that the active fractions A had several masses in common, which represent compounds that are produced among the different strains. The fractions C showed one cluster of three nodes from the strain *Synechococcus sp.* LEGE 07172 and several clusters (7) exclusively found on the strain *Lusitaniella coriacea* LEGE 07167. These two strains were the only that previously revealed activity on two assays, acid phosphatase and PI fluorescence (**Figure 1** and **2**).

FCUP 146

Cyanobacterial bioactive metabolites for anticancer drug discovery: characterization of new compounds and molecular mechanisms in physiologically relevant 3D cell culture

Figure 4 - GNPS-based LC-HRESIMS/MS molecular network analysis of active vs non active fractions. Dark green dots represent mass peaks of less polar fractions (Hexane – fractions A) that were active on the biological assays and light green dots represent control fractions A that were not biologically active. Dark pink dots represent mass peaks of more polar fractions (Methanol – fractions C) that were active on the biological assays and light pink dots represent control fractions C that were not biologically active. Light blue dots represent masses that are unspecific throughout all the fractions analysed.

Using the dereplication platforms of GNPS database (Insilico Peptidic Natural Product Dereplicator and Dereplicator+), the precursor mass of m/z 459.098 was identified as a 2'-O-Glutamyl-adenosine-3',5'-cyclic monophosphate, a cAMP analogue and primary metabolite. The 3',5'-cyclic adenosine monophosphate is an important secondary messenger involved in several biological processes and therefore, several analogues of cAMP were reported as having effects against breast cancer[47]. The related masses might be other cAMP analogues on the E14056C fraction (**Figure 5**), however, these

FCUP 147
Cyanobacterial bioactive metabolites for anticancer drug
discovery: characterization of new compounds and
molecular mechanisms in physiologically relevant 3D cell
culture

masses appeared with very low resolution at the mass spectra. Regarding the same fraction E14056C, the precursor masses with higher abundance on the TIC spectra were the mass peak of m/z 597.992 and 543.065 (**Figure 5**), but no known compounds were retrieved from the dereplication databases for the clusters in which they belong. All the remaining masses appear on the total ion current chromatogram with very low resolution and without signal in the UV-vis spectra. Important to note that the higher abundance indicates rather the ionization capacity of the metabolites than their quantities on the sample, similar to the UV vis spectra that rather shows photometric absorption[48].
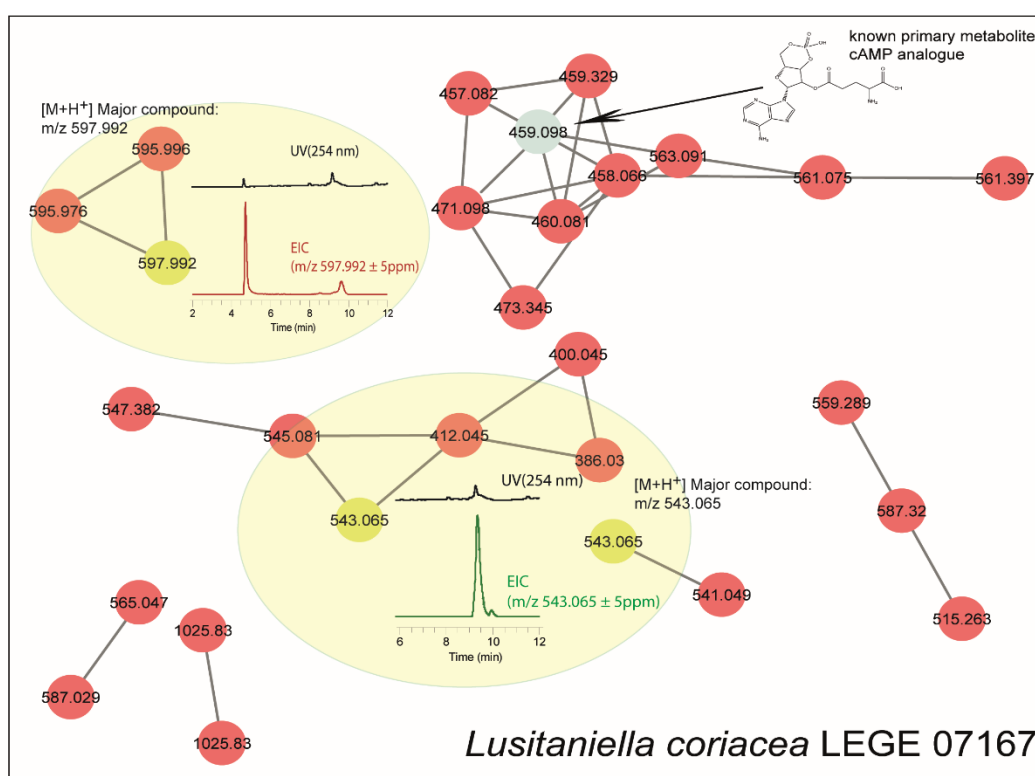
Figure 5 - Precursor masses analysis of the promising clusters. The precursor mass m/z 459.098 had a hit for a cAMP analogue. Most of the masses appear at very low resolution but two masses appear abundant on the UV spectra and extracted ion chromatogram (597.922, 543.065 m/z).

On the E14044C fraction, the three precursor masses of the cluster did not appear evidently peaked on TIC or on the EIC (**SI_Figure 2**).

From the fractions A, the clusters belonged to more than one strain, but only the fractions A of *Cyanobium sp.* LEGE 06026 revealed the present of the mass peak of 907.479 m/z on the general chromatogram in parallel with the UV spectra (Figure 6). All the other masses did not retrieve high peaks on TIC nor on UV spectra (**SI_Figure 3**SI_Figure , **SI_Figure 4** and **SI_Figure 5**).

FCUP 148
Cyanobacterial bioactive metabolites for anticancer drug
discovery: characterization of new compounds and
molecular mechanisms in physiologically relevant 3D cell
culture
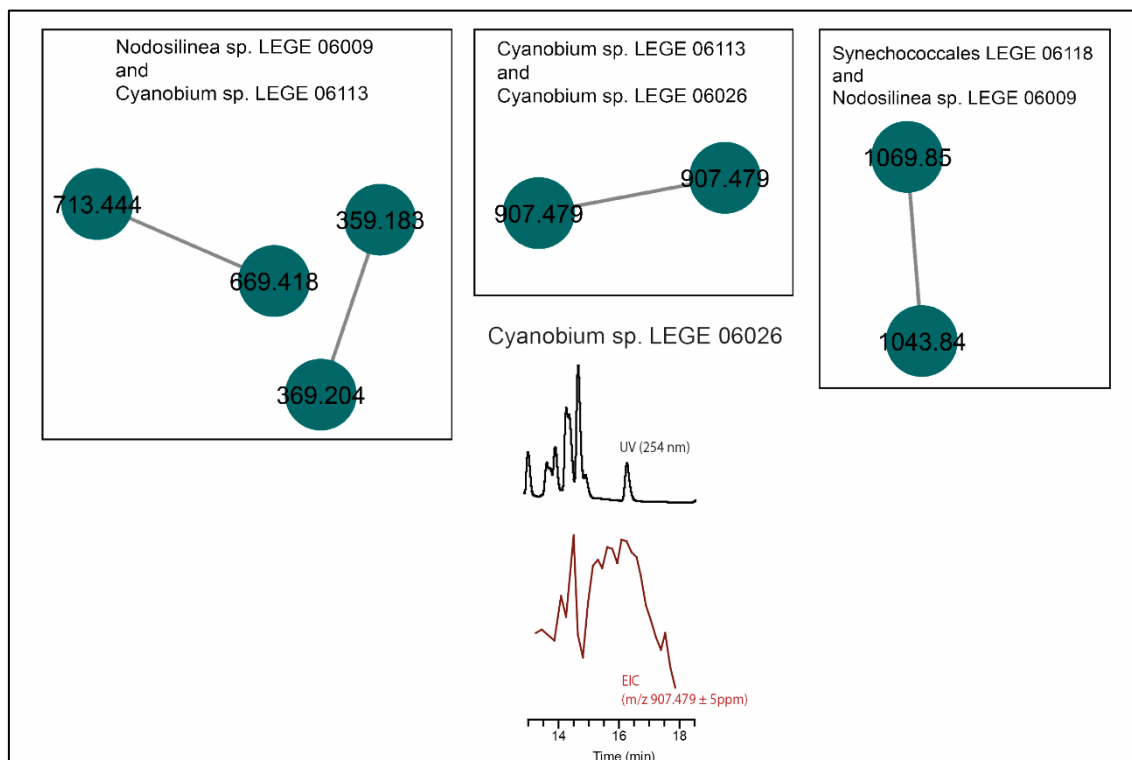
Figure 6 - Precursor masses analysis of the promising clusters. The precursor mass m/z 907.479 was the only that appeared relatively abundant but only on the EIC of the fraction A of *Cyanobium* sp. LEGE 06026 (E14053A) and not on the strain *Cyanobium* sp. LEGE 06113, which appears with very small resolution. Most of the masses appear at very low resolution but one mass (from two different clusters) appear abundant on the UV spectra and extracted ion chromatogram.

In a previous work on 61 isolates from LEGE culture collections, the presence of PKS and/or NRPS clusters genes were detected on a wide range of isolates, and many of those strains were used on the present work[24]. The presence of these genes suggested the potential for producing secondary metabolites[49-50]. The most promising strains in this research, *Lusitaniella coriacea* LEGE 07167, *Nodosilinea* sp. LEGE 06009, *Cyanobium* sp. LEGE 06113 and *Synechococcales* LEGE 06118 have PKS/NRPS sequences (**SI_Table 2**), but also the presence of compounds was predicted based on the PKS cluster sequences, using the NRPS Predictive Blast server[51] and NaPDos- Natural Product Domain Seeker[52]. Already reported before[24], none of the predictions of possible metabolites retrieved high percentage of identity, which means that new compounds related with PKS cluster remain to be discovered (**Table 3**) (nothing was retrieved from NRPS Predictive Blast server). No information on *Cyanobium sp.* LEGE 06026 polyketide synthase or non-ribosomal peptide synthetase DNA sequences are available in LEGE CC culture collection until now. Considering the present results, it would be interesting to identify if this strain has any of these cluster types, and perhaps predict their secondary metabolites.

FCUP | 149

Cyanobacterial bioactive metabolites for anticancer drug discovery: characterization of new compounds and molecular mechanisms in physiologically relevant 3D cell culture

Table 3 - Cyanobacterial KS domain sequence, based prediction of PKS using the NaPDoS software for the hit strains in GNPS. Adapted from Brito 2015[24].

Organism (LEGE code)	Accession Number 16S	Accession Number (product/gene /region)	Database match ID	% Identity	Pathway Product	Domain Class	Cluster type
Cyanobium sp. (06113)	KC469577	KC842298	CurA_AAT70096_mod	54	Curacin	KS	PKS
		KF010866[a]	JamE_AAS98777_KS1	51	jamaicamide	KS	KS
Lusitaniella coriacea (07167)	KU951853	KC842317	NosB_Q9RAH3_H	50	Nostopeptolide	Hybrid KS	PKS
Nodosilinea sp (06009)	JF708121	KC842331	StiB_Q8RJY5_1KSB	59	Stigmatellin	Modular	PKS
		KC842332	JamP_AAS98787_H	66	Jamaicamide	Hybrid KS	PKS
unidentified filamentous *Synechococcales* (06118)	KU951868	KC842358	NosB_Q9RAH3_H	59	Nostopeptolide	Hybrid KS	PKS
Cyanobium sp. LEGE 06026	KU951691	-	-	-	-	-	-

[a] Not present on Brito data (reference[24]). Runned on NaPDos at 30th September 2019.

FCUP 150
Cyanobacterial bioactive metabolites for anticancer drug
discovery: characterization of new compounds and
molecular mechanisms in physiologically relevant 3D cell
culture

Regarding the strain *Lusitaniella coriacea* LEGE 07167, a previous work analysed also the metabolite profile with the GNPS approach but using crude extracts and 105 reference cyanobacterial metabolites (seed compounds). This work identified nodes (m/z 516.982) connected with nodularin and microcystin[24]. The present results did not retrieve the same data, even though microcystin was present on some of the run samples (**SI_Table 1**). Some other m/z show up here, as promising and without connection neither to known compounds from the dereplication databases, neither with the referred m/z 516.982 from previous work[24]. Considering all our results, the strain *Lusitaniella coriacea* LEGE 07167 is a very promising one, focusing on the GNPS data[24], the decrease of viability in monolayer cultured cancer cell lines[17], and especially the reduction of viability on MSC, both using acid phosphatase and fluorescence analysis.

Conclusions

The present work demonstrates that the conjugation of biological data using more complex models, such as MSC, can increase the visualization of the more promising hits that are often observed on other screening methods. Some cyanobacterial fractions were found to reduce the activity of alkaline phosphatase and calcein AM staining and increased PI staining, all indicating a reduction of viability of MSC. In general, a low percentage of reduced cell viability was observed. This finding might be due to the complexity of the fractions, which can diminish the effectiveness of the assay. A more extensive fractionation of the cyanobacterial fractions will be a solution to diminish each fraction complexity. Nevertheless, the present work identified a promising strain, *Lusitaniella coriacea* LEGE 07167, in particular the most polar fraction, as producer of interesting metabolites. The molecular networking approach identified two potential metabolites with mass peaks of 597.992 and 543.065 m/z, which could be related to the observed bioactivities. Those metabolites should be explored in the future by mass guided isolation procedures.

References

1.   Schirrmeister, B. E.; Gugger, M.; Donoghue, P. C. J., Cyanobacteria and the Great Oxidation Event: evidence from genes and fossils. *Palaeontology* **2015,** *58* (5), 769-785.

2.   Huisman, J.; Codd, G. A.; Paerl, H. W.; Ibelings, B. W.; Verspagen, J. M. H.; Visser, P. M., Cyanobacterial blooms. *Nature Reviews Microbiology* **2018,** *16* (8), 471-483.

3.   Dittmann, E.; Wiegand, C., Cyanobacterial toxins – occurrence, biosynthesis and impact on human affairs. *Molecular Nutrition & Food Research* **2006,** *50* (1), 7-17.

4.   Wijffels, R. H.; Kruse, O.; Hellingwerf, K. J., Potential of industrial biotechnology with cyanobacteria and eukaryotic microalgae. *Current Opinion in Biotechnology* **2013,** *24* (3), 405-413.

5.   Tidgewell, K.; Clark, B.; Gerwick, W., The Natural Products Chemistry of Cyanobacteria. In *Comprehensive Natural Products II: Chemistry and Biology*, Mander, L.; Liu, H.-W., Eds. Elsevier: 2010; Vol. 2, pp 142-187

6.   Nozzi, N. E.; Oliver, J. W. K.; Atsumi, S., Cyanobacteria as a Platform for Biofuel Production. *Frontiers in bioengineering and biotechnology* **2013,** *1*, 7.

7.   Kehr, J.-C.; Gatte Picchi, D.; Dittmann, E. B., Natural product biosyntheses in cyanobacteria: A treasure trove of unique enzymes. *Beilstein Journal of Organic Chemistry* **2011,** (7), 1622–1635.

8.   Balaji, S.; Gopi, K.; Muthuvelan, B., A review on production of poly β hydroxybutyrates from cyanobacteria for the production of bio plastics. *Algal Research* **2013,** *2* (3), 278-285.

9.   Fusetani, N., Antifouling marine natural products. *Natural Product Reports* **2011,** *28* (2), 400-410.

10.   Dahms, H.-U.; Ying, X.; Pfeiffer, C., Antifouling potential of cyanobacteria: a mini-review. *Biofouling* **2006,** *22* (5), 317-327.

11.   Antunes, J.; Pereira, S.; Ribeiro, T.; Plowman, J. E.; Thomas, A.; Clerens, S.; Campos, A.; Vasconcelos, V.; Almeida, J. R., A Multi-Bioassay Integrated Approach to Assess the Antifouling Potential of the Cyanobacterial Metabolites Portoamides. *Marine Drugs* **2019,** *17* (2), 111.

12.   Tan, L. T., Pharmaceutical agents from filamentous marine cyanobacteria. *Drug discovery today* **2013,** *18* (17-18), 863-871.

13.   Singh, R. K.; Tiwari, S. P.; Rai, A. K.; Mohapatra, T. M., Cyanobacteria: an emerging source for drug discovery. *Japanese Journal of Antibiotics* **2011,** *64* (6), 401-412.

14.   Salvador-Reyes, L. A.; Luesch, H., Biological targets and mechanisms of action of natural products from marine cyanobacteria. *Natural Product Reports* **2015,** *32* (3), 478-503.

15.   Ribeiro, T.; Lemos, F.; Preto, M.; Azevedo, J.; Sousa, M. L.; Leão, P. N.; Campos, A.; Linder, S.; Vitorino, R.; Vasconcelos, V.; Urbatzka, R., Cytotoxicity of portoamides in human cancer cells and analysis of the molecular mechanisms of action. *PLOS ONE* **2017,** *12* (12), e0188817.

16.   Leão, P. N.; Costa, M.; Ramos, V.; Pereira, A. R.; Fernandes, V. C.; Domingues, V. F.; Gerwick, W. H.; Vasconcelos, V. M.; Martins, R., Antitumor Activity of Hierridin B, a Cyanobacterial Secondary Metabolite Found in both Filamentous and Unicellular Marine Strains. *PLOS ONE* **2013,** *8* (7), e69562.

17.   Costa, M.; Garcia, M.; Costa-Rodrigues, J.; Costa, S. M.; Ribeiro, J. M.; Fernandes, H. M.; Barros, P.; Barreiro, A.; Vasconcelos, V.; Martins, R., Exploring

Bioactive Properties of Marine Cyanobacteria Isolated from the Portuguese Coast: High Potential as a Source of Anticancer Compounds. *Marine Drugs* **2014,** *12* (1).

18. Margarida, C.; Ivo E., S.-D.; Raquel, C.-B.; Hugo, S.; Roberta, R. d. C.; Artur, S.; Maria Paula Cruz, S.; Maria João, A.; Rosário, M.; Valentina, F. D.; Fatima, N.; Vera, C.; Vitor M., V.; Pedro, L., *Structure,* Synthesis of Hierridin C and Discovery of Prevalent Alkylresorcinol Biosynthesis in Picocyanobacteria. *Journal of Natural Products*. 2018. 82 (2), 393-402.

19. Leão, P. N.; Nakamura, H.; Costa, M.; Pereira, A. R.; Martins, R.; Vasconcelos, V.; Gerwick, W. H.; Balskus, E. P., Biosynthesis-Assisted Structural Elucidation of the Bartolosides, Chlorinated Aromatic Glycolipids from Cyanobacteria. *Angewandte Chemie International Edition* **2015,** *54* (38), 11063-11067.

20. Martins, J.; Vasconcelos, V., Cyanobactins from Cyanobacteria: Current Genetic and Chemical State of Knowledge. *Marine drugs* **2015,** *13* (11), 6910-6946.

21. Martins, J.; Leikoski, N.; Wahlsten, M.; Azevedo, J.; Antunes, J.; Jokela, J.; Sivonen, K.; Vasconcelos, V.; Fewer, D. P.; Leão, P. N., Sphaerocyclamide, a prenylated cyanobactin from the cyanobacterium Sphaerospermopsis sp. LEGE 00249. *Scientific Reports* **2018,** *8* (1), 14537.

22. Ramos, V.; Morais, J.; Castelo-Branco, R.; Pinheiro, Â.; Martins, J.; Regueiras, A.; Pereira, A. L.; Lopes, V. R.; Frazão, B.; Gomes, D.; Moreira, C.; Costa, M. S.; Brûle, S.; Faustino, S.; Martins, R.; Saker, M.; Osswald, J.; Leão, P. N.; Vasconcelos, V. M., Cyanobacterial diversity held in microbial biological resource centers as a biotechnological asset: the case study of the newly established LEGE culture collection. *Journal of Applied Phycology* **2018**.

23. Leão, P. N.; Ramos, V.; Gonçalves, P. B.; Viana, F.; Lage, O. M.; Gerwick, W. H.; Vasconcelos, V. M., Chemoecological Screening Reveals High Bioactivity in Diverse Culturable Portuguese Marine Cyanobacteria. *Marine Drugs* **2013,** *11* (4), 1316-1335.

24. Brito, Â.; Gaifem, J.; Ramos, V.; Glukhov, E.; Dorrestein, P. C.; Gerwick, W. H.; Vasconcelos, V. M.; Mendes, M. V.; Tamagnini, P., Bioprospecting Portuguese Atlantic coast cyanobacteria for bioactive secondary metabolites reveals untapped chemodiversity. *Algal Research* **2015,** *9*, 218-226.

25. Costa, M.; Costa-Rodrigues, J.; Fernandes, M. H.; Barros, P.; Vasconcelos, V.; Martins, R., Marine Cyanobacteria Compounds with Anticancer Properties: A Review on the Implication of Apoptosis. *Marine Drugs* **2012,** *10* (10), 2181.

26. Voráčová, K.; Paichlová, J.; Vicková, K.; Hrouzek, P., Screening of cyanobacterial extracts for apoptotic inducers: a combined approach of caspase-3/7 homogeneous assay and time-lapse microscopy. *Journal of Applied Phycology* **2017,** *29* (4), 1933-1943.

27. Weiswald, L.-B.; Bellet, D.; Dangles-Marie, V., Spherical Cancer Models in Tumor Biology. *Neoplasia* **2015,** *17* (1), 1-15.

28. Langhans, S. A., Three-Dimensional *in vitro* Cell Culture Models in Drug Discovery and Drug Repositioning. *Frontiers in Pharmacology* **2018,** *9* (6).

29. Kunz-Schughart, L. A.; Kreutz, M.; Knuechel, R., Multicellular spheroids: a three-dimensional *in vitro* culture system to study tumour biology. *International Journal of Experimental Pathology* **1998,** *79* (1), 1-23.

30. Kunz-Schughart, L. A.; Freyer, J. P.; Hofstaedter, F.; Ebner, R., The Use of 3-D Cultures for High-Throughput Screening: The Multicellular Spheroid Model. *Journal of Biomolecular Screening* **2004,** *9* (4), 273-285.

31. Kondo, J.; Ekawa, T.; Endo, H.; Yamazaki, K.; Tanaka, N.; Kukita, Y.; Okuyama, H.; Okami, J.; Imamura, F.; Ohue, M.; Kato, K.; Nomura, T.; Kohara, A.; Mori, S.; Dan, S.; Inoue, M., High-throughput screening in colorectal cancer tissue-originated spheroids. *Cancer Science* **2019,** *110* (1), 345-355.

FCUP | 153
Cyanobacterial bioactive metabolites for anticancer drug
discovery: characterization of new compounds and
molecular mechanisms in physiologically relevant 3D cell
culture

32.   Hirschhaeuser, F.; Menne, H.; Dittfeld, C.; West, J.; Mueller-Klieser, W.; Kunz-Schughart, L. A., Multicellular tumor spheroids: An underestimated tool is catching up again. *Journal of Biotechnology* **2010,** *148* (1), 3-15.

33.   Friedrich, J.; Eder, W.; Castaneda, J.; Doss, M.; Huber, E.; Ebner, R.; Kunz-Schughart, L. A., A Reliable Tool to Determine Cell Viability in Complex 3-D Culture: The Acid Phosphatase Assay. *Journal of Biomolecular Screening* **2007,** *12* (7), 925-937.

34.   Oksana, S.; Trisha, M.; Jayne, H.; Steve, L.; Windsor, O.; F., C. E., High-Content Assays for Characterizing the Viability and Morphology of 3D Cancer Spheroid Cultures. *Assay and Drug Development Technologies* **2015,** *13* (7), 402-414.

35.   Wang, M.; Carver, J. J.; Phelan, V. V.; Sanchez, L. M.; Garg, N.; Peng, Y.; Nguyen, D. D.; Watrous, J.; Kapono, C. A.; Luzzatto-Knaan, T.; Porto, C.; Bouslimani, A.; Melnik, A. V.; Meehan, M. J.; Liu, W.-T.; Crüsemann, M.; Boudreau, P. D.; Esquenazi, E.; Sandoval-Calderón, M.; Kersten, R. D.; Pace, L. A.; Quinn, R. A.; Duncan, K. R.; Hsu, C.-C.; Floros, D. J.; Gavilan, R. G.; Kleigrewe, K.; Northen, T.; Dutton, R. J.; Parrot, D.; Carlson, E. E.; Aigle, B.; Michelsen, C. F.; Jelsbak, L.; Sohlenkamp, C.; Pevzner, P.; Edlund, A.; McLean, J.; Piel, J.; Murphy, B. T.; Gerwick, L.; Liaw, C.-C.; Yang, Y.-L.; Humpf, H.-U.; Maansson, M.; Keyzers, R. A.; Sims, A. C.; Johnson, A. R.; Sidebottom, A. M.; Sedio, B. E.; Klitgaard, A.; Larson, C. B.; Boya P, C. A.; Torres-Mendoza, D.; Gonzalez, D. J.; Silva, D. B.; Marques, L. M.; Demarque, D. P.; Pociute, E.; O'Neill, E. C.; Briand, E.; Helfrich, E. J. N.; Granatosky, E. A.; Glukhov, E.; Ryffel, F.; Houson, H.; Mohimani, H.; Kharbush, J. J.; Zeng, Y.; Vorholt, J. A.; Kurita, K. L.; Charusanti, P.; McPhail, K. L.; Nielsen, K. F.; Vuong, L.; Elfeki, M.; Traxler, M. F.; Engene, N.; Koyama, N.; Vining, O. B.; Baric, R.; Silva, R. R.; Mascuch, S. J.; Tomasi, S.; Jenkins, S.; Macherla, V.; Hoffman, T.; Agarwal, V.; Williams, P. G.; Dai, J.; Neupane, R.; Gurr, J.; Rodríguez, A. M. C.; Lamsa, A.; Zhang, C.; Dorrestein, K.; Duggan, B. M.; Almaliti, J.; Allard, P.-M.; Phapale, P.; Nothias, L.-F.; Alexandrov, T.; Litaudon, M.; Wolfender, J.-L.; Kyle, J. E.; Metz, T. O.; Peryea, T.; Nguyen, D.-T.; VanLeer, D.; Shinn, P.; Jadhav, A.; Müller, R.; Waters, K. M.; Shi, W.; Liu, X.; Zhang, L.; Knight, R.; Jensen, P. R.; Palsson, B. Ø.; Pogliano, K.; Linington, R. G.; Gutiérrez, M.; Lopes, N. P.; Gerwick, W. H.; Moore, B. S.; Dorrestein, P. C.; Bandeira, N., Sharing and community curation of mass spectrometry data with Global Natural Products Social Molecular Networking. *Nature Biotechnology* **2016,** *34*, 828.

36.   Carpenter, A. E.; Jones, T. R.; Lamprecht, M. R.; Clarke, C.; Kang, I. H.; Friman, O.; Guertin, D. A.; Chang, J. H.; Lindquist, R. A.; Moffat, J.; Golland, P.; Sabatini, D. M., CellProfiler: image analysis software for identifying and quantifying cell phenotypes. *Genome Biology* **2006,** *7* (10), R100.

37.   Mohimani, H.; Gurevich, A.; Mikheenko, A.; Garg, N.; Nothias, L.-F.; Ninomiya, A.; Takada, K.; Dorrestein, P. C.; Pevzner, P. A., Dereplication of peptidic natural products through database search of mass spectra. *Nature Chemical Biology* **2016,** *13*, 30.

38.   Gurevich, A.; Mikheenko, A.; Shlemov, A.; Korobeynikov, A.; Mohimani, H.; Pevzner, P. A., Increased diversity of peptidic natural products revealed by modification-tolerant database search of mass spectra. *Nature Microbiology* **2018,** *3* (3), 319-327.

39.   Mohimani, H.; Gurevich, A.; Shlemov, A.; Mikheenko, A.; Korobeynikov, A.; Cao, L.; Shcherbin, E.; Nothias, L.-F.; Dorrestein, P. C.; Pevzner, P. A., Dereplication of microbial metabolites through database search of mass spectra. *Nature Communications* **2018,** *9* (1), 4035.

40.   Shannon, P.; Markiel, A.; Ozier, O.; Baliga, N. S.; Wang, J. T.; Ramage, D.; Amin, N.; Schwikowski, B.; Ideker, T., Cytoscape: A Software Environment for Integrated Models of Biomolecular Interaction Networks. *Genome Research* **2003,** *13* (11), 2498-2504.

41. Kessel, S.; Cribbes, S.; Déry, O.; Kuksin, D.; Sincoff, E.; Qiu, J.; Chan, L. L.-Y., High-Throughput 3D Tumor Spheroid Screening Method for Cancer Drug Discovery Using Celigo Image Cytometry. *SLAS TECHNOLOGY: Translating Life Sciences Innovation* **2017,** *22* (4), 454-465.

42. Trédan, O.; Galmarini, C. M.; Patel, K.; Tannock, I. F., Drug Resistance and the Solid Tumor Microenvironment. *JNCI: Journal of the National Cancer Institute* **2007,** *99* (19), 1441-1454.

43. Minchinton, A. I.; Tannock, I. F., Drug penetration in solid tumours. *Nat Rev Cancer* **2006,** *6* (8), 583-592.

44. Herrmann, R.; Fayad, W.; Schwarz, S.; Berndtsson, M.; Linder, S., Screening for Compounds That Induce Apoptosis of Cancer Cells Grown as Multicellular Spheroids. *Journal of Biomolecular Screening* **2008,** *13* (1), 1-8.

45. Becher, P. G.; Baumann, H. I.; Gademann, K.; Jüttner, F., The cyanobacterial alkaloid nostocarboline: an inhibitor of acetylcholinesterase and trypsin. *Journal of Applied Phycology* **2008,** *21* (1), 103.

46. Sousa, M. L.; Preto, M.; Vasconcelos, V.; Linder, S.; Urbatzka, R., Antiproliferative Effects of the Natural Oxadiazine Nocuolin A Are Associated With Impairment of Mitochondrial Oxidative Phosphorylation. *Frontiers in Oncology* **2019,** *9* (224).

47. Valdés, F. Z.; Luna, V. Z.; Arévalo, B. R.; Brown, N. V.; Gutiérrez, M. C., Adenosine: Synthetic Methods of Its Derivatives and Antitumor Activity. *Mini-Reviews in Medicinal Chemistry* **2018,** *18* (20), 1684-1701.

48. Girão, M.; Ribeiro, I.; Ribeiro, T.; Azevedo, I. C.; Pereira, F.; Urbatzka, R.; Leão, P. N.; Carvalho, M. F., Actinobacteria Isolated From Laminaria ochroleuca: A Source of New Bioactive Compounds. *Frontiers in Microbiology* **2019,** *10* (683).

49. Ehrenreich, I. M.; Waterbury, J. B.; Webb, E. A., Distribution and diversity of natural product genes in marine and freshwater cyanobacterial cultures and genomes. *Applied and Environmental Microbiology* **2005,** *71* (11), 7401-7413.

50. Shih, P. M.; Wu, D.; Latifi, A.; Axen, S. D.; Fewer, D. P.; Talla, E.; Calteau, A.; Cai, F.; Tandeau de Marsac, N.; Rippka, R.; Herdman, M.; Sivonen, K.; Coursin, T.; Laurent, T.; Goodwin, L.; Nolan, M.; Davenport, K. W.; Han, C. S.; Rubin, E. M.; Eisen, J. A.; Woyke, T.; Gugger, M.; Kerfeld, C. A., Improving the coverage of the cyanobacterial phylum using diversity-driven genome sequencing. *Proceedings of the National Academy of Sciences* **2013,** *110* (3), 1053-1058.

51. Altschul, S. F.; Madden, T. L.; Schäffer, A. A.; Zhang, J.; Zhang, Z.; Miller, W.; Lipman, D. J., Gapped BLAST and PSI-BLAST: a new generation of protein database search programs. *Nucleic Acids Research* **1997,** *25* (17), 3389-3402.

52. Ziemert, N.; Podell, S.; Penn, K.; Badger, J. H.; Allen, E.; Jensen, P. R., The Natural Product Domain Seeker NaPDoS: A Phylogeny Based Bioinformatic Tool to Classify Secondary Metabolite Gene Diversity. *PLOS ONE* **2012,** *7* (3), e34064.

53. Afonso, T. B.; Costa, M. S.; Rezende de Castro, R.; Freitas, S.; Silva, A.; Schneider, M. P. C.; Martins, R.; Leão, P. N., Bartolosides E–K from a Marine Coccoid Cyanobacterium. *Journal of Natural Products* **2016,** *79* (10), 2504-2513.

Supplementary Information
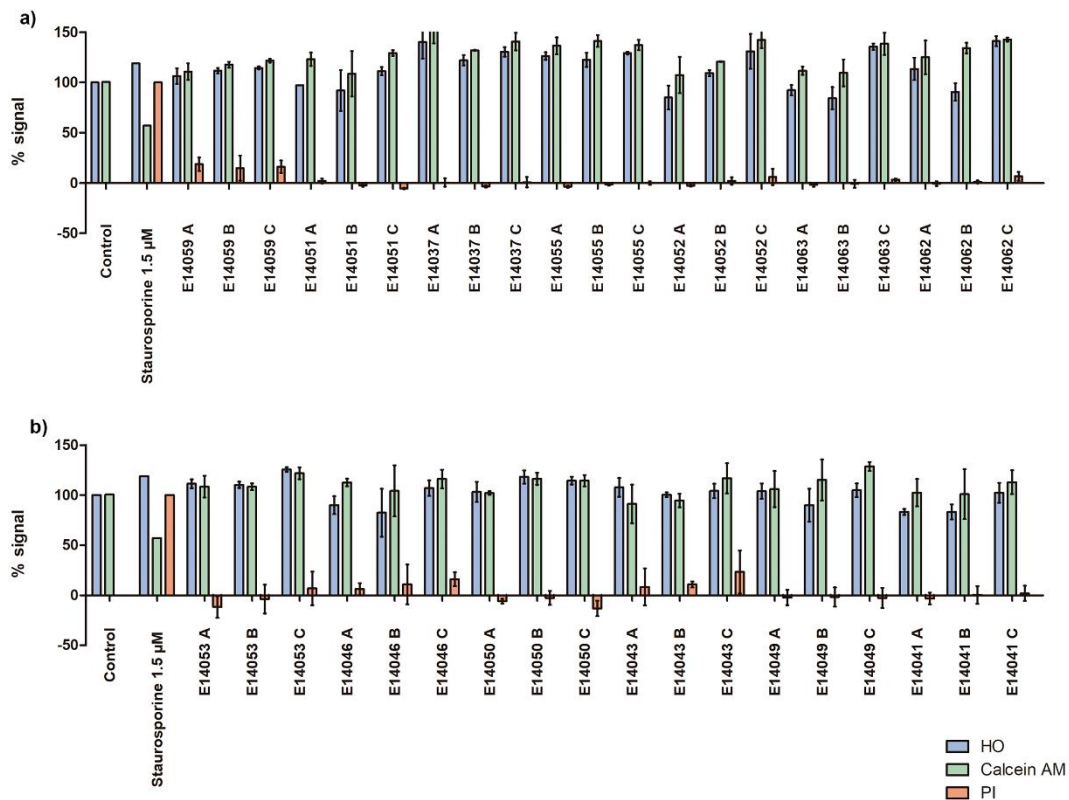
SI_Figure 1- Graphs representing part of the fluorescent analysis performed on MSC stained with Hoechst (HO) in blue, Calcein AM in green and Propidium Iodide (PI), in red; the data is normalized considering the solvent control as 100% for HO and Calcein and for PI solvent control represents 0% while staurosporine 1.5μM represents 100%. None of these fractions were considered for further GNPS. n=3.

Synechococcus sp. LEGE 07172
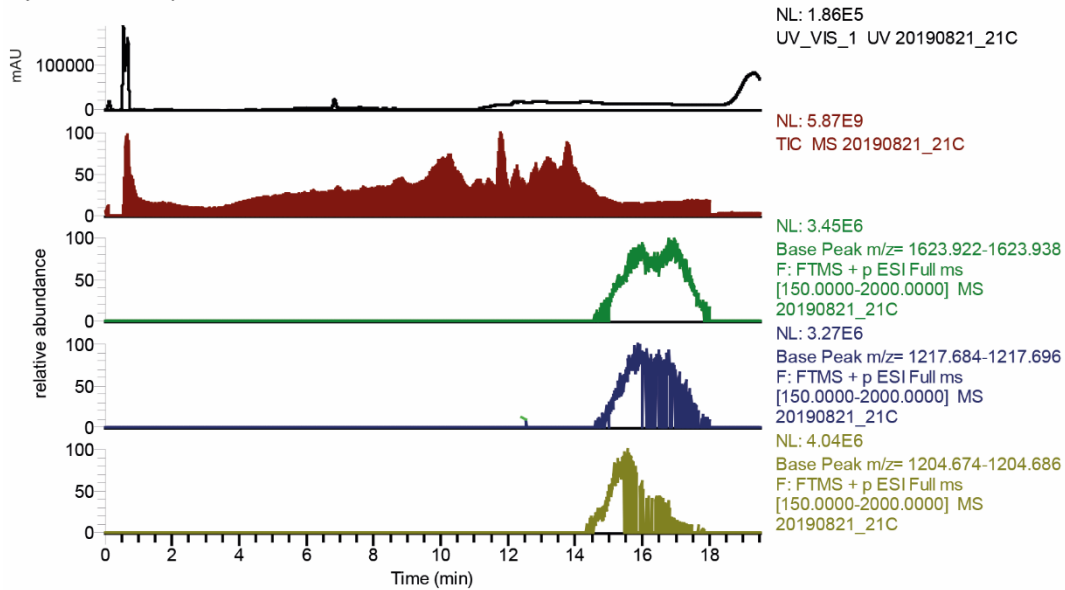
SI_Figure 2- Mass spectra exploration from *Synechococcus* sp. LEGE 07172 fraction C (E14044 C) regarding the isolated clusters from GNPS (Figure 4): m/z 1623.93; m/z 1217.69 and m/z 1204.68.

Cyanobium sp. LEGE 06113
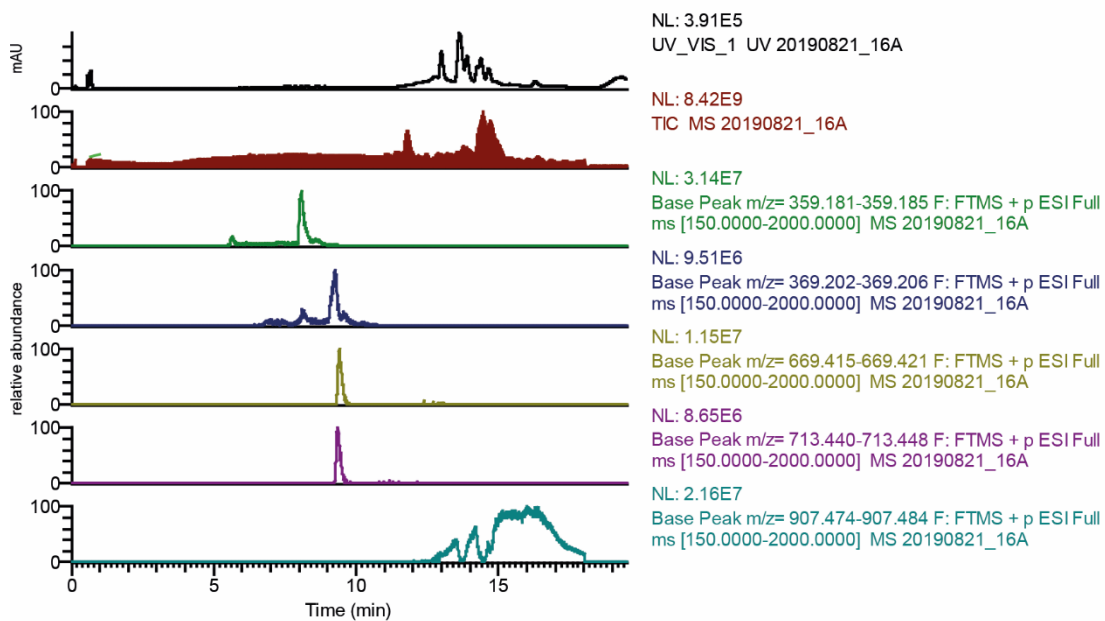
SI_Figure 3 - Mass spectra exploration from *Cyanobium* sp. LEGE 06113 fraction A (E14057 A) regarding the isolated clusters from GNPS (Figure 4): m/z 359.183, m/z369.204, m/z669.418, m/z 713.444 and m/z 907.479.

Nodosilinea sp. LEGE 06009

NL: 3.95E5
UV_VIS_1 UV 20190821_5A

NL: 8.36E9
TIC MS 20190821_5A

NL: 1.04E7
Base Peak m/z= 713.440-713.448 F: FTMS + p ESI Full ms [150.0000-2000.0000] MS 20190821_5A

NL: 1.30E7
Base Peak m/z= 669.415-669.421 F: FTMS + p ESI Full ms [150.0000-2000.0000] MS 20190821_5A

NL: 6.43E6
Base Peak m/z= 369.202-369.206 F: FTMS + p ESI Full ms [150.0000-2000.0000] MS 20190821_5A

NL: 4.13E7
Base Peak m/z= 359.181-359.185 F: FTMS + p ESI Full ms [150.0000-2000.0000] MS 20190821_5A

NL: 6.42E6
Base Peak m/z= 1069.845-1069.855 F: FTMS + p ESI Full ms [150.0000-2000.0000] MS 20190821_5A

NL: 2.09E7
Base Peak m/z= 1043.835-1043.845 F: FTMS + p ESI Full ms [150.0000-2000.0000] MS 20190821_5A

SI_Figure 4- Mass spectra exploration from *Cyanobium* sp. LEGE 06009 fraction A (E14060A) regarding the isolated clusters from GNPS (Figure 4): m/z 359.183, m/z369.204, m/z 669.418, m/z 713.444, m/z 1069.85 and m/z 1043.84.

unidentified filamentous Synechococcales LEGE 06118

NL: 1.72E5
UV_VIS_1 UV 20190821_4A

NL: 7.02E9
TIC MS 20190821_4A

NL: 5.52E6
Base Peak m/z= 1069.845-1069.855 F: FTMS + p ESI Full ms [150.0000-2000.0000] MS 20190821_4A

NL: 6.20E7
Base Peak m/z= 1043.835-1043.845 F: FTMS + p ESI Full ms [150.0000-2000.0000] MS 20190821_4A
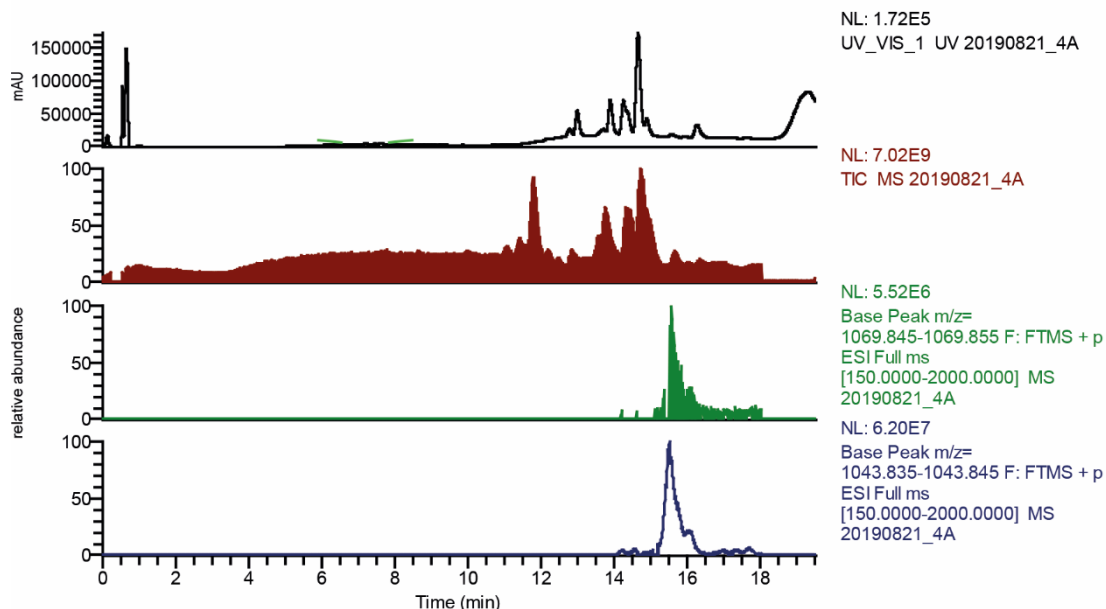
SI_Figure 5- Mass spectra exploration *Synechococcales* LEGE 06118 fraction A (E14058A) regarding the isolated clusters from GNPS (Figure 4): m/z 1069.85 and m/z 1043.84.

SI_Table 1 - Dereplication table with hits from Dereplicator + and Insilico Peptidic Natural Product Dereplicator databases. All those masses are identified in our samples, however non of those belong to the precursor masses identified on the clusters, with exception of 2'-O-Glutamyl-adenosine-3',5'-cyclic monophosphate.

FCUP | 158

Cyanobacterial bioactive metabolites for anticancer drug
discovery: characterization of new compounds and
molecular mechanisms in physiologically relevant 3D cell
culture

LibraryID	RTMean	precursor mass
[2,3-dihydroxypropoxy][3-(hexadecanoyloxy)-2-[octadec-9-enoyloxy]propoxy]phosphinic acid	986.478	771.514
1,2-dihydroxyheptadec-16-en-4-yl acetate	1049.352	329.269
MassbankEU:SM884701 N-Cyclohexyl-2-benzothiazol-amine|N-cyclohexyl-1,3-benzothiazol-2-amine	401.171	233.111
MoNA:936698 DBP	960.580	279.159
Pheophorbide A	748.304	593.276
Spectral Match to .beta.-Cryptoxanthin from NIST14	972.206	553.44
Spectral Match to 1,2-Dipalmitoyl-sn-glycero-3-phospho-(1'-rac-glycerol) from NIST14	1050.37	745.499
Spectral Match to 13-Docosenamide, (Z)- from NIST14	762.913	338.342
Spectral Match to 13-Docosenamide, (Z)- from NIST14	750.722	675.677
Spectral Match to 9-Octadecenamide, (Z)- from NIST14	726.726	282.279
Spectral Match to 9-Octadecenamide, (Z)- from NIST14	708.028	563.551
plakortone_N	1113.388	209.153
Spectral Match to cis,cis-9,12-Octadecadien-1-ol from NIST14	1126.286	267.268
Chaulmoogric Acid	1062.208	298.274
Spectral Match to Benzyldodecyldimethylammonium from NIST14	471.169	304.3
Spectral Match to cis-5,8,11,14-Eicosatetraenoic acid from NIST14	1145.835	305.247
Spectral Match to 1-Hexadecanoyl-sn-glycerol from NIST14	1118.141	331.284
Longicatenamycin;_S-520	760.673	419.277
Longicatenamycin;_S-520	628.088	419.277
Microcystin_Microcystin_	**575.4975**	**441.26**
Haliclonamide_B_O-(3-Methyl-2-butenyl) or Virotoxin_[Ala1]Viroidin	231.412	443.212
1-(2-Hydroxy-phenoxy)-trieicos-1-en-3-on	1028.284	445.367
1-De-[N-(1,2-dioxobutyl)-N-methylvaline]	271.867	453.343
Puwainaphycin_A_Puwainaphycin_A	323.191	456.939
2'-O-Glutamyl-adenosine-3',5'-cyclic_mon	550.225	459.098
3',4'-Didehydro-y,psi-carotene	920.544	535.43
Â§,Â§-carotene	760.264	537.451
1,2-Dihydrolycopene;_1',2'-Dihydrolycope	993.321	539.467
Sch_378167_5'-Amide	612.867	549.258
Sch_378199_5''-Amide	615.994	549.321
Cyclosporin,_9CI_N9-De-Me	**842.556**	**551.424**
Cyclosporin,_9CI_N9-De-Me or Clonostachysin_A_Clonostachysin_A	850.644	551.444
Spectral Match to .beta.-Cryptoxanthin from NIST14	876.846	552.432
Cyclosporin,_9CI_Cyclosporin_C	707.876	582.52
Sulfomycin_Sulfomycin_I	41.83425	583.131
Guaraxanthin;_7,8-Dihydroastaxanthin;3	742.0745	599.41
Destruxins_Î´Pro-Methyl,_3-isoleucine_homologue	750.469	600.417
(D-Hiv)2(Leu)4(Thr)7-Cyclosporin_A_10-L-Leucine_analogue or NVA2-g-hydroxy-Meleu4-cyclosporin	707.759	607.023
P10-B-1	773.725	623.407

1-O-Acyl_phillipsiaxanthin	745.846	639.402
Dehydrorhodopin_glucoside;1-Glycosylox	733.619	715.499
Petriellin_A_Petriellin_A	732.438	737.481
Amidomycin_Amidomycin	866.212	909.549
porphyrinolactone	899.665	931.594
Spectral Match to Bis(2-ethylhexyl) phthalate from NIST14	1050.143	391.284
Spectral Match to Glycerol 1-stearate from NIST14	1129.178	359.315
Spectral Match to Hexanedioic acid, bis(2-ethylhexyl) ester from NIST14	750.052	371.315
Spectral Match to Monopalmitolein (9c) from NIST14	960.854	311.258

SI_Table 2 – Summary table resuming the detected presence of NRPS or PKS genes and RiPPs on the strains used on the present work. This information was retrieved from Brito 2015[24] and Ramos 2018[22] previous work.

Strains	*NRPS/ PKS*	*RiPPs*	*extract code*	*OBS.:*
Nodosilinea nodulosa LEGE 06152	+		E14061	
Nodosilinea nodulosa LEGE 06102	+		E14048	Bartolosides[19,53]
Leptolyngbya mycoidea LEGE 06108	+		E14040	
unidentified filamentous *Synechococcales* LEGE 06118	+	+	E14058	
Nodosilinea sp. LEGE 06009	+		E14060	
Leptolyngbya fragilis LEGE 07167	+		E14056	
unidentified filamentous *Synechococcales* LEGE 07160	+		E14036	
Pseudanabaena aff. LEGE 07169	+		E14059	
Pseudanabaena aff. persicina LEGE 07163	+		E14051	
Pseudanabaena sp. LEGE 06144	+		E14037	
Pseudanabaena sp. LEGE 06194	+		E14055	
Cyanobium sp. LEGE 06098	+		E14052	
Cyanobium sp. LEGE 06134	+		E14063	
Cyanobium sp. LEGE 07175	-		no extracts available	
Cyanobium sp. LEGE 07186	+		E14062	
Cyanobium sp. LEGE 06113	+		E14057	Hierridin B[16]
Cyanobium sp. LEGE 06137	-		E14047	
Cyanobium sp. LEGE 06097	+		E14042	
Cyanobium sp. LEGE 06139	-		E14045	
Synechococcus nidulans LEGE 07171	-		E14039	
Synechococcus sp. LEGE 07172	-		E14044	
Synechococcus sp. LEGE 06005	-		E14038	
Cyanobium sp. LEGE 06026	-		E14053	
Synechocystis salina LEGE 06099	+	+	E14046	Bartolosides[53]
Synechocystis salina LEGE 06155	-	+	E14050	Bartolosides[19]
Synechocystis salina LEGE 07173	+		E14043	

| Romeria sp. LEGE 06013 | + | E14049 |
| Romeria aff. gracilis LEGE 07310 | - | E14041 |
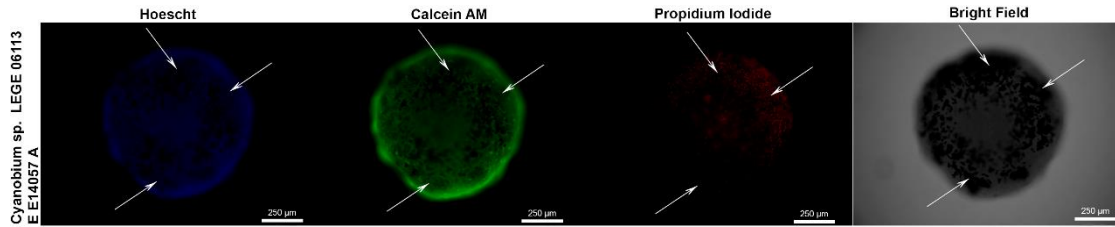
SI_Figure 6 - MSC with deposits of precipitated sample.

DISCUSSION

FCUP | 162
Cyanobacterial bioactive metabolites for anticancer drug
discovery: characterization of new compounds and
molecular mechanisms in physiologically relevant 3D cell
culture

Advances from a mechanistic perspective

As described on the introduction of the present thesis, nature has been the primordial source of new compounds to overcome a huge variety of human diseases such as cancer. Cyanobacterial compounds isolated on BBE laboratory are here presented as a solid proof of its importance regarding their bioactivity against cells, namely cancer cells cultured as spheroids, a more complex advanced model that better mimics real tumour environment and physiology.

Hereby we described the activity and mechanisms of action of two compounds, nocuolin A (designated as NocA on the following text) and portoamides AB (a mixture of two compounds designated as PAB on the following text).

NocA was first discovered by Vorácová[56] but also on BBE on *Nodularia* sp. LEGE 06071. The discovery of its mode of action took most of the time of the work presented on the current thesis. This compound was discovered through bio-guided isolation, which means that cytotoxic effects were known already throughout the process. However, the question remained of how potent such compound was, its selectivity, its mode of action and molecular targets, and if it would be active against cells cultured under circumstances similar to a real tumour. To the best of my knowledge, the present work shows the first study of a cyanobacterial compound on 3D cell culture.

We have chosen to use HCT116, a colon adenocarcinoma cell line, since it was described to form spheroids with good reproducibility and we could have access to genetically modified HCT116 cell lines with certain genes expression altered, namely BCL family genes. Regarding the mechanism of action, we demonstrated that NocA decreases viability of HCT116 cells cultured both monolayer and as spheroids. Moreover, such loss of viability was happening through apoptosis mechanisms, and on spheroid down to 2.5 µM, which is only 2.5-fold higher compared to its IC_{50} on monolayer cultures. NocA showed higher effectiveness on HCT116 cells than on the non-carcinogenic epithelial cell line RPE-1[hTERT]. This emphasizes the already discussed role of mitochondria on cancer cells and their dependence on mitochondrial energy production to keep proliferating[139], in opposition to non-continuously proliferating cells in which their energy requirements are not so high.

By performing a transcriptomic analysis of the breast cancer cell line MCF-7 (IC_{50} 1.6 µM), the Connectivity Map database (Broad Institute)[218] could be used to verify if NocA would have a similar mode of action to already known compounds of that database. No

FCUP 164

Cyanobacterial bioactive metabolites for anticancer drug discovery: characterization of new compounds and molecular mechanisms in physiologically relevant 3D cell culture

specific pathway was encountered, but rather several similarities with compounds with very different pharmacological classes, which did not allow further suggestion on the mechanism. However, a gene set enrichment analysis[219-220] orientated the further work, as some effects were elucidated, such as endoplasmic reticulum stress and autophagy. We followed these indications and no increase in phosphorylation of eIF2α was detected, usually related with ER stress, but rather an upregulation of LC3B-II. This would indicate autophagy and was confirmed by a fluorescent staining approach with MDC, although no assessment of the autophagic flux was measured[221]. Yet, such indications of autophagy lead us to search for bioenergetic failures. ATP level were decreased on cells exposed to NocA and seahorse assays showed that OXPHOS was impaired, without alteration of the mitochondrial polarization. Mitochondria has been recognized as a potential target for cancer therapies[139, 141, 143, 149], as cancer cells demand high energy amounts in order to keep proliferating.

PAB were discovered on *Phormidium sp.* due to their allelopathic behaviour towards other organisms[59]. The activity of these cyclic peptides against several human cancer cell lines (MG-63, HCT116, RKO, HT-29, A549, HepG2, T47D, SH-SY5Y) and non-carcinogenic cell lines (hCMEC/D3, HaCaT, RPE-1[hTERT]) were studied. The panel of the eleven cell lines tested with very different IC_{50} was the first indication that these compounds could be target specific. HT-29 was the most sensitive cell line detected, with an IC_{50} of 0.98 µM. As happened for NocA work, using HCT116 cell line forming spheroids (even though not the most sensitive, it was the one that could form spheroids and known mutations and transfections on this cell line were available for us to use) revealed that PAB are cytotoxic also to cells cultured as tumours, with significant reduction of spheroid viability at 10 µM. A closer analysis on PAB effects on spheroid, reveal that the outer layer, the most proliferating and metabolically more active is the most affected by PAB. Although PAB are molecules with high molecular weight (A ≈ 1532 g mol^{-1} and B ≈ 1502 g mol^{-1}) they are macrocyclic peptides, which can be proteolytic stabilized and can have higher penetrations rates[222]. Moreover, PAB induced cell death through apoptosis, and such effect was detected from 10 µM to 2.5 µM. Higher concentrations than 10 µM are probably too cytotoxic, presumably stressing the cells to a fast and deleterious necrosis death[223].

The first insights about PAB mode of action were elucidated by protein identification and mitochondrial membrane staining on the colon carcinoma cell line HT-29, exposed to these compounds for a 48h period. The detected proteins upregulated were related

with the functioning of complex I of the mitochondrial respiratory chain. Also, the protein level of transaldolase (TALDO) were increased, a key enzyme on the pentose phosphate pathway (PPP), which is essential to provide NADPH for lipid biosynthesis and to prevent oxidative stress. Further upregulated proteins include the peroxiredoxins 4 and 6, two important ROS scavengers, and two subunits of the proteasome, an intracellular structure responsible to keep cell free from unneeded or damage proteins, which is essential to maintain several processes, such as cell cycle and oxidative stress. These results led us to speculate that PAB either 1) induce oxidative stress or 2) impair energy metabolism due to mitochondrial respiration dysfunction. Oxidative stress induction was rapidly discarded by assessing the ROS levels using the redox-sensistive probe DCFDA and using HCT116 transfected with the transcriptor factor Nrf2 reporter.

Following the hypothesis that PAB could impair the mitochondria, ATP production was shown to be reduced in cells exposed to PAB cultured either with glucose or galactose medium, which indicated that the effects of PAB should affect mitochondrial respiratory chain primarily. With access to a Seahorse equipment, OXPHOS impairment was observed on the HCT116 cell line. Additionally, the presence of PAB led to mitochondrial hyperpolarization in a short period of 6h. However, the epithelial immortalized cell line RPE-1^{hTERT} was also sensitive to PAB and the mitochondrial impairment was also observed, demonstrating a general cytotoxic effect, not specific for cancer cells.

The effects on mitochondrial respiration performance were detected on monolayer culture systems, however, as largely explored on the present work, cells on living tumours respond to drugs very distinctively. Following the results related with mitochondrial respiration disruption, the analysis of PTEN-induced putative kinase 1 (PINK1), a sensor of mitochondrial dysfunction, in HCT116 spheroids revealed an upregulated expression after 48h, as well as an increase of protein synthesis stress response, which added further evidence for the proposed mechanism of action Sumarising, two very different compounds, NocA and PAB, interacted both with mitochondria and in particular with mitochondrial respiration, however, via very different modes of action.

Regarding the effects on 3D cell culture and mechanistic analyses of bartolosides and hierridins studies, we can say that the present work showed the two sides of the same coin. To check for the mechanism of action can be difficult and sometimes impossible (on a reasonable time). In fact, the aim of the work was to assess if bartolosides A, B

FCUP | 166
Cyanobacterial bioactive metabolites for anticancer drug
discovery: characterization of new compounds and
molecular mechanisms in physiologically relevant 3D cell
culture

and C and hierridins B and C would have evident effects on spheroids, despite of the fact that previous work showed weak or no effects on several cell lines cultured as monolayer. We knew in advance that only hierridin B had effects on the cell line HT-29 with an IC_{50} of 100.2 µM, but hierridin C did not have effects in eight cell lines tested (both cancer and non carcinogentic cell lines)[35, 62]. As for bartolosides, previous work showed weak activity on monolayer cultured cells[66-67].

Considering previous results, we decided for hierridins to use the concentration corresponding to the only IC_{50} found before, even though we knew that it would have low clinical relevance or activate off-target responses[229]. A low expression of p21 and an overexpression of p53 and c-myc genes were observed, in accordance with the previous results on HT-29 cell line cultured as monolayer. Alterations on target proteins were common in both hierridins on a more complex structure, as spheroids are, although no alterations on the general spheroid morphology was detected. No effects were verified either for bartolosides A or C to a concentration up to 20 µM. Yet, bartoloside B decreased the spheroid size in comparison to control, which means that somehow the spheroid growth was arrested, accompanied with some disaggregation of the spheroid structure after 24h and 48h. However, no alterations on viability or apoptosis induction was detected. No further effects were then detected, which means that future work remains for understanding the disaggregation of cells from the spheroids.

Toxicity issues of studied compounds

Often in the scientific literature, certain compounds are described with anticancer activity without assessing other type of toxicity[35,62]. Here, we previledge the use of human retina epithelial cell line immortalized with hTERT and zebrafish larvae as our toxicity controls. The tests that we performed on NocA revealed that effects on mitochondria of RPE-1[hTERT] cells were similar to the ones observed on the cancer cell line studied (HCT116), however, such effects were more catastrophic on HCT116. At the IC_{50} concentration of NocA on confluent grown HCT116 cells, no reduction of viability was observed on the non-carcinogenic cell line RPE-1[hTERT]. Although not present on the published paper of Frontiers in Oncology[37], primary toxicological assessment on zebrafish larvae (3 to 5 days post hatching) demonstrate that NocA LC_{50} was 2.83 µM at 48h, and high toxicity rates were present at 5 µM and higher. This assay was performed only after the publication; therefore, it was not included (Figure 1).
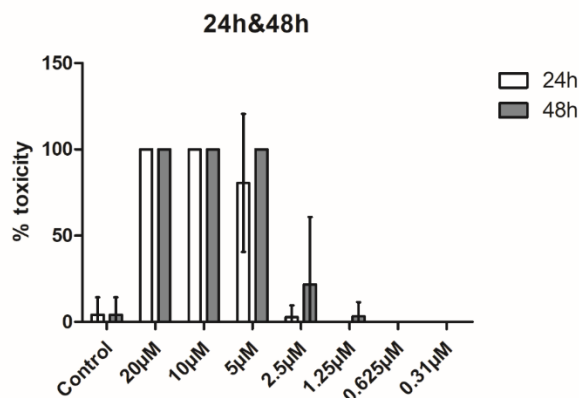
Figure 1 - Zebrafish toxicological assay of NocA. Toxicity was evaluated based on the number of dead embryos after 24h and 48h. n>15, 2 independent assays.

Regarding PAB, the first study showed cytotoxic against hCMEC/D3 (human blood-brain barrier cell line immortalized with hTERT) and HaCaT (immortalized keratinocytes) with IC_{50} below 4 µM on monolayer culture system. The second study with PAB improved those results showing that not only RPE-1[hTERT] cells were sensitive, but especially demonstrated that PAB is as effective in proliferating cells and non-proliferating cells. In other words, these results suggested that PAB would be effective against cells with high energy requirements, as cancer cells, or low energy demanding cells. Further confirmation of toxicity was obtained by the zebrafish toxicity assay, which demonstrated a very high toxicity against zebrafish larvae (in all the tested concentrations - 10µM to 0.31 µM) after 48h.

With such results, human non-carcinogenic cells, namely RPE-1[hTERT] were moderate predictors of toxicity, as they represented similar results (in the case of PAB) or underestimated toxicity (in the case of NocA) in comparison to results obtained with zebrafish larvae. However, although we cannot directly extrapolate such results to humans, it is important to emphasize that there is a crosslink between human cells and fish model with the same results, which indicates that such models give a good prediction of their toxicity, something that it is already supported by literature[189-196].

If we carefully look to the natural compounds currently in clinics, we will conclude that all of them exert cytotoxic effects on more than one type of cells since they affect a general mechanism of cell proliferation[1,5-11]. That is why chemotherapy has secondary effects. Anticancer compounds should be more effective in certain cells (cancer) than others. However, toxicity is not a dead end for compounds. In fact, compounds with

U. PORTO
FACULDADE DE CIÊNCIAS
UNIVERSIDADE DO PORTO

FCUP | 168
Cyanobacterial bioactive metabolites for anticancer drug discovery: characterization of new compounds and molecular mechanisms in physiologically relevant 3D cell culture

target specificity have been combined with antibodies, ADC (antibody drug conjugates) in order to increase its effectiveness in detriment of toxicity[226-228]. It is then not surprising that NocA is CZ patented as an ADC toxin (https://www.creative-biolabs.com/adc/nocuolin-a-820.htm). However, PAB is still a mixture of macrocyclic compounds in which this approach will probably need more studies, eventually to understand which part of the molecule is the active binding site and then modulate the chemical structure in order to either improve its activity[225], making it possible to be connected to a delivery vector, such as an antibody[20, 24, 226-227] or nanoparticle[228], or even diminish their general toxicity effects. The modulation of the chemical structure of hit compounds by medicinal chemistry is an interesting approach to improve the performance of compounds, for increasing the activity towards the molecular target and for decreasing associated toxicity or side effects. Such approach has been used for long time, being one of the famous examples the taxol derivatives Docetaxel and Cabazitaxel[1] but been applied on other compounds. The cyanobacterial natural product dolastatin derivatives, auristatin E, which are now under clinical trials[12] or even the further monomethylauristatin E which conjugated with antibody CD79b led to the latest marine drug approved by FDA Polatuzumab Vedotin[235].

Future application potential

The identification of the mechanisms of action is important for the definition of a specific application together with the analysis of toxicity issues. NocA showed target specificity and a mechanism of action that was dissimilar to the already used compounds[218]. This compound affected mitochondrial respiration but did not alter the mitochondrial membrane potential. Additionally, data pointed to autophagy, which could be a consequence of altered mitochondrial function. In the case of PAB, if we would have remained to only assess the cytotoxic activity, we would never know that, although directed therapies are often related with small molecules, macrocyclic peptides produced by cyanobacteria can also have a specific targets and penetrate intro complex structures as spheroids and kill cancer cells through impairment of mitochondrial respiration[222]. With this work we are now able to point out the importance of PAB as a potential compound mixture for future studies rather than just a potent cytotoxic compound. Hierridin C is described as an antimalarial agent[64] however no evident application was found on tumour spheroids, being the the same result for bartolosides.

On the case of the present thesis, the cytotoxicity towards cancer cells was explored, in order to understand their mechanisms of action and both NocA and PAB, due to their effects on mitochondria, have higher probability to be useful as anticancer drugs. However, these same compounds can have other applications, as other pharmacological purposes[27, 29, 44] or just different biotechnological applications, as antifouling as it was suggested for PAB[34, 231-232]. Unfortunately, toxicity issues were identified by the use of non-carcinogenic cells and zebrafish larvae as whole small animal model for the cyanobacterial compounds that had interesting bioactivities towards tumour spheroids, namely NocA and PAB. For any future use, the modification of these compounds would be necessary in order to reduce toxicity or specific shuttle systems that deliver compounds only to target cells avoiding catastrophic events on any cells.

Advances from a screening perspective

Since compounds isolated by traditional cytotoxic assays based on monolayer culture often result in compounds that do fail in the following steps of the drug discovery process, we aimed innovating this process. Here, we applied for the first-time spheroid cultures for a screening of beneficial effects of cyanobacterial extracts on solid tumours. The selection of extracts was done on data from a previous work of our[233], which used monolayer culture of several cancer cell lines (HepG2, RKO, MG-63, SK-BR-3, T47D, HT-29, SH-SY5Y, PC-3) and viability assessment with MTT assay and LDH release assay. Such work indicated a general cytotoxicity of several strains, but there was no idea of which compound or compounds were inducing the cytotoxicity, either if the positive effects would maintain in a more complex model. After this study, hierridins[35, 62-64] and bartolosides[66-67] were isolated (hierridins were not by bio guided assay), but, as shown on the present thesis, these compounds were not particularly interesting as anticancer drugs.

On the present work, we intended to use the spheroid assay to orientate more effectively to which could be the most interesting strains and fractions to search for new bioactive compounds. For that, the very same extracts were exposed to spheroids over a period of 48h. After that period, the viability of the spheroids was assessed using two distinct methods: an assay that evaluates the activity of cytosolic acid phosphatases, a method previously described as being a reliable tool to access spheroids viability[186] and fluorescence staining of dead cells with propidium iodide (PI) and calcein AM[173], a viability marker. The differences observed on the fractions were not as strong compared

to our positive control (Staurosporine 1.5 µM), but we selected those fractions which effects were visible in more than one marker: acid phosphatases, PI staining or Calcein staining. Those chosen fractions were subjected to a high-resolution liquid chromatography coupled with MS-MS (HR-LC–MS/MS) to identify unique masses present on mixtures, that could represent some promising compounds. The resulting masses were then analysed and organized on a network Global Natural Products Social Molecular Networking program[234] (GNPS), where common masses among active and non-active fractions were discarded as promising ones. Then, using online databases available on GNPS program, we dereplicated the known compounds and masses, not only to discard the possible known compounds but also to understand if similar ones were connected. Five strains appeared as producer of interesting mass peaks, *Cyanobium sp.* LEGE 06113, *Lusitaniella coriacea* LEGE 07167, *Nodosilinea sp* LEGE 06009, unidentified filamentous *Synechococcales* LEGE 06118, *Cyanobium sp.* LEGE 06026. From these five strains, we believe that *Lusitaniella coriacea* LEGE 07167 is most promising one. Previous work using this strain confirmed the selection as promising, based on biological assays[233] and the presence of genomic biosynthetic clusters of polyketide synthase genes.

Although this last work did not result on a new compound, we decreased the number of strains that we could follow up for further work. During the work, we noted that the fractionation procedure of the extracts should be changed in order to yield more fractions, in order to decrease fractions complexity and increase bioassays sensitivity.

This improvement is now already implemented on current screening project on the BBE lab. Now, an extract library and fractionation protocol are established where each extract of a cyanobacteria strain is fractionated into eight fractions of crescent polarity with further exposure to spheroids and acid phosphatase assay.

Future work

Even though a lot of work is presented on the current thesis, new questions were raised and remain unanswered. Regarding NocA, it would be interesting to perform assays using spheroids of other types of cells and detect in which we could have the lowest IC_{50} on such advanced models. Then, it would be interesting to make xenographs (in zebrafish) to test its effectiveness on cancer cell metastasis or tumour reduction in an *in vivo* environment using non-toxic concentrations. Its activity should be analysed as a free molecule and as antibody-drug conjugate or similar specific shuttle systems.

Regarding PAB, it should be studied if such compounds are still active on the core of spheroids, where the mitochondrial activity is essential for obtaining ATP. It is unknown how low pH conditions in this microenvironment might affect PAB cytotoxicity[224]. Furthermore, it could be interesting to study the pharmacophore of these macrocycle peptides. Finally, it would be important to perform mechanistic study regarding its effects on the compounds separately, even though lower cytotoxicity were reported on the initial paper [59].

The study of hierridins were not conclusive regarding the mode of action, only a confirmation of possible cell arrest on spheroids were shown. In order to better understand the mechanisms of action, it would be important to study hierridin C (and eventually hierridin B) on the anti-malarial model used before, *Plasmodium falciparum*.

Bartolosides, although interesting regarding its chemistry and biosynthetic pathways[65-67, 230], did not reveal to be particularly interesting as a bioactive compound against human cells, either cancer or non-carcinogenic cells. And I say, so far, because apparently small changes on the bartolosides chemical skeleton was enough to increase its activity, namely the presence of sugars and halogenation of the alkyl chains. A future and interesting work should focus on changing the chemical structure of bartolosides and test for bioactivity, in order to perhaps increase its activity towards cancer cells.

Conclusions

The present work demonstrates that clearly the investment on advanced models for drug screening and molecular mode of action assessment is crucial to give an importance and an application to the compounds that are discovered every day. The use of advanced models is more expensive as monolayer cultured cells but provide more promising results. With this I do not defend the retraction of using monolayer cells, but 3D models can be an important tool to let us focus on the most promising fractions (in the case of screening) or compounds.

Also, as already testified by other authors, cyanobacteria are definitely a auspicious source of new compounds. This search for new compounds from cyanobacteria needs to be aided by new technology and global databases, such as the connectivity map or GNPS, that are indubitable important tools to increase, improve and fasten the search for new compounds, understand their mode of action and maybe repurposing known compounds for different ends.

It is important to notice that drug screening has a high rate of failure. Considering that the present work explored the activity and mechanism of seven compounds (nocuolin A, portoamides A and B mixture, bartolosides A, B and C and hierridins B and C), it is normal that all compounds are not suitable to be developed into anticancer drugs in the present state. However, two compounds (nocuolin a, and portoamides AB) have shown interesting potential for further studies, due to their prominent, but different effects on mitochondria. Structural modifications by medicinal chemistry need to be analysed in order to reduce associated toxicity observed in a whole small animal model and to maintain or improve the activity towards their molecular targets.

References

1.   Kim, K.-W.; Roh, J. K.; Wee, H.-J.; Kim, C., Natural Product Anticancer Drugs. In *Cancer Drug Discovery: Science and History*, Springer Netherlands: Dordrecht, **2016**; pp 113-134.

2.   Harvey, A. L., Natural products in drug discovery. *Drug Discovery Today* **2008,** *13* (19–20), 894-901.

3.   Newman, D. J.; Cragg, G. M., Natural Products as Sources of New Drugs from 1981 to 2014. *Journal of Natural Products* **2016,** *79* (3), 629-661.

4.   Bensch, K. G.; Marantz, R.; Wisniewski, H.; Shelanski, M., Induction *in vitro* of Microtubular Crystals by Vinca Alkaloids. *Science* **1969,** *165* (3892), 495-496.

5.   Schiff, P. B.; Fant, J.; Horwitz, S. B., Promotion of microtubule assembly *in vitro* by taxol. *Nature* **1979,** *277* (5698), 665-667.

6.   Ross, W.; Rowe, T.; Glisson, B.; Yalowich, J.; Liu, L., Role of Topoisomerase II in Mediating Epipodophyllotoxin-induced DNA Cleavage. *Cancer Research* **1984,** *44* (12 Part 1), 5857-5860.

7.   Hsiang, Y. H.; Hertzberg, R.; Hecht, S.; Liu, L. F., Camptothecin induces protein-linked DNA breaks via mammalian DNA topoisomerase I. *Journal of Biological Chemistry* **1985,** *260* (27), 14873-14878.

8.   Huang, M.-T., Harringtonine, an Inhibitor of Initiation of Protein Biosynthesis. *Molecular Pharmacology* **1975,** *11* (5), 511-519.

9.   C. Tan, C. T.; Dargeon, H. W.; Burchenal, J. H., The effect of actinomycin D on cancer in childhood. *Pediatrics* **1959,** *24* (4), 544-561.

10.   Gothelf, A.; Mir, L. M.; Gehl, J., Electrochemotherapy: results of cancer treatment using enhanced delivery of bleomycin by electroporation. *Cancer Treatment Reviews* **2003,** *29* (5), 371-387.

11.   Hortobágyi, G. N., Anthracyclines in the Treatment of Cancer. *Drugs* **1997,** *54* (4), 1-7.

12.   Simmons, T. L.; Andrianasolo, E.; McPhail, K.; Flatt, P.; Gerwick, W. H., Marine natural products as anticancer drugs. *Molecular Cancer Therapeutics* **2005,** *4* (2), 333-342.

13.   Bergmann, W.; Feeney, R. J., Contributions to the study of marine products. XXXII. The nucleosides of sponges. I.1. *The Journal of Organic Chemistry* **1951,** *16* (6), 981-987.

14.	Shepshelovich, D.; Edel, Y.; Goldvaser, H.; Dujovny, T.; Wolach, O.; Raanani, P., Pharmacodynamics of cytarabine induced leucopenia: a retrospective cohort study. *Br J Clin Pharmacol* **2015,** *79* (4), 685-691.

15.	Towle, M. J.; Salvato, K. A.; Budrow, J.; Wels, B. F.; Kuznetsov, G.; Aalfs, K. K.; Welsh, S.; Zheng, W.; Seletsky, B. M.; Palme, M. H.; Habgood, G. J.; Singer, L. A.; DiPietro, L. V.; Wang, Y.; Chen, J. J.; Quincy, D. A.; Davis, A.; Yoshimatsu, K.; Kishi, Y.; Yu, M. J.; Littlefield, B. A., *In vitro* and *In vivo* Anticancer Activities of Synthetic Macrocyclic Ketone Analogues of Halichondrin B. *Cancer Research* **2001,** *61* (3), 1013-1021.

16.	Smith, J. A.; Wilson, L.; Azarenko, O.; Zhu, X.; Lewis, B. M.; Littlefield, B. A.; Jordan, M. A., Eribulin Binds at Microtubule Ends to a Single Site on Tubulin To Suppress Dynamic Instability. *Biochemistry* **2010,** *49* (6), 1331-1337.

17.	de Claro, R. A.; McGinn, K.; Kwitkowski, V.; Bullock, J.; Khandelwal, A.; Habtemariam, B.; Ouyang, Y.; Saber, H.; Lee, K.; Koti, K.; Rothmann, M.; Shapiro, M.; Borrego, F.; Clouse, K.; Chen, X. H.; Brown, J.; Akinsanya, L.; Kane, R.; Kaminskas, E.; Farrell, A.; Pazdur, R., U.S. Food and Drug Administration Approval Summary: Brentuximab Vedotin for the Treatment of Relapsed Hodgkin Lymphoma or Relapsed Systemic Anaplastic Large-Cell Lymphoma. *Clinical Cancer Research* **2012,** *18* (21), 5845-5849.

18.	Katz, J.; Janik, J. E.; Younes, A., Brentuximab Vedotin (SGN-35). *Clinical Cancer Research* **2011,** *17* (20), 6428-6436.

19.	Younes, A.; Yasothan, U.; Kirkpatrick, P., Brentuximab vedotin. *Nature Reviews Drug Discovery* **2012,** *11*, 19.

20.	Chari, R. V. J.; Miller, M. L.; Widdison, W. C., Antibody–Drug Conjugates: An Emerging Concept in Cancer Therapy. *Angewandte Chemie International Edition* **2014,** *53* (15), 3796-3827.

21.	In, G. K.; Hu, J. S.; Tseng, W. W., Treatment of advanced, metastatic soft tissue sarcoma: latest evidence and clinical considerations. *Therapeutic Advances in Medical Oncology* **2017,** *9* (8), 533-550.

22.	Rath, C. M.; Janto, B.; Earl, J.; Ahmed, A.; Hu, F. Z.; Hiller, L.; Dahlgren, M.; Kreft, R.; Yu, F.; Wolff, J. J.; Kweon, H. K.; Christiansen, M. A.; Håkansson, K.; Williams, R. M.; Ehrlich, G. D.; Sherman, D. H., Meta-omic Characterization of the Marine Invertebrate Microbial Consortium That Produces the Chemotherapeutic Natural Product ET-743. *ACS Chemical Biology* **2011,** *6* (11), 1244-1256.

U.PORTO
FACULDADE DE CIÊNCIAS
UNIVERSIDADE DO PORTO

FCUP 175
Cyanobacterial bioactive metabolites for anticancer drug discovery: characterization of new compounds and molecular mechanisms in physiologically relevant 3D cell culture

23.   Alonso-Álvarez, S.; Pardal, E.; Sánchez-Nieto, D.; Navarro, M.; Caballero, M. D.; Mateos, M. V.; Martín, A. Plitidepsin: design, development, and potential place in therapy *Drug Design, Development and Therapy* [Online], **2017**, p. 253-264. PubMed. https://doi.org/10.2147/DDDT.S94165 (accessed 2019).

24.   Shen, B.-Q.; Xu, K.; Liu, L.; Raab, H.; Bhakta, S.; Kenrick, M.; Parsons-Reponte, K. L.; Tien, J.; Yu, S.-F.; Mai, E.; Li, D.; Tibbitts, J.; Baudys, J.; Saad, O. M.; Scales, S. J.; McDonald, P. J.; Hass, P. E.; Eigenbrot, C.; Nguyen, T.; Solis, W. A.; Fuji, R. N.; Flagella, K. M.; Patel, D.; Spencer, S. D.; Khawli, L. A.; Ebens, A.; Wong, W. L.; Vandlen, R.; Kaur, S.; Sliwkowski, M. X.; Scheller, R. H.; Polakis, P.; Junutula, J. R., Conjugation site modulates the *in vivo* stability and therapeutic activity of antibody-drug conjugates. *Nature Biotechnology* **2012,** *30*, 184.

25.   Shih, P. M.; Wu, D.; Latifi, A.; Axen, S. D.; Fewer, D. P.; Talla, E.; Calteau, A.; Cai, F.; Tandeau de Marsac, N.; Rippka, R.; Herdman, M.; Sivonen, K.; Coursin, T.; Laurent, T.; Goodwin, L.; Nolan, M.; Davenport, K. W.; Han, C. S.; Rubin, E. M.; Eisen, J. A.; Woyke, T.; Gugger, M.; Kerfeld, C. A., Improving the coverage of the cyanobacterial phylum using diversity-driven genome sequencing. *Proceedings of the National Academy of Sciences* **2013,** *110* (3), 1053-1058.

26.   Leao, P. N.; Engene, N.; Antunes, A.; Gerwick, W. H.; Vasconcelos, V., The chemical ecology of cyanobacteria. *Natural Product Reports* **2012,** *29* (3), 372-391.

27.   Singh, R. K.; Tiwari, S. P.; Rai, A. K.; Mohapatra, T. M., Cyanobacteria: an emerging source for drug discovery. *Japanese Journal of Antibiotics* **2011,** *64* (6), 401-412.

28.   Osswald, J.; Rellán, S.; Gago, A.; Vasconcelos, V., Toxicology and detection methods of the alkaloid neurotoxin produced by cyanobacteria, anatoxin-a. *Environment International* **2007,** *33* (8), 1070-1089.

29.   Wijffels, R. H.; Kruse, O.; Hellingwerf, K. J., Potential of industrial biotechnology with cyanobacteria and eukaryotic microalgae. *Current Opinion in Biotechnology* **2013,** *24* (3), 405-413.

30.   Costa, M.; Rosa, F.; Ribeiro, T.; Hernandez-Bautista, R.; Bonaldo, M.; Gonçalves Silva, N.; Eiríksson, F.; Thorsteinsdóttir, M.; Ussar, S.; Urbatzka, R., Identification of Cyanobacterial Strains with Potential for the Treatment of Obesity-Related Co-Morbidities by Bioactivity, Toxicity Evaluation and Metabolite Profiling. *Marine Drugs* **2019,** *17* (5), 280.

31.   Freitas, S.; Silva, N. G.; Sousa, M. L.; Ribeiro, T.; Rosa, F.; Leão, P. N.; Vasconcelos, V.; Reis, M. A.; Urbatzka, R., Chlorophyll Derivatives from Marine Cyanobacteria with Lipid-Reducing Activities. *Marine Drugs* **2019,** *17* (4), 229.

32.   Nozzi, N. E.; Oliver, J. W. K.; Atsumi, S., Cyanobacteria as a Platform for Biofuel Production. *Frontiers in bioengineering and biotechnology* **2013,** *1*, 7.

33.   Balaji, S.; Gopi, K.; Muthuvelan, B., A review on production of poly β hydroxybutyrates from cyanobacteria for the production of bio plastics. *Algal Research* **2013,** *2* (3), 278-285.

34.   Antunes, J.; Pereira, S.; Ribeiro, T.; Plowman, J. E.; Thomas, A.; Clerens, S.; Campos, A.; Vasconcelos, V.; Almeida, J. R., A Multi-Bioassay Integrated Approach to Assess the Antifouling Potential of the Cyanobacterial Metabolites Portoamides. *Marine Drugs* **2019,** *17* (2), 111.

35.   Margarida, C.; Ivo E., S.-D.; Raquel, C.-B.; Hugo, S.; Roberta, R. d. C.; Artur, S.; Maria Paula Cruz, S.; Maria João, A.; Rosário, M.; Valentina, F. D.; Fatima, N.; Vera, C.; Vitor M., V.; Pedro, L., Structure, Synthesis of Hierridin C and Discovery of Prevalent Alkylresorcinol Biosynthesis in Picocyanobacteria. *Journal of Natural Products.* **2018**. 82 (2), 393-402.

36.   Martins, R. F.; Ramos, M. F.; Herfindal, L.; Sousa, J. A.; Skærven, K.; Vasconcelos, V. M., Antimicrobial and Cytotoxic Assessment of Marine Cyanobacteria - Synechocystis and *Synechococcus*. *Marine Drugs* **2008,** *6* (1), 1-11.

37.   Sousa, M. L.; Preto, M.; Vasconcelos, V.; Linder, S.; Urbatzka, R., Antiproliferative Effects of the Natural Oxadiazine Nocuolin A Are Associated With Impairment of Mitochondrial Oxidative Phosphorylation. *Frontiers in Oncology* **2019,** *9* (224).

38.   Ribeiro, T.; Lemos, F.; Preto, M.; Azevedo, J.; Sousa, M. L.; Leão, P. N.; Campos, A.; Linder, S.; Vitorino, R.; Vasconcelos, V.; Urbatzka, R., Cytotoxicity of portoamides in human cancer cells and analysis of the molecular mechanisms of action. *PLOS ONE* **2017,** *12* (12), e0188817.

39.   Freitas, S.; Martins, R.; Campos, A.; Azevedo, J.; Osório, H.; Costa, M.; Barros, P.; Vasconcelos, V.; Urbatzka, R., Insights into the potential of picoplanktonic marine cyanobacteria strains for cancer therapies – Cytotoxic mechanisms against the RKO colon cancer cell line. *Toxicon* **2016,** *119*, 140-151.

FCUP 177
Cyanobacterial bioactive metabolites for anticancer drug
discovery: characterization of new compounds and
molecular mechanisms in physiologically relevant 3D cell
culture

40.   Costa, M.; Costa-Rodrigues, J.; Fernandes, M. H.; Barros, P.; Vasconcelos, V.; Martins, R., Marine Cyanobacteria Compounds with Anticancer Properties: A Review on the Implication of Apoptosis. *Marine Drugs* **2012,** *10* (10), 2181.

41.   Leao, T.; Castelão, G.; Korobeynikov, A.; Monroe, E. A.; Podell, S.; Glukhov, E.; Allen, E. E.; Gerwick, W. H.; Gerwick, L., Comparative genomics uncovers the prolific and distinctive metabolic potential of the cyanobacterial genus *Moorea*. *Proceedings of the National Academy of Sciences* **2017,** *114* (12), 3198-3203.

42.   Ehrenreich, I. M.; Waterbury, J. B.; Webb, E. A., Distribution and diversity of natural product genes in marine and freshwater cyanobacterial cultures and genomes. *Applied and Environmental Microbiology* **2005,** *71* (11), 7401-7413.

43.   Zhang, Y.; Chen, M.; Bruner, S. D.; Ding, Y., Heterologous Production of Microbial Ribosomally Synthesized and Post-translationally Modified Peptides. *Frontiers in Microbiology* **2018,** *9* (1801).

44.   Kehr, J.-C.; Gatte Picchi, D.; Dittmann, E. B., Natural product biosyntheses in cyanobacteria: A treasure trove of unique enzymes. *Beilstein Journal of Organic Chemistry* **2011,** (7), 1622–1635.

45.   Gutiérrez, M.; Suyama, T. L.; Engene, N.; Wingerd, J. S.; Matainaho, T.; Gerwick, W. H., Apratoxin D, a Potent Cytotoxic Cyclodepsipeptide from Papua New Guinea Collections of the Marine Cyanobacteria Lyngbya majuscula and Lyngbya sordida. *Journal of Natural Products* **2008,** *71* (6), 1099-1103.

46.   Linington, R. G.; Edwards, D. J.; Shuman, C. F.; McPhail, K. L.; Matainaho, T.; Gerwick, W. H., Symplocamide A, a Potent Cytotoxin and Chymotrypsin Inhibitor from the Marine Cyanobacterium Symploca sp. *Journal of natural products* **2008,** *71* (1), 22-27.

47.   Zheng, L.-H.; Wang, Y.-J.; Sheng, J.; Wang, F.; Zheng, Y.; Lin, X.-K.; Sun, M., Antitumor Peptides from Marine Organisms. *Marine Drugs* **2011,** *9* (10), 1840.

48.   Giacomotto, J.; Ségalat, L., High-throughput screening and small animal models, where are we? *British Journal of Pharmacology* **2010,** *160* (2), 204-216.

49.   Gao, H.; Korn, J. M.; Ferretti, S.; Monahan, J. E.; Wang, Y.; Singh, M.; Zhang, C.; Schnell, C.; Yang, G.; Zhang, Y.; Balbin, O. A.; Barbe, S.; Cai, H.; Casey, F.; Chatterjee, S.; Chiang, D. Y.; Chuai, S.; Cogan, S. M.; Collins, S. D.; Dammassa, E.; Ebel, N.; Embry, M.; Green, J.; Kauffmann, A.; Kowal, C.; Leary, R. J.; Lehar, J.; Liang, Y.; Loo, A.; Lorenzana, E.; Robert McDonald Iii, E.; McLaughlin, M. E.; Merkin, J.; Meyer, R.; Naylor, T. L.; Patawaran, M.; Reddy, A.; Röelli, C.; Ruddy, D. A.; Salangsang, F.;

Santacroce, F.; Singh, A. P.; Tang, Y.; Tinetto, W.; Tobler, S.; Velazquez, R.; Venkatesan, K.; Von Arx, F.; Wang, H. Q.; Wang, Z.; Wiesmann, M.; Wyss, D.; Xu, F.; Bitter, H.; Atadja, P.; Lees, E.; Hofmann, F.; Li, E.; Keen, N.; Cozens, R.; Jensen, M. R.; Pryer, N. K.; Williams, J. A.; Sellers, W. R., High-throughput screening using patient-derived tumor xenografts to predict clinical trial drug response. *Nature Medicine* **2015,** *21*, 1318.

50.   Weaver, R. J.; Valentin, J.-P., Today's Challenges to De-Risk and Predict Drug Safety in Human "Mind-the-Gap". *Toxicological Sciences* **2018,** *167* (2), 307-321.

51.   Cook, D.; Brown, D.; Alexander, R.; March, R.; Morgan, P.; Satterthwaite, G.; Pangalos, M. N., Lessons learned from the fate of AstraZeneca's drug pipeline: a five-dimensional framework. *Nature Reviews Drug Discovery* **2014,** *13*, 419.

52.   Ravi, M.; Ramesh, A.; Pattabhi, A., Contributions of 3D Cell Cultures for Cancer Research. *Journal of Cellular Physiology* **2017,** *232* (10), 2679-2697.

53.   Langhans, S. A., Three-Dimensional *in vitro* Cell Culture Models in Drug Discovery and Drug Repositioning. *Frontiers in Pharmacology* **2018,** *9* (6).

54.   Hynds, R. E.; Vladimirou, E.; Janes, S. M., The secret lives of cancer cell lines. *Dis Model Mech* **2018,** *11* (11), dmm037366.

55.   Ramos, V.; Morais, J.; Castelo-Branco, R.; Pinheiro, Â.; Martins, J.; Regueiras, A.; Pereira, A. L.; Lopes, V. R.; Frazão, B.; Gomes, D.; Moreira, C.; Costa, M. S.; Brûle, S.; Faustino, S.; Martins, R.; Saker, M.; Osswald, J.; Leão, P. N.; Vasconcelos, V. M., Cyanobacterial diversity held in microbial biological resource centers as a biotechnological asset: the case study of the newly established LEGE culture collection. *Journal of Applied Phycology* **2018**. 30: 1437.

56.   Voráčová, K.; Hájek, J.; Mareš, J.; Urajová, P.; Kuzma, M.; Cheel, J.; Villunger, A.; Kapuscik, A.; Bally, M.; Novák, P.; Kabeláč, M.; Krumschnabel, G.; Lukeš, M.; Voloshko, L.; Kopecký, J.; Hrouzek, P., The cyanobacterial metabolite nocuolin a is a natural oxadiazine that triggers apoptosis in human cancer cells. *PLOS ONE* **2017,** *12* (3), e0172850.

57.   Lopes, V. R.; Fernández, N.; Martins, R. F.; Vasconcelos, V., Primary Screening of the Bioactivity of Brackishwater Cyanobacteria: Toxicity of Crude Extracts to Artemia salina Larvae and Paracentrotus lividus Embryos. *Marine Drugs* **2010,** *8* (3), 471-482.

58.   Tidgewell, K.; Clark, B.; Gerwick, W., The Natural Products Chemistry of Cyanobacteria. In *Comprehensive Natural Products II: Chemistry and Biology*, Mander, L.; Liu, H.-W., Eds. Elsevier: 2010; Vol. 2, pp 142-187

59. Leão, P. N.; Pereira, A. R.; Liu, W.-T.; Ng, J.; Pevzner, P. A.; Dorrestein, P. C.; König, G. M.; Vasconcelos, V. M.; Gerwick, W. H., Synergistic allelochemicals from a freshwater cyanobacterium. *Proceedings of the National Academy of Sciences* **2010,** *107* (25), 11183-11188.

60. Papendorf, O.; König, G. M.; Wright, A. D., Hierridin B and 2,4-dimethoxy-6-heptadecyl-phenol, secondary metabolites from the cyanobacterium *Phormidium* ectocarpi with antiplasmodial activity. *Phytochemistry* **1998,** *49* (8), 2383-2386.

61. Huneck, S., New Results on the Chemistry of Lichen Substances. In *Fortschritte der Chemie organischer Naturstoffe / Progress in the Chemistry of Organic Natural Products*, Herz, W.; Falk, H.; Kirby, G. W.; Moore, R. E., Eds. Springer Vienna: Vienna, **2001**; pp 1-276.

62. Leão, P. N.; Costa, M.; Ramos, V.; Pereira, A. R.; Fernandes, V. C.; Domingues, V. F.; Gerwick, W. H.; Vasconcelos, V. M.; Martins, R., Antitumor Activity of Hierridin B, a Cyanobacterial Secondary Metabolite Found in both Filamentous and Unicellular Marine Strains. *PLOS ONE* **2013,** *8* (7), e69562.

63. Freitas, S.; Martins, R.; Costa, M.; Leão, P.; Vitorino, R.; Vasconcelos, V.; Urbatzka, R., Hierridin B Isolated from a Marine Cyanobacterium Alters VDAC1, Mitochondrial Activity, and Cell Cycle Genes on HT-29 Colon Adenocarcinoma Cells. *Marine Drugs* **2016,** *14* (9), 158.

64. Leão, P., Rosário, M.M., Costa, M., Vasconcelos, V., Nogueira, F., Domingues, V. (2016) WO2016207869A1 - Antimalarial agent, methods and uses thereof. Applicants: Universidade do Porto, CIIMAR – Centro Interdisciplinar de Investigação Marinha e Ambiental, Instituto de Higiene e Medicina Tropical, Instituto Politécnico do Porto

65. Martins, T. P.; Rouger, C.; Glasser, N. R.; Freitas, S.; de Fraissinette, N. B.; Balskus, E. P.; Tasdemir, D.; Leão, P. N., Chemistry, bioactivity and biosynthesis of cyanobacterial alkylresorcinols. *Natural Product Reports* **2019**. Advanced article.

66. Leão, P. N.; Nakamura, H.; Costa, M.; Pereira, A. R.; Martins, R.; Vasconcelos, V.; Gerwick, W. H.; Balskus, E. P., Biosynthesis-Assisted Structural Elucidation of the Bartolosides, Chlorinated Aromatic Glycolipids from Cyanobacteria. *Angewandte Chemie International Edition* **2015,** *54* (38), 11063-11067.

67. Afonso, T. B.; Costa, M. S.; Rezende de Castro, R.; Freitas, S.; Silva, A.; Schneider, M. P. C.; Martins, R.; Leão, P. N., Bartolosides E–K from a Marine Coccoid Cyanobacterium. *Journal of Natural Products* **2016,** *79* (10), 2504-2513.

68.   Albuquerque, T. A. F.; Drummond do Val, L.; Doherty, A.; de Magalhães, J. P., From humans to hydra: patterns of cancer across the tree of life. *Biological Reviews* **2018,** *93* (3), 1715-1734.

69.   Aktipis, C. A.; Boddy, A. M.; Jansen, G.; Hibner, U.; Hochberg, M. E.; Maley, C. C.; Wilkinson, G. S., Cancer across the tree of life: cooperation and cheating in multicellularity. *Philosophical Transactions of the Royal Society B: Biological Sciences* **2015,** *370* (1673), 20140219.

70.   Mirzoyan, Z.; Sollazzo, M.; Allocca, M.; Valenza, A. M.; Grifoni, D.; Bellosta, P., Drosophila melanogaster: A Model Organism to Study Cancer. *Front Genet* **2019,** *10*, 51-51.

71.   Capasso, L. L., Antiquity of cancer. *International Journal of Cancer* **2005,** *113* (1), 2-13.

72.   Moodie, R. L., Tumors in the lower carboniferous.. *Science* **1927,** *66* (1718), 540-540.

73.   Faguet, G. B., A brief history of cancer: Age-old milestones underlying our current knowledge database. *International Journal of Cancer* **2015,** *136* (9), 2022-2036.

74.   Bray, F.; Ferlay, J.; Soerjomataram, I.; Siegel, R. L.; Torre, L. A.; Jemal, A., Global cancer statistics 2018: GLOBOCAN estimates of incidence and mortality worldwide for 36 cancers in 185 countries. *CA: A Cancer Journal for Clinicians* **2018,** *68* (6), 394-424.

75.   Siegel, R. L.; Miller, K. D.; Jemal, A., Cancer statistics, 2019. *CA: A Cancer Journal for Clinicians* **2019,** *69* (1), 7-34.

76.   Cancer, N. I. o. NCI Dictionary of Cancer Terms. https://www.cancer.gov/publications/dictionaries/cancer-terms (accessed 16.08.2019).

77.   Hanahan, D.; Weinberg, R. A., The Hallmarks of Cancer. *Cell* **2000,** *100* (1), 57-70.

78.   Hanahan, D.; Weinberg, Robert A., Hallmarks of Cancer: The Next Generation. *Cell* **2011,** *144* (5), 646-674.

79.   DeBerardinis, R. J.; Chandel, N. S., Fundamentals of cancer metabolism. *Science Advances* **2016,** *2* (5), e1600200-e1600200.

80.   Pavlova, N. N.; Thompson, C. B., The Emerging Hallmarks of Cancer Metabolism. *Cell Metab* **2016,** *23* (1), 27-47.

81.   Warburg, O.; Wind, F.; Negelein, E., The metabolism of tumors in the body. *The Journal of General Physiology .* **1927,** *8* (6), 519-530.

FCUP 181
Cyanobacterial bioactive metabolites for anticancer drug
discovery: characterization of new compounds and
molecular mechanisms in physiologically relevant 3D cell
culture

82.   Barker, J.; Khan, M. A. A.; Solomos, T., Mechanism of the Pasteur Effect. *Nature* **1964,** *201* (4924), 1126-1127.

83.   Koppenol, W. H.; Bounds, P. L.; Dang, C. V., Otto Warburg's contributions to current concepts of cancer metabolism. *Nature Reviews Cancer* **2011,** *11*, 325.

84.   Lunt, S. Y.; Heiden, M. G. V., Aerobic Glycolysis: Meeting the Metabolic Requirements of Cell Proliferation. *Annual Review of Cell and Developmental Biology* **2011,** *27* (1), 441-464.

85.   Lu, W.; Pelicano, H.; Huang, P., Cancer Metabolism: Is Glutamine Sweeter than Glucose? *Cancer Cell* **2010,** *18* (3), 199-200.

86.   Alberghina, L.; Gaglio, D., Redox control of glutamine utilization in cancer. *Cell Death &Amp; Disease* **2014,** *5*, e1561.

87.   Rohas, L. M.; St-Pierre, J.; Uldry, M.; Jäger, S.; Handschin, C.; Spiegelman, B. M., A fundamental system of cellular energy homeostasis regulated by PGC-1α. *Proceedings of the National Academy of Sciences* **2007,** *104* (19), 7933-7938.

88.   Vander Heiden, M. G.; Cantley, L. C.; Thompson, C. B., Understanding the Warburg Effect: The Metabolic Requirements of Cell Proliferation. *Science* **2009,** *324* (5930), 1029.

89.   Porporato, P. E.; Filigheddu, N.; Pedro, J. M. B.-S.; Kroemer, G.; Galluzzi, L., Mitochondrial metabolism and cancer. *Cell Research* **2017,** *28*, 265.

90.   Zheng, J., Energy metabolism of cancer: Glycolysis versus oxidative phosphorylation (Review). *Oncology Letters* **2012,** *4* (6), 1151-1157.

91.   Trédan, O.; Galmarini, C. M.; Patel, K.; Tannock, I. F., Drug Resistance and the Solid Tumor Microenvironment. *JNCI: Journal of the National Cancer Institute* **2007,** *99* (19), 1441-1454.

92.   Minchinton, A. I.; Tannock, I. F., Drug penetration in solid tumours. *Nature Reviews Cancer* **2006,** *6* (8), 583-592.

93.   Green, S. K.; Frankel, A.; Kerbel, R. S., Adhesion-dependent multicellular drug resistance. *Anti-Cancer Drug Design* **1999,** *14* (2), 153-168.

94.   Hirschhaeuser, F.; Sattler, U. G. A.; Mueller-Klieser, W., Lactate: A Metabolic Key Player in Cancer. *Cancer Research* **2011,** *71* (22), 6921-6925.

95.   Kolosenko, I.; Avnet, S.; Baldini, N.; Viklund, J.; De Milito, A., Therapeutic implications of tumor interstitial acidification. *Seminars in Cancer Biology* **2017,** *43*, 119-133.

96. Mellor, H. R.; Callaghan, R., Resistance to Chemotherapy in Cancer: A Complex and Integrated Cellular Response. *Pharmacology* **2008,** *81* (4), 275-300.

97. Olive, P. L.; Durand, R. E., Drug and radiation resistance in spheroids: cell contact and kinetics. *Cancer and Metastasis Reviews* **1994,** *13* (2), 121-138.

98. Pellegrini, P.; Serviss, J. T.; Lundbäck, T.; Bancaro, N.; Mazurkiewicz, M.; Kolosenko, I.; Yu, D.; Haraldsson, M.; D'Arcy, P.; Linder, S.; De Milito, A., A drug screening assay on cancer cells chronically adapted to acidosis. *Cancer Cell International* **2018,** *18* (1), 147.

99. Renschler, M. F., The emerging role of reactive oxygen species in cancer therapy. *European Journal of Cancer* **2004,** *40* (13), 1934-1940.

100. Carmeliet, P.; Jain, R. K., Angiogenesis in cancer and other diseases. *Nature* **2000,** *407* (6801), 249-257.

101. Bhandari, V.; Hoey, C.; Liu, L. Y.; Lalonde, E.; Ray, J.; Livingstone, J.; Lesurf, R.; Shiah, Y.-J.; Vujcic, T.; Huang, X.; Espiritu, S. M. G.; Heisler, L. E.; Yousif, F.; Huang, V.; Yamaguchi, T. N.; Yao, C. Q.; Sabelnykova, V. Y.; Fraser, M.; Chua, M. L. K.; van der Kwast, T.; Liu, S. K.; Boutros, P. C.; Bristow, R. G., Molecular landmarks of tumor hypoxia across cancer types. *Nature Genetics* **2019,** *51* (2), 308-318.

102. Forster, J. C.; Harriss-Phillips, W. M.; Douglass, M. J.; Bezak, E., A review of the development of tumor vasculature and its effects on the tumor microenvironment. *Hypoxia (Auckl)* **2017,** *5*, 21-32.

103. Helmlinger, G.; Yuan, F.; Dellian, M.; Jain, R. K., Interstitial pH and pO2 gradients in solid tumors *in vivo*: High-resolution measurements reveal a lack of correlation. *Nature Medicine* **1997,** *3* (2), 177-182.

104. Guppy, M., The hypoxic core: a possible answer to the cancer paradox. *Biochemical and Biophysical Research Communications* **2002,** *299* (4), 676-680.

105. Carmeliet, P., Angiogenesis in health and disease. *Nature Medicine* **2003,** *9* (6), 653-660.

106. Greijer, A. E.; van der Wall, E., The role of hypoxia inducible factor 1 (HIF-1) in hypoxia induced apoptosis. *Journal of Clinical Pathology* **2004,** *57* (10), 1009-1014.

107. Yamakuchi, M.; Lotterman, C. D.; Bao, C.; Hruban, R. H.; Karim, B.; Mendell, J. T.; Huso, D.; Lowenstein, C. J., P53-induced microRNA-107 inhibits HIF-1 and tumor angiogenesis. *Proceedings of the National Academy of Sciences* **2010,** *107* (14), 6334-6339.

108.   Carmeliet, P.; Dor, Y.; Herbert, J.-M.; Fukumura, D.; Brusselmans, K.; Dewerchin, M.; Neeman, M.; Bono, F.; Abramovitch, R.; Maxwell, P.; Koch, C. J.; Ratcliffe, P.; Moons, L.; Jain, R. K.; Collen, D.; Keshet, E., Role of HIF-1α in hypoxia-mediated apoptosis, cell proliferation and tumour angiogenesis. *Nature* **1998,** *394* (6692), 485-490.

109.   Petrova, V.; Annicchiarico-Petruzzelli, M.; Melino, G.; Amelio, I., The hypoxic tumour microenvironment. *Oncogenesis* **2018,** *7* (1), 10.

110.   Sattler, U. G. A.; Mueller-Klieser, W., The anti-oxidant capacity of tumour glycolysis. *International Journal of Radiation Biology* **2009,** *85* (11), 963-971.

111.   Brown, J. E.; Cook, R. J.; Lipton, A.; Coleman, R. E., Serum Lactate Dehydrogenase Is Prognostic for Survival in Patients with Bone Metastases from Breast Cancer: A Retrospective Analysis in Bisphosphonate-Treated Patients. *Clinical Cancer Research* **2012,** *18* (22), 6348-6355.

112.   Le Scodan, R.; Massard, C.; Jouanneau, L.; Coussy, F.; Gutierrez, M.; Kirova, Y.; Lerebours, F.; Labib, A.; Mouret-Fourme, E., Brain metastases from breast cancer: proposition of new prognostic score including molecular subtypes and treatment. *Journal of Neuro-Oncology* **2012,** *106* (1), 169-176.

113.   Pellegrini, P.; Dyczynski, M.; Sbrana, F. V.; Karlgren, M.; Buoncervello, M.; Hägg-Olofsson, M.; Ma, R.; Hartman, J.; Bajalica-Lagercrantz, S.; Grander, D.; Kharaziha, P.; De Milito, A., Tumor acidosis enhances cytotoxic effects and autophagy inhibition by salinomycin on cancer cell lines and cancer stem cells. *Oncotarget* **2016,** *7* (24), 35703-35723.

114.   Pellegrini, P.; Strambi, A.; Zipoli, C.; Hägg-Olofsson, M.; Buoncervello, M.; Linder, S.; De Milito, A., Acidic extracellular pH neutralizes the autophagy-inhibiting activity of chloroquine: implications for cancer therapies. *Autophagy* **2014,** *10* (4), 562-571.

115.   Yaromina, A.; Quennet, V.; Zips, D.; Meyer, S.; Shakirin, G.; Walenta, S.; Mueller-Klieser, W.; Baumann, M., Co-localisation of hypoxia and perfusion markers with parameters of glucose metabolism in human squamous cell carcinoma (hSCC) xenografts. *International Journal of Radiation Biology* **2009,** *85* (11), 972-980.

116.   Moscat, J.; Richardson, A.; Diaz-Meco, M. T., Nutrient stress revamps cancer cell metabolism. *Cell Research* **2015,** *25*, 537.

117.   MacFarlane, M.; Robinson, G. L.; Cain, K., Glucose—a sweet way to die. *Cell Cycle* **2012,** *11* (21), 3919-3925.

118.   Zu, X. L.; Guppy, M., Cancer metabolism: facts, fantasy, and fiction. *Biochemical and Biophysical Research Communications* **2004,** *313* (3), 459-465.

119. Madan, E.; Gogna, R.; Bhatt, M.; Pati, U.; Kuppusamy, P.; Mahdi, A. A., Regulation of glucose metabolism by p53: emerging new roles for the tumor suppressor. *Oncotarget* **2011,** *2* (12), 948-957.

120. Park, H.-R.; Tomida, A.; Sato, S.; Tsukumo, Y.; Yun, J.; Yamori, T.; Hayakawa, Y.; Tsuruo, T.; Shin-ya, K., Effect on Tumor Cells of Blocking Survival Response to Glucose Deprivation. *JNCI: Journal of the National Cancer Institute* **2004,** *96* (17), 1300-1310.

121. Wek, R. C.; Staschke, K. A., How do tumours adapt to nutrient stress? *The EMBO Journal* **2010,** *29* (12), 1946-1947.

122. Knott, S. R. V.; Wagenblast, E.; Khan, S.; Kim, S. Y.; Soto, M.; Wagner, M.; Turgeon, M.-O.; Fish, L.; Erard, N.; Gable, A. L.; Maceli, A. R.; Dickopf, S.; Papachristou, E. K.; D'Santos, C. S.; Carey, L. A.; Wilkinson, J. E.; Harrell, J. C.; Perou, C. M.; Goodarzi, H.; Poulogiannis, G.; Hannon, G. J., Asparagine bioavailability governs metastasis in a model of breast cancer. *Nature* **2018,** *554*, 378.

123. Krall, A. S.; Xu, S.; Graeber, T. G.; Braas, D.; Christofk, H. R., Asparagine promotes cancer cell proliferation through use as an amino acid exchange factor. *Nature Communications* **2016,** *7*, 11457.

124. Chabner, B. A.; Roberts, T. G., Chemotherapy and the war on cancer. *Nature Reviews Cancer* **2005,** *5* (1), 65-72.

125. Kim, K.-W.; Roh, J. K.; Wee, H.-J.; Kim, C., Chronology of Anticancer Drug Development. In *Cancer Drug Discovery: Science and History*, Springer Netherlands: Dordrecht, 2016; pp 59-70.

126. Warwick, G. P., The Mechanism of Action of Alkylating Agents. *Cancer Research* **1963,** *23* (8 Part 1), 1315-1333.

127. Sarkaria, J. N.; Kitange, G. J.; James, C. D.; Plummer, R.; Calvert, H.; Weller, M.; Wick, W., Mechanisms of Chemoresistance to Alkylating Agents in Malignant Glioma. *Clinical Cancer Research* **2008,** *14* (10), 2900-2908.

128. Kobayashi, H.; Man, S.; Graham, C. H.; Kapitain, S. J.; Teicher, B. A.; Kerbel, R. S., Acquired multicellular-mediated resistance to alkylating agents in cancer. *Proceedings of the National Academy of Sciences* **1993,** *90* (8), 3294-3298.

129. Hall, A. G.; Tilby, M. J., Mechanisms of action of, and modes of resistance to, alkylating agents used in the treatment of haematological malignancies. *Blood Reviews* **1992,** *6* (3), 163-173.

130. Kim, K.-W.; Roh, J. K.; Wee, H.-J.; Kim, C., Alkylating Anticancer Drugs. In *Cancer Drug Discovery: Science and History*, Springer Netherlands: Dordrecht, 2016; pp 71-94.

131. Falzone, L.; Salomone, S.; Libra, M., Evolution of Cancer Pharmacological Treatments at the Turn of the Third Millennium. *Frontiers in pharmacology* **2018,** *9*, 1300-1300.

132. Tiwari, M., Antimetabolites: Established cancer therapy. *Journal of Cancer Research & Therapeutics* **2012,** *8* (4), 510-519.

133. Hagner, N.; Joerger, M., Cancer chemotherapy: targeting folic acid synthesis. *Cancer Manag Res* **2010,** *2*, 293-301.

134. Kaye, S. B., New antimetabolites in cancer chemotherapy and their clinical impact. *British journal of cancer* **1998,** *78 Suppl 3*, 1-7.

135. Kim, K.-W.; Roh, J. K.; Wee, H.-J.; Kim, C., Antimetabolic Anticancer Drugs. In *Cancer Drug Discovery: Science and History*, Springer Netherlands: Dordrecht, **2016**; pp 95-112.

136. Pommier, Y., Drugging Topoisomerases: Lessons and Challenges. *ACS Chemical Biology* **2013,** *8* (1), 82-95.

137. Manchado, E.; Guillamot, M.; Malumbres, M., Killing cells by targeting mitosis. *Cell Death And Differentiation* **2012,** *19*, 369.

138. Shi, J.; Orth, J. D.; Mitchison, T., Cell Type Variation in Responses to Antimitotic Drugs that Target Microtubules and Kinesin-5. *Cancer Research* **2008,** *68* (9), 3269-3276.

139. Wallace, D. C., Mitochondria and cancer. *Nature Reviews Cancer* **2012,** *12*, 685.

140. Martinez-Outschoorn, U. E.; Peiris-Pagés, M.; Pestell, R. G.; Sotgia, F.; Lisanti, M. P., Cancer metabolism: a therapeutic perspective. *Nature Reviews Clinical Oncology* **2016,** *14*, 11.

141. Weinberg, S. E.; Chandel, N. S., Targeting mitochondria metabolism for cancer therapy. *Nature Chemical Biology* **2014,** *11*, 9.

142. Zhang, X.; Fryknäs, M.; Hernlund, E.; Fayad, W.; De Milito, A.; Olofsson, M. H.; Gogvadze, V.; Dang, L.; Påhlman, S.; Schughart, L. A. K.; Rickardson, L.; D'Arcy, P.; Gullbo, J.; Nygren, P.; Larsson, R.; Linder, S., Induction of mitochondrial dysfunction as a strategy for targeting tumour cells in metabolically compromised microenvironments. *Nature Communications* **2014,** *5*, 3295.

FCUP 186
Cyanobacterial bioactive metabolites for anticancer drug
discovery: characterization of new compounds and
molecular mechanisms in physiologically relevant 3D cell
culture

143. Zhang, X.; de Milito, A.; Olofsson, M.; Gullbo, J.; D'Arcy, P.; Linder, S., Targeting Mitochondrial Function to Treat Quiescent Tumor Cells in Solid Tumors. *International Journal of Molecular Sciences* **2015,** *16* (11), 26020.

144. Vazquez, F.; Lim, J.-H.; Chim, H.; Bhalla, K.; Girnun, G.; Pierce, K.; Clish, Clary B.; Granter, Scott R.; Widlund, Hans R.; Spiegelman, Bruce M.; Puigserver, P., PGC1α Expression Defines a Subset of Human Melanoma Tumors with Increased Mitochondrial Capacity and Resistance to Oxidative Stress. *Cancer Cell* **2013,** *23* (3), 287-301.

145. Akins, N. S.; Nielson, T. C.; Le, H. V., Inhibition of Glycolysis and Glutaminolysis: An Emerging Drug Discovery Approach to Combat Cancer. *Current Topics in Medicinal Chemistry* **2018,** *18* (6), 494-504.

146. Dalva-Aydemir, S.; Bajpai, R.; Martinez, M.; Adekola, K. U. A.; Kandela, I.; Wei, C.; Singhal, S.; Koblinski, J. E.; Raje, N. S.; Rosen, S. T.; Shanmugam, M., Targeting the Metabolic Plasticity of Multiple Myeloma with FDA-Approved Ritonavir and Metformin. *Clinical Cancer Research* **2015,** *21* (5), 1161-1171.

147. Formosa, L. E.; Ryan, M. T., Mitochondrial OXPHOS complex assembly lines. *Nature Cell Biology* **2018,** *20* (5), 511-513.

148. Gautier, C. A.; Kitada, T.; Shen, J., Loss of PINK1 causes mitochondrial functional defects and increased sensitivity to oxidative stress. *Proceedings of the National Academy of Sciences* **2008,** *105* (32), 11364-11369.

149. Stephen, J. R.; Pauline, L.; Langfeng, D.; Alfons, L.; Jiri, N., Mitocans: Mitochondrial Targeted Anti-Cancer Drugs as Improved Therapies and Related Patent Documents. *Recent Patents on Anti-Cancer Drug Discovery* **2006,** *1* (3), 327-346.

150. Sánchez-Alcázar, J. A.; Ault, J. G.; Khodjakov, A.; Schneider, E., Increased mitochondrial cytochrome c levels and mitochondrial hyperpolarization precede camptothecin-induced apoptosis in Jurkat cells. *Cell Death And Differentiation* **2000,** *7,* 1090.

151. Graves, J. A.; Wang, Y.; Sims-Lucas, S.; Cherok, E.; Rothermund, K.; Branca, M. F.; Elster, J.; Beer-Stolz, D.; Van Houten, B.; Vockley, J.; Prochownik, E. V., Mitochondrial Structure, Function and Dynamics Are Temporally Controlled by c-Myc. *PLOS ONE* **2012,** *7* (5), e37699.

152. Fantin, V. R.; Berardi, M. J.; Scorrano, L.; Korsmeyer, S. J.; Leder, P., A novel mitochondriotoxic small molecule that selectively inhibits tumor cell growth. *Cancer Cell* **2002,** *2* (1), 29-42.

153. Zhang, X.; Mofers, A.; Hydbring, P.; Olofsson, M. H.; Guo, J.; Linder, S.; D'Arcy, P. MYC is downregulated by a mitochondrial checkpoint mechanism *Oncotarget*, **2017**, p. 90225-90237. PubMed. https://doi.org/10.18632/oncotarget.21653.

154. Miller, D. M.; Thomas, S. D.; Islam, A.; Muench, D.; Sedoris, K., c-Myc and cancer metabolism. *Clinical cancer research : an official journal of the American Association for Cancer Research* **2012,** *18* (20), 5546-5553.

155. Martínez-Reyes, I.; Sánchez-Aragó, M.; Cuezva, José M., AMPK and GCN2–ATF4 signal the repression of mitochondria in colon cancer cells. *Biochemical Journal* **2012,** *444* (2), 249.

156. Jung, P.; Hermeking, H., The c-MYC-AP4-p21 cascade. *Cell Cycle* **2009,** *8* (7), 982-989.

157. Colwy, W. B., The Classic: The Treatment of Malignant Tumors by Repeated Inoculations of Erysipelas with a Report of Ten Original Cases. *Clinical Orthopaedics and Related Research®* **1991,** *262*, 3-11.

158. Lamm, D. L.; Blumenstein, B. A.; Crawford, E. D.; Montie, J. E.; Scardino, P.; Grossman, H. B.; Stanisic, T. H.; Smith, J. A.; Sullivan, J.; Sarosdy, M. F.; Crissman, J. D.; Coltman, C. A., A Randomized Trial of Intravesical Doxorubicin and Immunotherapy with Bacille Calmette–Guérin for Transitional-Cell Carcinoma of the Bladder. *New England Journal of Medicine* **1991,** *325* (17), 1205-1209.

159. Rouprêt, M.; Babjuk, M.; Compérat, E.; Zigeuner, R.; Sylvester, R. J.; Burger, M.; Cowan, N. C.; Gontero, P.; Van Rhijn, B. W. G.; Mostafid, A. H.; Palou, J.; Shariat, S. F., European Association of Urology Guidelines on Upper Urinary Tract Urothelial Carcinoma: 2017 Update. *European Urology* **2018,** *73* (1), 111-122.

160. Kantoff, P. W.; Higano, C. S.; Shore, N. D.; Berger, E. R.; Small, E. J.; Penson, D. F.; Redfern, C. H.; Ferrari, A. C.; Dreicer, R.; Sims, R. B.; Xu, Y.; Frohlich, M. W.; Schellhammer, P. F., Sipuleucel-T Immunotherapy for Castration-Resistant Prostate Cancer. *New England Journal of Medicine* **2010,** *363* (5), 411-422.

161. Higano, C. S.; Small, E. J.; Schellhammer, P.; Yasothan, U.; Gubernick, S.; Kirkpatrick, P.; Kantoff, P. W., Sipuleucel-T. *Nature Reviews Drug Discovery* **2010,** *9*, 513.

162. Ribas, A.; Wolchok, J. D., Cancer immunotherapy using checkpoint blockade. *Science* **2018,** *359* (6382), 1350-1355.

163.   Kim, K.-W.; Roh, J. K.; Wee, H.-J.; Kim, C., Immunotherapeutic Anticancer Drugs and Other Miscellaneous Anticancer Drugs. In *Cancer Drug Discovery: Science and History*, Springer Netherlands: Dordrecht, 2016; pp 135-153.

164.   Motzer, R. J.; Penkov, K.; Haanen, J.; Rini, B.; Albiges, L.; Campbell, M. T.; Venugopal, B.; Kollmannsberger, C.; Negrier, S.; Uemura, M.; Lee, J. L.; Vasiliev, A.; Miller, W. H.; Gurney, H.; Schmidinger, M.; Larkin, J.; Atkins, M. B.; Bedke, J.; Alekseev, B.; Wang, J.; Mariani, M.; Robbins, P. B.; Chudnovsky, A.; Fowst, C.; Hariharan, S.; Huang, B.; di Pietro, A.; Choueiri, T. K., Avelumab plus Axitinib versus Sunitinib for Advanced Renal-Cell Carcinoma. *The New England Journal of Medicine* **2019,** *380* (12), 1103-1115.

165.   D'Arcy, P.; Brnjic, S.; Olofsson, M. H.; Fryknäs, M.; Lindsten, K.; De Cesare, M.; Perego, P.; Sadeghi, B.; Hassan, M.; Larsson, R.; Linder, S., Inhibition of proteasome deubiquitinating activity as a new cancer therapy. *Nature Medicine* **2011,** *17*, 1636.

166.   Brnjic, S.; Mazurkiewicz, M.; Fryknäs, M.; Sun, C.; Zhang, X.; Larsson, R.; D'Arcy, P.; Linder, S., Induction of Tumor Cell Apoptosis by a Proteasome Deubiquitinase Inhibitor Is Associated with Oxidative Stress. *Antioxidants & Redox Signaling* **2014,** *21* (17), 2271-2285.

167.   Mofers, A.; Pellegrini, P.; Linder, S.; D'Arcy, P., Proteasome-associated deubiquitinases and cancer. *Cancer Metastasis Reviews* **2017,** *36* (4), 635-653.

168.   Vanneman, M.; Dranoff, G., Combining immunotherapy and targeted therapies in cancer treatment. *Nature Reviews Cancer* **2012,** *12*, 237.

169.   Pauraic Mc, C.; Aisling, C.; Denis, O. S.; Malachy, M.; Orla, H.; Mary, H.; Michael, D., Targeting the Folate Receptor: Improving Efficacy in Inorganic Medicinal Chemistry. *Current Medicinal Chemistry* **2018,** *25* (23), 2675-2708.

170.   Vergote, I.; Leamon, C. P., Vintafolide: a novel targeted therapy for the treatment of folate receptor expressing tumors. *Therapeutic advances in medical oncology* **2015,** *7* (4), 206-218.

171.   Srinivasarao, M.; Low, P. S., Ligand-Targeted Drug Delivery. *Chemical Reviews* **2017,** *117* (19), 12133-12164.

172.   Eglen, R. M.; Randle, D. H., Drug Discovery Goes Three-Dimensional: Goodbye to Flat High-Throughput Screening? *ASSAY and Drug Development Technologies* **2015,** *13* (5), 262-265.

FCUP 189
Cyanobacterial bioactive metabolites for anticancer drug
discovery: characterization of new compounds and
molecular mechanisms in physiologically relevant 3D cell
culture

173.   Oksana, S.; Trisha, M.; Jayne, H.; Steve, L.; Windsor, O.; F., C. E., High-Content Assays for Characterizing the Viability and Morphology of 3D Cancer Spheroid Cultures. *Assay and Drug Development Technologies* **2015,** *13* (7), 402-414.

174.   Antunes, J.; Gaspar, V. M.; Ferreira, L.; Monteiro, M.; Henrique, R.; Jerónimo, C.; Mano, J. F., In-air production of 3D co-culture tumor spheroid hydrogels for expedited drug screening. *Acta Biomaterialia* **2019,** *94*, 392-409.

175.   Nzou, G.; Wicks, R. T.; Wicks, E. E.; Seale, S. A.; Sane, C. H.; Chen, A.; Murphy, S. V.; Jackson, J. D.; Atala, A. J., Human Cortex Spheroid with a Functional Blood Brain Barrier for High-Throughput Neurotoxicity Screening and Disease Modeling. *Scientific Reports* **2018,** *8* (1), 7413.

176.   Yildirimer, L.; Zhang, Q.; Kuang, S.; Cheung, C.-W. J.; Chu, K. A.; He, Y.; Yang, M.; Zhao, X., Engineering three-dimensional microenvironments towards *in vitro* disease models of the central nervous system. *Biofabrication* **2019,** *11* (3), 032003.

177.   Wong, C.-W.; Han, H.-W.; Tien, Y.-W.; Hsu, S.-h., Biomaterial substrate-derived compact cellular spheroids mimicking the behavior of pancreatic cancer and microenvironment. *Biomaterials* **2019,** *213*, 119202.

178.   Kondo, J.; Ekawa, T.; Endo, H.; Yamazaki, K.; Tanaka, N.; Kukita, Y.; Okuyama, H.; Okami, J.; Imamura, F.; Ohue, M.; Kato, K.; Nomura, T.; Kohara, A.; Mori, S.; Dan, S.; Inoue, M., High-throughput screening in colorectal cancer tissue-originated spheroids. *Cancer Sci* **2019,** *110* (1), 345-355.

179.   Turner, P. A.; Garrett, M. R.; Didion, S. P.; Janorkar, A. V., Spheroid Culture System Confers Differentiated Transcriptome Profile and Functional Advantage to 3T3-L1 Adipocytes. *Annals of Biomedical Engineering* **2018,** *46* (5), 772-787.

180.   Turner, P. A.; Harris, L. M.; Purser, C. A.; Baker, R. C.; Janorkar, A. V., A surface-tethered spheroid model for functional evaluation of 3T3-L1 adipocytes. *Biotechnology and Bioengineering* **2014,** *111* (1), 174-183.

181.   Pampaloni, F.; Reynaud, E. G.; Stelzer, E. H. K., The third dimension bridges the gap between cell culture and live tissue. *Nat Rev Mol Cell Biol* **2007,** *8* (10), 839-845.

182.   Hirschhaeuser, F.; Menne, H.; Dittfeld, C.; West, J.; Mueller-Klieser, W.; Kunz-Schughart, L. A., Multicellular tumor spheroids: An underestimated tool is catching up again. *Journal of Biotechnology* **2010,** *148* (1), 3-15.

183.   Kunz-Schughart, L. A.; Kreutz, M.; Knuechel, R., Multicellular spheroids: a three-dimensional *in vitro* culture system to study tumour biology. *International Journal of Experimental Pathology* **1998,** *79* (1), 1-23.

184. Sutherland, R. M., Cell and environment interactions in tumor microregions: the multicell spheroid model. *Science* **1988,** *240* (4849), 177.

185. Weiswald, L.-B.; Bellet, D.; Dangles-Marie, V., Spherical Cancer Models in Tumor Biology. *Neoplasia* **2015,** *17* (1), 1-15.

186. Friedrich, J.; Eder, W.; Castaneda, J.; Doss, M.; Huber, E.; Ebner, R.; Kunz-Schughart, L. A., A Reliable Tool to Determine Cell Viability in Complex 3-D Culture: The Acid Phosphatase Assay. *Journal of Biomolecular Screening* **2007,** *12* (7), 925-937.

187. Friedrich, J.; Seidel, C.; Ebner, R.; Kunz-Schughart, L. A., Spheroid-based drug screen: considerations and practical approach. *Nature Protocols* **2009,** *4* (3), 309-324.

188. Mehta, G.; Hsiao, A. Y.; Ingram, M.; Luker, G. D.; Takayama, S., Opportunities and challenges for use of tumor spheroids as models to test drug delivery and efficacy. *Journal of Controlled Release* **2012,** *164* (2), 192-204.

189. Zon, L. I.; Peterson, R. T., *In vivo* drug discovery in the zebrafish. *Nature Reviews Drug Discovery* **2005,** *4* (1), 35-44.

190. Stoletov, K.; Klemke, R., Catch of the day: zebrafish as a human cancer model. *Oncogene* **2008,** *27*, 4509.

191. Lieschke, G. J.; Currie, P. D., Animal models of human disease: zebrafish swim into view. *Nature Reviews Genetics* **2007,** *8*, 353.

192. Amatruda, J. F.; Shepard, J. L.; Stern, H. M.; Zon, L. I., Zebrafish as a cancer model system. *Cancer Cell* **2002,** *1* (3), 229-231.

193. Haffter, P.; Granato, M.; Brand, M.; Mullins, M. C.; Hammerschmidt, M.; Kane, D. A.; Odenthal, J.; van Eeden, F. J.; Jiang, Y. J.; Heisenberg, C. P.; Kelsh, R. N.; Furutani-Seiki, M.; Vogelsang, E.; Beuchle, D.; Schach, U.; Fabian, C.; Nusslein-Volhard, C., The identification of genes with unique and essential functions in the development of the zebrafish, Danio rerio. *Development* **1996,** *123* (1), 1-36.

194. Tanguay, R. L., The Rise of Zebrafish as a Model for Toxicology. *Toxicological Sciences* **2018,** *163* (1), 3-4.

195. Kari, G.; Rodeck, U.; Dicker, A. P., Zebrafish: An Emerging Model System for Human Disease and Drug Discovery. *Clinical Pharmacology & Therapeutics* **2007,** *82* (1), 70-80.

196. Stern, H. M.; Zon, L. I., Cancer genetics and drug discovery in the zebrafish. *Nature Reviews Cancer* **2003,** *3* (7), 533-539.

197.   Stanton, M. F., Diethylnitrosamine-Induced Hepatic Degeneration and Neoplasia in the Aquarium Fish, Brachydanio rerio. *JNCI: Journal of the National Cancer Institute* **1965,** *34* (1), 117-130.

198.   Berghmans, S.; Murphey, R. D.; Wienholds, E.; Neuberg, D.; Kutok, J. L.; Fletcher, C. D. M.; Morris, J. P.; Liu, T. X.; Schulte-Merker, S.; Kanki, J. P.; Plasterk, R.; Zon, L. I.; Look, A. T., tp53 mutant zebrafish develop malignant peripheral nerve sheath tumors. *Proceedings of the National Academy of Sciences of the United States of America* **2005,** *102* (2), 407-412.

199.   Faucherre, A.; Taylor, G. S.; Overvoorde, J.; Dixon, J. E.; Hertog, J. d., Zebrafish pten genes have overlapping and non-redundant functions in tumorigenesis and embryonic development. *Oncogene* **2007,** *27*, 1079.

200.   Lu, J.-W.; Ho, Y.-J.; Ciou, S.-C.; Gong, Z., Innovative Disease Model: Zebrafish as an *In vivo* Platform for Intestinal Disorder and Tumors. *Biomedicines* **2017,** *5* (4), 58.

201.   White, R.; Rose, K.; Zon, L., Zebrafish cancer: the state of the art and the path forward. *Nature Reviews Cancer* **2013,** *13*, 624.

202.   Cornet, C.; Di Donato, V.; Terriente, J., Combining Zebrafish and CRISPR/Cas9: Toward a More Efficient Drug Discovery Pipeline. *Frontiers in Pharmacology* **2018,** *9* (703).

203.   Selvaraju, K.; Mofers, A.; Pellegrini, P.; Salomonsson, J.; Ahlner, A.; Morad, V.; Hillert, E.-K.; Espinosa, B.; Arnér, E. S. J.; Jensen, L.; Malmström, J.; Turkina, M. V.; D'Arcy, P.; Walters, M. A.; Sunnerhagen, M.; Linder, S., Cytotoxic unsaturated electrophilic compounds commonly target the ubiquitin proteasome system. *Scientific Reports* **2019,** *9* (1), 9841.

204.   Letrado, P.; de Miguel, I.; Lamberto, I.; Díez-Martínez, R.; Oyarzabal, J., Zebrafish: Speeding Up the Cancer Drug Discovery Process. *Cancer Research* **2018,** *78* (21), 6048-6058.

205.   Wu, J.-Q.; Zhai, J.; Li, C.-Y.; Tan, A.-M.; Wei, P.; Shen, L.-Z.; He, M.-F., Patient-derived xenograft in zebrafish embryos: a new platform for translational research in gastric cancer. *Journal of Experimental & Clinical Cancer Research* **2017,** *36* (1), 160.

206.   Lessman, C. A., The developing zebrafish (Danio rerio): A vertebrate model for high-throughput screening of chemical libraries. *Birth Defects Research Part C: Embryo Today: Reviews* **2011,** *93* (3), 268-280.

207.   Pardo-Martin, C.; Chang, T.-Y.; Koo, B. K.; Gilleland, C. L.; Wasserman, S. C.; Yanik, M. F., High-throughput *in vivo* vertebrate screening. *Nature Methods* **2010,** *7*, 634.

208.   Shlush, L. I.; Mitchell, A.; Heisler, L.; Abelson, S.; Ng, S. W. K.; Trotman-Grant, A.; Medeiros, J. J. F.; Rao-Bhatia, A.; Jaciw-Zurakowsky, I.; Marke, R.; McLeod, J. L.; Doedens, M.; Bader, G.; Voisin, V.; Xu, C.; McPherson, J. D.; Hudson, T. J.; Wang, J. C. Y.; Minden, M. D.; Dick, J. E., Tracing the origins of relapse in acute myeloid leukaemia to stem cells. *Nature* **2017,** *547*, 104.

209.   Maiuthed, A.; Chantarawong, W.; Chanvorachote, P., Lung Cancer Stem Cells and Cancer Stem Cell-targeting Natural Compounds. *Anticancer Research* **2018,** *38* (7), 3797-3809.

210.   Reya, T.; Morrison, S. J.; Clarke, M. F.; Weissman, I. L., Stem cells, cancer, and cancer stem cells. *Nature* **2001,** *414* (6859), 105-111.

211.   Greaves, M.; Maley, C. C., Clonal evolution in cancer. *Nature* **2012,** *481* (7381), 306-313.

212.   Kai, M.; Kanaya, N.; Wu, S. V.; Mendez, C.; Nguyen, D.; Luu, T.; Chen, S., Targeting breast cancer stem cells in triple-negative breast cancer using a combination of LBH589 and salinomycin. *Breast Cancer Research and Treatment* **2015,** *151* (2), 281-294.

213.   Rather, R. A.; Bhagat, M., Cancer Chemoprevention and Piperine: Molecular Mechanisms and Therapeutic Opportunities. *Frontiers in Cell and Developmental Biology* **2018,** *6*, 10-10.

214.   Li, Y.; Zhang, T., Targeting cancer stem cells by curcumin and clinical applications. *Cancer Letters* **2014,** *346* (2), 197-205.

215.   Burnett, J.; Newman, B.; Sun, D., Targeting Cancer Stem Cells with Natural Products. *Current Drug Targets* **2012,** *13* (8), 1054-1064.

216.   Moselhy, J.; Srinivasan, S.; Ankem, M. K.; Damodaran, C., Natural Products That Target Cancer Stem Cells. *Anticancer Research* **2015,** *35* (11), 5773-5788.

217.   Tofoli, F. A.; Dasso, M.; Morato-Marques, M.; Nunes, K.; Pereira, L. A.; da Silva, G. S.; Fonseca, S. A. S.; Costas, R. M.; Santos, H. C.; da Costa Pereira, A.; Lotufo, P. A.; Bensenor, I. M.; Meyer, D.; Pereira, L. V., Increasing The Genetic Admixture of Available Lines of Human Pluripotent Stem Cells. *Scientific reports* **2016,** *6*, 34699-34699.

218.   Subramanian, A.; Narayan, R.; Corsello, S. M.; Peck, D. D.; Natoli, T. E.; Lu, X.; Gould, J.; Davis, J. F.; Tubelli, A. A.; Asiedu, J. K.; Lahr, D. L.; Hirschman, J. E.; Liu, Z.; Donahue, M.; Julian, B.; Khan, M.; Wadden, D.; Smith, I. C.; Lam, D.; Liberzon, A.; Toder, C.; Bagul, M.; Orzechowski, M.; Enache, O. M.; Piccioni, F.; Johnson, S. A.; Lyons, N.

FCUP 193
Cyanobacterial bioactive metabolites for anticancer drug
discovery: characterization of new compounds and
molecular mechanisms in physiologically relevant 3D cell
culture

J.; Berger, A. H.; Shamji, A. F.; Brooks, A. N.; Vrcic, A.; Flynn, C.; Rosains, J.; Takeda, D. Y.; Hu, R.; Davison, D.; Lamb, J.; Ardlie, K.; Hogstrom, L.; Greenside, P.; Gray, N. S.; Clemons, P. A.; Silver, S.; Wu, X.; Zhao, W.-N.; Read-Button, W.; Wu, X.; Haggarty, S. J.; Ronco, L. V.; Boehm, J. S.; Schreiber, S. L.; Doench, J. G.; Bittker, J. A.; Root, D. E.; Wong, B.; Golub, T. R., A Next Generation Connectivity Map: L1000 Platform and the First 1,000,000 Profiles. *Cell* **2017,** *171* (6), 1437-1452.e17.

219.   Subramanian, A.; Tamayo, P.; Mootha, V. K.; Mukherjee, S.; Ebert, B. L.; Gillette, M. A.; Paulovich, A.; Pomeroy, S. L.; Golub, T. R.; Lander, E. S.; Mesirov, J. P., Gene set enrichment analysis: A knowledge-based approach for interpreting genome-wide expression profiles. *Proceedings of the National Academy of Sciences* **2005,** *102* (43), 15545.

220.   Merico, D.; Isserlin, R.; Stueker, O.; Emili, A.; Bader, G. D., Enrichment Map: A Network-Based Method for Gene-Set Enrichment Visualization and Interpretation. *PLOS ONE* **2010,** *5* (11), e13984.

221.   White, E., Deconvoluting the context-dependent role for autophagy in cancer. *Nature Reviews Cancer* **2012,** *12*, 401.

222.   Appiah Kubi, G.; Dougherty, P. G.; Pei, D., Designing Cell-Permeable Macrocyclic Peptides. In *Cyclic Peptide Design*, Goetz, G., Ed. Springer New York: New York, NY, **2019**; pp 41-59.

223.   Herrmann, R.; Fayad, W.; Schwarz, S.; Berndtsson, M.; Linder, S., Screening for Compounds That Induce Apoptosis of Cancer Cells Grown as Multicellular Spheroids. *Journal of Biomolecular Screening* **2008,** *13* (1), 1-8.

224.   Weerakkody, D.; Moshnikova, A.; El-Sayed, N. S.; Adochite, R.-C.; Slaybaugh, G.; Golijanin, J.; Tiwari, R. K.; Andreev, O. A.; Parang, K.; Reshetnyak, Y. K., Novel pH-Sensitive Cyclic Peptides. *Scientific Reports* **2016,** *6*, 31322.

225.   Hruby, V. J., Designing peptide receptor agonists and antagonists. *Nature Reviews Drug Discovery* **2002,** *1* (11), 847-858.

226.   Sievers, E. L.; Senter, P. D., Antibody-Drug Conjugates in Cancer Therapy. *Annual Review of Medicine* **2013,** *64* (1), 15-29.

227.   Beck, A.; Goetsch, L.; Dumontet, C.; Corvaïa, N., Strategies and challenges for the next generation of antibody–drug conjugates. *Nature Reviews Drug Discovery* **2017,** *16*, 315.

228.   Tran, S.; DeGiovanni, P.-J.; Piel, B.; Rai, P., Cancer nanomedicine: a review of recent success in drug delivery. *Clin Transl Med* **2017,** *6* (1), 44-44.

229.   Liston, D. R.; Davis, M., Clinically Relevant Concentrations of Anticancer Drugs: A Guide for Nonclinical Studies. *Clinical cancer research : an official journal of the American Association for Cancer Research* **2017,** *23* (14), 3489-3498.

230.   João P. A., R.; Sandra A. C., F.; Pedro, L., BrtB Is a Novel O-Alkylating Enzyme That Generates Fatty Acid-Bartoloside Esters. **2019**. *Preprint on ChemRxiv*.

231.   Fusetani, N., Antifouling marine natural products. *Natural Product Reports* **2011,** *28* (2), 400-410.

232.   Dahms, H.-U.; Ying, X.; Pfeiffer, C., Antifouling potential of cyanobacteria: a mini-review. *Biofouling* **2006,** *22* (5), 317-327.

233.   Costa, M.; Garcia, M.; Costa-Rodrigues, J.; Costa, S. M.; Ribeiro, J. M.; Fernandes, H. M.; Barros, P.; Barreiro, A.; Vasconcelos, V.; Martins, R., Exploring Bioactive Properties of Marine Cyanobacteria Isolated from the Portuguese Coast: High Potential as a Source of Anticancer Compounds. *Marine Drugs* **2014,** *12* (1).

234.   Wang, M.; Carver, J. J.; Phelan, V. V.; Sanchez, L. M.; Garg, N.; Peng, Y.; Nguyen, D. D.; Watrous, J.; Kapono, C. A.; Luzzatto-Knaan, T.; Porto, C.; Bouslimani, A.; Melnik, A. V.; Meehan, M. J.; Liu, W.-T.; Crüsemann, M.; Boudreau, P. D.; Esquenazi, E.; Sandoval-Calderón, M.; Kersten, R. D.; Pace, L. A.; Quinn, R. A.; Duncan, K. R.; Hsu, C.-C.; Floros, D. J.; Gavilan, R. G.; Kleigrewe, K.; Northen, T.; Dutton, R. J.; Parrot, D.; Carlson, E. E.; Aigle, B.; Michelsen, C. F.; Jelsbak, L.; Sohlenkamp, C.; Pevzner, P.; Edlund, A.; McLean, J.; Piel, J.; Murphy, B. T.; Gerwick, L.; Liaw, C.-C.; Yang, Y.-L.; Humpf, H.-U.; Maansson, M.; Keyzers, R. A.; Sims, A. C.; Johnson, A. R.; Sidebottom, A. M.; Sedio, B. E.; Klitgaard, A.; Larson, C. B.; Boya P, C. A.; Torres-Mendoza, D.; Gonzalez, D. J.; Silva, D. B.; Marques, L. M.; Demarque, D. P.; Pociute, E.; O'Neill, E. C.; Briand, E.; Helfrich, E. J. N.; Granatosky, E. A.; Glukhov, E.; Ryffel, F.; Houson, H.; Mohimani, H.; Kharbush, J. J.; Zeng, Y.; Vorholt, J. A.; Kurita, K. L.; Charusanti, P.; McPhail, K. L.; Nielsen, K. F.; Vuong, L.; Elfeki, M.; Traxler, M. F.; Engene, N.; Koyama, N.; Vining, O. B.; Baric, R.; Silva, R. R.; Mascuch, S. J.; Tomasi, S.; Jenkins, S.; Macherla, V.; Hoffman, T.; Agarwal, V.; Williams, P. G.; Dai, J.; Neupane, R.; Gurr, J.; Rodríguez, A. M. C.; Lamsa, A.; Zhang, C.; Dorrestein, K.; Duggan, B. M.; Almaliti, J.; Allard, P.-M.; Phapale, P.; Nothias, L.-F.; Alexandrov, T.; Litaudon, M.; Wolfender, J.-L.; Kyle, J. E.; Metz, T. O.; Peryea, T.; Nguyen, D.-T.; VanLeer, D.; Shinn, P.; Jadhav, A.; Müller, R.; Waters, K. M.; Shi, W.; Liu, X.; Zhang, L.; Knight, R.; Jensen, P. R.; Palsson, B. Ø.; Pogliano, K.; Linington, R. G.; Gutiérrez, M.; Lopes, N. P.; Gerwick, W. H.; Moore, B. S.; Dorrestein, P. C.; Bandeira, N., Sharing and community curation of mass

FCUP | 195
Cyanobacterial bioactive metabolites for anticancer drug
discovery: characterization of new compounds and
molecular mechanisms in physiologically relevant 3D cell
culture

spectrometry data with Global Natural Products Social Molecular Networking. *Nature Biotechnology* **2016,** *34*, 828.

235. Deeks, Emma D. Polatuzumab Vedotin: First Global Approval. *Drugs.* **2019**, 79 (13), 1467-1475.

FCUP | 197
Cyanobacterial bioactive metabolites for anticancer drug
discovery: characterization of new compounds and
molecular mechanisms in physiologically relevant 3D cell
culture

Publications, conference proceedings and attended courses

Publications during PhD period included on the present thesis

Sousa ML, Preto M, Vasconcelos V, Linder S and Urbatzka R. **2019**. *Antiproliferative Effects of the Natural Oxadiazine Nocuolin A Are Associated With Impairment of Mitochondrial Oxidative Phosphorylation*. Frontiers in Oncology. http://dx.doi.org/10.3389/fonc.2019.00224.

Ribeiro T, Lemos F, Preto M, Azevedo J, **Sousa ML**, Leão PN, Campos, A, Linder, S, Vitorino, R, Vasconcelos, V, Urbatzka, R. **2017**. *Cytotoxicity of portoamides in human cancer cells and analysis of the molecular mechanisms of action.* PLOS ONE 12 (12): e0188817. http://dx.doi.org/10.1371/journal.pone.0188817.

Conference proceedings during PhD period

Sousa, Maria Lígia, Ribeiro, Tiago, Vasconcelos, Vítor, Linder, Stig, Urbatzka, Ralph. **2019**. "Portoamides A and B isolated from *Phormidium sp.* LEGE 05292 Induces Cytotoxicity on the Proliferative Cell Layer of *In vitro* Microtumours". XVI International Symposium on Marine Natural Products and XI European Conference on Marine Natural Products. Peniche, Portugal. Poster Presentation.

Sousa, M.L., Preto, M., Vasconcelos, V., Linder, S.; Urbatzka, R.. **2019**. "Cyanobacteria isolated Nocuolin A impairs mitochondrial oxidative phosphorylation on cancer spheroids. PSE meeting Lisbon 2019 - Natural Products in Drug Discovery and Human Health. Lisbon 28th-31st July 2019. Oral Communication.

Sousa, M.L., Preto, M., Vasconcelos, V., Linder, S.; Urbatzka, R. **2019**. "Effects of Cyanobacteria Origin Oxadiazine Nocuolin A on HCT116 Cells Cultured on 2D and 3D Cell Systems". Università degli studi di Napoli Federico II (Nápoles, Itália) - ISSNP - International Summer School on Natural Products. Naples and Maratea 1st -5th July 2019. Oral communication.

Sousa, Maria Lígia, Preto, M., Vasconcelos, V., Linder, S.; Urbatzka, R.. **2018**. "A natural oxadiazine isolated from cyanobacteria kills cancer cells in multicellular culture systems by impairing cellular respiration". 30th International Symposium on the Chemistry of Natural Products and the 10th International Congress on Biodiversity (ISCNP30 & ICOB10). Athens, Greece. Poster presentation.

Sousa, Maria Lígia, Preto, M., Leão, P., Martins, R., Vasconcelos, V., Linder, S.; Urbatzka, R. **2017**. "Generation of spheroids of cancer cells for screening of anti-tumour

activity of cyanobacterial extracts and isolated compounds". 8th International Conference on Marine Biotechnology (BIOPROSP_17). TrØmso, Norway. Poster presentation.

Attended courses

The project Blue and Green (European Union's Horizon 2020 Research and Innovation programme, under grant agreement No 692419) training courses:

1. High Throughput Screening & Safety Course, 5-7 November 2018;
2. Structure Elucidation Course, 25-28 June 2018;
3. Bioactivities Course, 13-16 November 2017, CIIMAR.
4. Análise De Dados Provenientes De Técnicas Moleculares, 15 November – 2 December 2016.

Publications, during PhD period not included on the present thesis

Freitas, Sara; Silva, Natália; **Sousa, Maria Lígia**, Ribeiro, Tiago; Rosa, Filipa; Leão, Pedro Nuno; Vasconcelos, Vítor; Reis, Mariana Alves; Urbatzka, Ralph. **2019**. *Chlorophyll Derivatives from Marine Cyanobacteria with Lipid-Reducing Activities.* Marine Drugs 17(4), 229. http://dx.doi.org/10.3390/md17040229.

Frommlet, Jörg C.; Wangpraseurt, Daniel; **Sousa, Maria L.**, Guimarães, Bárbara; Silva, Mariana M.; Küh, Michael, Serôdio, João. **2018**. *Symbiodinium-Induced Formation of Microbialites: Mechanistic Insights From in Vitro Experiments and the Prospect of Its Occurrence in Nature.* Frontiers in Microbiology 9, 224. http://dx.doi.org/10.3389/fmicb.2018.00998.

Sousa, Maria Lígia; Figueiredo, Francisco; Pinheiro, Catarina, Silva, Ana, Malhão, Fernanda, Rocha, Maria João, Rocha, Eduardo, Urbatzka, Ralph. **2015**. *Morphological and molecular effects of cortisol and ACTH on zebrafish stage I and II follicles.* Reproduction 150 (5): 429-436. http://dx.doi.org/10.1530/rep-15-0271.

Patent submission, during PhD period not included on the present thesis

Co - author of the patent submission 20191000013283 - INPI - Instituto Nacional da Propriedade Industrial, with Ralph Urbatzka, Sara, Pedro Leão, **Maria Ligia Sousa**, Mariana Reis, Natália Gonçalves Silva, Vitor Vasconcelos. "Hydroxypheophorbide compounds, methods and uses thereof".